ADVANCED LIGHT SOURCE | Activity Report 2001

Advanced Light Source
Ernest Orlando Lawrence Berkeley National Laboratory
University of California, Berkeley, California 94720-8226

Supported by the U.S. Department of Energy under Contract No. DE-AC03-76SF00098

LBNL- 49628

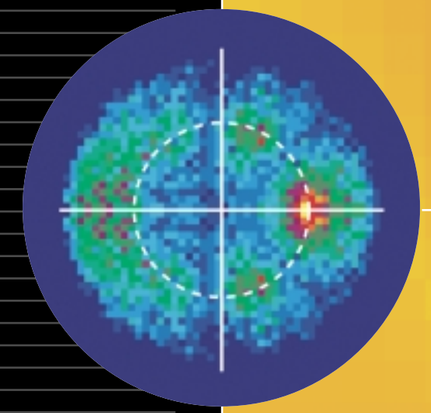

ADVANCED LIGHT SOURCE

Activity Report 2001

APRIL 2002

Ernest Orlando Lawrence Berkeley National Laboratory
University of California • Berkeley, California 94720
LBNL- 49628

Editors:
Annette Greiner
Elizabeth Moxon
Arthur L. Robinson
Lori Tamura

Proofreaders:
Richard Albert
Teresa Duque

Design, layout, photography:
Berkeley Lab's Technical and Electronic Information Department (TEID)
Creative Services

The editors gratefully acknowledge the ALS users and staff for their contributions, advice, and patience.

On the cover: The circular image is an electron momentum map for carbon monoxide, generated by a new multiparticle coincidence technique for photoelectron diffraction (see highlight, p. 42).

Disclaimer

This document was prepared as an account of work sponsored by the United States Government. While this document is believed to contain correct information, neither the United States Government nor any agency thereof, nor The Regents of the University of California, nor any of their employees, makes any warranty, express or implied, or assumes any legal responsibility for the accuracy, completeness, or usefulness of any information, apparatus, product, or process disclosed, or represents that its use would not infringe privately owned rights. Reference herein to any specific commercial product, process, or service by its trade name, trademark, manufacturer, or otherwise, does not necessarily constitute or imply its endorsement, recommendation, or favoring by the United States Government or any agency thereof, or The Regents of the University of California. The views and opinions of authors expressed herein do not necessarily state or reflect those of the United States Government or any agency thereof, or The Regents of the University of California.

Available to DOE and DOE Contractors from the Office of Scientific and Technical Communication, P.O. Box 62, Oak Ridge, TN 37831. Prices available from (615) 576-8401.

Available to the public from the National Technical Information Service, U.S. Department of Commerce, 5285 Port Royal Road, Springfield, VA 22161.

Ernest Orlando Lawrence Berkeley National Laboratory is an equal opportunity employer.

For More Information

For information about using the ALS, contact

Gary Krebs
User Services Group Leader
Advanced Light Source
Lawrence Berkeley National Laboratory
MS 6R2100
Berkeley, CA 94720-8226
Tel: (510) 486-7727
Fax: (510) 486-4773
Email: gfkrebs@lbl.gov

For all other information concerning the ALS, contact

Jeremy Coyne
User Services Program Administrator
Advanced Light Source
Lawrence Berkeley National Laboratory
MS 6R2100
Berkeley, CA 94720-8226
Tel: (510) 486-4518
Fax: (510) 486-4773
Email: alsuser@lbl.gov

ALS home page
http://www-als.lbl.gov/

ADVANCED LIGHT SOURCE

Activity Report 2001

April 2002
Ernest Orlando Lawrence Berkeley National Laboratory
University of California
Berkeley, California, 94720
LBNL-49628

This work was supported by the Director, Office of Science, Office of Basic Energy Sciences, Materials Sciences Division, of the U.S. Department of Energy under Contract No. DE-AC03-76SF00098.

Contents

Introduction iv

Note from the UEC Chair v

Science Highlights 1

- Overview 2
- Feature: Making the Microchips of the Future 3
- Complex Materials 9
- Magnetism and Magnetic Materials 16
- Polymers, Biomaterials, and Soft Matter 22
- Nanostructures and Semiconductors 24
- Environmental and Earth Science 26
- Protein Crystallography 30
- Atomic and Molecular Science 42
- Chemical Dynamics 53
- Accelerator Physics 55

Facility Report 59

- Feature: Superbends at the ALS 60
- Operations 66
- Accelerator Physics 69
- Experimental Systems 75
- Scientific Support 83
- User Services 90

Special Events 93

ALS Advisory Panels 111

ALS Staff 112

Facts and Figures 114

2001 Publications 119

Introduction

Daniel Chemla, *ALS Director*

When I was appointed Director of the ALS, I agreed to do it for two to three years. I am now well into my fourth year and finding the job as stimulating and challenging as ever. It is a pleasure to work with such a talented user community and a dedicated ALS staff towards a common goal—the delivery of outstanding science.

The biggest event of 2001 was undoubtedly the installation of the superbends. I congratulate the superbend team for its flawless achievement (and for putting to rest the sleepless nights I had been experiencing!). No one was surprised by the decision of the UEC's Award Selection Committee to recognize this accomplishment with the Halbach Prize. Superbend beamlines for macromolecular crystallography are already generating protein structures. We have now enhanced our capability in the hard x-ray region without compromising our core mission, which is to excel in the soft x-ray and VUV regions of the spectrum.

The ALS is continually being reviewed. The key event in 2001 was the review of the ALS as a Division of Berkeley Lab by the University of California, which operates the Laboratory for the U.S. Department of Energy. The principal conclusion of the committee, chaired by Jene Golovchenko (Harvard University), was "We cannot overstate our view that the ALS is now an extremely valuable regional, national and international scientific resource…it deserves the continued attention and support from the highest levels of management within LBNL, the University of California, and the Department of Energy to maintain this state of affairs." Towards the end of 2001, we were preparing for a DOE/BES review scheduled for February 2002. We will report on the outcome of this review in next year's Activity Report.

Finally, let me say how dependent I am on input from the ALS advisory committees, particularly the UEC and the SAC. I say a special thank-you to the members of those committees and to their respective chairs, Harald Ade (North Carolina State University) and Steve Kevan (University of Oregon). Let us trust that 2002 will see the ALS as successful as it was in 2001.

Note From the UEC Chair

Harald Ade, *UEC Chair for 2001*

My tenure as ALS UEC Chair during 2001 has confirmed my belief that ALS users are very fortunate to be able to work at such a fantastic facility. The diversity and strength of the ALS community and its accomplishments were readily observable at the annual ALS Users' Meeting on October 16–18, 2001. The meeting was a great success, with a record number of participants and excellent workshops that focused on diverse scientific and technological themes. After the *al fresco* dinner on the ALS terrace, I had the pleasure to present the Shirley Award to Ed Rightor and Gary Mitchell, the Halbach Award to the superbend team, the Renner Award to Elke Arenholz and Ken Barat, and the award for best student poster to Hendrik Ohldag and Christoph Bostedt. I am deeply grateful to UEC members Rupert Perera and Dennis Lindle for organizing the meeting. (See the Special Events section for more about the Users' Meeting.)

Despite excellent reviews during the recent past, the ALS and its users must not rest on their laurels. Active planning must take place to keep the facility state-of-the-art in the years to come. An event that symbolizes this quest for renewal and continuing leadership was the implementation of the superbend magnets, allowing the ALS to serve a larger protein crystallography and hard x-ray community. No one will look at synchrotron facilities in quite the same way again.

The UEC is looking forward to working actively with ALS management on a number of challenging problems, such as sufficient staging areas, office space, weekend transportation, and the difficult issue of adequate and cheap housing at or near the Berkeley Lab.

The ALS user community is growing rapidly. The number of beamline scientists in the Scientific Support Group is growing in order to provide vital support functions. Yet more staff is needed to truly exploit the opportunities. The need for user support has "spilled over" into the Experimental Systems Group, a large fraction of which now provides user support functions. Hence, the growing user base and their needs are putting a severe strain on the facility and constrain the innovative developments the Experimental Systems Group should undertake. We are starting to devour our future.

While the users can work with ALS management to strike an appropriate balance between present and future needs, the users also need to vigorously attempt to increase the available resources. Individual users have written letters to Congress, and UEC representatives from all four DOE synchrotron facilities have met in Washington with members of Congress and their staff, as well as staff in the Office of Management and Budget. I strongly believe that we have to continue these activities and to further broaden them by including visits of users with their Congresspersons and Senators in their district or state offices.

During my term as UEC chair, I got a much deeper appreciation of the various accomplishments of the ALS and its users. It was truly an honor to have served this vibrant community as UEC chair.

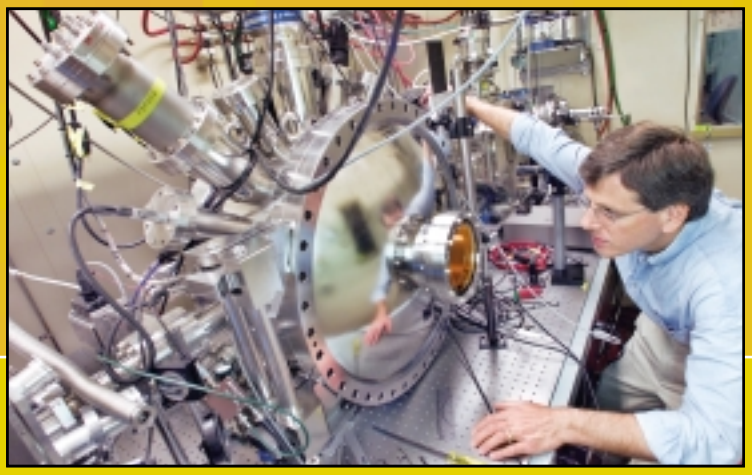

Science Highlights

As a national user facility, the Advanced Light Source generates light for cutting-edge scientific and technological research. Users come from industry, academia, and government laboratories around the world to take advantage of the bright synchrotron light (primarily x rays) generated by accelerated electrons circulating in the ALS storage ring. The light is directed along specialized beamlines to deliver the desired range of wavelengths to a precise spot on a sample in an experiment endstation. The types of samples and techniques for collecting data span a tremendous range, enabling a broad spectrum of research and applications, from protein folding to atomic physics. Competition for time on a beamline ("beam time") is keen, and prospective users earn the opportunity through a peer-review process, either as independent investigators or by joining a Participating Research Team for a particular beamline. These highlights represent a selection from that already elite group. A fuller accounting of the year's experiments is nestled inside the back cover of this volume—the Compendium of User Abstracts on CD.

Overview

Neville Smith, *Division Deputy for Science*

We present in this section a selection of scientific highlights of work published in 2001. As usual, the selection was difficult and, as usual, we offer apologies to those whose meritorious work does not appear. In making the selection, we strive for balance over the diversity of disciplines practiced at the ALS while still emphasizing work appearing in the "high-profile" journals that our sponsors watch carefully. Your comments are welcome.

One balancing act not used in the selection was the relative contributions of Participating Research Team (PRT) members and independent investigators (IIs). A retrospective inspection shows that a substantial fraction of the highlights (around 50%) were initiated through II proposals. Of course, IIs frequently publish with PRT members as co-authors, making it difficult to disentangle the contributions. Nevertheless, our II program is looking healthy.

One of my responsibilities is to oversee the II program. I am assisted in this task by two hard-working Proposal Study Panels (PSPs), the Protein Crystallography PSP and the General Sciences PSP. The procedures of the two PSPs are different, but the end product is the same: namely, a rank ordering of the proposals by merit that is then used for the purposes of beam-time allocation. For each beamline, there is then a meeting of the various stakeholders in which we go down the list allocating beam time until all the available II shifts are exhausted. Drawing this cutoff line is one of the most agonizing decisions we are called upon to make, and our preference is to allocate a few shifts to a large number of proposals rather than a large number of shifts to a few proposals.

Towards the end of 2001, the Protein Crystallography PSP switched from a six-month cycle to a one-month cycle in order to be more responsive to the faster turnaround required to serve this community. So far the new procedure seems to be working well, but we will monitor it through 2002 and describe the results in next year's Activity Report.

Neville Smith (front left) with the General Sciences Proposal Study Panel for 2001. *Back row,* Adam Hitchcock, Theodore Madey, and Dale Sayers; *center row,* Yves Idzerda, Gwyn Williams, Kevin Smith, Tomas Baer, and Stephen Southworth.

Making the Microchips of the Future

EUV Lithography Measures Up

An old adage says, "If you can't measure it, you can't make it." So it's no accident that EUV metrology beamlines built and operated at the Advanced Light Source under the auspices of Berkeley Lab's Center for X-Ray Optics (CXRO) have been instrumental in a 5-year, $250-million industry–national laboratory effort to bring extreme ultraviolet (EUV) lithography to fruition (see the timeline). EUV lithography is the future chip-printing technology that the Semiconductor Industry Association began backing last year as the likely successor, around the year 2007, to the reigning family of refractive optical lithography techniques. The EUV promise is that with wavelengths 50 times smaller than those of visible light, it will be able to draw circuit patterns just tens of nanometers wide.

In conformance with Intel co-founder Gordon Moore's prediction, now known as Moore's Law, the density of circuit elements on microchips has doubled roughly every 12 to 18 months for more than 30 years, resulting in ever smaller, faster, and cheaper computers (Figure 1). However, optical lithography based on traditional refractive optics cannot continue indefinitely on this course. One alternative is to switch to reflective optics—that is, from lenses to mirrors. The availability of molybdenum/silicon multilayer coatings that radically boost the weak normal-incidence reflectance of mirrors in the EUV to almost 70% makes this alternative practical. The operating wavelength of 13 nm is set primarily by the multilayer coating, which has a high reflectance over a relatively narrow range of wavelengths.

To advance the technology to the commercial stage, a consortium of companies (Intel, Motorola, Advanced Micro Devices, IBM, Micron Technology, and Infineon Technologies) established the EUV Limited Liability Corporation (EUV LLC), which partnered with the "Virtual National Laboratory" consisting of groups from Lawrence Livermore National Laboratory, Sandia National Laboratories, and Berkeley Lab in a five-year, $250-million Cooperative Research and Development Agreement (CRADA). Under the 1997 agreement, Livermore took on the multilayer coatings for the mirrors and mask, as well as the optical design and alignment; Sandia, the laser-plasma source, the EUV-sensitive polymer layer (resist) that covers the silicon wafer and is the entity

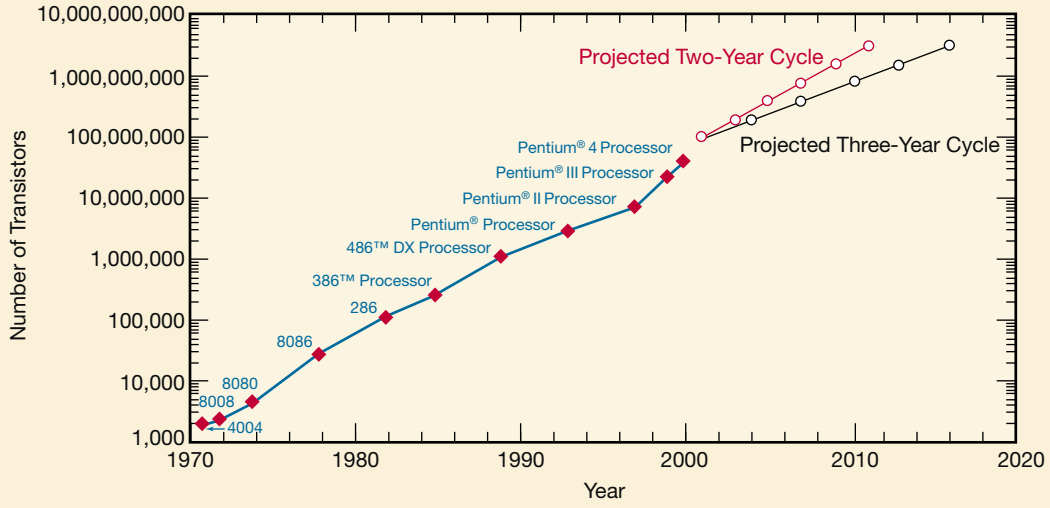

Figure 1 In 1965, Gordon Moore of the Intel Corporation predicted an exponential growth in the number of circuit elements on microchips over time, a forecast borne out by the transistor count on the generations of Intel microprocessors. Two future scenarios are shown *(open circles)* based on the three-year cycle for introduction of new chips used in the Semiconductor Industry Association's 2001 edition of the *International Technology Roadmap for Semiconductors* and an accelerated two-year cycle advocated by some manufacturers.

actually exposed to EUV light, and integrating the overall stepper system; and Berkeley Lab's CXRO, the at-wavelength metrology (measuring performance at 13 nm).

Heralding progress was an April 2001 announcement that the first full-scale prototype printing tool (alpha stepper) based on EUV lithography had met its initial performance milestone. The prototype stepper (known as the Engineering Test Stand, or ETS, Figure 2) demonstrates all the critical capabilities required for making future generations of computer chips with 13-nm light. The ETS includes a four-mirror camera that transfers a reduced image of the circuit pattern on a reflective mask to the resist on a wafer. For proper focusing, the imaging mirrors must be precisely manufactured in a curved but not spherical (aspherical) shape. The EUV source in the ETS is a laser-heated ionized gas (plasma). Successor versions of the ETS during the next few years will refine the technology and lead to pre-production machines (beta steppers) that meet industry requirements for chip manufacture.

Because EUV lithography places extremely demanding tolerances on the fabrication of mirror substrates and their multilayer coatings, as well as on assembling the optics into a camera, teams working at three CXRO beamlines at the ALS have played a key role in reaching the milestone represented by a functioning ETS. At Beamline 6.3.2, work focused on measuring the reflectivity and uniformity of critically important molybdenum-silicon multilayer coatings (Figure 3). The ability to characterize the coatings with high accuracy has turned out to be essential for successfully making mirrors. Beamline 11.3.2 was dedicated to finding tiny defects in the reflective, multilayer-coated "mask blanks" that will carry the circuit patterns—a task sometimes equated to searching for golf balls in an area the size of Rhode Island (Figure 4).

Finally, at Beamline 12.0.1, the CXRO team has exploited the coherence of ALS light in the EUV to perfect an at-wavelength phase-shifting point-diffraction interferometer (PS/PDI, Figure 5). This novel interferometer, arguably the most accurate wavefront-measuring device in the world, has been indispensable for characterizing EUV cameras and predicting their performance for printing circuit patterns. Interferograms reveal the departures of the optics from the designed shape. The measurement accuracy the team has

A Timeline for EUV Lithography

1965

Moore's Law proposed for semiconductor integrated circuits (G. Moore, Intel)

1972

Effective multilayer mirror designs published (E. Spiller, IBM)

1996

First working transistor produced by EUV lithography (K. Nguyen et al., Sandia, UC Berkeley)

1997

$250-million CRADA between Virtual National Laboratory (Sandia, LLNL, and LBNL) and EUV Limited Liability Corporation (Intel, Advanced Micro Devices, Motorola, IBM, Micron Technology, Infineon Technologies)

First of five different two-mirror Schwarzschild 10× prototype EUV optics tested with Phase-Shifting Point Diffraction Interferometer (PS/PDI) on ALS Beamline 12.0.1 with a measurement accuracy of $\lambda/300$ (0.04 nm), well beyond expectations (K. Goldberg et al., CXRO, UC Berkeley)

1999

Wavelength precision of 0.02% achieved with Calibrations and Standards Beamline 6.3.2 enables fabrication of multilayer coatings for EUV projection optics to be used in the Engineering Test Stand (prototype or alpha stepper). (J. Underwood, E. Gullikson et al., CXRO, LLNL)

2000

First projection optics (Set-1) for Engineering Test Stand measured with a new PS/PDI on Beamline 12.0.1 dedicated to testing four-mirror lithographic-quality EUV optics. A 1.0-nm wavefront error achieved after at-wavelength testing and realignment. (K. Goldberg, CXRO, LLNL, UC Berkeley)

SIA roadmap places EUV lithography at top of list for candidates for 70-nm technology generation

2001

ETS with Set-1 optic prints patterns with 100-nm features (D. Titchenor et al., Sandia, LLNL, CXRO)

Higher-quality projection optic (Set-2) for Engineering Test Stand measured with PS/PDI (K. Goldberg et al., CXRO)

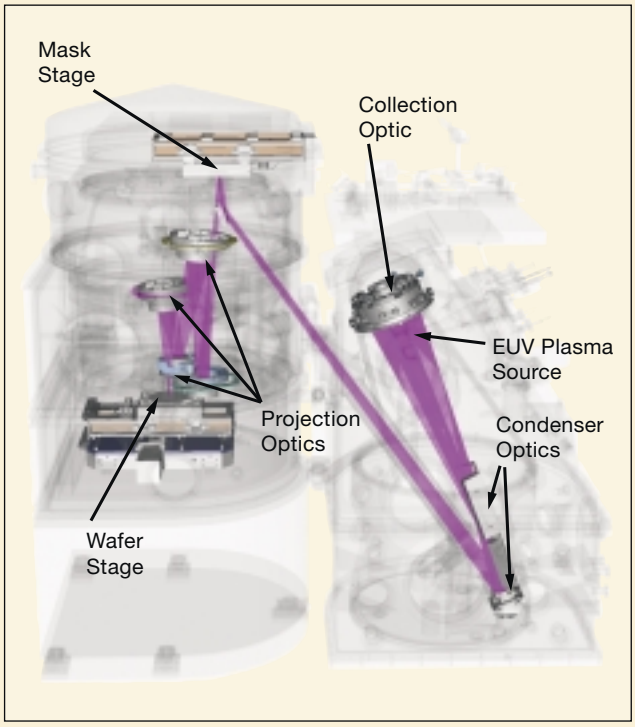

Figure 2 Elements of the Engineering Test Stand manufactured at Sandia National Laboratories. All told, there are nine reflective surfaces, hence the premium on the maximum possible reflectance for the mirrors. Chip patterns are not printed one at a time but by a coordinated scanning motion of the stages containing the mask and wafer through the EUV beam. A commercial stepper would also incorporate a system for handling multiple wafers, each of which contains several hundred chips.

1981

Multilayer mirrors with very high reflectance reported (E. Spiller, IBM; T. Barbee, Stanford)

First demonstration of x-ray imaging with normal-incidence optics (J. Underwood, Jet Propulsion Laboratory, and T. Barbee, Stanford)

1985

First molybdenum/silicon multilayer mirror demonstrated (T. Barbee et al., LLNL)

1988

EUV lithography proposed based on multilayer mirrors at wavelength near 13 nm (N. Ceglio, A. Hawryluk, and L. Seppala, LLNL; W. Silvfast and L. Wood, AT&T Bell Labs)

1989

First demonstration of EUV lithography at 13 nm (H. Kinoshita et al., Japan)

1990

50-nm features with EUV lithography demonstrated (J. Bjorkholm et al., AT&T Bell Labs)

1992

EUV programs begin at National Laboratories (Sandia w/AT&T Bell Labs CRADA; LLNL w/Ultratech CRADA, Berkeley Lab's CXRO w/DARPA grant)

1994

EUV lithography appears on Semiconductor Industry Association (SIA) National Technology Roadmap for Semiconductors

PS/PDI station modified and prints test patterns with Set-2 optic (P. Naulleau et al., CXRO, UC Berkeley, LLNL)

Wavelength and reflectance precisions of 0.007% and 0.08% achieved with Calibrations and Standards Beamline near the goals of 0.005% and 0.06% for production multilayer-coated mirrors (Gullikson et al., CXRO)

EUV LLC announces successful operation of prototype stepper (Engineering Test Stand) and industry commitment to EUV lithography

2004

Expected completion of preproduction (beta) stepper for EUV lithography

2007

45-nm technology generation to begin production with commercial stepper for EUV projection lithography

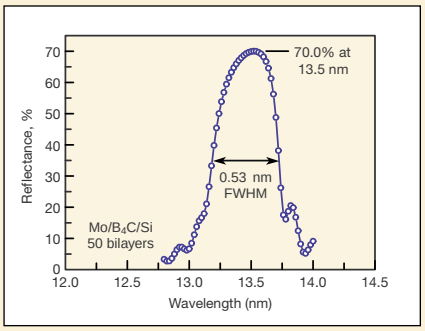

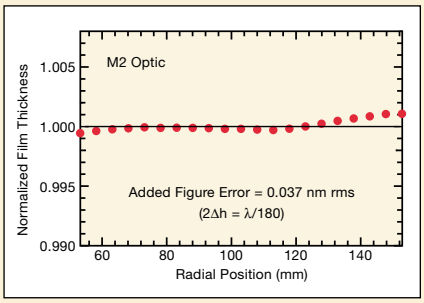

Figure 3 In the photo, Eric Gullikson *(left)* and Jim Underwood *(right)* stand by the reflectometer on CXRO's Calibration and Standards Beamline 6.3.2 that they pioneered. The graphs show typical results, a multilayer coating reflectivity spectrum demonstrating a 70% reflectance and a plot of multilayer-coating thickness inferred from optical measurements. The thickness must be highly uniform to avoid degrading the figure of the aspherical mirror.

achieved has been as fine as 0.04 nm—a distance smaller than the Bohr radius of a hydrogen atom! The precision (repeatability) is even better, at 0.01 nm. Two sets of four-mirror optics (ETS-1 and ETS-2 optics) manufactured at Tinsley/ASML (Richmond, CA) have already been tested with very satisfactory results (Figure 6).

The first computer processors produced with EUV technology are expected to be almost ten times faster than today's most powerful chips, and the storage capacity of memory chips will increase even more. Some chip manufacturers are illustrating the future with projections that the computer will become as easy to use as a telephone. The resulting economic impact of EUV lithography will plainly be significant, both in investment (the cost of a single chip-fabrication facility—and there will be many—is about $2 billion) and in the wealth generated, and it might well justify the cost of the entire U.S. synchrotron program, let alone the ALS.

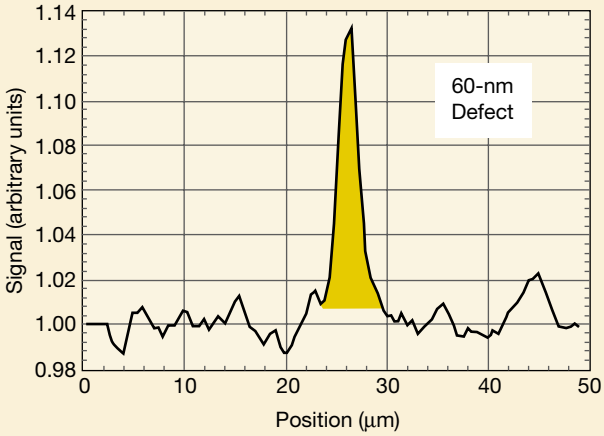

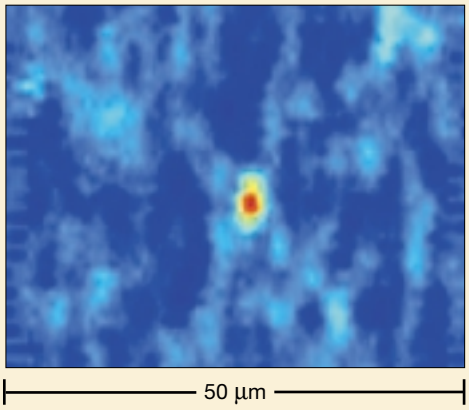

Figure 4 The multilayer-coated "blanks" on which masks (which carry the circuit pattern to be printed) will be formed must be free of defects with diameters above a fraction of the minimum size of a feature in the pattern (such as the width of a conducting line). Finding such defects has been likened to searching for golf balls in an area the size of Rhode Island, but it is being successfully done at Beamline 11.3.2, as shown by the 60-nm defect found here.

The Proof Is in the Printing

While interferometry is routinely used for the characterization and alignment of optics for EUV lithography, the ultimate performance metric is printing. The comparison of a lithographic image with that predicted from wavefront quality is also useful for verifying and improving the predictive power of wavefront metrology. To address these issues, Berkeley Lab's Center for X-Ray Optics (CXRO) added small-field printing capabilities to the EUV phase-shifting/point diffraction interferometer (PS/PDI) on ALS Beamline 12.0.1.

In the printing configuration, the test station is referred to as the static exposure station (SES). Static means that the scanning and stepping systems required to print complete circuit patterns on all the chips on a silicon wafer are not implemented. Instead, only small ("microfield") test patterns are imaged. A key feature of the SES is the ability to control the coherence of the illuminating EUV light. The combined PS/PDI–SES system remains extremely flexible in that switching between interferometry and printing modes can be accomplished in approximately two weeks.

Two 4× optical systems have been developed as part of the joint industry–DOE national laboratory EUV lithography program (see main story). The second, much higher quality, Set-2 optic is destined for integration into the prototype printing machine (the Engineering Test Stand or ETS) for full-field scanned imaging, but the CXRO team has already obtained valuable information by using the SES to lithographically characterize the static imaging performance of the Set-2 optic. Excellent performance was demonstrated down to 70 nm for elbow test patterns with a 1:1 ratio of line widths and line spacings (Figure 1). The team printed even finer features by adjusting the illumination pattern and/or the exposure dose (Figure 2).

These printing results reveal the extraordinarily high quality of the ETS Set-2 optic and in doing so demonstrate the success of CXRO's EUV metrology beamlines in helping to achieve very tight specifications for figure, finish, and multilayer coatings.

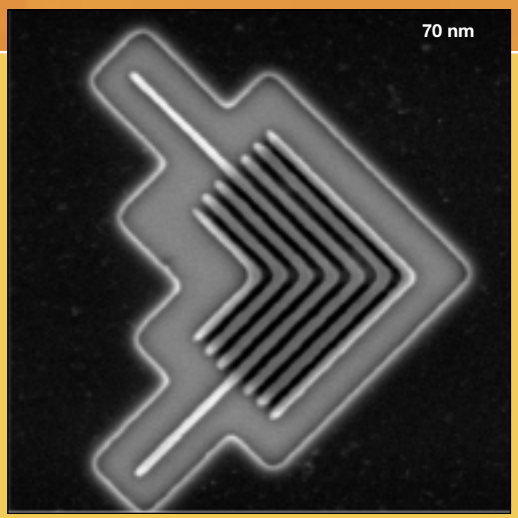

Figure 1 The ETS Set-2 Optic was designed for printing patterns with sub-100-nm features. Exposures by the CXRO team with the SES station on ALS Beamline 12.0.1 have pushed the performance to well below 70 nm with the use of resolution-enhancement techniques. In comparison, the current industry state-of-the-art chips required printing patterns with 130-nm lines and spaces.

Figure 2 Modifying the exposure process can decrease the minimum feature size for some types of patterns. Here, by overexposing an elbow test pattern with the lines somewhat farther apart than in the pattern with equal line widths and spacing imaged in Figure 1, the CXRO team was able to print line widths down to 39 nm with the ETS Set-2 Optic.

Figure 5 Members of the Beamline 12.0.1 EUV interferometry team stand by the newest phase-shifting/point-diffraction interferometer (PS/PDI), which is capable of characterizing four-mirror optics for EUV lithography with sub-angstrom accuracy. *Left to right, front,* Patrick Naulleau, Dave Richardson, Rene Delano, Senajith Rekawa; *second row,* Keith Jackson, Jeffrey Bokor, Ron Tackaberry, Kenneth Goldberg; *third row,* Farhad Salmassi, Paul Denham, Phillip Batson, Brian Hoef, Gideon Jones; *back row,* Drew Kemp.

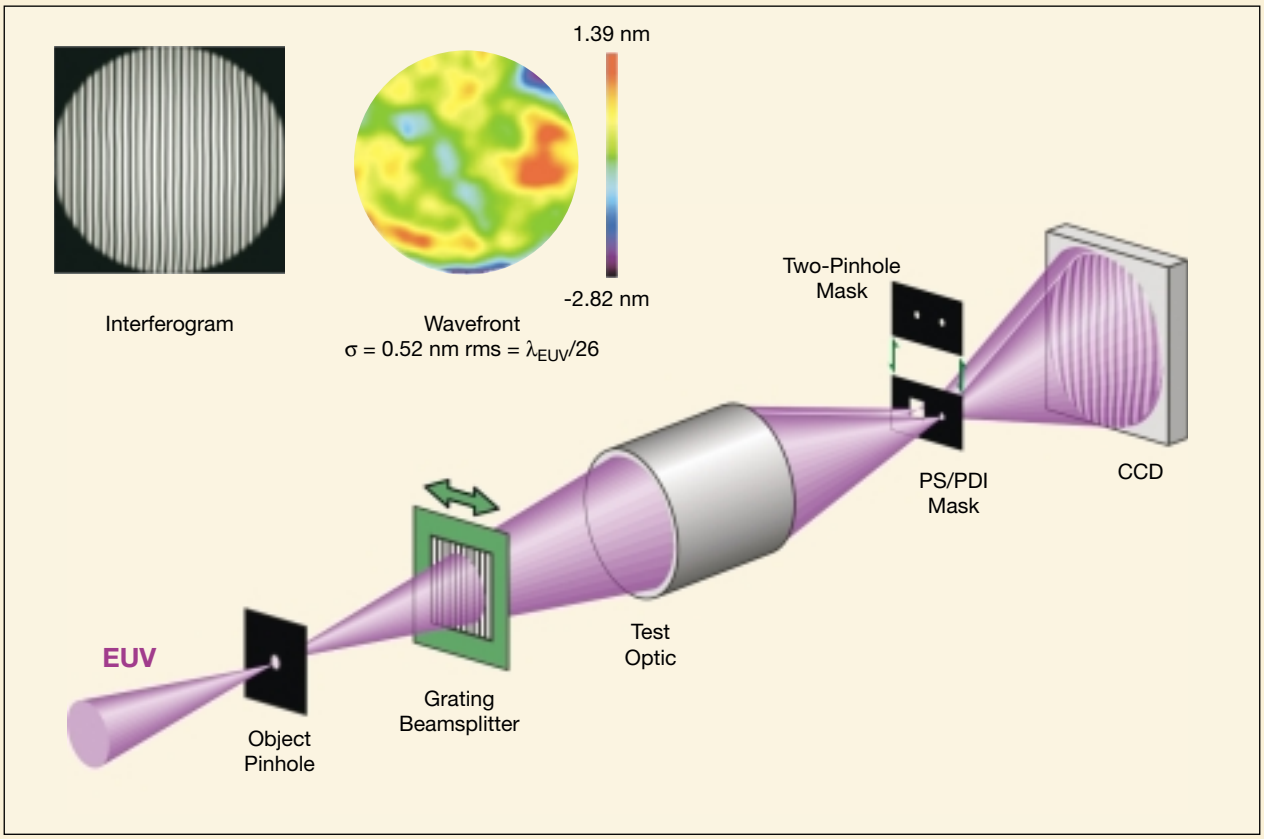

Figure 6 Diagram of the PS/PDI and a typical result. Analysis of the interferogram *(above, left)* resulting from the interference between the aberrated wave from the test optic passing through the large pinhole and a reference wave from the small pinhole yields a wavefront map *(above,center)* showing the deviation from the ideal, unaberrated map. (The two-pinhole mask is used to determine the measurement accuracy of the interferometer.) For this example, the measured wavefront has an rms error of 0.52 nm, or $\lambda_{EUV}/26$. Many such maps are made for light focused on different areas of the optic.

Complex Materials

Fermi Surface Drives Fluctuating Nanoscale Phase Separation in CMR Oxides

Rapid fluctuations are one of the themes of modern physical science, sometimes occurring during a transition from one state of matter to another. Chuang et al. have invoked fluctuations to understand one of the current hot topics in solid-state science, the "colossal" magnetoresistance (CMR) effect in certain compounds containing manganese and oxygen atoms (manganites). Application of a magnetic field decreases the ability of a CMR material to carry electric current by a factor of 1000 or more, a phenomenon both for physicists to explain and for technologists someday to convert into useful devices, such as high-density magnetic data-storage devices. In this work, the researchers made x-ray measurements of the behavior of electrons in a CMR manganite with the added elements lanthanum and strontium. The results provided a chain of evidence for fluctuations that involve minute (nanometer-sized) electrically conducting regions that coexist with nonconducting (insulating) regions in the current-conducting state but cease to exist in the insulating state.

Complex (or correlated-electron) materials are on the frontier of materials physics because conventional solid-state theory is often unable to explain their frequently novel behavior, high-temperature superconductivity being a prime example. Among these materials are the manganese oxide compounds that exhibit the colossal magnetoresistance (CMR) effect. Our collaboration working at the ALS has now shown that the quasiparticle concept, a pillar of current solid-state theory, does retain its validity in CMR oxides, but the peculiarities of the electronic structure result in rapid fluctuations at the nanometer length scale of separate conducting and insulating phases, fluctuations that appear to underlie the CMR effect.

Ordinary solids are complicated enough with every cubic centimeter containing around 10^{23} electrons whose every move not only affects but is influenced by the motion of all their neighbors—an insoluble problem. Remarkably, theorists are now able to transform this confusion of strongly interacting electrons into a mathematically tractable collection of weakly interacting quasiparticles whose properties match the results of experiments. For example, one can visualize a quasielectron as an electron surrounded by a cloud of displaced neighboring electrons. So far, so good, but when the electrons interact too strongly, the quasiparticle model breaks down, and so far no tractable alternative has arisen.

The CMR oxides undergo a transition from a paramagnetic insulator to a ferromagnetic "poor" metal as the temperature is lowered. Poor means the electrical resistivity is relatively high. An externally applied magnetic field can also drive this transition, which results in a "colossal" thousandfold decrease in the resistivity (Figure 1). Our American-Japanese team studied the manganite compound $La_{1.2}Sr_{1.8}Mn_2O_7$, whose crystal structure is built around double planes of manganese and oxygen atoms separated by lanthanum and strontium atoms. The CMR effect is thought to take place in these planes.

At ALS Beamline 10.0.1, we were able to make angle-resolved photoemission spectroscopy (ARPES) measurements with much higher angular and energy resolution than before, which allowed us to conduct a comprehensive examination of the electronic structure of the material at low temperature in the conducting state. For example, we were able to resolve an energy band associated with the manganese–oxygen layers that exhibited the classic steplike drop in photoemission intensity as the band crossed the Fermi energy above which electron quantum states are unoccupied, a telltale signature of quasiparticles with well-defined energies and momenta

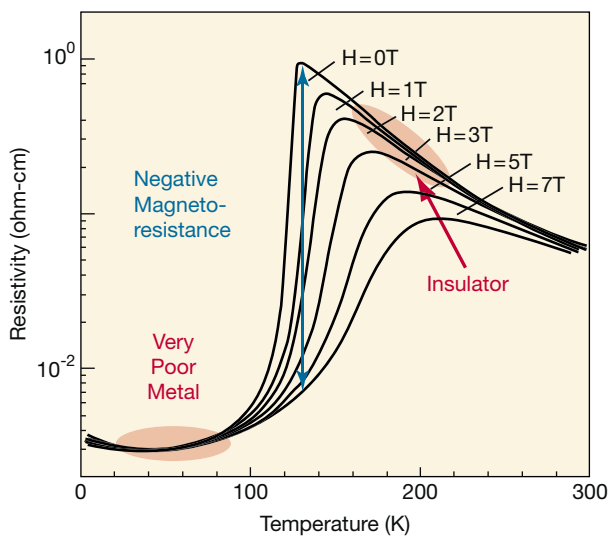

Figure 1 CMR oxides undergo a transition from a paramagnetic insulator to a ferromagnetic "poor" metal as the temperature (T) is lowered. An externally applied magnetic field (H) can also drive this transition, which results in a "colossal" thousandfold decrease in the resistivity.

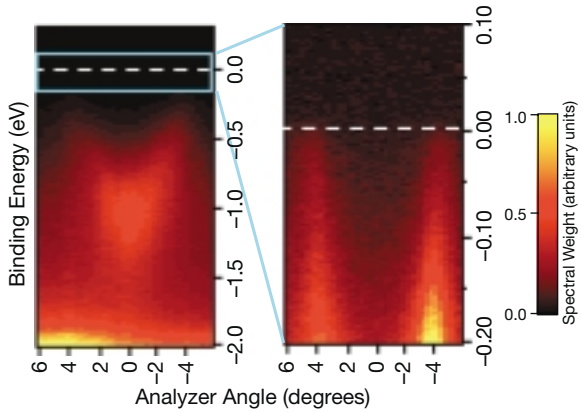

Figure 2 A quasielectron band extends to the Fermi energy *(dashed line)* in the low-temperature metallic state, but the low photoemission intensity (low spectral weight) is indicative of a pseudogap that pushes most of the electrons to lower energies (higher binding energies).

(Figure 2). We were also able to map the Fermi surface (the contour in momentum space of the Fermi energy).

Here, the story becomes too complicated to tell in detail. In brief, calculation of the electrical resistivity from parameters extracted from the Fermi surface, the energy band, and other details of the photoemission spectra resulted in a value ten times lower than measured experimentally. The shape of the Fermi surface, which has parallel straight lines, provided a clue as to why (Figure 3). Such lines are associated with electronic and structural instabilities (charge/orbital density waves cooperating with a Jahn–Teller distortion), for which there is

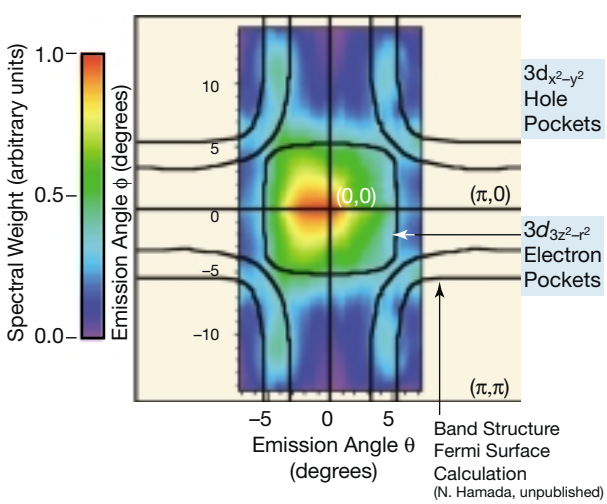

Figure 3 The experimentally measured Fermi surface *(false-color image)* matches well that calculated by theorists *(black lines).* The long parallel sections of the Fermi surface are associated with instabilities that drive nanoscale fluctuating phase separation of conducting and insulating regions and give rise to the pseudogap.

evidence in $La_{1.2}Sr_{1.8}Mn_20_7$ from neutron and x-ray scattering experiments by other groups.

These instabilities give rise to a "pseudogap" (seen in the present, as well as in past, ARPES measurements) in which the electron energy bands are pushed well below the Fermi energy and hence do not contribute to the conductivity. In the low-temperature conducting state, the pseudogap is not total, however, because there are nanometer-sized conducting regions with no pseudogap (where the quasiparticles are seen) as well as insulating regions with charge/orbital ordering. Moreover, competition between these regions causes fluctuations in their size and location with time. The net result is a poor metal at low temperature and an insulator at high temperature when the conducting regions disappear as the pseudogap grows stronger (Figure 4).

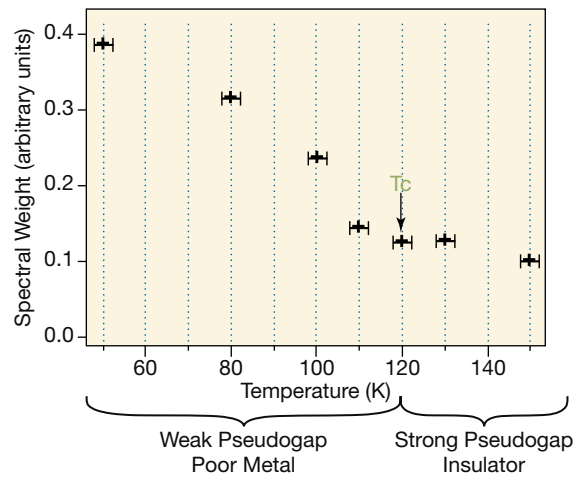

Figure 4 Near the Fermi energy, the change in the spectral weight with temperature shows that the pseudogap grows stronger at higher temperatures, resulting in an insulating state.

INVESTIGATORS

Y.-D. Chuang (University of Colorado and ALS); A.D. Gromko and D.S. Dessau (University of Colorado); T. Kimura (University of Tokyo); and Y. Tokura (University of Tokyo and Joint Research Center for Atom Technology, Tsukuba).

FUNDING

National Science Foundation and U. S. Department of Energy, Office of Basic Energy Sciences.

PUBLICATION

1. Y.-D. Chuang, A.D. Gromko, D.S. Dessau, T. Kimura, and Y. Tokura, "Fermi surface nesting and nanoscale fluctuating charge/orbital ordering in colossal magnetoresistive oxides," *Science* ***292,*** 1509 (2001).

Electron–Phonon Coupling Suggests a Strong Lattice Vibration Role in High-Temperature Superconductivity

Scientists call materials in which electrical current can flow without resistance superconductors. Originally discovered in 1911 in metallic mercury that was cooled to within a few degrees of absolute zero (0 Kelvin), superconductivity entered an intriguing new era 75 years later with the first report of "high-temperature" superconductivity in certain ceramic oxide compounds. Some materials in this broad family remain superconducting at temperatures well above 100 K. So, for the last 15 years, some researchers have worked to turn high-temperature superconductors into practical devices, such as power transmission cables, while others have joined the quest to learn what causes high-temperature superconductivity. In contrast to what many had believed, recent experiments at the ALS by Lanzara et al. suggest that some form of interaction between electrons and lattice vibrations may play an important role in high-temperature superconductors, just as it does in the earlier metallic superconductors. This controversial result has stimulated a flurry of research designed to explore its consequences for one of the important unsolved problems in solid-state physics.

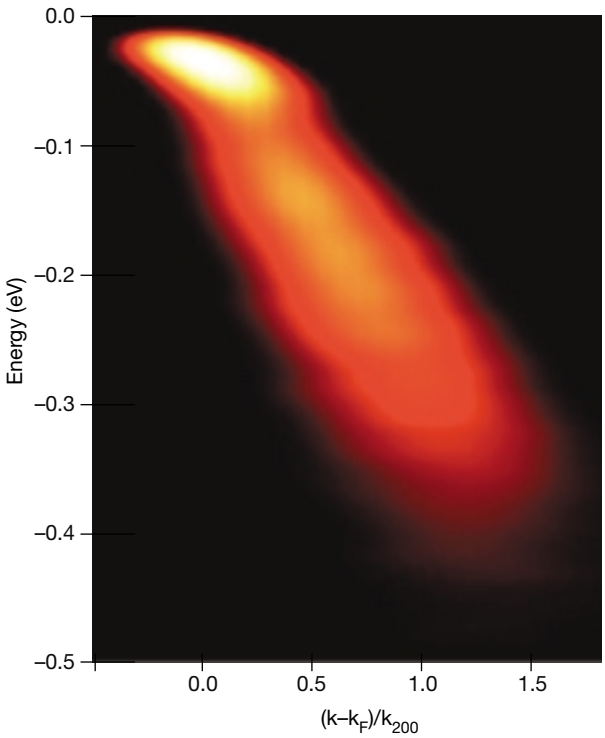

Figure 5 Raw ARPES data set showing photoemission intensity as a function of energy and the normalized reduced crystal momentum $(k - k_F)/k_{200}$, where k_F is the momentum at the Fermi surface, k is the actual momentum, and k_{200} is the momentum at an energy of 200 meV.

The mechanism responsible for high-temperature superconductivity remains elusive. The observation of spectral features occurring at a characteristic energy (an energy scale) often provides significant insight into physical processes in the material. Now, our international collaboration has evidence from high-resolution angle-resolved photoemission spectroscopy (ARPES) at the ALS for a common energy scale in three different families of high-temperature superconductors. Several chains of evidence argue that, in contrast to most recent thinking, lattice vibrations must have a role in the superconductivity in these materials.

ARPES measures the photoemission intensity as a function of two variables, the electron binding energy (obtained from the photoelectron kinetic energy) and electron momentum (obtained from the angle of emission from the sample surface) (Figure 5). With its ability to directly reveal energy–momentum relationships (dispersion curves) and lifetimes, ARPES provides a unique opportunity to look for energy scales that manifest themselves in dynamical parameters, such as the velocity (slope of energy–momentum curve) and scattering rate (Figure 6). The angular resolution of ±0.1 degrees, which is about an order of magnitude better than in many previous ARPES studies of these materials, made the new results possible.

The experimenters recorded their spectra at ALS Beamline 10.0.1 (some data were also taken at Stanford Synchrotron Radiation Laboratory Beamline 5-4) at several temperatures and photon energies on single crystals of $Bi_2Sr_2CaCu_2O_8$ (Bi2212), lead-doped $Bi_2Sr_2CaCu_2O_8$ (Pb-Bi2212), lead-doped $Bi_2Sr_2CuO_6$ (Pb-Bi2201), and $La_{2-x}Sr_xCuO_4$ (LSCO). These representative high-temperature superconductors exhibited a range of transition temperatures and energy-gap values.

A typical momentum distribution curve (MDC), obtained by plotting the photoemission intensity as a function of scanning angle at a constant binding energy, shows a peak on a constant background that can be fitted to obtain one point on an energy–momentum curve. The dispersion curves derived from many MDCs for each material clearly

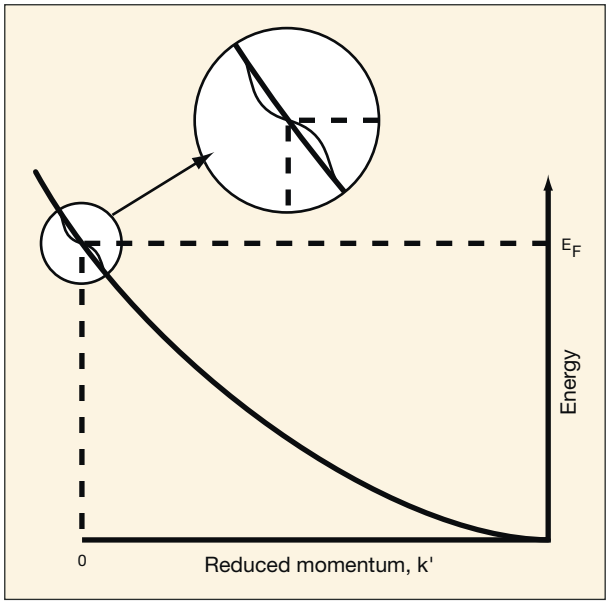

Figure 6 Electron–phonon coupling modifies the electron-momentum dispersion curve near the Fermi energy (E_F). The reduced momentum $k' = k - k_F$.

showed the energy moving linearly towards the Fermi energy (binding energy = 0) as the momentum decreased. Most important, however, the curves exhibited an obvious kink in the slope near a binding energy of 50–80 meV, independent of the material's superconducting transition temperature and energy gap (Figure 7).

The change in slope to a lower value close to the Fermi energy suggests the onset of a many-body effect involving electrons and some other entity to form a heavier, slower quasiparticle. Universality of the kink in the various materials and its uniformity for different directions of momentum in the Brillouin zone lead naturally to the conclusion that a very strong electron–phonon coupling is responsible. Persistence of the kink above the transition temperature further supports this conclusion, because phonons would be active over a wide temperature range. Neutron-scattering experiments by another group on $La_{2-x}Sr_xCuO_4$ show that the energy of an oxygen stretching vibration (longitudinal optical phonon) matches that of the kink, suggesting that this phonon mode is involved.

Additional evidence comes from energy distribution curves (EDCs), obtained from the photoemission intensity variation with binding energy at a fixed angle for several $Bi_2Sr_2CaCu_2O_8$ samples with different transition temperatures (Figure 8). The set of EDCs for each material exhibited a common structure showing a quasiparticle peak at energies close to the Fermi energy, a dip occurring approximately at the phonon energy, and a broad feature at higher energy. Similar EDCs are observed for the beryllium surface, whose

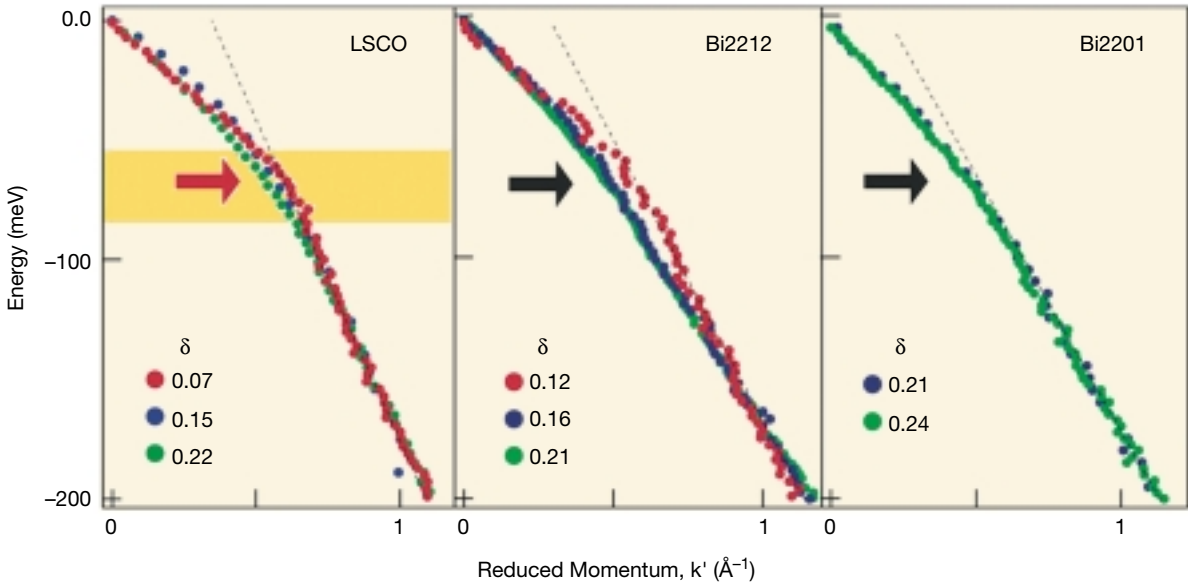

Figure 7 Dispersion curves for three families of high-temperature superconductors show a common kink at an energy *(arrow)* that matches an oxygen lattice vibration. The parameter δ is the doping concentration that determines the transition temperatures in the materials.

electrons are known to have a strong coupling to a single phonon mode, and to simulated EDC spectra for the simple case of isotropic coupling to a single phonon mode.

These findings, and others obtained from additional detailed analysis of the ARPES data, bring the electron–phonon interaction back as an important player in the high-temperature superconductivity puzzle.

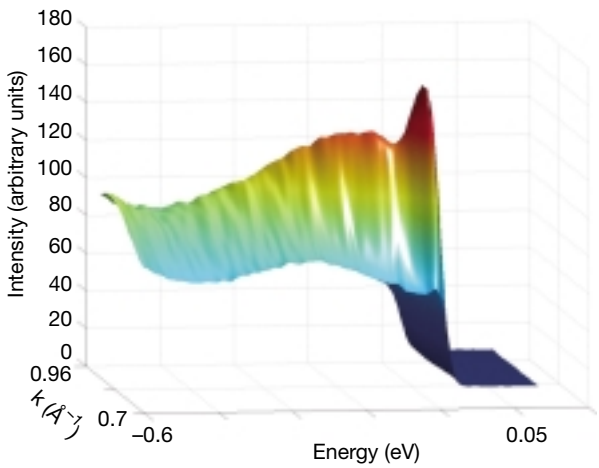

Figure 8 Set of photoemission energy distribution curves (EDCs) at different angles (colors) for a high-temperature superconductor (HTSC). Similar sets measured for three families of HTSCs and the nonsuperconducting beryllium surface and simulated for the simple case of isotropic coupling to a single phonon mode share common features, suggesting electron–phonon coupling is operative in HTSCs.

INVESTIGATORS

A. Lanzara (Stanford University, Stanford Synchrotron Radiation Laboratory, and ALS); P.V. Bogdanov, X.J. Zhou, S.A. Kellar, D.L. Feng, H. Eisaki, and Z.-X. Shen (Stanford University and Stanford Synchrotron Radiation Laboratory); E.D. Lu and Z. Hussain (ALS); and T. Yoshida, A. Fujimori, K. Kishio, J.I. Shimoyama, T. Noda, and S. Uchida (University of Tokyo).

FUNDING

U.S. Department of Energy, Office of Basic Energy Sciences; National Science Foundation; Istituto Nazionale Fisica della Materia (INFM); and University of Rome "La Sapienza."

PUBLICATION

1. A. Lanzara et al., "Evidence for ubiquitous strong electron–phonon coupling in high-temperature superconductors," *Nature* **412,** 510 (2001).

High-Temperature Superconductors: *c*-Axis Interlayer Coupling and the Possibility of a Magnetically Mediated Pairing Mechanism

The discovery of superconductivity in certain ceramic compounds beginning in late 1986 opened a new chapter in solid-state physics. How they remain superconducting at such relatively high temperatures as compared to other types of superconductors—up to 150 Kelvin or halfway between absolute zero and the thermometer reading on a balmy day—is just one of the riddles these compounds pose, but the answer may have important technological ramifications, especially if scientists could use information to design a superconductor that does not need to be cooled to a cryogenic temperature. One clue may lie in the structure of these compounds, which features layers one atom thick (i.e., atomic planes) comprising copper and oxygen atoms interspersed with planes containing other atoms. Chuang et al. now report the first direct experimental evidence identifying an electronic connection between nearby copper–oxygen planes that may help explain a long-observed correlation between the transition temperature below which superconductivity occurs and the number of nearby copper–oxygen planes.

One of the hallmarks of copper oxide (cuprate) high-temperature superconductors is that the transition temperature, T_c, is strongly dependent upon the number of CuO_2 planes per unit cell, as shown in Figure 9 for the Bi-Sr-Ca-Cu-O family of compounds, where T_c jumps from 35 K to 105 K as the number of planes rises from one to three. This trend seems to indicate that electronic coupling between the planes within a unit cell is very important, although to date there has been no direct experimental evidence identifying this coupling, and scientists usually neglect it in their models. Our recent high-resolution angle-resolved photoemission spectroscopy (ARPES) experiments at the High Energy Resolution Spectrometer (HERS) endstation at ALS Beamline 10.0.1 and at Stanford Synchrotron Radiation Laboratory (SSRL) Beamline 5-4 has dramatically changed this situation.

We studied the double-plane material Bi2212 and the single-plane material Bi2201. In Bi2212, we have directly observed the coupling between the CuO_2 planes, which splits the CuO_2 bands into a bonding and an antibonding set, just as the energy levels of atomic hydrogen are split in molecular

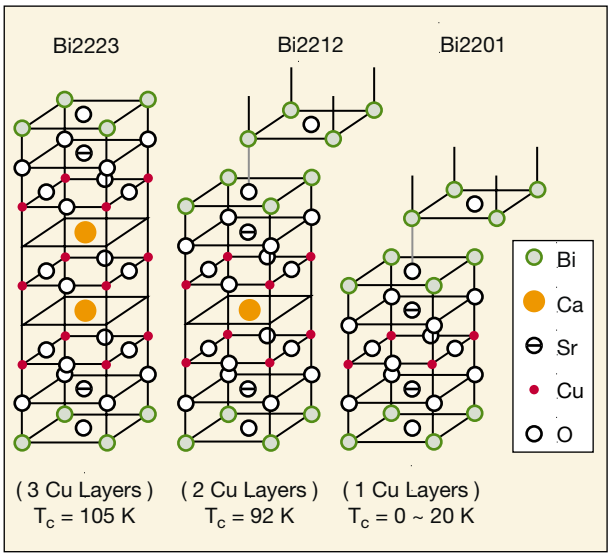

Figure 9 Correlation between the superconducting transition temperature and the number of CuO_2 planes per unit cell in the Bi-Sr-Ca-Cu-O compounds: the single-plane family $Bi_2Sr_2CuO_6$ (Bi2201) has a maximum T_c of 35 K, the double-plane family $Bi_2Sr_2CaCu_2O_8$ (Bi2212) has a maximum T_c near 90 K, and the triple-plane family $Bi_2Sr_2Ca_2Cu_3O_{10}$ (Bi2223) has a maximum T_c near 105 K.

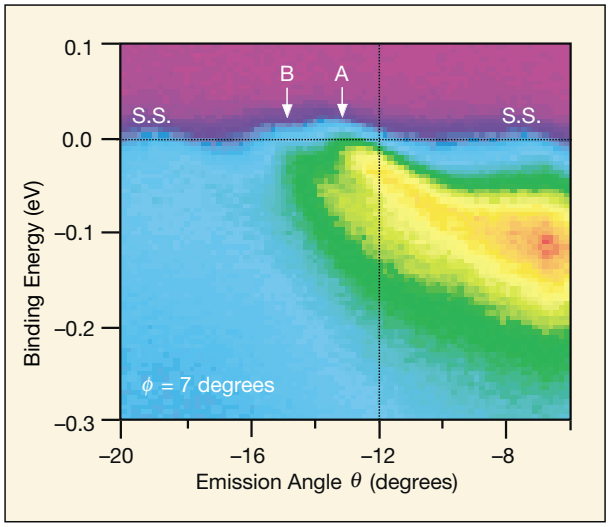

Figure 10 Typical computer-reconstructed false-color rendition of ARPES data for the double-plane material $Bi_2Sr_2CaCu_2O_8$ (Bi2212) showing the photoemission intensity as a function of binding energy (energy relative to the Fermi level) and scanning angle (θ) at a fixed perpendicular angle (ϕ).

hydrogen. In Bi2201, there is only one CuO_2 plane per unit cell, so there should be no splitting of the energy levels, as confirmed in our experiments. As compared to previous experiments, we studied single-crystal samples of especially high quality. The ARPES spectra of these samples had much sharper features than spectra of lower-quality samples, and we were able to investigate these with the very high resolution Scienta energy analyzers and undulator beamlines at both the ALS and SSRL.

Raw ARPES spectra plot photoemission intensity as a function of electron energy and angle (Figure 10). Figure 11 shows for a heavily overdoped Bi2212 sample some of our energy (E) vs. momentum (k) data taken along the blue cut in the two-dimensional Brillouin zone. Two features labeled A (antibonding) and B (bonding) are clearly seen, each of these giving rise to its own piece of the Fermi surface. It is seen that the separation between the pieces of the Fermi surface due to features A and B approaches zero along the zone diagonal and is maximal at the center of the zone edge [(π, 0) point], in agreement with theoretical predictions.

We measured the energy splitting between the A and B bands at (π, 0) to be about 100 meV, which is big enough to indicate sizeable coupling between the planes. Because the splitting is large compared to other relevant energy scales, such as the superconducting gap and the pseudogap, it cannot be ignored when discussing these parameters. Since band structure calculations have predicted a splitting of about 300 meV, we believe that electron correlation effects not included in the calculations are responsible for a factor of three decrease in the splitting. This reduction would normally be considered to be a huge reduction, except in the context of this example, where the splitting had previously been assumed to be essentially zero.

The (π, 0) point is probably the most important location in the Brillouin zone for the physics of the cuprates, because it is where the d-wave superconducting gap and normal-state pseudogap are the largest. Measurements of these key properties had previously been hindered by the inability to deconvolve the bilayer splitting. With this new ability, we have already observed "dispersion kinks" for the first time in this data. The details of this new kink data point to strong coupling between the (π, 0) electrons and the magnetic resonance mode observed by others in neutron scattering. This coupling greatly increases the possibility that this magnetic mode mediates the pairing of the electrons in the high-T_c superconductors.

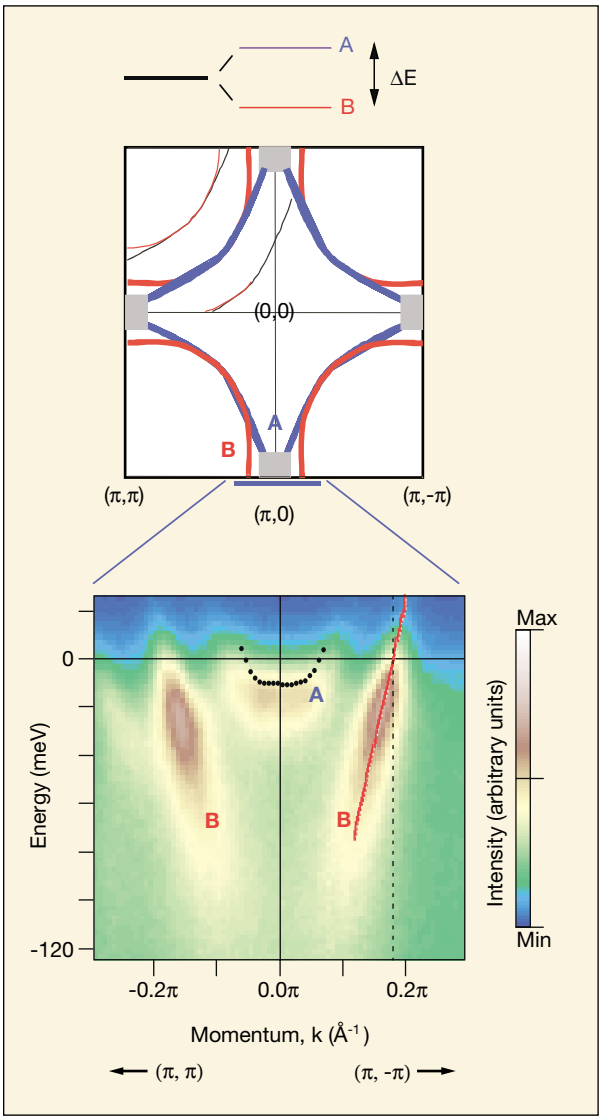

Figure 11 *Top,* two-dimensional Fermi surface for the double-plane material $Bi_2Sr_2CaCu_2O_8$ (Bi2212) reveals a momentum-dependent splitting between two bands (A and B) that is largest near the (π, 0) point of the Brillouin zone. *Bottom,* Photoemission intensity as a function of energy and momentum for this material along the blue line through the (π, 0) point in the Brillouin zone *(top)* shows the two bands (A and B) that are attributable to a coupling between the two copper–oxygen planes per unit cell.

INVESTIGATORS

Y.-D. Chuang, A.V. Fedorov (University of Colorado, Boulder, and ALS); A.D. Gromko, J.D. Koralek, and D.S. Dessau (University of Colorado, Boulder); Y. Aiura, Y. Yamaguchi, and K. Oka (National Institute of Advanced Industrial Science and Technology, Tsukuba); Y. Ando (Central Research Institute of Electric Power Industry, Tokyo), and H. Eisaki and S.I. Uchida (University of Tokyo).

FUNDING

National Science Foundation and U.S. Department of Energy, Office of Basic Energy Sciences.

PUBLICATIONS

1. Y.-D. Chuang et al., "Doubling of the bands in overdoped $Bi_2Sr_2CaCu_2O_{8+\delta}$: Evidence for *c*-axis bilayer coupling," *Phys. Rev. Lett.* **87,** 117002 (2001).

2. Y.-D. Chuang et al., "Constancy of the bilayer splitting as a function of doping in $Bi_2Sr_2CaCu_2O_{8+\delta}$," preprint available at http://xxx.lanl.gov/abs/cond-mat/0107002.

3. A.D. Gromko et al., "Mass-renormalized electronic excitations at (π, 0) in the superconducting state of $Bi_2Sr_2CaCu_2O_{8+\delta}$," preprint available at http://xxx.lanl.gov/abs/cond-mat/0202329.

Magnetism and Magnetic Materials

Antiferromagnetic Spin Reorientation at the NiO Interface in Response to an Adjacent Co Layer

In magnets, electrons act like tiny spinning tops all spinning in the same direction, but in materials called antiferromagnets, the magnetically important electrons on neighboring atoms spin in opposite directions. Manufacturers of computer hard disks and other advanced magnetic devices are keenly interested in what happens—and why—when one places a thin layer of magnetic material on top of an antiferromagnet. It turns out that the antiferromagnet pins the magnet's spins so they cannot respond to an external applied field, a still poorly understood effect known as exchange bias. This refusal to budge provides a reference direction that is essential to the function of modern magnetic devices. Ohldag et al. have used x-ray microscopy techniques to graphically show how the electron spins in an antiferromagnet twist after a magnetic layer is deposited. Their finding will force those trying to explain exchange bias to consider the actual arrangement of electron spins at the boundary between antiferromagnetic and magnetic layers rather than assuming the spin orientation is the same as in the interior.

One of the vexing mysteries facing researchers in magnetic materials is the origin of the exchange-bias effect, in which an antiferromagnetic layer pins the magnetization of an adjacent ferromagnetic layer so that it doesn't reverse in an external magnetic field. Building on earlier work with the photoemission electron microscope (PEEM) on Beamline 7.3.1.1 at the Advanced Light Source, our collaboration has taken an important step toward unveiling the secret of exchange bias by observing that spins near a nickel oxide antiferromagnet's surface reorient after deposition of a cobalt ferromagnetic layer. This discovery rules out models of exchange bias based on the common assumption that the spin configuration at the surface of the antiferromagnet is the same as that in its interior (bulk).

Exchange bias is more than a curious phenomenon. It plays a key role in magnetic-device technology, such as the giant-magnetoresistance-effect (GMR) read heads in high-density magnetic data-storage systems (hard disks) already on the market and magnetic random access memory chips under development for low-power, nonvolatile computer memory. But exactly how exchange bias works is not understood. The spin orientation on each side of the antiferromagnet/ferromagnet interface is one of the missing pieces of information. In the previous experiments, our group achieved a major advance by demonstrating that the alignment of the ferromagnetic spins in a cobalt overlayer is in fact correlated with the spin orientation in a $LaFeO_3$ antiferromagnetic layer. However, owing to the complex crystallography of the $LaFeO_3$, we could not verify a full three-dimensional correlation between ferromagnetic and antiferromagnetic spins.

In the new work, we used nickel oxide single crystals oriented to expose a (100) surface. Nickel oxide single crystals have been well characterized in the literature and exhibit large

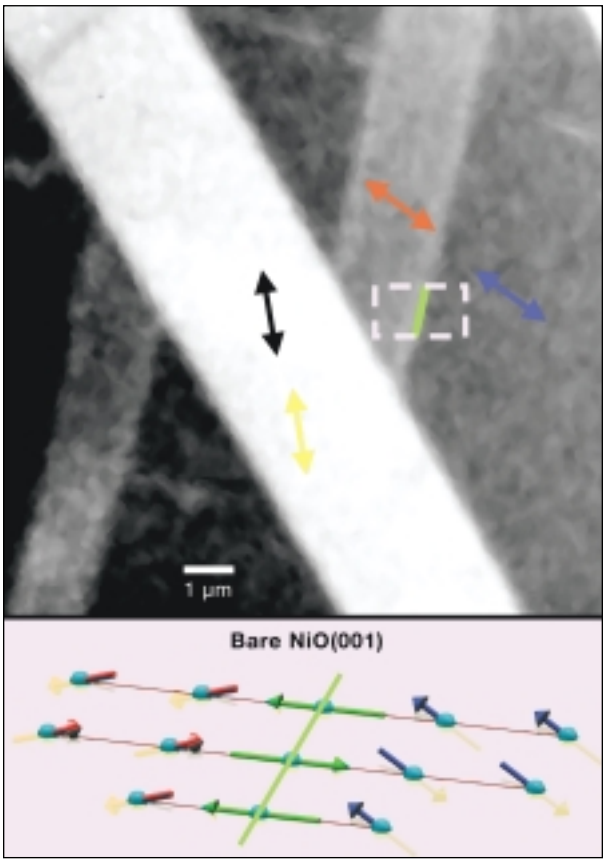

Figure 1 Antiferromagnetic domains on NiO(001) in an area 12 μm across. The colored arrows indicate the projections of the antiferromagnetic axes in the surface plane for four types of domains. Domains with identical in-plane projections (e.g., those marked with red and blue arrows) can be distinguished by examining their orientation out of the surface plane, as illustrated in the sketch at the bottom for the area in the dashed box. The green line represents a domain wall where the spins are in-plane.

antiferromagnetic domains that the PEEM, with a spatial resolution of 50 nm for magnetic structures, can easily image using the technique of x-ray magnetic linear dichroism (XMLD). Image contrast arises because the relative orientation of the polarization of the x-ray beam and the magnetic axis in the antiferromagnetic domains (changeable by rotating the crystal) determines the absorption. To image the cobalt ferromagnetic layer, our group used the now traditional x-ray magnetic circular dichroism (XMCD) with circularly polarized light.

The first set of XMLD measurements, made on bare nickel oxide, revealed a complex domain pattern related to that previously known for bulk single crystals, but with some differences (Figure 1). In the bulk, the domains are defined by the (111) crystallographic planes in which the spins lie and the [211] directions in which they are aligned. Analysis of the PEEM images yielded the same [211] magnetic axes but in a different arrangement. In addition, the PEEM data showed that some of the boundaries between the domains (domain walls) had decreased magnetic symmetry. Noting that the PEEM is sensitive to material only a few nanometers below the surface, we concluded that the surface domain structure deviated from that of the bulk.

When a ferromagnetic cobalt layer 12 monolayers thick was deposited on the nickel oxide, the story changed dramatically. The spins in the nickel oxide reoriented themselves in such a way that only domains with walls in (100) crystallographic planes remained (Figure 2). Moreover, the spins in the domains assumed [110] directions parallel to the interface. The XMCD measurements showed that the magnetization in the cobalt domains was aligned, domain by domain, parallel to the magnetic axes of the nickel oxide domains. Heating the sample to above the antiferromagnetic transition (Néel) temperature destroyed this correlation. This graphic demonstration of spin reorientation near the nickel oxide surface means that the exchange bias mechanism is not based on the bulk spin structure of the antiferromagnet.

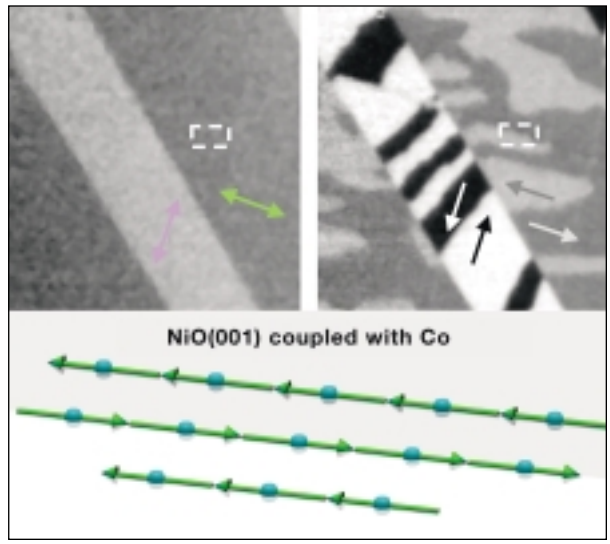

Figure 2 Antiferromagnetic (*left*) and ferromagnetic (*right*) domains after deposition of 12 monolayers of cobalt. The antiferromagnetic axes have rotated into the surface plane so that only two types of domains can now be distinguished. On top of each antiferromagnetic domain, two ferromagnetic domains can be formed with their magnetization in either of two directions parallel to the antiferromagnetic axis underneath. The sketch shows the nickel oxide spins for the area in the dashed box, which is overlaid by two cobalt domains *(light and dark areas).*

INVESTIGATORS

H. Ohldag (ALS, Stanford Synchrotron Radiation Laboratory, and Universität Düsseldorf); A. Scholl and S. Anders (ALS); F. Nolting (Stanford Synchrotron Radiation Laboratory and ALS); F.U. Hillebrecht (Max Planck Institute for Microstructure Physics, Halle); and J. Stöhr (Stanford Synchrotron Radiation Laboratory).

FUNDING

U. S. Department of Energy, Office of Basic Energy Sciences.

PUBLICATION

1. H. Ohldag et al., "Spin reorientation at the antiferromagnetic NiO(001) surface in response to an adjacent ferromagnet," *Phys. Rev. Lett.* **86,** 2878 (2001).

Shining Light on Interfaces—How X Rays Helped Solve a Long-standing Challenge in Materials Sciences

Unraveling the details of geometric structure (where the atoms are) and the electronic or magnetic behavior specific to the boundaries (interfaces) between materials remains one of the great challenges in materials science. A case in point is finding the cause of exchange bias, an effect discovered more than 40 years ago that is a key ingredient of advanced magnetic sensors and memory cells based on multiple layers of thin films. The difficulty is that the number of atoms in the thin interface region is much smaller than in the thicker surrounding material, so it is hard to separate out the signal from the interface against a much larger background. Ohldag et al. have found one way to accomplish

this feat by combining the results of two types of experiments that together isolated the chemical and magnetic behavior at the interface to show that a new compound is formed in this region, a compound that may lie at the heart of exchange bias.

When a ferromagnet (FM) is grown on an antiferromagnet (AFM), the exchange coupling between the two systems leads to an increased coercivity of the ferromagnet (Figure 3), but the ferromagnetic hysteresis loop remains symmetric, indicating two equivalent easy directions. If the AFM–FM system is grown in a magnetic field or, after growth, is annealed in a magnetic field to temperatures above the AFM Néel temperature, the hysteresis loop shifts in one direction, a unidirectional shift called exchange bias. It is clear that exchange bias has to originate from the coupling of the spins in the AFM to those in the FM, but because of the magnetic neutrality of the AFM, the coupling must involve uncompensated spins at the AFM–FM interface. The key to the exchange-bias puzzle is identifying the origin of these interfacial spins.

X-ray magnetic circular (XMCD) and linear (XMLD) dichroism are providing a fresh look at the decades-old exchange-bias problem and hold the promise of finally solving it. Previous experiments using the photoemission electron microscope (PEEM) on Beamline 7.3.1.1 at the ALS established the link between AFM and FM domain structure (see previous highlight). Our latest results with complementary spectroscopy and magnetic imaging experiments home in on the all-important interface.

Spectroscopy experiments with high energy resolution (150 meV) were performed at Beamline 10-1 at the Stanford Synchrotron Radiation Laboratory (SSRL). From the spectra in Figure 4, we deduced that a thin cobalt layer deposited on top of bulk nickel oxide (Co/NiO) contains nickel atoms that are in an environment somewhere between nickel oxide and nickel metal and cobalt atoms in an environment somewhere between cobalt metal and cobalt oxide. This is explained by an interfacial reaction in which the original nickel is reduced and the original cobalt is oxidized. A new interfacial layer is formed that we called NiCoOx.

We obtained magnetic images of the Co/NiO sandwich with the PEEM microscope at the ALS. The images were interpreted in the light of the spectroscopic information from Figure 4. In Figure 5, the original images are put together layer by layer to illustrate the magnetic structures. We imaged the

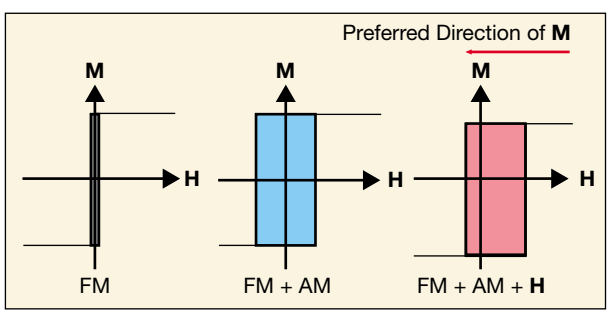

Figure 3 *Left,* hysteresis loops (magnetization, *M,* vs. applied magnetic field, *H*) of a pure ferromagnet are symmetric. *Center,* once the ferromagnet is in contact with an antiferromagnet, the loop widens (coercivity increases). *Right,* when the two materials are heated above the Néel temperature in a magnetic field, the loop shifts in one direction (exchange bias).

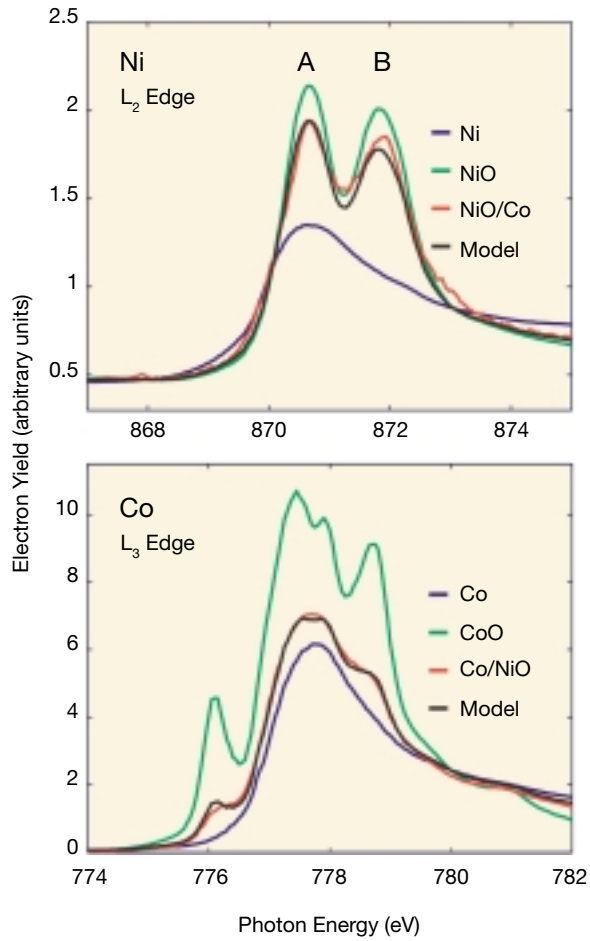

Figure 4 High-resolution x-ray absorption spectra *(red)* for a MgO(100)/NiO (1 nm)/Co(1 nm)/Ru(2 nm) sample recorded at the nickel L_2 and cobalt L_3 edges in comparison to reference spectra for pure metals *(blue)* and monoxides *(green).* The black curve is a weighted superposition of the blue and green spectra.

Figure 5 Magnetic structure, assembled layer by layer from original PEEM images, of a magnetic sandwich comprising ferromagnetic cobalt *(blue)* deposited on top of antiferromagnetic nickel oxide *(green).* By combining chemical specificity (x-ray energy), magnetic specificity (x-ray polarization), and limited depth sensitivity (electron yield detection), it was possible to image, for the first time, the magnetic structure of the interfacial NiCoOx-like layer *(golden)* formed by a chemical reaction.

antiferromagnetic nickel oxide domain with XMLD at the nickel L_2 peaks (A and B in Figure 4) in nickel oxide, the ferromagnetic cobalt domain with XMCD at the Co metal L_3 peak, and the domain structure of the NiCoOx interface layer with XMCD at the nickel L_2 peak energy of 870.5 eV. Since XMCD yields only ferromagnetic contrast, the observed domain structure of the interface has to arise from uncompensated nickel spins formed by reduction of nickel oxide. Close inspection reveals that the domains mimic the antiferromagnetic nickel oxide domains below and the ferromagnetic cobalt domains above and therefore form the bridge between the two.

Additional experiments show that, in an external magnetic field, most of the interfacial spins rotate with those of the ferromagnet, but they increase the rotational drag that leads to the widened magnetization loop. These results indicate that the increase in coercivity in AFM–FM sandwiches originates from the interfacial spins created by a chemical reaction. We believe that only a small, yet to be isolated fraction of the interfacial spins remains fixed in an external field, because the spins are tightly coupled to the antiferromagnetic NiO lattice underneath. We believe these fixed spins give rise to the exchange-bias phenomenon. Because their low abundance corresponds to a fraction of a monolayer, the isolation of their magnetic signal and the determination of their spatial location remain great challenges for future experiments.

INVESTIGATORS

H. Ohldag (Stanford Synchrotron Radiation Laboratory, ALS, and Universität Düsseldorf); A. Scholl (ALS); T.J. Regan and R.L. White (Stanford University); F. Nolting (Stanford Synchrotron Radiation Laboratory and ALS); and J. Lüning and J. Stöhr (Stanford Synchrotron Radiation Laboratory).

FUNDING

U.S. Department of Energy, Office of Basic Energy Sciences.

PUBLICATIONS

1. T. J. Regan et al., "Chemical effects at metal/oxide interfaces studied by x-ray-absorption spectroscopy," *Phys. Rev. B* **64,** 214422 (2001).

2. H. Ohldag et al., "Spectroscopic identification and direct imaging of interfacial magnetic spins," *Phys. Rev. Lett.* **87,** 247201 (2001).

Modified Magnetism at a Buried Co/Pd Interface Resolved with X-Ray Standing Waves

The novel behavior of very thin magnetic layers only a few atoms thick forms the basis for advanced magnetic data storage and other devices. Some years ago, researchers discovered the curious phenomenon of perpendicular magnetic anisotropy (PMA) in such layers that are sandwiched between nonmagnetic metals. Usually, the magnetic field direction lies in the layer, but PMA causes it to sometimes point up or down out of the layer. Understanding just why thinness causes these effects requires the ability to peer into each layer and especially at the boundaries (interfaces) between the magnetic layer and its neighbors, which scientists suspect may hold the keys to what is going on. Kim and Kortright have combined two established x-ray techniques that together allow them to probe magnetism at any selected depth below the surface. In this way, they demonstrated that magnetic behavior at the interface between a layer only two nanometers thick of the PMA material cobalt and a bounding palladium metal layer is indeed different from that in the center of the cobalt.

As we enter into the era of nanoscience, where effects due to surfaces and interfaces often dominate, researchers more than ever need experimental techniques that allow them to discriminate between what goes on at the boundaries and in the interior of nanostructures. Our team has used x-ray standing waves generated with circularly polarized soft x rays at the ALS to do just that for palladium/cobalt/palladium trilayers similar to those that exhibit perpendicular magnetic anisotropy (PMA). With this technique, we demonstrated quantitatively that the magnetic properties at a palladium/cobalt interface differed from those in the center of the cobalt layer. Other groups are already adopting this approach in their own studies of buried interfaces in nanolayer structures.

In a magnetic material, the magnetization usually prefers to point in certain "easy" crystallographic directions because the energy is lower. In a thin film, the easy directions typically lie in the plane of the film. The PMA effect refers to the tendency in some ultrathin magnetic layers for the magnetization to point out of the plane, especially if the magnetic layer is also bounded by top and bottom metallic layers. It is one of several phenomena, such as giant magnetoresistance, exchange bias, and spin tunneling, that make devices based on nanolayer structures attractive for magnetic data storage, memory, and related applications.

To explain the basics of PMA, researchers often use a phenomenological model originated by Néel in which a surface term inversely proportional to the layer thickness lowers the energy of the perpendicular relative to the in-plane orientation as the thickness decreases. However, researchers are not able to rule out other microstructural effects, such as anisotropic strain or chemical intermixing at the interface between the magnetic and metal layers, in part because experimental techniques generally average over depths of two to three nanometers and thus cannot resolve physical effects localized at an interface.

To address this issue, we adapted the established technique of x-ray standing wave spectroscopy by combining it with circularly polarized synchrotron radiation. Standing waves build up within multilayer mirrors because of the constructive and destructive interference of the waves reflected from each interface in the multilayer. Such a standing wave extends through a magnetic trilayer grown on top of the standing-wave generator (Figure 6). The difference in the absorption of left and right circularly polarized x rays (magnetic circular dichroism, or MCD) at the cobalt L edges probes the cobalt magnetic properties (both spin and orbital moments). Since the depths of the periodic intensity maxima depend on the reflection (incidence) angle, it is possible by varying the angle to scan the standing wave vertically through portions of the trilayer and thereby study the depth dependence of the dichroism (Figure 7).

We investigated a palladium/cobalt/palladium trilayer on a W/B_4C multilayer standing-wave generator. At the 2-nm thickness we chose, the cobalt layer does not exhibit PMA, and our goal was to look for precursor interfacial effects. Our cobalt MCD spectra obtained over a range of angles show

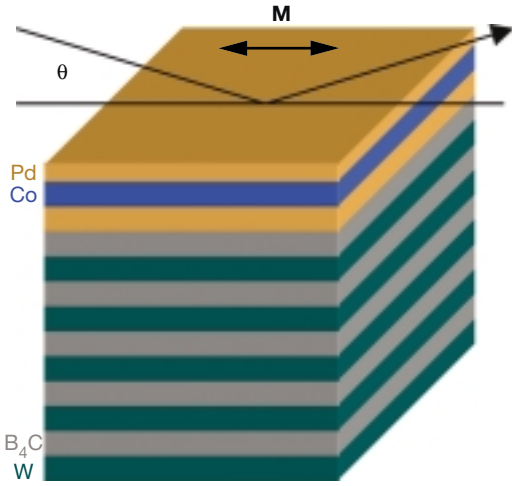

Figure 6 X rays reflecting from the W/B_4C multilayer generate a standing wave pattern that extends into the overlying Pd/Co/Pd trilayer. M is the in-plane easy axis of magnetization in the cobalt.

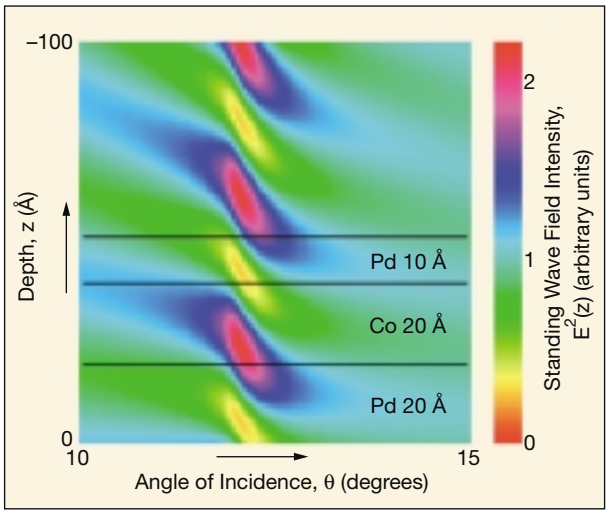

Figure 7 The intensity distribution of the standing wave varies with angle of incidence, θ, thereby providing a way to examine how magnetic behavior varies with depth, *z,* in the cobalt.

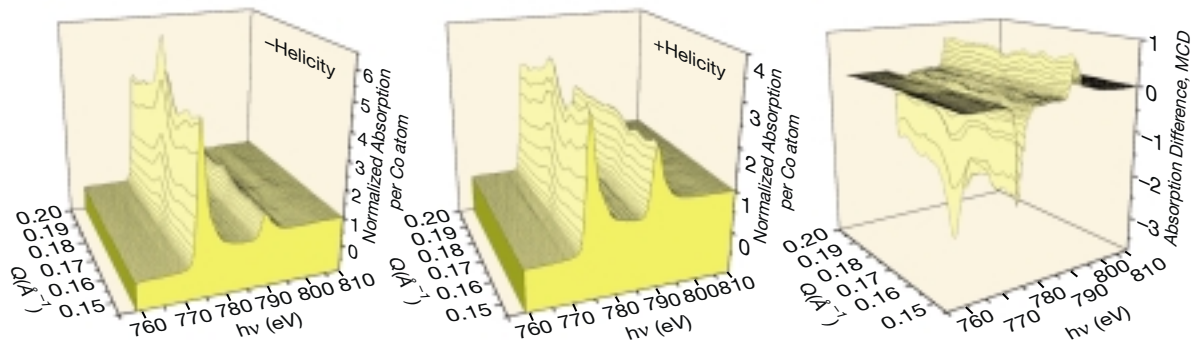

Figure 8 Absorption by cobalt of a standing wave consisting of circularly polarized x rays varies not only with photon energy and the helicity of the polarization but also with the scattering vector, *Q* (related to the reflection angle, θ). *Q* scans show that the absorption and, hence, the magnetic properties are different in the middle of the cobalt layer (*Q* = 0.16) and at the interface with Pd (*Q* = 0.17).

strong differences do exist between interfacial cobalt atoms and those at the center of the cobalt layer (Figure 8). From the MCD data, we extracted values of the number of missing electrons (holes) in the magnetically active cobalt d states and of the associated spin and orbital magnetic moments (Figure 9). We interpreted increases in the number of d holes and the orbital moment near the interface in terms of hybridization of cobalt with palladium states at the interface. The strong enhancement in orbital moment we observed was oriented in-plane (not perpendicular), leading us to conclude that the two-term surface magnetocrystalline anisotropy model of Néel is oversimplified (Figure 10).

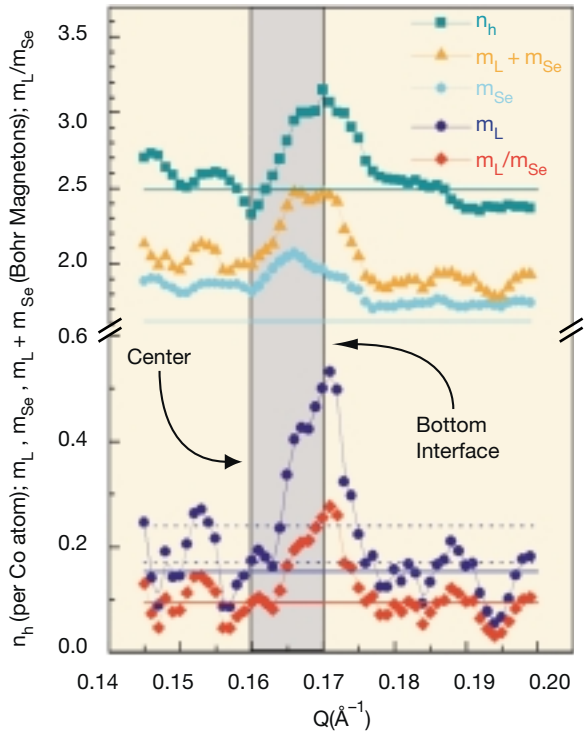

Figure 9 Analysis of the depth-dependent magnetic circular dichroism spectra yields the number of holes, n_h, in d states and their orbital and spin magnetic moments in the cobalt layer near and far from cobalt/palladium.

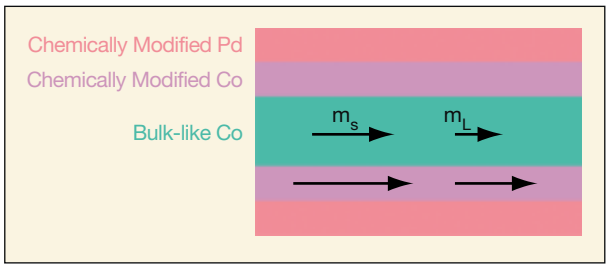

Figure 10 The changing values of the number of holes and the magnetic moments with depth suggest a model attributing the behavior to chemical modifications near the cobalt/palladium interface.

INVESTIGATORS

S.-K. Kim (Berkeley Lab and Korea Advanced Institute of Science and Technology) and J.B. Kortright (Berkeley Lab).

FUNDING

U. S. Department of Energy, Office of Basic Energy Sciences.

PUBLICATION

1. S.-K. Kim and J. B. Kortright, "Modified magnetism at a buried Co/Pd interface resolved with x-ray standing waves," *Phys. Rev. Lett.* **86,** 1347 (2001).

Polymers, Biomaterials, and Soft Matter

X-Ray Spectromicroscopy of Crosslink Density in Superabsorbent Polymers

The global market for disposable diapers is $20 billion annually, but manufacturers face a twofold challenge. To keep the baby dry, the diaper must be able to take up a large quantity of liquid and then hold it "under load" (i.e., as the baby moves around). Superabsorbent polymers (SAPs), materials comprising long chains of intertwining molecules with the happy ability to soak up lots of liquid, now dominate the disposable diaper market. By means of chemical reactions on the surfaces of submillimeter-sized SAP beads, polymer makers form thin shells of "tightly crosslinked polymer" that make it more difficult for liquid to leak out. The actual performance depends on microscopic details of the shell structure, but this kind of detail has been hard to come by. Mitchell et al. have now successfully applied x-ray microscopy to map the variation in crosslink density through shells formed in different ways, thereby providing a way to gauge the effect of shell-formation processes at the microscopic level and to improve the production process.

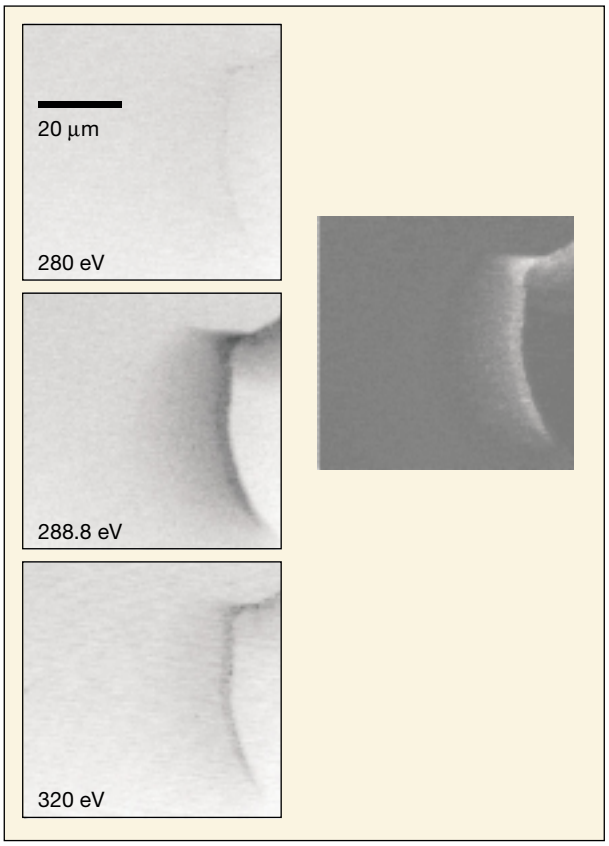

Figure 1 *Left,* NEXAFS spectromicroscopy images at three photon energies of the shell formed around an SAP bead crosslinked with ethylene glycol diglycidyl ether. The shell is the arc of graded density with the outer surface to the right. *Right,* map of the polymer concentration obtained from analysis of the three images.

Often viewed as primarily a tool for basic research, synchrotron radiation nonetheless has its share of industrial users looking for solutions to their problems. At the ALS, we formed an industrial–academic collaboration to conduct x-ray spectromicroscopy studies of superabsorbent polymers (SAPs), materials with a $2 billion annual market for a wide range of products including disposable baby diapers. The experiments were such a success that Dow Chemical has been able to use the results to help develop the process technology now being designed for a new SAP-manufacturing plant. Because of this and related work on x-ray spectromicroscopy of polymeric materials, Dow's Analytical Sciences division has conferred on two of us (GM and ER) its highest internal award.

Superabsorbent polymers are a specific example of a polymer gel. Occurring in both natural and synthetic forms, gels exhibit an intriguing combination of the properties of both liquids and solids. One feature that makes gels useful is their ability to respond strongly to very weak external stimuli, such as minute changes in pH or temperature. For example, a polymer gel might first absorb a quantity of liquid and later release it as the external conditions change. Timed release of pharmaceuticals is one example among many in which a control stimulus determines the rate of release. Crosslinking is a key feature of the polymer microstructure that governs actual performance.

Dow sells SAP in the form of small (less than 1.0 mm in size) beads of sodium polyacrylate that is lightly crosslinked to form an insoluble, hydrophilic gel. The ability to soak up great quantities of fluid makes SAPs attractive for use in diapers. But, like a sponge when compressed, some of the fluid is squeezed back out when the baby moves, negating part of the benefit. The strategy for preventing leakage under weight-bearing load is the formation of a thin shell of more tightly crosslinked polymer. The effectiveness of the shell depends in part on the density profile of the crosslinking through the

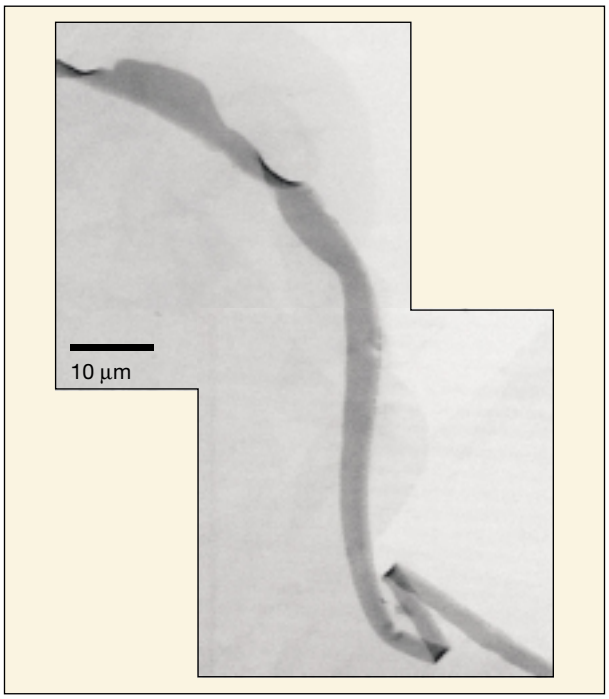

Figure 2 NEXAFS spectromicroscopy map of the polymer concentration in the shell formed around an SAP bead crosslinked with glycerol showing a sharply delineated density profile.

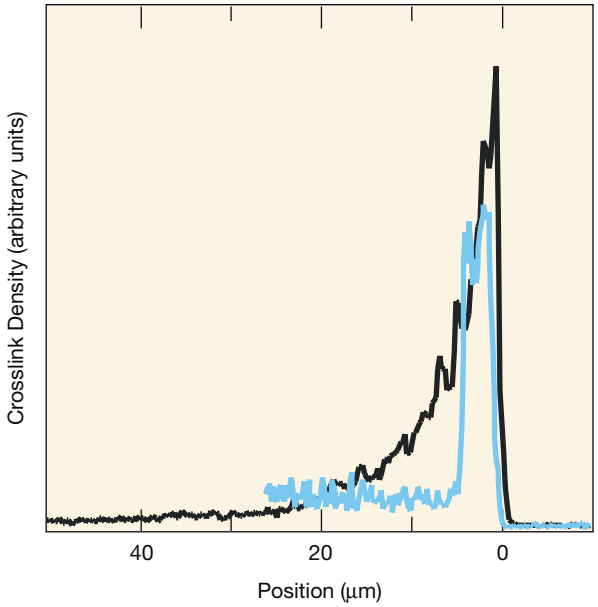

Figure 3 Crosslink density across the shells from the outer surface (position 0) to the interior of SAP beads treated in two different ways. Comparison shows strikingly different profiles that reflect the complicated kinetics of the SAP swelling when exposed to liquid and the different shell-formation processes.

shell, a distance of several microns. Several different methods have been developed to make surface crosslinked SAP gels, but there has been no good way to visualize and assess the resulting core-shell structure and the crosslink density profile.

To obtain the desired information, we turned to near-edge x-ray absorption fine structure (NEXAFS) spectromicroscopy, using the scanning transmission x-ray microscope (STXM) on Beamline 7.0.1 to make images of the polymers in the fully hydrated state (in excess water). Because the x-ray energy could be tuned to a value where the carbon in the polymer absorbs and the water is almost transparent, we could map the areas where crosslinking was higher by observing the increased carbon content in these regions.

Crosslinking was stimulated by treating the surface of SAP beads with varying amounts of either ethylene glycol diglycidyl ether or glycerol. Sectioned beads were then exposed to 0.9% saline solution to put them in the fully swollen state for imaging. Analysis of the images yielded two extreme cases for the crosslink profile through the shell. In one, the crosslink density decreased smoothly over a distance of 18 microns from a maximum at the outer surface (Figure 1). In the other, the density was uniform over a distance of 5 microns and then dropped abruptly (Figure 2). These differences (Figure 3) reflect a complicated interplay between the dynamics of the swelling of the bead in water, the diffusion rate of the crosslinker in the water phase, and the rate of the crosslinking reaction. Dow was able to use this kind of information in designing new products, which will be produced by its new SAP-manufacturing plant.

INVESTIGATORS

G.E. Mitchell, L.R. Wilson, M.T. Dineen, F. Hayes, and E.G. Rightor (The Dow Chemical Company); S.G. Urquhart and H.W. Ade (North Carolina State University); and A.P. Hitchcock (McMaster University).

FUNDING

The Dow Chemical Company, National Science Foundation, and Natural Science and Engineering Research Council of Canada.

PUBLICATION

1. G.E Mitchell et al., "Quantitative characterization of microscopic variations in the crosslink density of gels," *Macromolecules* **35,** 1336 (2002).

Nanostructures and Semiconductors

Fluctations of a Quasi-One-Dimensional Solid Between Metallic and Insulating States

While we live in a three-dimensional world, many physical systems effectively exist in two or one dimension. For example, a wire only one atom wide would be a one-dimensional system. Physicists study systems with reduced dimensionality in part because they are simple yet still provide insight into the fully three-dimensional world and in part because they exhibit novel behaviors that do not occur elsewhere. The compound $NbSe_3$ grows in the form of needle-like whiskers and serves as a model system to study exceptional effects predicted for one dimension, such as a transition from an electrically conducting state at everyday temperatures to an insulating state when cooled sufficiently. The switch results from a structural change (Peierls distortion). Schaefer et al. have used x-ray spectroscopy at the ALS to show that a shadow of the Peierls distortion remains even at room temperature in the form of fluctuations between conducting and insulating states that only gradually disappear as the temperature increases.

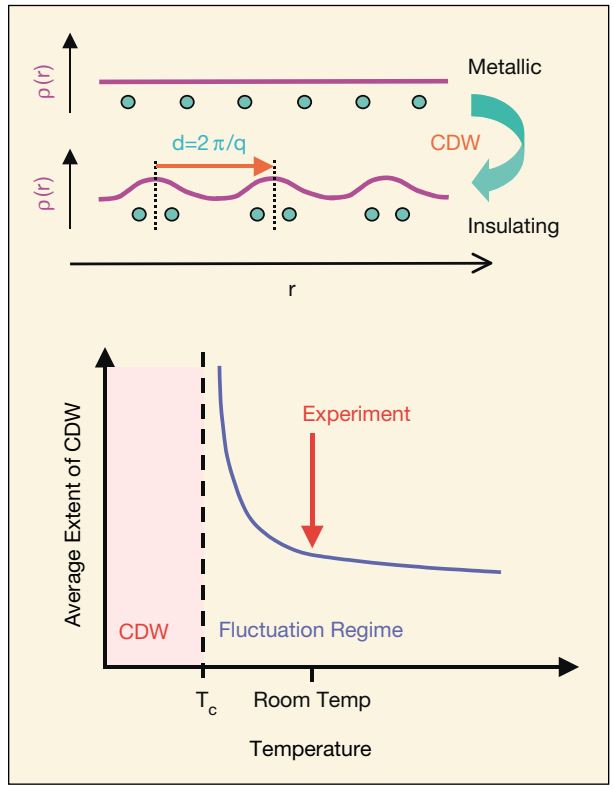

Figure 1 *Top,* schematic of the mechanism of a charge density wave in which distortion of the atom positions leads to a lowering of the energy. *Bottom,* precursors of the CDW can occur above the transition temperature, T_c.

Photoemission is particularly suited to probing exotic one-dimensional (1D) electronic properties, such as a Peierls instability, oftentimes referred to as a charge density wave (CDW). A CDW leads to a new crystal periodicity by grouping atoms and hence to an increased size of the crystal unit cell (Figure 1). The distortion lowers the total energy of the solid and implies a removal of electron states available for conduction, so that, in principle, the solid becomes an insulator. Thermal fluctuations limit this phase transition to relatively low temperatures, but local instabilities of the metallic phase can occur above the transition temperature, T_c. Such CDW precursor fluctuations affect the binding energies of the electrons.

One of the most intriguing compounds in this respect is $NbSe_3$. Its crystals take the form of needle-like whiskers roughly 10 µm in diameter. A CDW transition directed along the needle axis at T_c = 145 K leads to a significantly reduced conductivity. Our angle-resolved photoemission (ARPES) experiments were performed at ALS Beamline 7.0.1. The incident light beam was focused to a spot size of approximately 50 µm to ensure that only the whiskers were illuminated. All measurements were performed at room temperature (300 K)with the whiskers nominally in the metallic state. We obtained, for the first time, ARPES spectra that allowed us to determine the electronic states that satisfy the so-called "nesting" conditions for the CDW by changing their bonding configuration.

The photoemission angle (momentum) scan along the whisker direction in Figure 2 provides an overview of the experimental band structure along the whiskers. The features of the band map relevant for our study are the two sets of parabolic bands that appear to cross the Fermi level on each side of the Y symmetry point. The close-up view in Figure 3 shows the two bands in more detail. The lower band with a minimum at ~0.58 eV binding energy is the deepest one predicted by our density functional calculation. The upper band with a minimum at about 0.28 eV is consistent with a calculated doubly degenerate band.

The upper band exhibits a close approach to the Fermi level at momentum k_F = 0.22 Å^{-1}, which is in excellent agreement with theoretical results. This momentum immediately

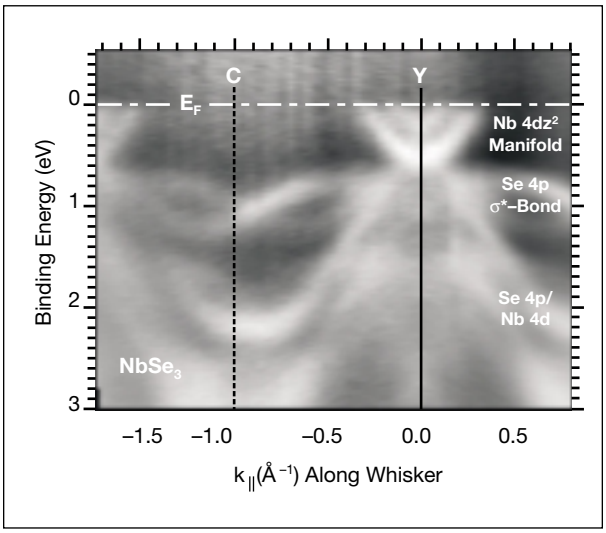

Figure 2 Electronic band structure from ARPES along the whiskers. Near the Fermi level, two sets of parabolic bands are clearly discernible around the Y point. They originate from Nb 4d states and satisfy the nesting conditions for the CDWs.

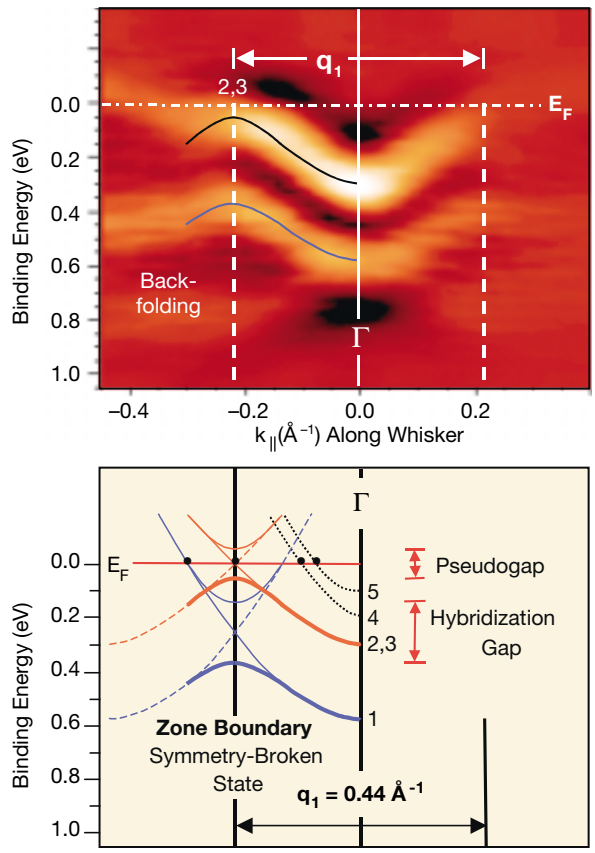

Figure 3 *Top,* close-up of bandmap data from ARPES. The CDW distortion superimposes new zone boundaries that induce a band backfolding, which weakens the metallic character—even above the actual transition temperature. *Bottom,* the band diagram using theoretical Fermi level crossings is in excellent agreement with the data.

satisfies the nesting condition for the known CDW vector $q_1 = 2k_F = 0.44$ Å^{-1}. This to our knowledge is the first determination of the nesting condition for the CDW along the principal axis in $NbSe_3$. Although close to E_F, the band does not exhibit a metallic crossing because the q_1 zone boundary induces backfolding of both bands. Instead of the bands reaching the Fermi level (as expected for a metal), both bands exhibit energy gaps so that they do not provide states for electron conduction.

The observation of an energy gap at room temperature is in stunning contrast to the fact that the pure CDW phase only exists below $T_1 = 145$ K. We believe that the thermal fluctuations above the critical temperature T_c, which lead to short-range order, affect the electron energies on the scale of the thermal energy, so that even for $T > 2T_c$, conventional metallic band crossings are absent and the symmetry of the electronic band structure is broken. To our knowledge, this effect has not previously been observed directly.

The remnant CDW implies the coexistence of metallic and insulating regions in $NbSe_3$, which is therefore not fully metallic at room temperature. With higher temperature, more and more conduction electrons would be provided. Our results imply that all earlier work on temperature-dependent conductivity reflects changes in the fraction of insulating sections in the sample.

INVESTIGATORS

J. Schäfer and S.D. Kevan (University of Oregon), E. Rotenberg (ALS), P. Blaha (Technische Universität Wien, Austria), R. Claessen (Universität Augsburg, Germany), and R.E. Thorne (Cornell University).

FUNDING

U.S. Department of Energy, Office of Basic Energy Sciences.

PUBLICATIONS

1. J. Schäfer et al., "High-temperature symmetry-breaking in the electronic band structure of the quasi-one-dimensional solid $NbSe_3$," *Phys. Rev. Lett.* **87,** 196403 (2001).

2. J. Schäfer et al. "Electronic precursor states of the charge density wave in $NbSe_3$," *Physica B: Cond. Mat.*, **312–313,** 650 (2002).

Environmental and Earth Science

Characterization of the Water Surface by Soft X-Ray Spectroscopy of Liquid Microjets

Everybody is familiar with liquid water, but when it comes to the details, scientists find they actually know a lot less about water than about many other common substances. Experiments and computer simulations do reveal that liquid water comprises hydrogen and oxygen atoms in a network of weakly bonded H_2O molecules characterized by, for example, a well-established average distance between the nearest oxygen atoms in neighboring molecules. However, researchers are only just now beginning to get a grip on the all-important water surface where interactions with surrounding matter take place. Wilson et al. have recently conducted x-ray absorption measurements on tiny streams (microjets) of water in a way that minimizes the obscuring water vapor cloud that normally lies over the surface and that specifically probes the surface in the presence of a much larger mass of bulk water. In this fashion, they were able to determine that the separation between oxygen atoms at the surface is larger than that in the interior, a valuable piece of information for theorists calculating the behavior of liquid water.

Developing a detailed molecular picture of liquid interfaces is important for understanding the accommodation of gaseous solutes in liquids, the dynamics of condensation and evaporation, and many problems in heterogeneous chemistry. In an effort to probe liquid interfaces on a molecular level, we have developed an endstation on ALS Beamline 8.0.1 that allows us to examine the surface of volatile liquids in the form of microjets. In our first experiments, we have demonstrated a 5% lengthening of the intermolecular oxygen–oxygen distance at the surface relative to the bulk, a lengthening that is not explained by current molecular-dynamics simulations of the structure of liquid water.

Previous measurements of macroscopic surface properties (e.g., surface tension and potential) have contributed to our overall understanding of liquid surfaces and provided important benchmarks for molecular-dynamics simulations. However, with the exception of sum-frequency generation for measuring the surface vibrational spectrum, no experimental techniques have been able to elucidate the interface molecular structure. Interface experiments are complicated by the large equilibrium vapor pressure above the liquid surface that obscures direct interrogation by traditional scattering techniques based on electrons, ions, or neutrals. In addition, the surface region persists for several molecular diameters (about 5 Å), which further necessitates the use of techniques with monolayer sensitivity.

Microjets, as pioneered by Faubel et al., allow us to maintain a base pressure of 10^{-5} torr and windowless coupling to the UHV environment of the beamline. More important, total electron, ion, and fluorescence yields can be simultaneously measured with an order-of-magnitude enhancement of signals relative to that of the vapor phase because of the beamline's small spot size (80×80 μm) and high photon flux. The total electron yield is dominated by a secondary electron cascade, which escapes into vacuum from an average depth of about 25 Å, thereby probing many monolayers. In contrast, ions are ejected into vacuum by Coulombic desorption, which is primarily sensitive to the outermost surface layer (1–5 Å).

By simultaneously measuring the near-edge x-ray absorption fine structure (NEXAFS) and extended x-ray absorption fine structure (EXAFS) spectra as a function of electron and ion yields, we directly compared the distribution of nearest-neighbor atoms and the structure of antibonding molecular orbitals at the surface to those of the bulk liquid. Additional bulk data by total fluorescence yield directly connects our measurements of liquid jets to those of other groups studying liquids at the ALS.

In particular, analysis of the EXAFS spectra obtained by total ion and electron yields revealed a change in the average near-neighbor distance at the surface of liquid water. The raw EXAFS spectra for the surface and bulk are shown in Figure 1, while the inset contains the Fourier transform of the data. We determined the average bulk intermolecular oxygen–oxygen distance to be 2.85±0.06 Å, in good agreement with previous diffraction measurements. However, when the same analysis was applied to the surface-sensitive EXAFS spectrum, we found a 5% lengthening of this intermolecular near-neighbor or first coordination shell distance at the liquid-water surface to 3.00±0.06 Å.

While this surface relaxation is qualitatively consistent with the breakdown of the three-dimensional network of hydrogen bonds observed in computer simulations, this effect is not accurately reproduced in current classical molecular

dynamics studies. As a result, this observation provides an important benchmark for developing a more accurate force field to be used in a theoretical description of liquid water.

Our microjet studies are currently being extended to other hydrogen bonding liquids (e.g., alcohols) in an effort to see whether this surface relaxation is indeed a general phenomenon in hydrogen-bonding liquids or one of the many unique properties observed in liquid water.

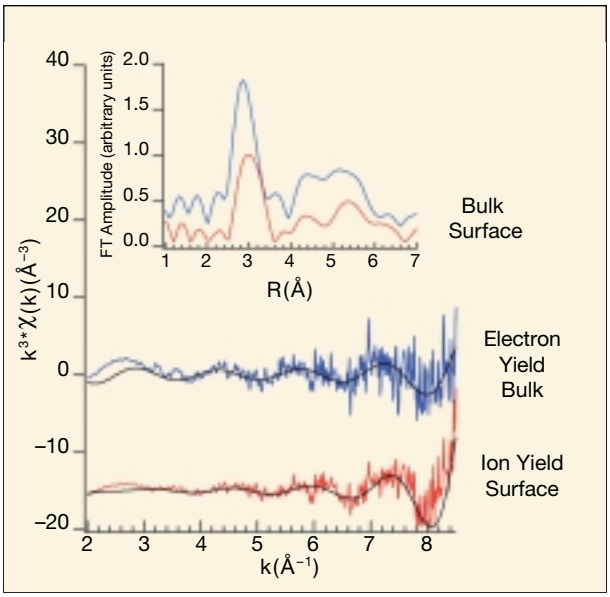

Figure 1 Raw EXAFS spectra above the oxygen K edge for the surface (electron yield) and bulk (ion yield) of a liquid-water microjet. *Inset,* the Fourier transforms of the EXAFS spectra show a 5% lengthening of the intermolecular oxygen–oxygen distance at the surface relative to the bulk.

INVESTIGATORS

K.R. Wilson, R. Schaller, D.T. Co, and R.J. Saykally (University of California, Berkeley); B.S. Rude and T. Catalano (ALS); and J.G. Tobin (Lawrence Livermore National Laboratory).

FUNDING

National Science Foundation.

PUBLICATION

1. K.R. Wilson et al., "X-ray spectroscopy of liquid water microjets," *J. Phys. Chem. B* **105,** 3346 (2001).

Monitoring Anthropogenic Metal Released in the Environment at Micrometer Scales of Resolution

Synergy, the added productivity of working together, is particularly beneficial when a complex problem is being attacked whose solution requires multiple skills and combined resources. Practitioners of the relatively new field of molecular environmental science, who strive to discern at the molecular level the myriad chemical transformations and modes of transport of harmful contaminants as they make their way through the environment, are finding that drawing on synergy in the form of multiple techniques is essential to their arduous task. A prime example comes from Manceau et al., who have combined three different x-ray techniques to determine the structural forms of compounds containing trace amounts of iron, zinc, and manganese in heterogeneous nodules from the floor of the Baltic Sea. Devised with the hope of using the nodules as monitors of long-term environmental changes, this approach is expected to be widely used in the growing arsenal of analytical methods available to both environmental and materials scientists.

Ferromanganese nodules are common in lakes, shallow marine environments, and the oceanic seafloor. They generally have a banded structure consisting of alternating iron- and manganese-rich layers separated by mixed iron-manganese zones, a growth pattern that implies a continuously growing substrate with invariable sorption efficiency for trace elements. Our goals were to measure metal fluxes into these nodules by dating individual nodule growth layers and to compare these fluxes with the changes in anthropogenic emissions in the last century in order to assess their use for retrospective monitoring of excess metal input.

We examined a nodule collected from the shallow water of the southwest Baltic Sea, where nodules are relatively fast growing and enriched in metal contaminants. Owing to the slow nodule accretion, high spatial resolution is a prerequisite, so we applied synchrotron-based micro-x-ray fluorescence (μSXRF) to obtain in-situ trace element profiles. Then, in-situ, micrometer-lateral-resolution x-ray diffraction (μXRD) and extended x-ray absorption fine structure (μEXAFS) spectroscopy at the manganese and zinc K edges were performed to determine how anthropogenic zinc is taken up in the concretions. We prepared a micropolished 30-μm-thick thin section and recorded μXRD patterns of

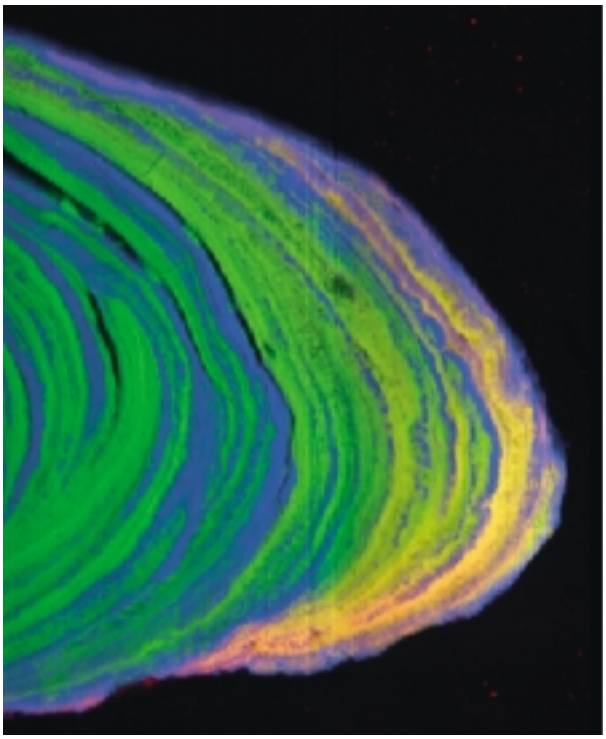

Figure 2 Synchrotron-based micro-x-ray fluorescence (μSXRF) maps of the outermost iron and manganese layers of a ferromanganese nodule from the Baltic sea (6600 μm × 3780 μm, step size 15 μm, *red* = zinc, *green* = manganese, *blue* = iron). The onion-like structure of growth rims is clearly discernible as iron- and manganese-rich bandings a few hundred microns thick. Zinc is exclusively associated with manganese, as indicated by the orange color of the zinc-containing manganese layers, and its concentration increases towards the surface.

iron- and manganese-rich layers on Beamline 7.3.3 and μEXAFS spectra at Beamline 10.3.2. In both cases, μSXRF maps were first recorded to image the iron and manganese layers.

The μSXRF elemental map of iron and manganese (Figure 2) shows the typically cuspate zebra-type banded structure with the thicknesses of manganese-rich layers typically from 200 to 500 μm and of the iron-rich layers from about 100 to 200 μm. Of the trace elements investigated (cobalt, nickel, copper, and zinc), zinc showed the most significant enrichment, with values in the outermost surface manganese layers up to six times higher than those found in the older nodule core. Assuming a continuous accretion of these relatively fast growing nodules (on average 20 μm/year) over the last century, we concluded that the zinc enrichment commenced in the period 1880 to1890, reflecting the enhanced heavy metal emissions with rising industrialization in Europe.

The μXRD patterns collected in iron-rich regions (Figure 3) contain only a broad and faint double hump with the centroid at about 2.5 Å, indicative of poorly crystallized two-line ferrihydrite (hydrous ferric oxide). The μXRD patterns taken in the manganese-rich layers look completely different, consisting of a series of basal and *hk*0 peaks whose positions, together with the noteworthy asymmetrical shape of the (200) reflection at 2.45 Å, are characteristic of turbostratic hexagonal birnessite (δ-MnO_2). The absence of *hkl* reflections with index $l \neq 0$ indicates that the structure is defective with no three-dimensional periodicity.

To determine the zinc sorption mechanism at the molecular level, we collected zinc K-edge μEXAFS spectra in a zinc "hot spot." Qualitative information about the local

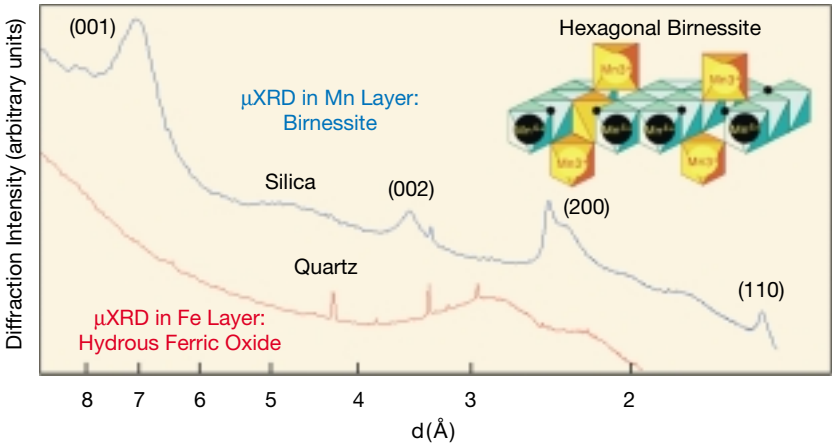

Figure 3 X-ray microdiffractograms collected in manganese (λ = 1.252 Å) and iron (λ = 1.758 Å) layers. The peak pattern from the manganese layers, a series of basal reflection peaks at 7.07 Å (001) and 3.51 Å (002) and *hk*0 peaks at 2.46 Å (200) and 1.43 Å (110), together with the noteworthy asymmetrical shape of the (200) reflection, identifies the manganese species as turbostratic hexagonal birnessite (δ-MnO_2). The pattern from the iron layers, a broad and faint double hump with maxima at about 2.85 Å and 2.25 Å and a centroid at about 2.5 Å, is characteristic of hydrous ferric oxide. Quartz grains (sharp peaks) and silica particles (d ≈ 4.6 Å) were detected throughout the sample.

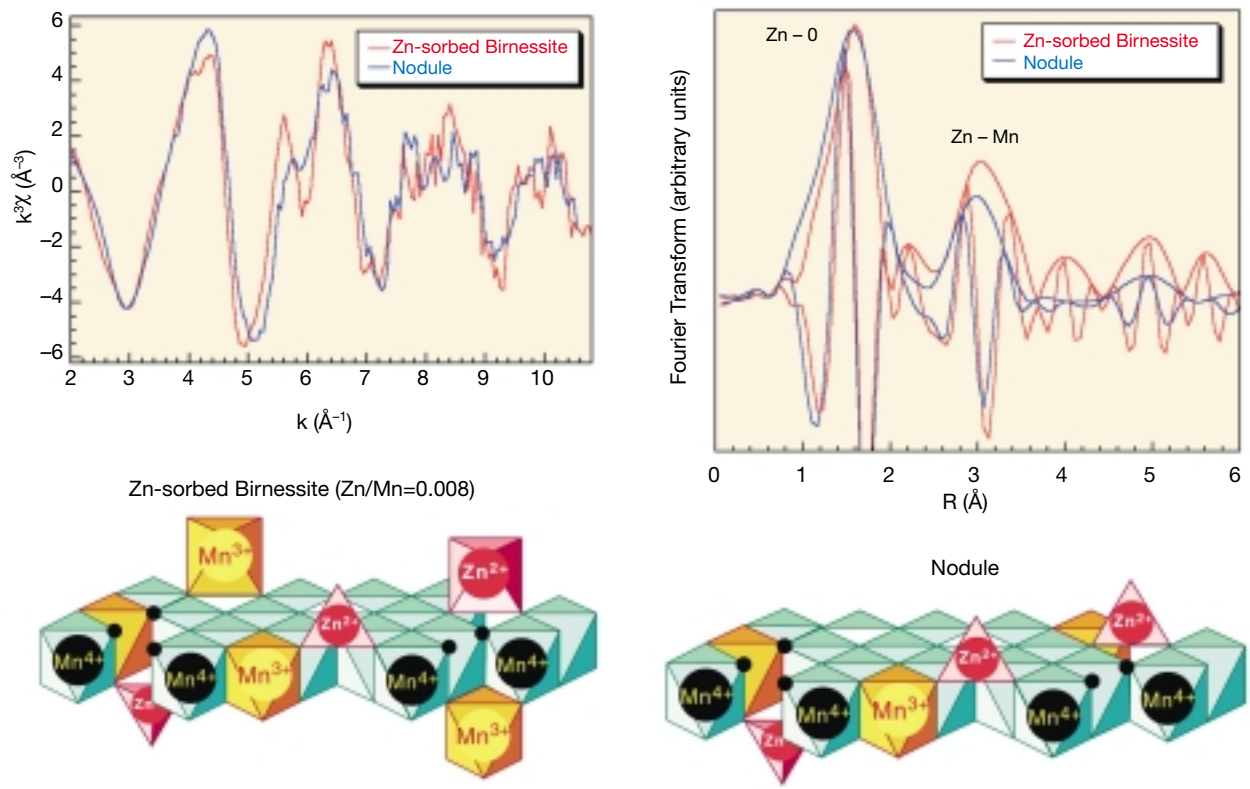

Figure 4 *Left*, zinc K-edge μEXAFS spectrum and *right,* Fourier transform (modulus plus imaginary part) from a zinc "hot spot" of the nodule rim compared to the spectrum from a zinc-sorbed birnessite reference, in which zinc is sorbed as a mix of Zn^{IV} and Zn^{VI} complexes above vacant layer manganese sites. The spectra look similar, indicating that zinc is taken up in a similar manner in both nodule and reference. However, the zinc–oxygen and zinc–manganese distances are clearly shorter in the nodule, and the experimental data were satisfactorily fit by assuming the presence of Zn^{IV} complex only.

structure of zinc can be obtained by comparing the unknown μEXAFS spectrum to reference EXAFS spectra from relevant model compounds. The best spectral match was obtained with the zinc-sorbed birnessite reference, in which zinc is predominantly tetrahedrally, and secondarily octahedrally, coordinated and complexed above vacant sites of the manganese layer (Figure 4). Comparison of radial structure functions indicates the presence of the Zn^{IV} but not the Zn^{VI} complex.

Our unprecedented combination of parallel fluorescence, diffraction, and absorption studies with micrometer spatial resolution allowed us to determine the structural form of trace elements in heterogeneous matrices with an unequaled precision. Since much of nature and synthetic materials are heterogeneous on micron and submicron length scales, we anticipate that the synergistic use of μSXRF, μSXRD, and μEXAFS will have broad applications and add to the arsenal of analytical methods available in environmental and materials science.

INVESTIGATORS

A. Manceau (ALS, Université J. Fourier, and CNRS, France); M.A. Marcus, N. Tamura, A.A. MacDowell, R.S. Celestre, R.E. Sublett, and H.A. Padmore (ALS); and M. Kersten (Gutenberg University, Germany).

FUNDING

U.S. Department of Energy, Office of Basic Energy Sciences; and Berkeley Lab.

PUBLICATION

1. Hlawatsch et al., "Trace metal fluxes to ferromanganese nodules from the western Baltic Sea as a record for long-term environmental changes," *Chemical Geology* **182,** 697 (2001).

Protein Crystallography

Zooming in on Ribosomes: Resolution Improves to 5.5 Å

The ribosome promises to answer one of mankind's oldest questions: How is life perpetuated? Stripped down to biological basics, the question can be posed as "How is the genetic code read to make proteins?" This process occurs on the surface of the ribosome. The code for a specific protein is carried out of the cell's nucleus on a string of messenger RNA (mRNA). A ribosome translates the code into a growing chain of amino acids that will become the protein. Amino acids arrive via transfer RNA (tRNA). Each tRNA carries a specific amino acid to be paired with a corresponding sequence of three bases (a codon) on the mRNA and added to the amino acid chain. The physical mechanism behind all this activity remains unclear. Yusupov et al. have taken a step toward the answer by determining the ribosome's structure with nearly atomic-scale resolution and using this structure to examine the path of RNA through the ribosome.

The structure of the ribosome—the site for the crucial process of turning genetic code into functional proteins—is coming into focus, in part because of the contribution of our team from the University of California, Santa Cruz. Working at the Macromolecular Crystallography Facility (MCF) at the ALS (Beamline 5.0.2), we have determined the structure of the ribosome with bound messenger RNA (mRNA) and transfer RNA (tRNA) at 5.5 Å resolution. This work builds on our group's previous efforts at the MCF, in which we solved the structure to 7.8 Å. Among the new observations is structural evidence that the two main parts of the ribosome (the 30S and 50S subunits) move relative to each other during protein synthesis. The new view also offers insight into how the ribosome interacts with tRNA.

The structure was solved by using multiple-wavelength anomalous diffraction (MAD) from crystallized ribosomes of Thermus thermophilus bacteria. The crystals contained a synthetic mRNA analog and tRNA molecules bound to two sites (the P and E sites). The high flux from the ALS wiggler yielded diffraction data with a resolution of 5.5 Å after density-modification algorithms were applied. Our group additionally used ribosome complexes with and without tRNA bound to a third site (the A site) to make a Fourier difference map that showed the A-site position at 7 Å resolution.

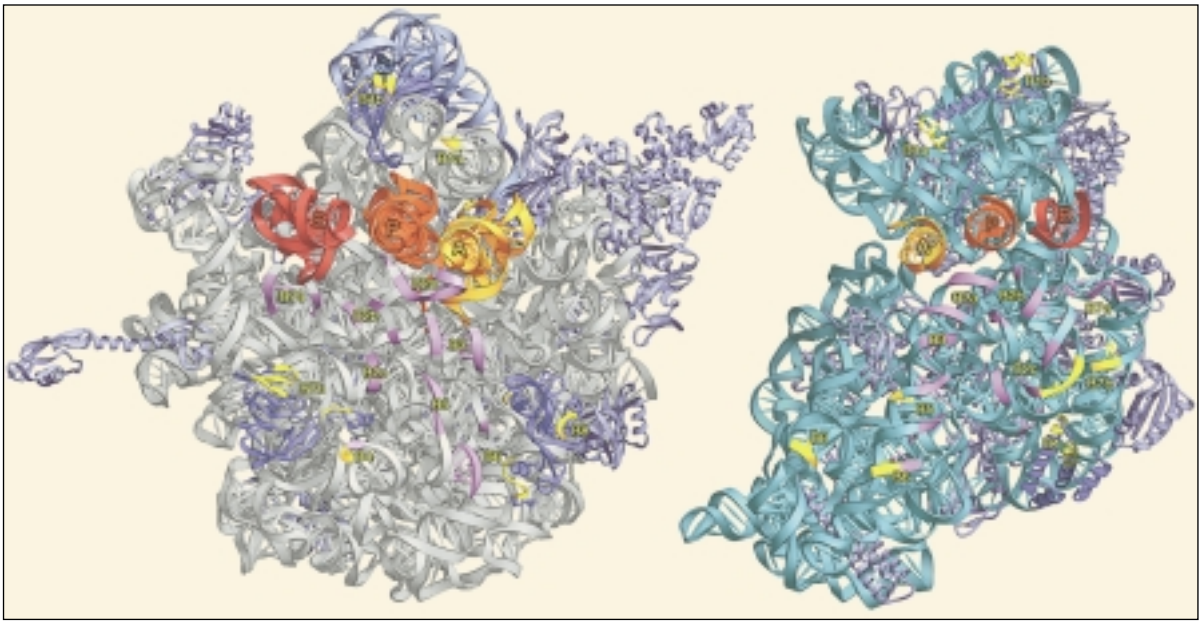

Figure 1 Interfaces of the 50S *(left)* and 30S *(right)* subunits of the ribosome with intersubunit bridges numbered. *Magenta,* RNA–RNA contacts; *yellow,* protein–protein and protein–RNA contacts; A, P, and E mark tRNAs at left and tRNA anticodon stem loops at right.

Ribosomes consist of ribosomal RNA (rRNA) and proteins. The ribosome's ability to function is known to depend more on RNA than on protein, but until now scientists did not know why. The high-resolution structure shows the answer: the protein–protein and protein–RNA interfaces tend to occur away from functional sites, whereas the RNA–RNA interactions exist near functional centers. In addition, the interactions between the ribosome and tRNA occur mainly through contacts with rRNA.

Central to the function of the ribosome and to the revelations of this latest view of it are the intersubunit bridges (Figure 1). These join the two subunits, holding them together around the string of mRNA that is being decoded and the tRNA molecules whose anticodons pair with codons on the mRNA. The new crystal structure shows all the molecular components of the known contacts between the two subunits, plus two new bridges.

Previous studies have shown that the tRNAs move through the space between subunits, translocating from the A site to the P site to the E site. Now, an important structural clue to the mechanism of this motion has been glimpsed. The new structure shows that these sites are all adjacent to intersubunit bridges. Since motion occurs around these sites, and the bridges are near enough to change shape as it occurs, it is likely that this motion is coupled with movement of the subunits relative to each other.

This structural information complements cryo-electron microscopy and neutron scattering studies suggesting intersubunit movement. Such studies have also made a strong case for movement of the head of the 30S subunit, relative to both the rest of that subunit and the rest of the ribosome. This case is reinforced in the new structure by the finding that the four domains making up 16S rRNA are nearly structurally independent of each other (and hence can move relative to each other with little change in shape). In addition, the four domains converge near sites of functional interactions with mRNA and tRNA, suggesting that their relative movements could be closely coupled with ribosome function.

Much work remains to be done before we have a complete solution to the mystery of how the ribosome works, but this latest effort provides vital structural information against which to test models of the ribosome's machinations.

INVESTIGATORS

M.M. Yusupov, G.Zh. Yusupova, A. Baucom, K. Lieberman, and H.F. Noller (University of California, Santa Cruz); T.N. Earnest (Berkeley Lab); and J.H.D. Cate (Whitehead Institute).

FUNDING

National Institutes of Health, Agouron Institute, W.M. Keck Foundation, Whitehead Institute for Biomedical Research, and Searle Scholars Program.

PUBLICATIONS

1. M.M. Yusupov, G.Zh. Yusupova, A. Baucom, K. Lieberman, T.N. Earnest, J.H.D. Cate, and H. F. Noller, "Crystal structure of the ribosome at 5.5 Å resolution," *Science* **292,** 883 (2001).

2. G.Zh. Yusupova, M.M. Yusupov, J.H.D. Cate, and H. F. Noller, "The path of messenger RNA through the ribosome," *Cell* **106,** 233 (2001).

Switch-Based Mechanism of Kinesin: Motor-Enzyme Action Captured in "Snapshots" of Two Key States

When you hear futurists speak with great excitement about the promise of nanotechnology, remember that they are speaking of artificial *nanomachines, because* natural *nanomachines already exist in every cell of your body. Kinesin, for example, is an amazing motor enzyme that "walks" in eight-nanometer steps along microscopic filaments called microtubules, dragging along various cargoes of mitochondria, chromosomes, or other cellular organelles. Nerve cells rely on kinesin to carry neurotransmitters out to tendril-like extremities that can extend several feet from the cell's main body. When a cell is ready to divide, its tangled microtubules align into a "spindle," and it is kinesin that propels the chromosome pairs into their separate corners. Needless to say, breakdowns in this complex transport system can have serious health consequences. By looking closely at kinesin's molecular structure in two key states, Kikkawa et al. have added to the growing store of knowledge about these nanoscale engines of life.*

Without infrastructure, business grinds to a halt, and the business of a cell is no exception. Cells require an internal transportation system reliable and flexible enough to accommodate both the routine movement of organelles and the dramatic choreography of mitosis. In response, nature has

engineered an intracellular rail system of sorts, in which a "motor" enzyme called kinesin hauls chromosomes and other cellular freight along microtubule tracks. Disruption of this system can lead to certain neurological disorders as well as cancer. To better understand how this system works, our team of researchers, working at the ALS and Stanford Synchrotron Radiation Laboratory, compared the structures of the kinesin mechanism when crystallized in two functionally critical states.

Kinesin's kinetic energy comes from the energy released when adenosine triphosphate (ATP) is hydrolyzed to produce adenosine diphosphate (ADP). The energy is thought to drive a stepping sequence in the kinesin molecule, which, in its conventional dimeric form, has a two-headed bilateral symmetry: one "head" remains attached to the microtubule surface while the other is free to move forward (Figure 2). However, the core region of a monomeric form of kinesin (KIF1A) has been observed to take multiple steps before detaching, suggesting that the KIF1A core region plays a vital role in kinesin's mobility.

In this work, we determined the structure of the KIF1A core region bound to ADP (to 2.2 Å) and to a nonhydrolyzable analogue of ATP (to 2.0 Å). Previously, all attempts to crystallize the ATP-like complex had failed. Our success in crystallizing this complex provided an excellent opportunity to compare "snapshots" of two key moments in the kinesin stepping sequence. Although the two structures look very similar overall, marked differences were observed in two "switch" regions near the ATP/ADP binding site (Figure 3).

In the switch I region, a helix flanked by two short loops in the ADP state forms a short β-hairpin structure in the ATP-like state. The switch II region shows a series of structural changes, including the partial unwinding of a helix and its rotation by roughly 20 degrees in the ATP-like state. To visualize the effect of these changes when the kinesin is attached to a microtubule, we embedded the molecular structures within cryo-electron microscope (cryo-EM) images of kinesin in contact with a microtubule surface (Figure 4). The results indicate that the switch II region actually remains fixed relative to the microtubule, while the rest of the KIF1A core rotates by about 20 degrees in the opposite direction. We suggest that this rotation binds the kinesin more tightly to the microtubule and creates a directional bias by pointing the tip of the KIF1A core in the direction of motion.

Another important difference between the two states was found in the "neck linker" domain, which connects the two heads in the dimeric form of kinesin (and which was "grafted" onto the KIF1A monomer for this experiment). The structures show that the linker is "docked" near the core in the

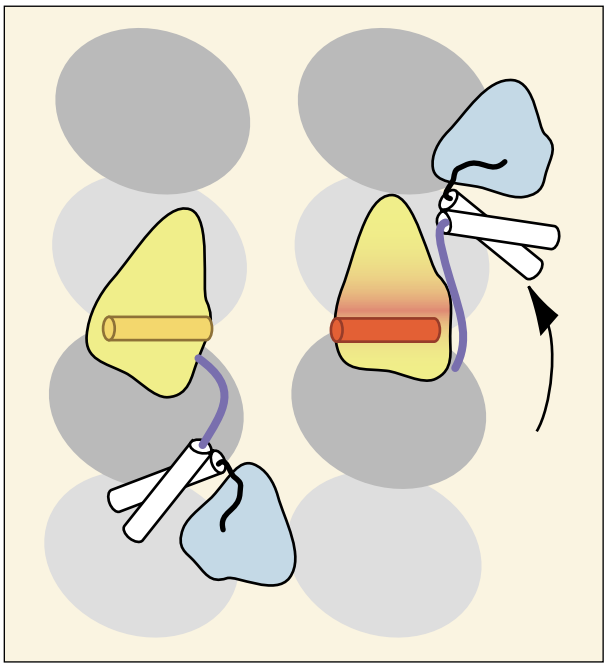

Figure 2 Movement of dimeric kinesin along a microtubule. One head *(yellow)* attaches to the microtubule surface *(gray)* while the other head *(blue)*, attached to the neck linker *(purple)*, swings forward.

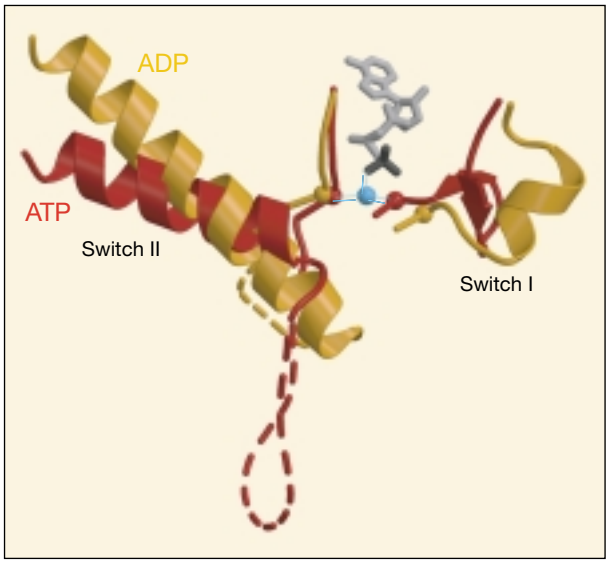

Figure 3 Comparison of KIF1A switch regions in the ADP *(yellow)* and ATP-like *(red)* states. Part of the bound ATP is shown in gray.

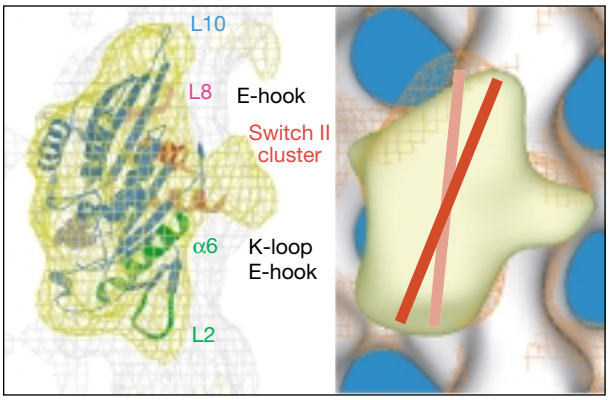

Figure 4 Rotation of KIF1A core *(yellow)* relative to microtubule surface *(gray). Left,* kinesin molecular model embedded within a cryo-electron-microscopy map of kinesin. *Right,* kinesin orientation in ADP *(pink line and orange grid)* and ATP-like *(red line)* states.

ATP-like state but is undocked and disordered in the ADP state. This finding supports the hypothesis that the neck linker is a crucial part of the mechanism that drives kinesin. In this view, the kinesin core is a modular base onto which different types of neck domains serve as mechanical amplifiers and transmitters (transmissions and drive shafts) whose exact function depends on the kinesin variant to which the neck linker belongs.

In general, these results confirm expectations—arrived at by analogy to previously studied, structurally similar proteins—that the conformational changes observed in KIF1A are modular and extend to all kinesins. They also suggest a rationale for kinesin's tendency to move in a given direction along a microtubule.

INVESTIGATORS

M. Kikkawa, Y. Okada, H. Yajima, and N. Hirokawa (University of Tokyo); E.P. Sablin and R.J. Fletterick (University of California, San Francisco)

FUNDING

Ministry of Education, Science, Sports, and Culture of Japan; National Institutes of Health.

PUBLICATION

1. M. Kikkawa et al., "Switch-based mechanism of kinesin motors," *Nature* **411**, 439 (2001).

Structure and Mechanism of a DNA Polymerase Processivity Clamp Loader

If DNA is the instruction book for life, then accurately replicating its DNA during cell division is a must for every organism that wants to grow and to generate offspring. Replication occurs when a double-stranded DNA molecule unzips to form two single strands, which then separate and become templates for the formation of new strands from surrounding chemicals (nucleotides). However, this work doesn't happen all by itself. Linking the nucleotides of the growing DNA strand to the template is performed by protein molecules (enzymes) called DNA polymerases with the assistance of still other proteins. Jeruzalmi et al. turned to x-ray crystallography to determine the structure of one such assisting protein, the polymerase processivity clamp loader. Their work also revealed the structure of a key portion of the loader while operating on the clamp protein. These structures not only are of fundamental interest but may also be useful to those developing pharmaceuticals, such as antibiotics and anticancer drugs, whose action depends on blocking cell replication.

We have been studying the molecular machines that are used to rapidly and accurately replicate the bacterial genome. The centrally important DNA polymerases in these machines are augmented by assemblies of other proteins that enable the polymerases to perform more effectively. We have determined the structure of one such assembly, an intact and functional clamp-loader machine. This structure, along with a second structure of the clamp caught in the act of being opened, has allowed us to construct a model of the clamp-loading reaction. While our work has focused on obtaining a basic understanding of this fundamental biological process, we can envision applications to the design of novel antibiotics and anticancer agents.

The general mechanism that we study in bacteria is conserved in all the kingdoms of life. During high-speed DNA replication, the DNA polymerase is tethered to DNA by the processivity clamp, which is a ring-shaped protein assembly that encircles DNA and slides freely along it. The processivity, or sliding, clamp is physically opened and loaded onto DNA by a multiprotein assembly known as the clamp loader. For historical reasons, the processivity clamp in bacteria is referred to as the β subunit. The clamp loader is composed of the γ subunit (an ATPase that acts as the motor in the

assembly), the δ subunit (a molecular "wrench" that binds to and opens the β ring) and the δ′ subunit (a stator in the motor). In eukaryotes, the homologous proteins are PCNA (proliferating cell nuclear antigen, the sliding clamp) and the five subunits of the RFC (replication factor C, the clamp loader) complex.

We have determined the structures of the bacterial clamp loader ($\gamma_3\delta\delta'$) and that of the δ wrench in complex with a clamp subunit (β). Owing to the large size and asymmetric nature of these assemblies, synchrotron x rays from insertion devices were required in the structure determination, and we made extensive use of ALS Beamline 5.0.2, as well as Beamline X-25 at the National Synchrotron Light Source, Beamline ID-19 at the Structural Biology Center at the Advanced Photon Source, and Beamline 9-2 at the Stanford Synchrotron Radiation Laboratory.

The crystal structure of the β:δ complex reveals how the δ wrench opens the β ring (Figure 5). The δ subunit, which adopts the same fold as the other clamp-loader subunits, places its N-terminal domain containing the β-interacting element into a binding site composed of two domains (2 and 3) on β_1. Binding of the δ subunit requires a conformational change in β that renders the clamp interface incapable of closing. With respect to its structure in the dimeric clamp, β from the β:δ complex adopts a conformation of reduced curvature. This observation, along with molecular dynamics simulations, suggests a spring-loaded mechanism in which the β ring opens spontaneously once a dimer interface is perturbed by the δ wrench.

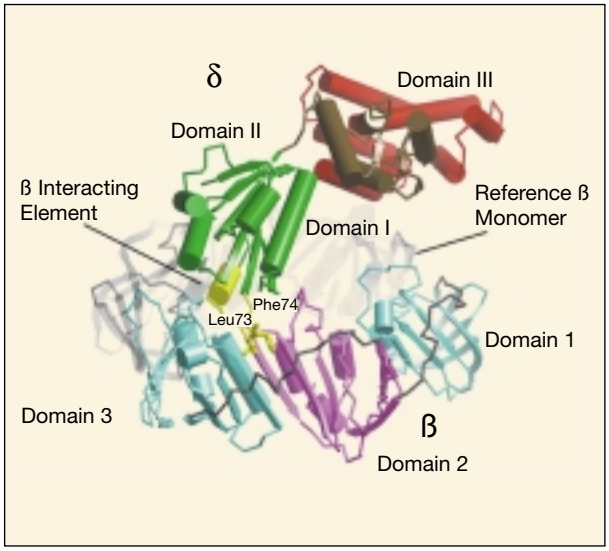

Figure 5 Structure of the β:δ complex within the clamp loader, which is composed of the γ subunit, the δ subunit (a molecular "wrench" that binds to and opens the β ring), and the δ′ subunit (a stator in the motor).

The 2.7–3.0-Å crystal structure of the clamp-loader complex reveals a pentameric arrangement of subunits, with a stoichiometry $\delta':\gamma_3:\delta$ (Figure 6). The C-terminal domains of the subunits form a circular collar that supports an asymmetric arrangement of the N-terminal ATP binding domains of the γ motor and the structurally related domains of the δ′ stator and the δ wrench. The three ATP binding sites on the γ motor subunits are located near clamp-loader-subunit interfaces. The structure crystallizes with only two of three sites available for ATP binding; the third site is blocked by the presence of structural elements from a neighboring subunit. The structure suggests a mechanism by which the γ complex switches between a closed state, in which the β-interacting element of δ is hidden by δ′, and an open form similar to the crystal structure, in which δ is free to bind to β.

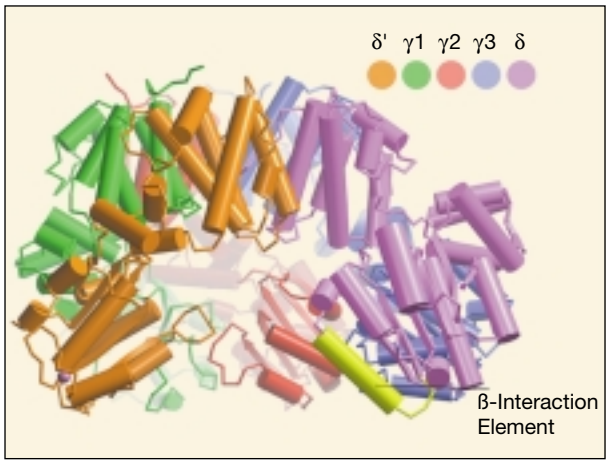

Figure 6 Structure of the γ complex within the clamp loader. The γ subunit is an ATPase that acts as the motor in the assembly.

INVESTIGATORS

David Jeruzalmi (University of California, Berkeley, and Berkeley Lab), Mike O'Donnell (Rockefeller University and Howard Hughes Medical Institute), and John Kuriyan (University of California, Berkeley, and Howard Hughes Medical Institute).

FUNDING

National Institutes of Health.

PUBLICATIONS

1. D. Jeruzalmi, M. O'Donnell, and J. Kuriyan, "Crystal

structure of the processivity clamp loader gamma complex of *E. coli* DNA polymerase III," *Cell* **106,** 429 (2001).

2. D. Jeruzalmi et al., "Mechanism of processivity clamp opening by the delta subunit wrench of the clamp loader complex of *E. coli* DNA polymerase III," *Cell* **106,** 417 (2001).

3. J. Stewart et al., "Mechanism of beta clamp opening by the delta subunit of *Escherichia coli* DNA polymerase III holoenzyme," *J. Biol. Chem.* **276,** 19182 (2001).

Allosteric Activation of a Spring-Loaded Natriuretic Peptide Receptor Dimer by a Hormone

Because vasoactive hormones regulate the volume of fluid in blood vessels, they are important players in diseases like high blood pressure and congestive heart failure. Like all biomolecules that carry out the cellular processes in our bodies, these hormones need open sites on the surfaces of cells to bind to before their work can begin. Known as receptors, these sites have a molecular structure that exactly complements that of the docking molecule, somewhat like a lock and key. When cellular processes go awry, the receptors provide a possible way to cure the problem. For example, a drug molecule crafted to either block or enhance binding to the receptor could slow down or accelerate the process, as appropriate. He et al. have taken this tack in their study of the structure of a receptor known as NPR-C alone and as it binds a hormone (C-type natriuretic peptide). Their structure may help in the design of a pharmaceutical that can stimulate fluid excretion and hence treat congestive heart failure.

Natriuretic peptides are vasoactive, cyclic-peptide hormones that play a major role in volume homeostasis and blood-pressure regulation through interaction with cell-surface receptors, of which the C-type natriuretic receptor (NPR-C) is the most abundant. NPR-C functions as both a clearance and a signaling receptor through activation of G proteins, and it is a primary therapeutic target for treatment of renal and cardiovascular disorders. Our goal was to visualize the mode of binding of these hormones responsible for blood-pressure regulation to their receptors on cell surfaces.

Towards this end, we crystallized the natriuretic hormone receptor both alone and complexed with a vasoactive peptide hormone called C-type natriuretic peptide (CNP). This combination enabled us to see the three-dimensional structure of the receptor in both the basal and activated states. We solved the three-dimensional structure using x-ray crystallography. Our use of ALS Beamline 5.0.2 was critical for the structure determination. The high brightness of the beamline enabled us to collect data with very high resolution, which was essential for seeing the interatomic contacts between the receptor and the hormone. Furthermore, the microfocused x rays on the beamline allowed us to collect data on very small crystals. Therefore, if not for the brightness and narrowly focused beam at the ALS, this project could not have been accomplished.

We determined the crystal structures of both the unliganded human C-type natriuretic peptide receptor extracellular domain and its complex with CNP, a potent 22-amino-acid natriuretic peptide (Figure 7). A single CNP molecule is

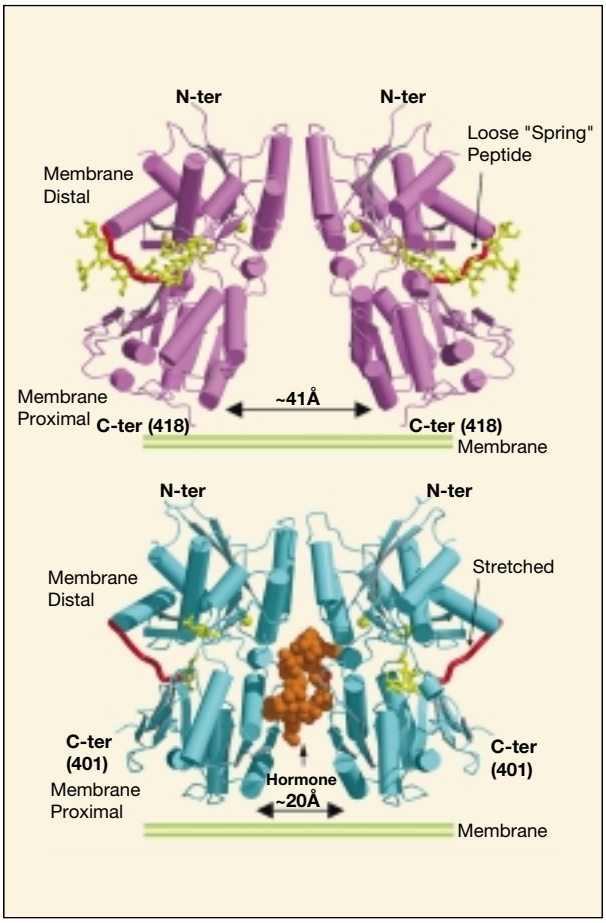

Figure 7 Ribbon diagrams of the three-dimensional structures of *(top)* the unliganded human C-type natriuretic receptor (NPR-C) dimer and *(bottom)* NPR-C bound to a human vasoactive peptide hormone called C-type natriuretic peptide (CNP). The cell surface is shown schematically at the base of the receptors, although on the cell surface, the receptor would enter the cell membrane.

bound in a ring-like conformation in the interface between two dimerized NPR-C extracellular domains, resulting in asymmetric interactions between the hormone and the symmetrically related receptors. Hormone binding induces large conformational changes in which the receptor monomers are straightened into an "open" state by a hinge movement, forcing a closer juxtaposition of the membrane-proximal domains of the dimer by 20Å, which is likely the activation trigger for the intracellular signal. A linker peptide tethering the two domains of the dumbbell-shaped receptor is stretched upon hormone binding and appears to act as a molecular spring, in concert with a large N-linked glycan, to constrain the receptors in the non-activated orientation in the absence of hormone. The delineation of two separate hormone interaction interfaces on NPR-C expands the scope of chemistries possible for development of NPR-C antagonists for the treatment of cardiovascular diseases.

The practical ramifications of this work are profound. Currently, no effective drug exists for treatment of congestive heart failure. The standard therapy is to use diuretics to stimulate the unloading of excess volume that the heart cannot pump, but this therapy is generally ineffective. Now, with the visualization of the structure of the receptor directly responsible for volume excretion, targeted drugs can be designed to activate this protein in a very specific fashion.

INVESTIGATORS

X.-L. He, D.-C. Chow, M.M. Martick, and K.C. Garcia (Stanford University School of Medicine).

FUNDING

American Heart Association; National Institutes of Health; and Rita Allen Foundation, Pew Scholars, and Frederick Terman Scholar Awards.

PUBLICATION

1. X.-L. He, D.-C. Chow, M.M. Martick, and K.C. Garcia, "Allosteric activation of a spring-loaded natriuretic peptide receptor dimer by hormone," *Science* **293,**1657 (2001).

The Structure of a Catalytic RNA Reveals an Active-Site Architecture Similar to That of a Protein Enzyme

One of the wonders of the chemical world, catalysts are substances with the remarkable ability to promote specific chemical reactions or biochemical processes without being themselves permanently transformed or consumed along the way. A large number of the proteins called enzymes that ply their trades in the cells of creatures large and small are catalysts, and it is safe to say that without enzymes, life would come to a halt. As it happens, however, there is a second category of biomolecule that also has catalytic talents: ribonucleic acid, or RNA. While RNA catalysts, also known as ribozymes, are just as important as enzymes, scientists have found it more difficult to study their three-dimensional structure, whose specific pattern of folds and crevasses carries the keys to how they do their work. Rupert and Ferré-D'Amaré have now determined the structure of one ribozyme and found that its structure has some of the same features as an analogous protein enzyme, which suggests the knowledge base of enzyme structure can be applied to ribozymes.

Two classes of macromolecules can fold into complex three-dimensional structures capable of biological catalysis: proteins and ribonucleic acid (RNA). Whereas thousands of structures of protein enzymes have been determined, only a handful of structures of catalytic RNAs, or ribozymes, have been solved to date. In the work summarized here, we have determined the three-dimensional structure of a catalytic RNA called the hairpin ribozyme, in complex with a specific inhibitor. The biological role of this ribozyme is that of a sequence-specific endonuclease; that is, it catalyzes cleavage of RNA at a particular site. Remarkably, the structural features we found for the ribozyme are quite similar to those of a protein enzyme that promotes the same cleavage reaction.

A few things are known about the differences between the structures of proteins and ribozymes that set the stage for our investigation. Proteins have an electrically neutral backbone and a choice of twenty amino acids for the formation of side chains with a broad spectrum of functional groups. RNA, in contrast, has a negatively charged backbone and only four types of side chains, all of which display limited chemical variety. These differences lead naturally to major questions: How can an electrically charged polymer fold into a compact

three-dimensional structure? How does RNA exploit its small repertory of functional groups to construct catalytically proficient active sites?

Our work addresses four principal points. First, how does the RNA fold? Previous biochemical studies had suggested that the active structure of the ribozyme resulted from association of two double-helical RNA segments. If this is so, what molecular interactions stabilize the close apposition of two negatively charged helices? Second, how does the ribozyme distort its substrate to activate it for cleavage? The cleavage reaction catalyzed by this RNA is a transesterification that requires that the reactant chemical groups be aligned. In the ground-state structure of the substrate, the chemical groups are far from being aligned. Third, what chemical groups does the ribozyme use to achieve catalysis? It is known that the hairpin ribozyme does not rely on metal ions or other cofactors for catalysis. All functional groups must be provided by the RNA itself. Fourth, how does the active site of the hairpin ribozyme compare to those of protein enzymes that catalyze the same reaction?

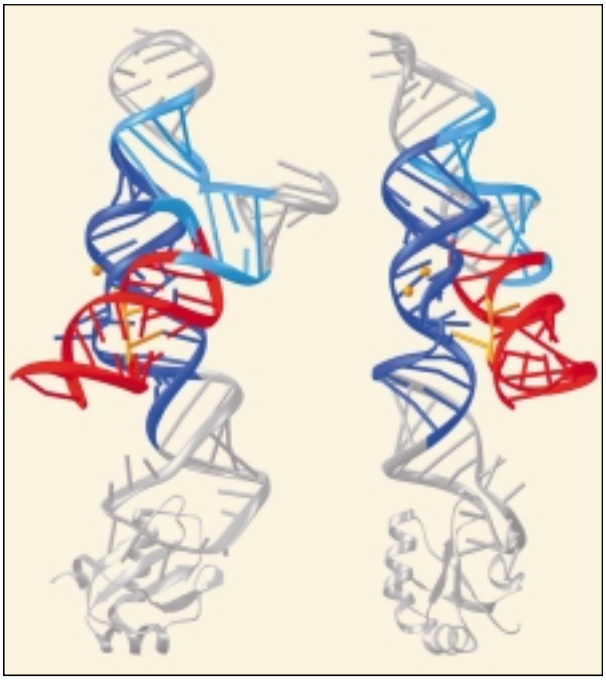

Figure 8 Schematic representation of the three-dimensional structure of the hairpin ribozyme. The path of the RNA backbone is shown as a ribbon; the nucleotides are indicated as sticks. The double helices colored dark blue and red in the two orthogonal views pack together to form the active structure of this catalytic RNA. The RNA bond that is cleaved lies between the two yellow nucleotides. The yellow spheres are tightly bound calcium ions that stabilize the RNA.

We obtained well-ordered crystals of a hairpin ribozyme–inhibitor complex and solved its structure at 2.4-Å resolution by taking advantage of the bright, tunable x rays from ALS Beamline 5.0.2. The structure shows that two of the four RNA helices that comprise the ribozyme have irregular, extremely wide minor grooves (Figure 8). The two widened minor grooves pack together, forming a network of specific hydrogen bonds and stacking interactions. The active site lies at the helical interface. The active conformation of the ribozyme is stabilized by the large molecular surface area buried between the two helices and by the binding of calcium ions in the adjacent major groove of one of the helices.

Our structure reveals that the hairpin ribozyme aligns the reactive groups of its substrate by splaying apart the nucleotides

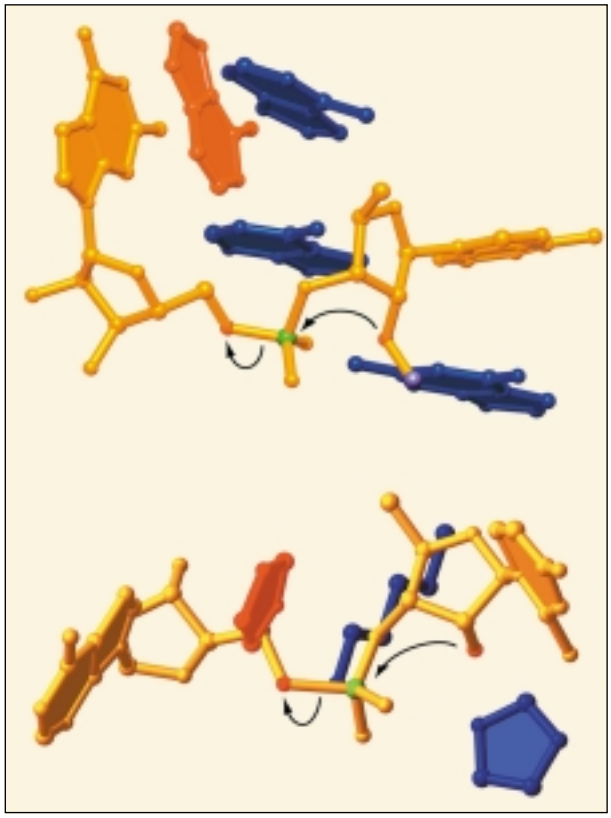

Figure 9 Comparison of the active sites of an RNA and a protein enzyme that catalyze the same RNA cleavage reaction. The conformations of the substrate in the active sites of the hairpin ribozyme *(top)* and in the ribonuclease-A *(bottom)* are remarkably similar. Splaying apart of the two nucleotides *(in yellow)* that flank the scissile phosphate (the phosphorus atom is colored green) aligns the nucleophile and leaving groups for the transesterification reaction *(arrows)*. Some of the functional groups contributed by the ribozyme and the protein enzyme to the active site are shown in red and blue.

that flank the phosphate group at the site of cleavage. Both the splayed conformation of the substrate and the arrangement of catalytic groups around the scissile phosphate are remarkably similar to the disposition of substrate within the active site of a protein enzyme, ribonuclease-A, that catalyzes the same RNA-cleavage reaction (Figure 9). Thus, two completely unrelated molecules, an RNA and a protein, with a similar problem have arrived at the same structural solution, suggesting that the understanding already achieved for protein-enzyme function can probably be extended without much alteration to understanding RNA active sites.

INVESTIGATORS

P.B. Rupert and A.R. Ferré-D'Amaré (Fred Hutchinson Cancer Research Center).

FUNDING

National Institutes of Health, American Cancer Society, and Rita Allen Foundation.

PUBLICATION

1. P.B Rupert and A.R. Ferré-D'Amaré, "Crystal structure of a hairpin ribozyme–inhibitor complex with implications for catalysis," *Nature* **410,** 780 (2001).

Structure of the B7-1/CTLA-4 Complex, a Key Inhibitor of Human Immune Responses

An efficiently functioning immune system recognizes foreign organisms that invade our bodies, destroys the attackers, and builds up immunity against future invasions. Thymus lymphocytes, or T cells, are key members of the immune system and are responsible for recognizing and destroying cells infected by viruses or bacteria. T-cell activity is driven by two signal types, a recognition signal and so-called co-stimulatory signal that in effect tells the T cell how active to be. Both overly zealous and underactive immune responses can lead to disease. Inhibitors are molecular complexes that act to slow down or attenuate cellular processes. Stamper et al. have determined the structure of a particular inhibitor complex that spans the space between a T-cell and a foreign antigen-presenting cell (the antigen is the specific molecule that is recognized as alien), where it delivers a co-stimulatory signal that attenuates T-cell activity. The robustness of the structure is an indicator of the importance in cell function of inhibitory signaling.

Modulation of T-cell responses plays a primary role in determining the outcome of autoimmune disease, the development of tumor immunity, and graft survival following transplantation. Optimal T-cell responses require both an antigen-specific and a second (nonspecific) co-stimulatory signal. Shared ligands, B7-1 and B7-2, on antigen-presenting cells deliver this co-stimulatory signal through receptors on the T-cell surface: CD28, which augments the T-cell response, and CTLA-4 , which attenuates the response. With the consequences of these signals well established and details of the downstream signaling events emerging, understanding the molecular nature of these extracellular interactions becomes crucial.

In this work, we have determined the crystal structure of the human CTLA-4/B7-1 co-stimulatory complex. The extracellular domains of human soluble CTLA-4 and B7-1 were expressed in Chinese hamster ovary cells, and the complex was purified and crystallized. Saccharides accounted for about half of the molecular weight of the crystallized complex, resulting in very fragile crystals that only diffracted to 3.6-Å resolution when we used a laboratory x-ray source. At ALS Beamline 5.0.2, the combination of cryogenic cooling and extremely intense synchrotron radiation allowed us to obtain data up to a resolution of 3.0 Å from a single crystal at 100 K, and the structure was solved by the molecular-replacement method.

In our crystals, CTLA-4 and B7-1 monomers each associate as noncrystallographic, roughly twofold symmetric homodimers; single copies of each homodimer together form the asymmetric unit (Figure 10). The association of the four monomers in the asymmetric unit is driven by the interaction of three surfaces: the surface-mediating sB7-1 homodimerization, the CTLA-4 homodimer interface, and the receptor–ligand binding interface.

Receptor–ligand recognition occurs in an orthogonal mode (Figure 11), representing a recurrent theme for immunoglobulin superfamily interactions. However, in contrast to other interacting cell surface molecules, the relatively small ligand binding interface exhibits an unusually high degree of shape complementarity. Overall, we observe 85 interatomic contacts (van der Waals radius, 3.9 Å) between 13 residues of CTLA-4 and 13 residues of B7-1. Most of these are hydrophobic contacts but include also five hydrogen bonds. The hydrophobic ^{99}MYPPPYY^{105} loop, which is strictly conserved in CTLA-4 and CD28, dominates the interaction (Figure 11).

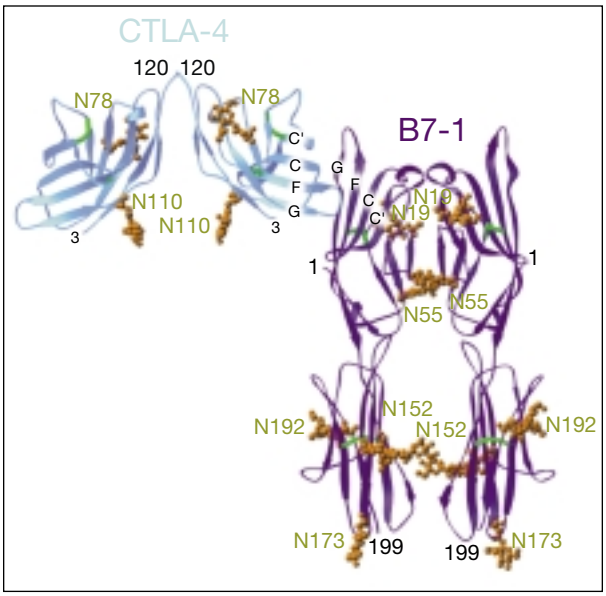

Figure 10 Ribbon diagram of the CTLA-4/B7-1 complex showing two B7-1 *(purple)* and two sCTLA-4 *(cyan)* molecules in the asymmetric unit. Disulfide bonds *(green)* and sugar moieties *(orange)* are also shown. Beta sheets involved in the receptor–ligand interaction are labeled. Glycosylation sites on sCTLA-4 (Asn 76 and Asn 108) and on sB7-1 (Asn 19, Asn 55, Asn 152, Asn 173, and Asn 192) are all surface exposed. None of the ordered glycosides are involved in the receptor–ligand recognition.

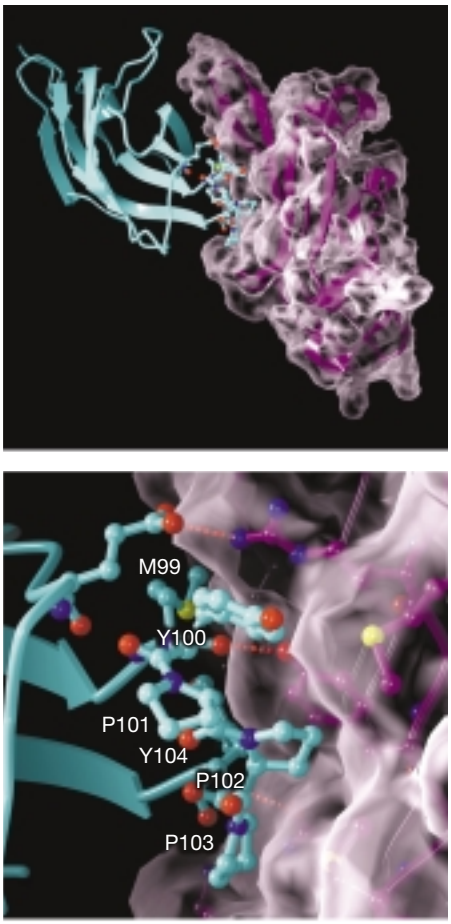

Figure 11 Overview of receptor–ligand interactions. *Top,* ribbon diagram showing orthogonal interaction between sCTLA-4 *(cyan)* and sB7-1 *(purple)* monomers. Also drawn is the molecular surface representation *(transparent white)* of the ligand binding domain of sB7-1 to emphasize the high geometric match between the two interacting surfaces. *Bottom,* direct receptor–ligand contacts with the same color coding. The ^{99}MYPPPYY^{105} loop of sCTLA-4 is buried in a shallow depression of the sB7-1 GFCC′ surface. Three out of five hydrogen bonds formed across the β sheets of the interacting domains are depicted as red dashed lines. Several other side chains on CTLA-4 and B7-1 (not shown) may contribute to the binding through appreciable, but not direct, contacts formed on the periphery of the binding interface.

In the crystal lattice, the CTLA-4 and B7-1 homodimers pack together to form a periodic arrangement in which bivalent CTLA-4 homodimers bridge bivalent sB7-1 homodimers (Figure 12). The B7-1 and shorter CTLA-4 homodimers associate orthogonally, thus generating a "skewed zipper" arrangement. It has long been clear that CTLA-4 exists as a constitutive, bivalent homodimer, and the affinity of sB7-1 for self-association indicates that B7-1 is also likely to exist as a dimer at the cell surface, albeit in dynamic monomer–dimer equilibrium. We therefore expect oligomeric arrays similar, if not identical, to those seen in the crystals to form at the membrane interface between T cells and antigen-presenting cells. Including the "stalk" regions, the extracellular domains of the ligated receptors are expected to span a distance of about 140 Å between the opposing cell membranes, a distance compatible with that required by other complexes involved in intercellular interactions.

As far as is generally known, cell surface molecules bind their ligands monovalently and with very low affinities. The submicromolar affinity of B7-1 for CTLA-4 is thus unusually high for interacting cell surface molecules. Our structural analysis implies that potent B7-mediated inhibitory signaling is not based exclusively on the stability of association between individual homodimers, but rather that the counter-receptor oligomeric arrays will also strengthen the interaction between the opposing cells. We believe this zipper-like oligomerization represents the structural basis for formation of unusually stable signaling complexes at the T-cell surface, a conclusion that underscores the importance of potent inhibitory signaling in human immune responses.

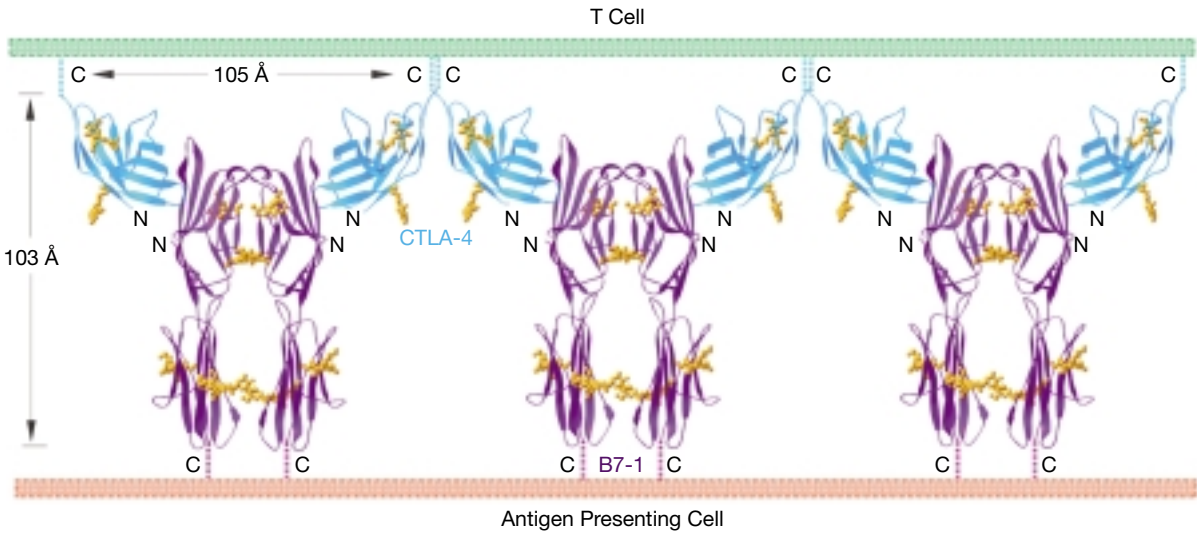

Figure 12 The molecular association of CTLA-4 and B7-1 in the crystal lattice as "Skewed zipper" ribbons in which CTLA-4/B7-1 complexes would be evenly spaced along membrane surfaces with a separation of 105 Å. In the perpendicular direction, across membranes, ligated receptors would span 103 Å. Geometrically, sugar chains attached at Asn 76 on sCTLA-4 and those attached at Asn 173 on B7-1 are close to the opposing T-cell and antigen-presenting-cell membranes, implying their potential involvement in interaction with the membranes, perhaps by stabilizing the orientation of the CTLA-4 and B7-1 dimers.

INVESTIGATORS

C.C. Stamper, Y. Zhang, J.F. Tobin, D.V. Erbe, M.L. Stahl, J. Seehra, W.S. Somers, and L. Mosyak (Wyeth Research/Genetics Institute); S.J. Davis and S. Ikemizu (The University of Oxford).

FUNDING

Wyeth Research/Genetics Institute.

PUBLICATION

1. C.C. Stamper et al., "Crystal structure of the B7-1/CTLA-4 complex that inhibits human immune responses," *Nature* **410,** 608 (2001).

The Activated Complex between Human gp130 and Viral Interleukin-6: A Structural Paradigm for gp130 Cytokine Signaling Assemblies

If biological cells are like tiny factories filled with molecular-scale engines churning out products three shifts a day, various signaling mechanisms are needed to tell the machines when to start and stop their particular operations. The signaling generally comes about by way of biochemical reactions involving molecules connecting one cell location to another. Cytokines comprise a family of protein molecules collectively responsible for signaling that is essential to many functional activities. In action, a cytokine operates as a member of a molecular complex based on a receptor protein that binds the cytokine, a basic unit that then forms an assembly of one or more such units. Chow et al. have determined the molecular structure of a particular cytokine signaling assembly involving the receptor protein gp130 and the cytokine interleukin-6. Since gp130 cytokines are implicated in many diseases associated with defective cell growth and differentiation, such as cancers, a knowledge of their structure could lead to the design of drugs that work by altering cytokine action.

The engagement of cell-surface receptors by extracellular ligands is a basic biological mechanism to initiate intracellular signaling cascades. The protein gp130 is a shared signal-transducing receptor for a family of soluble proteins and peptides known as cytokines that modulate the functional activities of individual cells and tissues. In many tissue systems, cytokines are critical to normal biological homeostasis (physiological equilibrium) and biological responses in vivo. Signaling via gp130 is crucial to the normal growth and differentiation of hematopoietic (blood-forming) cells, bone, neurons, muscle, heart, adipose tissue, liver, and testes. The gp130 cytokines have been implicated in a large number of diseases and neoplastic disorders, such as multiple myeloma.

The activities of gp130 cytokines are mediated through formation of oligomeric complexes containing one or more copies of gp130. Activation of gp130 occurs in a stepwise fashion initiated by recognition of a ligand through its cytokine-binding homology region (CHR), followed by oligomerization into a higher-order signaling complex, leading to intracellular signaling cascades. Long-standing questions in cytokine signaling have included the architecture of this higher-order signaling complex and the structural basis for the unique promiscuous recognition properties inherent in gp130's role as a shared receptor. Kaposi's sarcoma herpes virus (KSHV) encodes a functional homologue of the cytokine human interleukin-6, termed viral IL-6, which activates human gp130 and is a growth factor in KSHV-related neoplastic diseases.

We have determined the 2.4-Å crystal structure of the higher-order signaling complex between KSHV IL-6 and the three N-terminal domains of human gp130 (Figure 13). The x-ray data was primarily collected on ALS Beamline 5.0.2, whose microfocused beam enabled us to collect data on a very small crystal. Owing to the very small quantities of protein we could express, an intense, highly collimated x-ray source was essential. In total, we were only able to grow five or six usable crystals, and we were able to extract sufficient data from one of these crystals for a structure determination.

The molecular mimicry of human IL-6 by the viral cytokine is achieved largely through utilization of hydrophobic amino acids to contact gp130, in contrast to hydrophilic residues in human IL-6. This difference substantially enhances the complementarity of the viral IL-6/gp130 binding interfaces. The remarkable cross-reactivity of gp130 appears to be due to a chemical, rather than structural, plasticity evident in the amphipathic gp130 cytokine-binding sites. Two viral IL-6/gp130 complexes are cross-linked into a tetramer that is bridged through extensive interaction between the activation domain of gp130 and a conserved region of viral IL-6 termed site III, a site necessary for receptor activation. From the structure of this complex, the architecture of higher-order signaling assemblies for other members of the gp130 family of cytokines can be inferred.

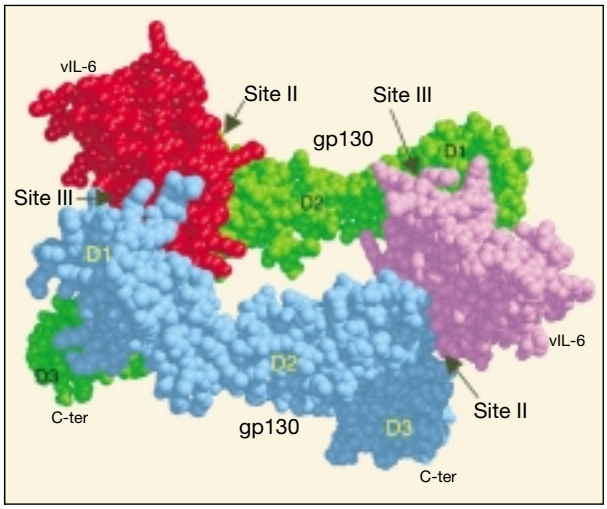

Figure 13 A view of a space-filling model of viral IL-6 complexed to gp130 in the 2:2 tetrameric oligomer. One can simultaneously see the hole in the middle and the D3 domains underneath the "canopy" of viral IL-6 and D1/D2 domains that dominate the uppermost portion of the complex. The twofold axis runs through the hole.

On the basis of this x-ray structure, pharmacological manipulation of the IL-6 signaling cascade could target both the extracellular recognition and oligomerization sites on the protein. An optimal strategy, then, for inhibition of IL-6 activity would be to design an IL-6 variant with increased affinity for the receptor IL-6Rα, or simply Rα, so that it will displace wild-type IL-6 from Rα, and decreased affinity for gp130, so signaling will not occur. Atomic models of the site-II and site-III receptor-binding interfaces of vIL-6 have greatly facilitated the design of this molecule.

Overall, the presence of numerous structurally related cytokines that act through common receptors and intracellular signal transducers makes the task of engineering specificity into modified molecules extremely difficult. Therefore, high-resolution atomic models of the receptor/ligand interfaces are critical for this highly redundant system in order to glean specificity determinants that have eluded functional studies. Our x-ray structure of the first gp130 cytokine complex now paves the way for the development of specific inhibitors.

INVESTIGATORS

D.-C. Chow, X.-L. He, A.L. Snow, and K.C. Garcia (Stanford University School of Medicine); S. Rose-John (Christian-Albrechts-Universität zu Kiel, Germany).

FUNDING

National Institutes of Health, California Cancer Program, Pew Scholars, and Cancer Research Institute.

PUBLICATION

1. D. Chow, X. He, A.L. Snow, S. Rose-John, and K.C. Garcia, "Structure of an extracellular gp130 cytokine receptor signaling complex," *Science* **291,** 2150 (2001).

Atomic and Molecular Science

Photoelectron Diffraction Mapping: Gas-Phase Molecules Illuminated from Within

Scientists can learn a lot about molecules by observing electrons ejected when the molecules are illuminated by x rays. The way such electrons end up distributed in space reveals information about the state of the molecule. However, to relate the emission pattern to the molecule, researchers need to know how the randomly moving molecule was oriented at the time of emission. For a simple molecule, like carbon monoxide with its two atoms, orientation can be determined by breaking the molecules apart and observing which way the fragments fly. Previous experiments in this vein provided only glimpses of the electron distribution for a few selected directions or molecular orientations. This is like trying to watch a defective television that displays only a few narrow slices of the picture at a time. The technique described by Landers et al. captures the full picture with high efficiency and resolution, allowing scientists to see the entire electron distribution for a given molecular orientation, as well as how the image evolves as the molecule rotates.

Seeing is believing, and the importance of visualization is obvious at the molecular level, which lies outside the realm of everyday experience. Gas-phase molecules, however, present some difficulties because traditional techniques for probing within molecules, such as photoelectron diffraction, require knowledge of the molecule's orientation. Addressing this problem, our international collaboration has demonstrated a multiparticle coincidence technique at the ALS that yields comprehensive photoelectron diffraction data for gaseous carbon monoxide (CO) as if the molecules were fixed in space. The most striking aspect of viewing molecules "illuminated" from within this way is how the results reveal, nearly at a glance, the major physical features at play.

In x-ray photoelectron diffraction (XPD), a core-level electron is ejected from one atom in a molecule by an incoming x ray. The ejected photoelectron wave, diffracted by neighboring atoms, provides a signature of the nonspherical potential of the molecule. However, to fully observe the rich, three-dimensional structure of the electron wave, knowledge of the orientation of the molecule is required. In most cases, the material under investigation is in solid form (crystal or adsorbate) and can be easily oriented in the laboratory. Determining the orientation of a freely moving molecule, however, requires some experimental finesse.

At Beamline 9.3.2, a beam of CO gas can be crossed with a beam of linearly polarized x rays, thereby removing the carbon 1s electrons and leaving the molecules in highly excited states. The molecules then rapidly dissociate into carbon and oxygen positive ions. The fragments (ions and electrons) are drawn by electric and magnetic fields toward position-sensitive detectors (Figure 1). Only triple coincidences between two ions and one electron are recorded. From the times of flight and the impact positions, the momenta of all particles in all directions are calculated. Because the dissociation time of ionized CO is substantially shorter than its rotation period, measurement of the carbon and oxygen momentum vectors gives the molecule's orientation upon photoionization. In contrast to previous experiments, this technique records, with high efficiency and resolution, the full picture of the outgoing electron wave for all orientations of the molecule simultaneously. One can, by computer analysis, select and organize the results to show the electron emission pattern as if all the molecules were oriented in the same way.

For example, the data can be displayed in a map of the photoelectron momentum vectors, where the azimuthal angle gives the direction of the photoelectron emission, the radial distance gives the photoelectron energy, and the emission

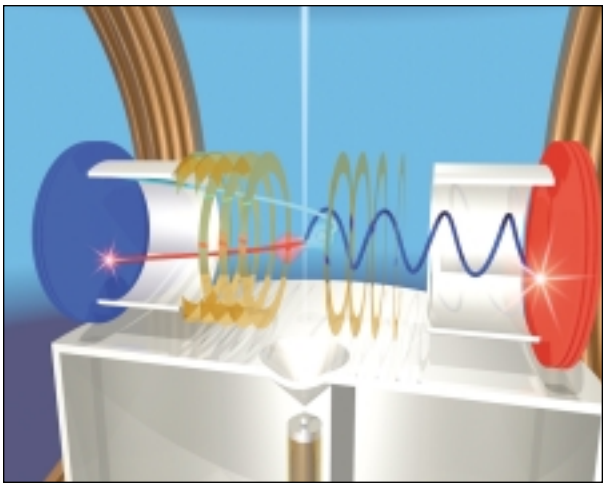

Figure 1 Experimental apparatus. A beam of carbon monoxide gas from below intersects with photons from Beamline 9.3.2. The negatively charged electrons *(red)* and positively charged ions *(blue)* produced in the interaction are captured by electrodes of the opposite sign and recorded to reconstruct momentum vectors.

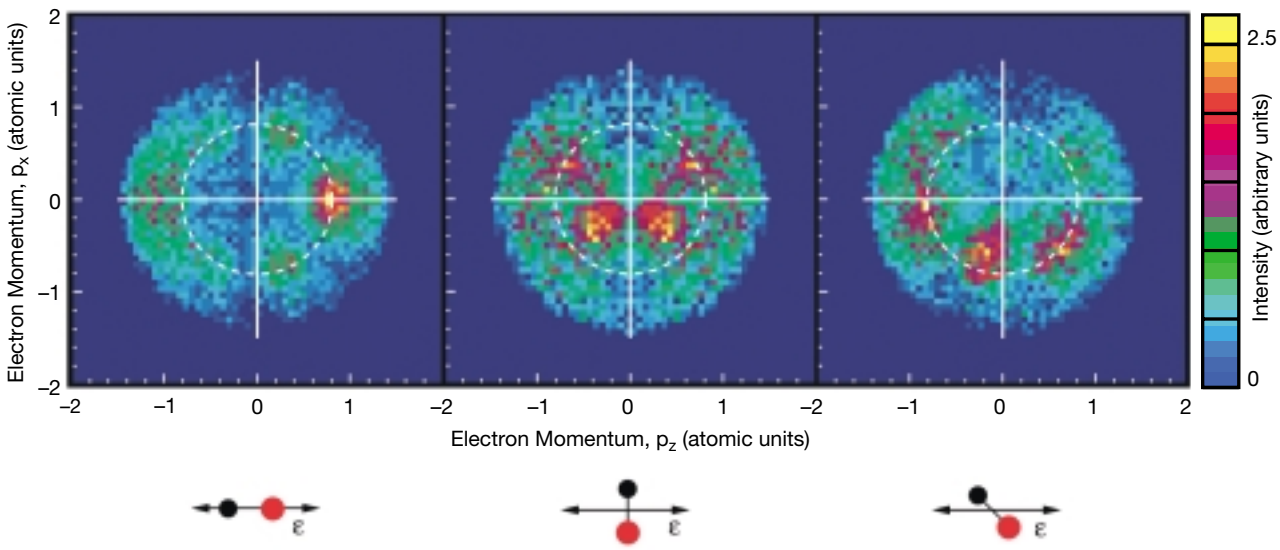

Figure 2 Electron momentum maps for three different molecular orientations with respect to the direction of the photon polarization, ε. *Black circle,* carbon atom; *red circle,* oxygen atom.

intensity is indicated by color (Figure 2). The resulting pictures are rich in physics: one sees the outgoing wave resonating in the molecular potential at a certain energy (i.e., at a constant radius) and displaying interference from reflection off of the oxygen partner ("bright" spot when the molecular axis is aligned with the x-ray polarization, ε). An alternative depiction, in polar coordinates, lets us compare the experimental photoelectron momentum data to calculations based on linear combinations of partial waves (Figure 3). The high fidelity of the fitted curves to the data demonstrates that the contributions of different partial waves to the photoelectron wave can be successfully extracted from the data.

While we chose a simple ground-state molecule for this demonstration, the technique might also be used to produce time-dependent snapshots of transient species. It may be possible to map the evolution of molecular potentials by initiating a photochemical reaction with a short laser pulse and later probing the molecule with a photoelectron wave generated by a time-delayed x-ray pulse. Thus, this approach to viewing molecules is a major step forward in our ability to

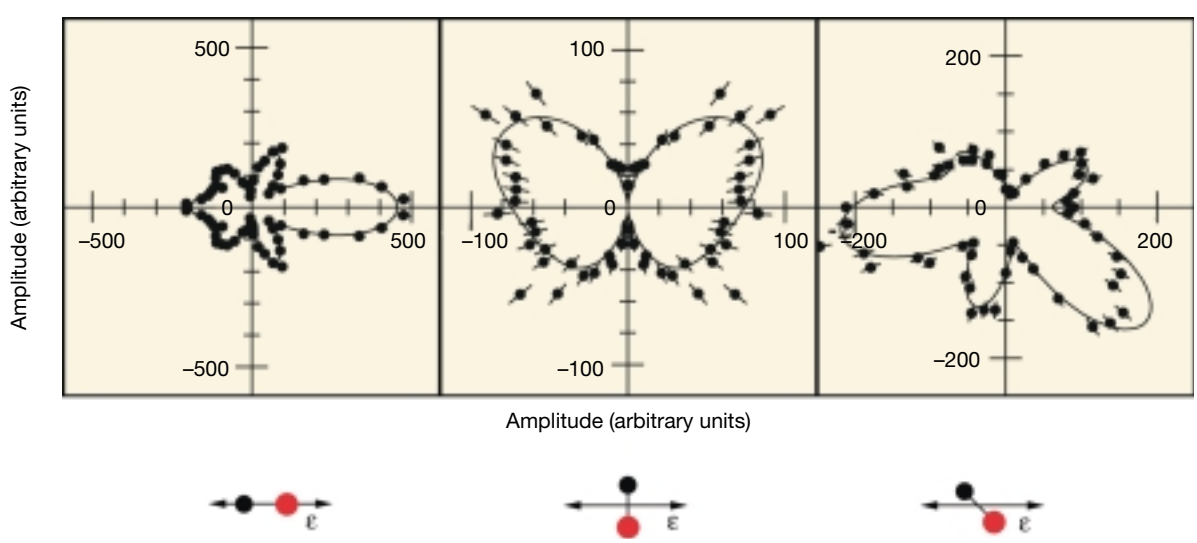

Figure 3 Comparison (in polar coordinates) of calculated and experimental angular distributions for 10.2-eV photoelectrons (corresponding to electrons at the dotted circles in Figure 2). *Black circle,* carbon atom; *red circle,* oxygen atom.

obtain comprehensive information about molecular dynamics and structure from photoelectron emission.

INVESTIGATORS

A. Landers (Western Michigan University); Th. Weber, M. Hattass, O. Jagutzki, A. Nauert, and H. Schmidt-Böcking (Universität Frankfurt); I. Ali, T. Osipov, and C.L. Cocke (Kansas State University); A. Cassimi (Université de Caen); A. Staudte (Universität Frankfurt and Berkeley Lab); M.H. Prior (Berkeley Lab); and R. Dörner (Universität Frankfurt).

FUNDING

Bundesministerium für Bildung und Forschung; Deutsche Forschungsgemeinschaft; and the U.S. Department of Energy, Office of Basic Energy Sciences.

PUBLICATION

1. A. Landers et al., "Photoelectron diffraction mapping: Molecules illuminated from within," *Phys. Rev. Lett.* **87,** 013002 (2001).

Anionic Photofragmentation of CO: A Selective Probe of Molecular Core-Level Resonances

Belying their relative simplicity, small molecules with only a few atoms display a bewildering forest of spectral signatures when beams of x rays illuminate them over a range of wavelengths. Since deciphering spectra is the key to understanding molecular behavior, any new tool that can selectively cut through the forest and classify specific spectral features is more than welcome. Stolte et al. have hit upon a way to conclusively identify hitherto elusive shape resonances—relatively broad and featureless spectral peaks that researchers widely believe to be present in molecular x-ray spectra but nonetheless find hard to pin down. The key is the fragmentation into both positively and negatively charged entities (cations and anions, respectively) that often occurs after x-ray absorption. In experiments on carbon monoxide, where a shape resonance is known to exist, the group found that the resonance does not show up when measuring the yield of oxygen anions but it does for cations. Comparing the spectra for both species thereby unmasks the shape resonance.

Shape resonances are a controversial subject among molecular spectroscopists, in part because there has been no agreed-upon way even to identify them when they occur, which is thought to be rather frequently in both gas-phase and adsorbed molecules. The work of our international team comprising researchers from the USA, Italy, Mexico, and Sweden has now resulted in the discovery of a method for verifying their presence. The team's approach, demonstrated in carbon monoxide, is to measure the yields of both cation and anion fragments above the molecular photoionization threshold. We showed that, unlike cation spectra, the anion spectra do not contain the shape resonance, whose energy is well known in this molecule. Measuring both therefore pinpointed the shape resonance.

As the x-ray photon energy scans from (say) 20 eV below to 20 eV above the photoionization threshold for 1s electrons in molecules comprising atoms with low atomic numbers and π bonding, a progression of typical spectral features appears. The sequence begins at the lower-energy end with the familiar π^* (Feshbach) resonances that are so useful in molecular fingerprinting and in calibrating monochromators, progresses through a number of Rydberg series just below threshold, and ends above threshold with overlapping features due to doubly excited (two electrons in excited states) molecules and shape resonances.

The shape resonance results from a potential barrier that temporarily prevents electrons excited in the resonance energy range from leaving the molecule (Figure 4). Their apparent simplicity, broad energy widths, and well-defined symmetries have made shape resonances a popular object of study in gas-phase molecular science and a common tool for probing

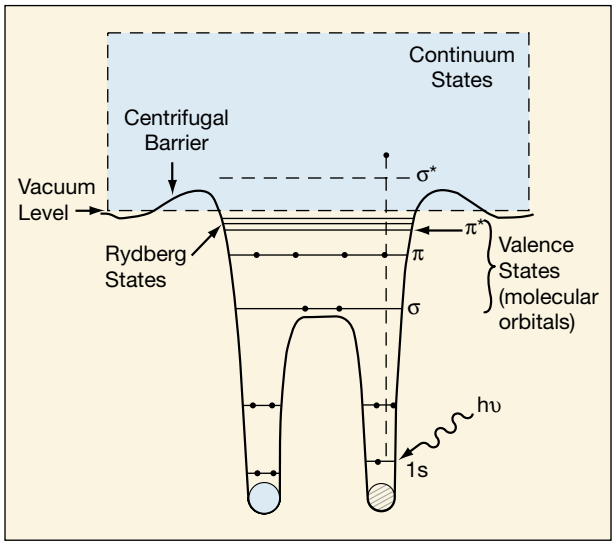

Figure 4 A σ^* shape resonance above the ionization potential results from a potential (centrifugal) barrier that temporarily prevents electrons excited in the resonance energy range from leaving the molecule.

orientations and bond lengths in molecules adsorbed on solid substrates. Unfortunately, picking out shape resonances from other spectral features is not so straightforward. This difficulty has raised questions about the validity of parameters extracted from the analysis of shape resonances. For example, peaks due to double excitation can be experimentally indistinguishable from them.

Against this background, carbon monoxide presents itself as a valuable test-bed. It displays a broad peak that is known to be due to a shape resonance and is readily distinguishable from sharper features at somewhat lower energy from doubly excited molecules. Our team extended the well-known technique of ion-yield spectroscopy to examine negatively charged ion species, as well as the commonly measured positively charged ions, both of which may be created when the molecule breaks into fragments during the decay process following x-ray excitation. The high spectral resolution and signal intensity achieved at ALS Beamline 8.0.1 made anion spectroscopy feasible.

Several pathways exist for creation of ions. These range from simple photoemission, which leaves a CO^{2+} ion, to photofragmentation, which can result in several cation species and O^- as the primary anion. Measuring the O^- production as a function of photon energy near the carbon K edge yielded a spectrum containing the various features enumerated above but with no apparent contribution from the known shape resonance (Figure 5). Detailed comparison of cation and anion spectra above the photoionization threshold conclusively demonstrated the absence of the resonance clearly visible in the cation spectra (Figure 6). Anion measurements at the oxygen K edge were only somewhat less conclusive, owing to more overlap with the region of doubly excited states.

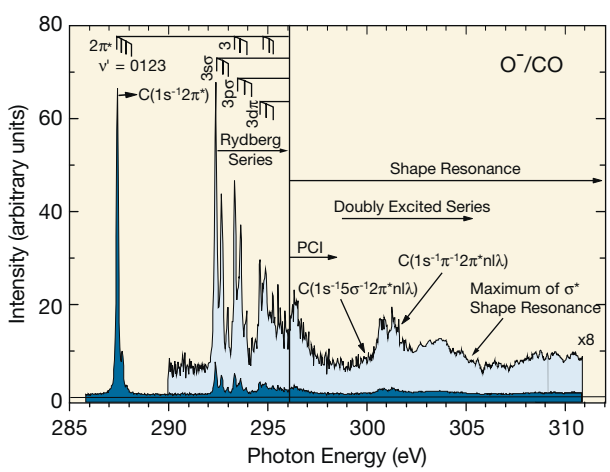

Figure 5 Partial oxygen-ion-yield spectrum at the carbon K edge of carbon monoxide shows the typical collection of spectral features, but the shape resonance is conspicuously absent.

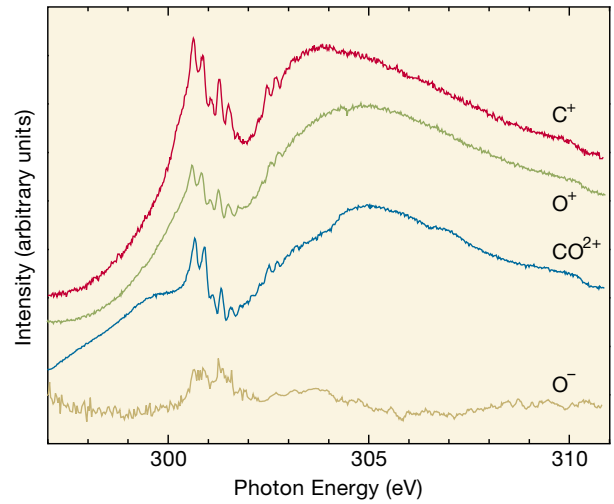

Figure 6 Detailed comparison of partial cation- and anion-yield spectra above the carbon K edge graphically demonstrates the absence in the anion spectrum of the broad shape resonance seen in the cation spectra.

The main message is that shape resonances are completely absent in anion yields. Moreover, there is nothing special about carbon monoxide, so we are confident that this new approach will apply to many small molecules, thereby providing a new tool to examine core-level resonant processes in general and sort out shape resonances in particular.

INVESTIGATORS

W.C. Stolte (University of Nevada, Las Vegas, and ALS); D.L. Hansen (Jet Propulsion Laboratory); M.N. Piancastelli (University of Rome, "Tor Vergata," and ALS); I. Dominguez Lopez (Centro Nacional de Metrologia, México); A. Rizvi and A.S. Schlachter (ALS); O. Hemmers and D.W. Lindle (University of Nevada, Las Vegas); H. Wang (Lund University, Sweden); and M.S. Lubell (City College of New York).

FUNDING

National Science Foundation; U. S. Department of Energy, Nevada Experimental Program to Stimulate Competitive Research (EPSCOR); and National Research Council.

PUBLICATION

1. W.C. Stolte et al., "Anionic photofragmentation of CO: A selective probe of core-level resonances," *Phys. Rev. Lett.* **86,** 4504 (2001).

Quantum Chaos in Helium: Transition to Chaos Observed in a Simple Quantum System

We tend to think of chaos as a state of randomness, a complex situation where chance alone ultimately determines what is going on. For physicists, chaos is more ordered than random, and it shows up in seemingly simple systems. It is defined as an extreme sensitivity to initial conditions, to the point where small changes in these conditions lead to larger and larger differences in outcomes over time, ultimately yielding wildly divergent results. The result is a dynamic system whose future behavior we cannot predict by observation of its past behavior, even though its dynamics follow a set of determined rules. Incredibly common, chaotic behavior has been noted in weather patterns, chemical reactions, and the evolution of insect populations. Studies of chaos help us to understand the behavior of earthquakes, lasers, fluids, mechanical structures, neural networks, and even biological rhythms. Püttner et al. have now observed chaos in atomic helium, which is described by quantum mechanics, thereby providing another key to understanding the dynamics of our world.

Two's a party, three's a crowd—especially in a tiny space. Two objects that exert electrostatic or gravitational forces on each other have relatively simple dynamics: the forces scale as the square of the distance between the objects. A three-body system, however, cannot be solved analytically (it is nonintegrable), which indicates that the dynamics involve a mixture of regularity and chaos. Add to that the constraints of quantum mechanics, and things get truly challenging. Now, our investigation into the transition from quantum dynamics to chaos in the spectrum of helium has shed a little bit of light on one of physics's blackest boxes—quantum chaos.

Since the work of Poincaré a century ago, the problem of three bodies interacting under their mutual gravitational forces (such as the earth, moon, and sun) has been known to exhibit a mixture of classical and chaotic dynamics. A system of three charged particles should have similar dynamics (within a sign), even in very small systems. But as yet, scientists don't know how to reconcile chaos with a quantum-mechanical view of the universe. Classical dynamics allows for the chaotic motion of three bodies, because the mechanics can be described with nonlinear equations of motion; quantum mechanics, however, does not have this way to account for chaos, because the Schrödinger equation is linear. Furthermore, the quantum states of the helium atom, the prototypical three-body charged- particle system, occur in seemingly regular progressions, labeled by sets of quantum numbers. How, then, can classical chaos and quantum mechanics be reconciled? What are the manifestations of the underlying classical chaos in the quantum spectrum of helium?

To answer these questions, our group has used Beamline 9.0.1 (now Beamline 10.0.1) along with theoretical modeling to search for quantum chaos in the photoabsorption spectrum of helium—and we've found it. The high brightness on this undulator beamline allowed the resolution (about 2 meV) necessary to distinguish tightly spaced states near helium's double-ionization threshold. Electrons in these high-energy, doubly excited states are known to show more classical behavior than those lying closer to the nucleus. But the states are so close together that a third-generation light source is needed to resolve them. The resulting spectrum was compared to a new theoretical model based on a random matrix approach to chaotic systems (Figure 7). Agreement between the model and the data was excellent, allowing us to extend the statistical analysis even to states above those seen in the experimental spectrum.

The electronic states of doubly excited helium can be labeled as N,K_n, where N is the principal quantum number of the inner electron, n is that of the outer electron, and K is the angular correlation between the two. States with the same N

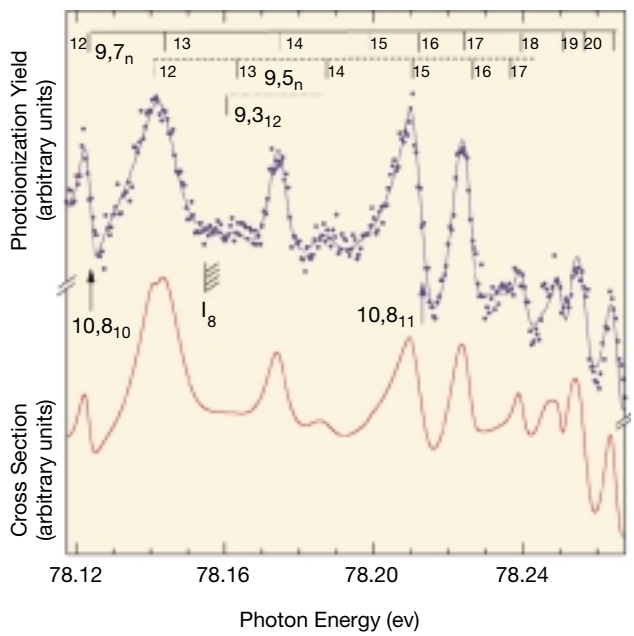

Figure 7 Photoabsorption spectrum of helium gas after double-electron excitation. *Blue,* experimental spectrum *(data points)* and best fit *(solid line through the data points). Red,* spectrum calculated from theoretical model.

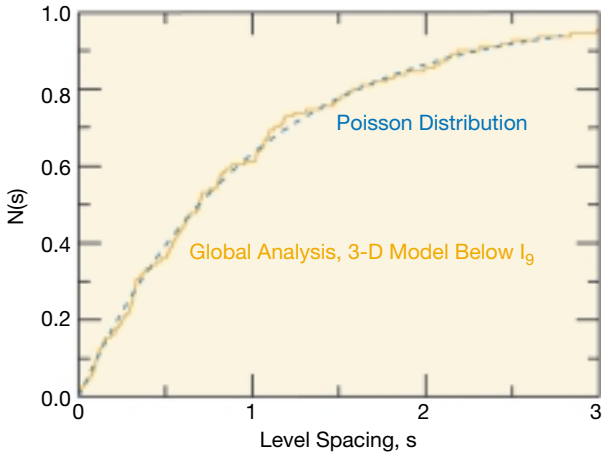

Figure 8 Cumulative distribution of nearest-neighbor spacings for the $^1P^o$ states of helium below I_9. The data agree very well with a cumulative Poisson distribution *(dashed blue line),* which is indicative of a nonchaotic system.

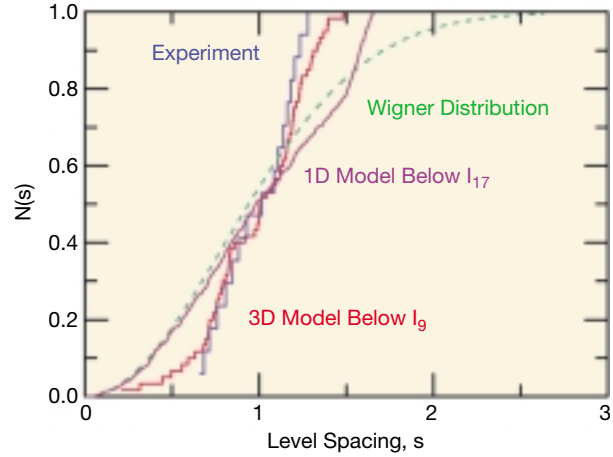

Figure 9 Cumulative distributions of nearest-neighbor spacings for the $^1P^o$ states of helium, analyzed individually for each series associated with a given value of N–K. *Blue,* distribution derived from experiment; *red,* best fit from three-dimensional model calculations for states below I_9; *purple,* best fit from one-dimensional model calculations for states below I_{17}; *dashed green line,* Wigner distribution. The marked tendency toward a Wigner distribution as higher lying states are included indicates the onset of chaos.

converge to an ionization threshold, I_N. We found that, as the electron energies approach the ionization threshold for electrons with higher N, the statistical properties of the spacing between neighboring energy levels clearly display a transition toward quantum chaos. Where $I_N > 4$, the N–1 series begins to be perturbed by higher series. Where $I_N > 8$, the effect is strong enough that traditional quantum numbers can no longer describe the dynamics. Statistical analyses also showed that, as I_N increases, plots of the spacings between nearest-neighbor states move from being best described by a Poisson distribution (associated with regular systems, Figure 8) to more closely approximating a Wigner distribution (associated with chaotic systems, Figure 9). This observation of the onset of chaotic dynamics in a simple three-body system shows, for the first time, how the underlying classical chaos manifests in a simple and well-studied quantum system.

INVESTIGATORS

R. Püttner, M. Domke, M. Martins, and G. Kaindl (Freie Universität Berlin); B. Grémaud and D. Delande (Université Pierre et Marie Curie); and A.S. Schlachter (ALS).

FUNDING

Deutsche Forschungsgemeinschaft, Bunderminister für Bildung und Forschung, and Centre National de la Recherche Scientifique (CNRS).

PUBLICATION

1. R. Püttner et al., "Statistical properties of inter-series mixing in helium: From integrability to chaos," *Phys. Rev. Lett.* **86**, 3747 (2001).

Quantifying Relativistic Interactions in Photoionization from the Polarization of Ionic Fluorescence

Are the electrons in atoms and molecules loners or team players? Sometimes the electrons behave like noninteracting entities that go their own ways (single-electron phenomena), but in other instances, they act together in an organized way (multielectron phenomena). When an energetic x ray is absorbed by an atom, it transfers all its energy and angular momentum to just one of the atom's electrons. This electron may keep these quantities to itself or share them with its neighbors. Physicists customarily study the sharing process by examining those electrons that receive enough energy to be ejected from the atom and the positively charged "photoion" left behind. Jaecks et al. have added a new twist to this old photoionization formula by measuring the polarization properties of the visible light emitted when the photoion loses some of its extra energy. This new experimental method and the theoretical analysis of the data enable scientists to obtain information about collective electron behavior that cannot be efficiently obtained with traditional techniques.

One of the current goals of atomic and molecular physics is to quantify the degree and nature of organized motion of

electrons in dynamic processes. Studying photoionization is an effective method of gaining insight about the measurable consequences of such organized motion in isolated atoms. Because a photon interacts with only a single electron, any multielectron phenomena must result from dynamic inter-electron interactions. Historically, measurements of the properties of the emitted electrons, e.g., the energy dependence of the total and differential photoionization cross-sections and the angular and spin distributions of the photoelectrons, have allowed physicists to identify, quantify, and explain much of the multielectron photoionization dynamics of isolated atoms.

In our work, we have developed a new paradigm beyond the measurements of these photoelectron parameters. In this new procedure, we measure both linear and circular polarization of visible fluorescent light emitted by the residual ions that are photoionized by circularly polarized vacuum ultraviolet (VUV) radiation. The analysis of the polarization of the fluorescence leads to information about the photoionization dynamics that cannot be obtained with traditional techniques.

We photoionized argon in the energy range (35.5 to 37 eV) of double excitations of the outer 3p electrons with circularly polarized VUV radiation. The measured linear and circular polarization of the visible fluorescence from the excited residual ion carries away information about how the absorbed circularly polarized photon's angular momentum is shared among different electrons of the atom. By using the remarkable quantum dependence between the angular-momentum properties of the photoelectron and those of the residual photoion, even when they are infinitely separated, we determined the partial-wave probabilities of the emitted photoelectron.

There are several key experimental requirements for our method. One needs highly focused, circularly polarized synchrotron radiation with high spectral resolution and high brightness. Since our method is based on how the single unit of angular momentum is shared by the ionic electrons and the photoelectron, it is important to unambiguously specify the direction of the photon's angular momentum, which requires the use of circularly polarized radiation. On ALS Beamline 10.0.1, we installed and characterized a quarter-wave phase retarder that converts the linearly polarized synchrotron radiation into circularly polarized radiation. We verified that the retarder transformed the linearly polarized VUV radiation from the beamline undulator into 99.7% circularly polarized radiation in the energy range of our experiments. The transmission efficiency of the retarder is typically 1%.

We used narrow-band interference filters to unambiguously determine the fine-structure-resolved ionic states that emit the characteristic fluorescence. When the residual ion is in the $Ar^{+}\{3p^{4}[^{3}P]4p\ ^{2}P^{o}_{1/2}\}$ state, conservation of angular momentum and parity laws restrict the allowed partial waves of the photoelectron to s and d partial waves with total angular momentum of 1/2 and 3/2, respectively. Figure 10 shows the probability of $s_{1/2}$ partial waves as a function of ionizing photon energy.

Before the absorption of the circularly polarized photon, the argon ground state has no spin. Our analytical procedures allow us to determine the z-components of the angular momenta of the residual excited ion and the photoelectron. Our analysis surprisingly shows that, after the absorption, the expectation value for the z-component of the total spin of the residual ion–photoelectron system is nonzero. Since the absorption of the photon cannot alter the total spin of the system, we conclude that the nonzero net spin polarization of the system must result from spin-dependent relativistic interactions.

In summary, we have developed a novel technique for quantifying the importance of spin-dependent relativistic interactions in photoionization dynamics. The application of this technique to argon has shown that these interactions are significant for the observed photoionization process.

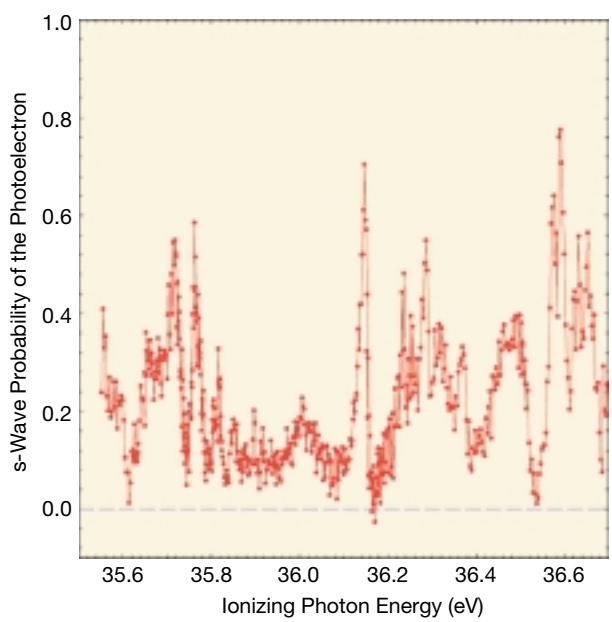

Figure 10 s partial wave probability of the photoelectron for the $h\nu + Ar\{3p^{6}\ ^{1}S_{0}\} \rightarrow (Ar^{+})^{**} \rightarrow Ar^{+}\{3p^{4}[^{3}P]4p\ ^{2}P^{o}_{1/2}\} + e^{-}$ photoionization channel.

INVESTIGATORS

D.H. Jaecks, O. Yenen (University of Nebraska-Lincoln), K.W. McLaughlin (Loras College), M.M. Sant'Anna (ALS), and E.A. Seddon (CLRC Daresbury Laboratory, UK).

FUNDING

National Science Foundation.

PUBLICATION

1. O. Yenen, K.W. McLaughlin, D.H. Jaecks, M.M. Sant'Anna, and E.A. Seddon, "Quantifying relativistic interactions in photoionization from angular momentum partitioning measurements during photoionization," *Phys. Rev. Lett.* **86,** 979 (2001).

Photoionization of Metastable O^+ Ions

Atoms are electrically neutral because the number of positively charged protons in the nucleus is the same as the number of orbiting negatively charged electrons. However, it is relatively easy to remove one or more of the loosely attached outer electrons to make a positively charged ion. In fact, it is so easy that almost all of the atoms in the universe are ionized, as found in stars, interstellar space, and the upper reaches of our Earth's atmosphere. For scientists using x rays, the main difficulty in studying ions in the laboratory is collecting enough of them in a small space to produce a strong signal. Covington et al. have developed a new apparatus in which the ions and x rays travel in opposite directions through a long tube, so that the x rays "see" a large number of ions on their trip. The subjects of their first experiments, positively charged oxygen ions, play important roles in both terrestrial and stellar atmospheres.

More than 99.9% of the atoms in the known universe exist in the ionized "plasma" state, and the light they emit and absorb carries most of our knowledge about distant stars and nebulae. A detailed understanding of the structure of ions and their interactions with photons is therefore critical to astrophysics as well as to the study of laboratory plasmas and their application to the development of fusion energy. Until recently, most of this understanding was based on theoretical calculations, with few experimental benchmarks. Our group has developed a new apparatus that will help redress the imbalance. In our first measurements, we obtained the absolute photoionization cross sections for a mixture of metastable and ground-state O^+ ions.

Photoionization of ions is a fundamental process that occurs primarily by two mechanisms. Direct photoionization is the transfer of energy from a photon to a bound electron, and it may occur at any photon energy greater than the ionization potential of the ion. Indirect photoionization may be viewed as a two-step process involving the excitation of the ion's electronic core, creating an unstable state that relaxes by

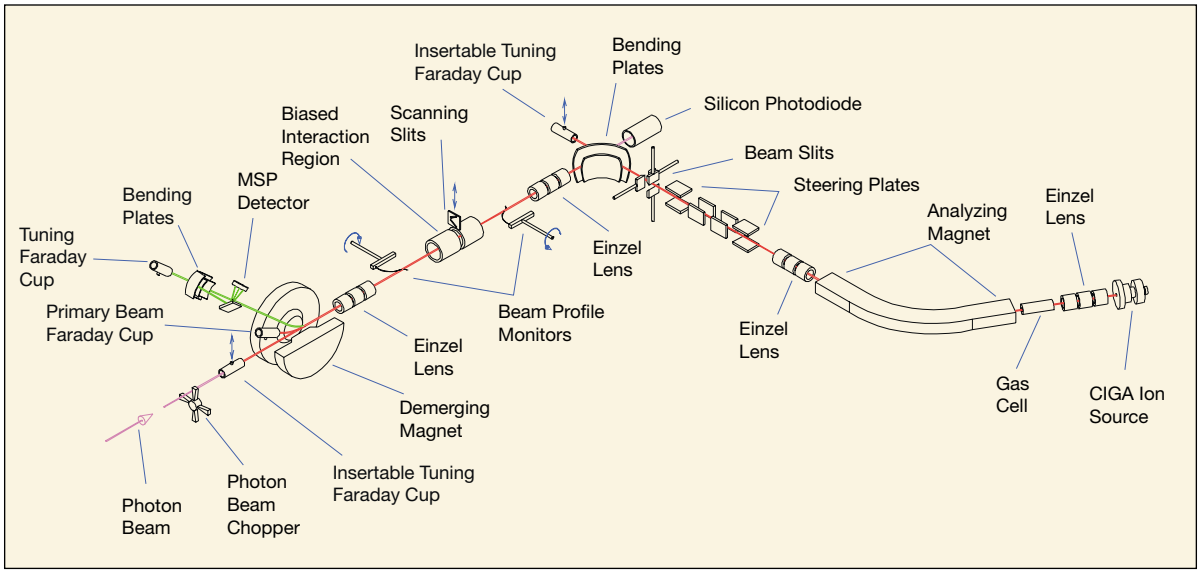

Figure 11 Schematic diagram of the ion-photon-beam endstation at ALS Beamline 10.0.1, in which a fast ion beam is merged with a counterpropagating photon beam whose energy can be continuously scanned for photoionization measurements.

ejecting an electron. Since the photon's energy is completely absorbed by the ion in the initial step, indirect ionization may occur only at discrete photon energies that exceed the ionization potential and that correspond to differences between energy levels of the ion. It is therefore a resonant process, whereas direct photoionization is a nonresonant process.

The total ionization probability is represented by the photoionization cross-section, which corresponds to a superposition of the direct and indirect mechanisms. The probabilities for these two processes may interfere, producing characteristic ionization profiles with changing photon energy. Thus, by uncovering the energies, widths, and shapes of these resonances, photons provide a powerful probe of the internal electronic structure and dynamics of ions.

Oxygen is the third most abundant element in the universe, and its ions play important roles in terrestrial and stellar atmospheres. Long-lived metastable states of positively charged oxygen ions (O^+) are produced by photoionization of oxygen atoms in the F-region of the earth's ionosphere and are known to strongly influence the chemistry of the thermosphere. Metastable states of O^+ are abundant in laboratory electrical-discharge sources, ion sources, and beams.

The high brightness and high spectral resolution available at the ALS in the VUV spectral region have made possible the first absolute measurements of photoionization of a metastable ion, O^+. Our experiments were carried out at undulator Beamline 10.0.1, where there is a newly developed ion-photon-beam endstation (Figure 11). In this station, a fast O^+ ion beam was merged with a counterpropagating photon beam whose energy could be continuously scanned. Photoionization was studied by separating and counting the number of fast O^{2+} photoion products while simultaneously measuring the ion and photon beam fluxes. We measured the initial metastable-state fraction (57%) in an independent experiment.

We compared the absolute photoionization cross-section measurements for a mixture of metastable and ground-state O^+ ions with the predictions of two independent theoretical calculations representative of the current state of the art (Figure 12). The ionization potential of ground-state (^4S) O^+ ions is 35.12 eV. Therefore the measurements below that energy must correspond solely to metastable (^2P and ^2D) O^+ ions. The theoretical results have been multiplied by the measured metastable and ground-state fractions and convoluted with a Gaussian photon energy distribution of width 17 meV to match the energy resolution of the experiment. While there is correspondence between the energy positions

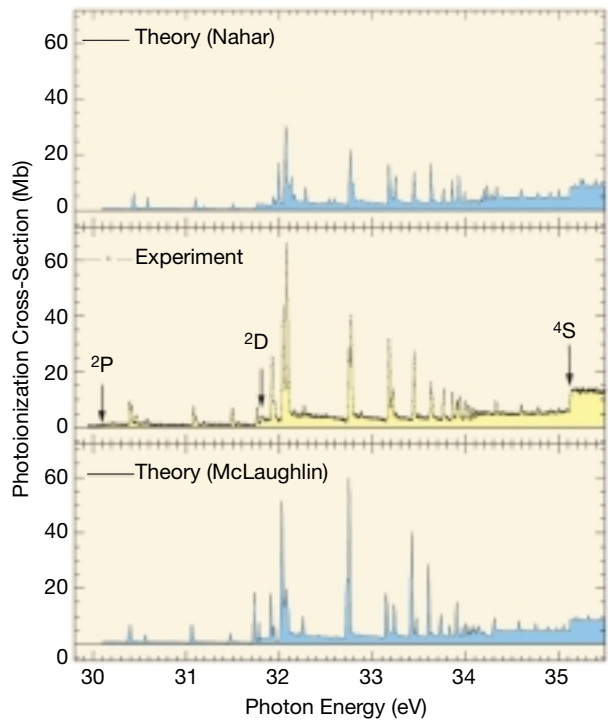

Figure 12 Comparison of experimentally measured photoionization cross-section and two theoretical models for photoionization of a mixture of metastable and ground-state O^+ ions. The energy resolution is 0.017 eV.

and strengths of some of the resonances, the differences indicate sensitivity of the theory to the set of mathematical functions that represent the electronic states of O^+.

INVESTIGATORS

A.M. Covington, A. Aguilar, I.R. Covington, M F. Gharaibeh, C.A. Shirley, and R.A. Phaneuf (University of Nevada, Reno); I. Álvarez, C. Cisneros, and G. Hinojosa (Universidad Nacional Autónoma de México, México); J.D. Bozek, I. Dominguez, M.M. Sant'Anna, and A.S. Schlachter (ALS); N. Berrah (Western Michigan University); S.N. Nahar (Ohio State University); and B.M. McLaughlin (Harvard Smithsonian Center for Astrophysics).

FUNDING

U.S. Department of Energy, Office of Basic Energy Sciences and Nevada Experimental Program to Stimulate Competitive Research (EPSCOR); National Science Foundation, Consejo Nacional de Ciencia y Tecnología, México; Dirección General de Asuntos del Personal Académico, Universidad Nacional Autónoma de México;. Conselho Nacional de Desenvolvimento Científico e

Tecnológico, Brazil; Ohio Supercomputer Center; Engineering and Physical Sciences Research Council, United Kingdom; and Institute for Theoretical Atomic and Molecular Physics, Harvard Smithsonian Center for Astrophysics.

PUBLICATION

A.M. Covington et al., "Photoionization of metastable O^+ ions: Experiment and theory," *Phys. Rev. Lett.* **87**, 243002 (2001).

K-Shell Photodetachment of Negative Ions: Li^-

Negative ions are formerly neutral atoms to which an electron has been added. While it's comparatively easy to make a positive ion by stripping electrons away from an atom, making an extra electron stick is a bit trickier. It is worthwhile to make the effort, however, because ions, including the negative variety, are so widespread throughout the universe. A successful understanding of the inner life of ions forms a foundation for scientists to use in other fields, such as astrophysics, atmospheric science, and plasma physics (where plasma refers to a collection of ions and electrons). An additional benefit of studying negative ions is that they only exist because of the correlated motion of multiple electrons in the ion, a fact that makes them particularly valuable for study of the effects of one electron on another. Berrah et al. have contributed new data to this field by studying how absorption of an x ray results in the detachment of two electrons from a singly charged negative lithium ion.

Investigation of the properties and dynamics of negative ions provides several valuable insights to the general problem of the correlated motion of electrons in many-particle systems, such as heavy atoms, molecules, clusters, and solids. In particular, photoexcitation and photodetachment processes of negative ions stand out as an extremely sensitive probe and theoretical test-bed for electron–electron interactions because of the weak coupling between the photons and the target electrons. While it has long been known that negative ions only exist because of electron correlation, it has usually been thought that it is correlation of the valence shell electrons that underlies negative-ion formation. In contrast, we have now shown that the correlation involves all four of the electrons of Li^-.

In the past, outer-shell resonance structures in the photodetachment cross section of Li^- have been investigated both experimentally and theoretically. However, up until a very recent calculation of K-shell photodetachment in Li^-, no published work of any kind on inner-shell photodetachment of negative ions has been available. In particular, there has been no publication of experimental results. With the advent of third-generation synchrotron light sources, it is now possible to experimentally investigate inner-shell processes in extremely tenuous negative ion targets.

Our experiment was performed at ALS undulator Beamline 10.0.1. Li^- ions produced by means of a cesium sputtering source were used in the photon-ion experimental apparatus described in the previous highlight. We have measured and calculated dramatic structure in the photodetachment

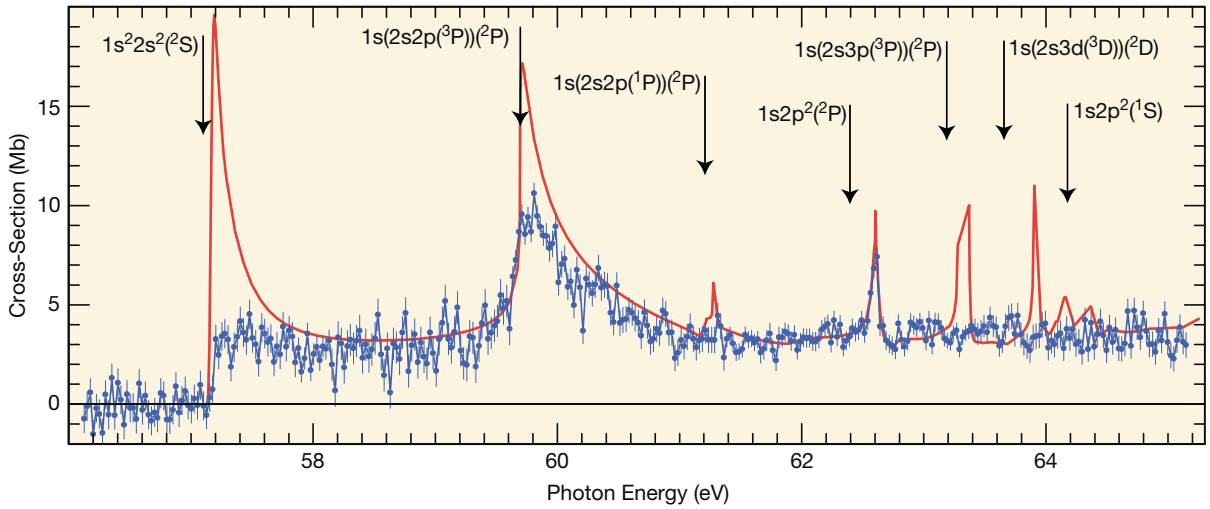

Figure 13 Total double-photodetachment cross-section of Li^- giving rise to Li^+ in the vicinity of the 1s threshold. The solid curve is the R-matrix calculation, and the dots with error bars are the experimental data normalized to the calculated value at 62 eV. The arrows indicate neutral Li thresholds.

cross-section of the Li^- K shell (Figure 13). This structure stands in stark contrast to the structureless, slowly decreasing 1s photoionization cross-sections of Li and Li^+. The photodetachment process leads to a core-excited state of Li which decays predominantly to the Li^+ ion (Figure 14).

The demonstration of four-electron correlation is unambiguous because inner-shell photoionization of Li or Li^+ in this energy range is structureless, whereas the Li^- spectrum is clearly structured by a variety of negative ion resonances, as shown in Figure 13. The agreement between measured and calculated Li^+ ion spectra is good in some energy regions but only fair in others, indicating the complex dynamics even in a simple four-electron system. Our data also agrees well with that from a similar experiment conducted recently by another group.

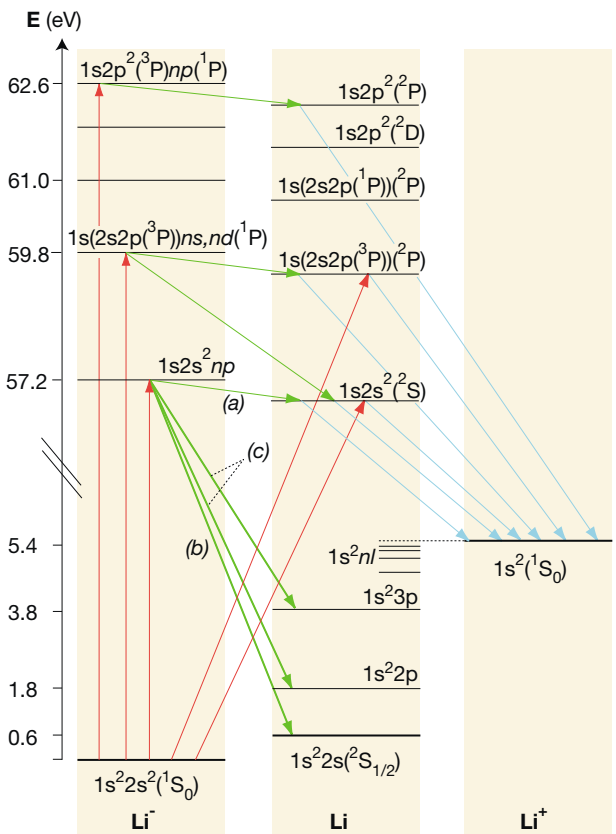

Figure 14 Schematic energy level diagrams for Li^-, Li, and Li^+. The arrows indicate some of the possible decay channels for the excited Li^- ion.

We hope that the investigation of inner-shell photoexcitation processes in negative ions will offer a new perspective for a fundamental understanding of strongly correlated systems such as nanostructures and superconducting materials. However, the impact of this finding extends beyond condensed-matter science. For example, negative ions are produced and destroyed in dilute plasmas in the outer atmospheres of stars (thus contributing to stellar opacity) as well as in interstellar space and in cold molecular clouds. Because ionic-photoionization processes have applications in fields including atmospheric science, astrophysics, and plasma physics, photoexcitation studies can be considered enabling science for these disciplines.

INVESTIGATORS

N. Berrah, A.A. Wills, G. Turri, and S.M. Ferguson (Western Michigan University); J.D. Bozek, G. Turri, G. Ackerman, and B. Rude (ALS); H.-L. Zhou and S.T. Manson (Georgia State University); N.D. Gibson and C.W. Walter (Denison University); L. VoKy (DAMAP, UMR 8588 du CNRS, France) and A. Hibbert (Queen's University of Belfast, UK).

FUNDING

U.S. Department of Energy, Office of Basic Energy Sciences; National Science Foundation; and National Aeronautics and Space Administration.

PUBLICATION

1. N. Berrah et al., "K-shell photodetachment of Li^-: Experiment and theory," *Phys. Rev. Lett.* **87**, 253002 (2001).

Chemical Dynamics

Observation of Accurate Ion-Dissociation Thresholds in Pulsed-Field Ionization–Photoelectron Studies

One of the most important parameters for molecules and molecular ions (molecules with one or more electrons removed) is the energy it takes to break a single chemical bond, resulting in molecular fragmentation. Dissociation of this type is one of the most basic chemical reactions and is ubiquitous in nature, not only in our day-to-day world but also in the distant reaches of interstellar space, which remarkably is home to a large number of molecules. One way to obtain accurate bond-dissociation energies is by illuminating the molecules or ions with a bright beam of vacuum-ultraviolet (short-wavelength) light and measuring quantities from which the bond-dissociation energy can be calculated, such as the longest wavelength of light that will generate the formation of molecular fragments. Weitzel et al. have now shown how to use vacuum-ultraviolet light in a new way. They used a sophisticated new technique previously used to measure the energy needed to remove an electron from a molecule (ionization energy) to obtain highly accurate values of the dissociation threshold, also known as the appearance energy.

A major technique for research in physical sciences, photoionization–photoelectron spectroscopy allows scientists to obtain ionization energies (IEs) and ion-dissociation thresholds or appearance energies (AEs), from which bond-dissociation energies for neutral molecules and for cations can be deduced. Recent developments in vacuum-ultraviolet (VUV) lasers and third-generation synchrotron sources, together with the introduction of pulsed-field ionization (PFI) techniques, have revolutionized this field by significantly improving the energy resolution.

For many simple molecules, the PFI–photoelectron (PFI–PE) method allows the measurement of rotationally resolved photoelectron spectra, yielding definitive IEs with uncertainties on the order of 0.5 meV (4 cm^{-1}). Here, we show for the first time that highly accurate 0 K (ground state) AE values for a range of molecules can also be determined in PFI–PE studies.

The recent successful implementation of PFI schemes that use the high-resolution VUV synchrotron radiation at the ALS has made possible the routine examination of molecular dissociative photoionization processes by means of PFI techniques. The PFI–PE experiments presented here were conducted at chemical dynamics Beamline 9.0.2.2 with the ALS operating in multibunch mode with a dark gap of 144 ns. Excited parent species in high-n (n>100) Rydberg states, formed by VUV excitation of the supersonic-beam sample are field ionized by an electric field pulse (height ≈ 1.5 V/cm, width ≈ 40 ns) applied in the dark gap. Electrons formed in this way are selected in a time-of-flight spectrometer with a detection time gate.

As a first example, we show in Figure 1 the PFI–PE spectrum for CH_4 measured in the region of 14.25–14.40 eV. The most distinctive feature discovered in the spectrum is the sharp steplike feature at 14.323 eV. In recent PFI–PE–photoion coincidence (PFI–PEPICO) studies at the chemical dynamics beamline, we examined the formation of CH_3^+ from CH_4 near its threshold. The breakdown curves obtained from these experiments for CH_3^+ and CH_4^+ are also presented in Figure 1 for comparison with the PFI–PE spectrum of CH_4. The 0 K AE for CH_3^+ was determined to be 14.323±0.001 eV from the disappearance energy of the parent CH_4^+ ion, i.e., the lowest energy at which the branching ratio for CH_4^+ becomes zero.

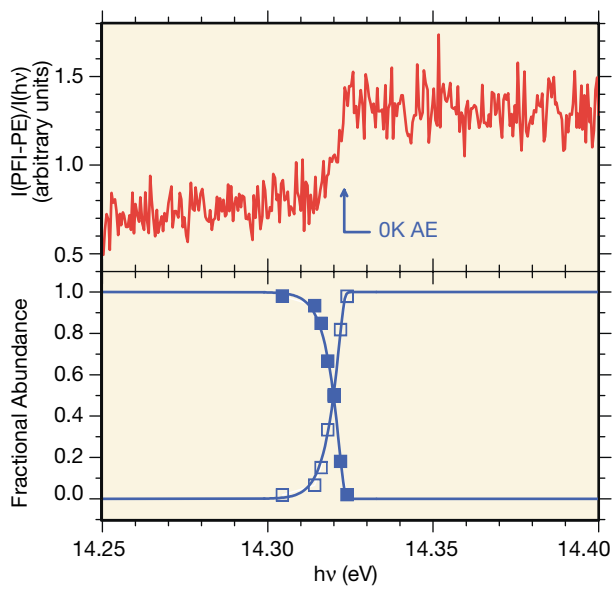

Figure 1 Comparison of the PFI–PE spectrum and breakdown diagram for CH_4 in the energy range of 14.25–14.44 eV. *Top,* PFI–PE spectrum for CH_4. I(PFI–PE) and I(hν) represent the PFI–PE and VUV intensity, respectively. The arrow marks the 0 K AE for CH_3^+. *Bottom,* the breakdown curves for CH_3^+ *(open squares)* and CH_4^+ *(solid squares).*

The comparison of the PFI–PE spectrum and the breakdown diagram of CH_4 reveals excellent correlation between the step observed and the 0 K AE for CH_3^+. The step in the PFI–PE spectrum occurs because photoexcited CH_4^* molecules in high-*n* Rydberg states predominantly decay by autoionization below the dissociation threshold but decay by fragmentation above the threshold. Since the latter process leads to CH_3^* molecules below the first IE, the overall PFI–PE signal sharply increases at the dissociation threshold.

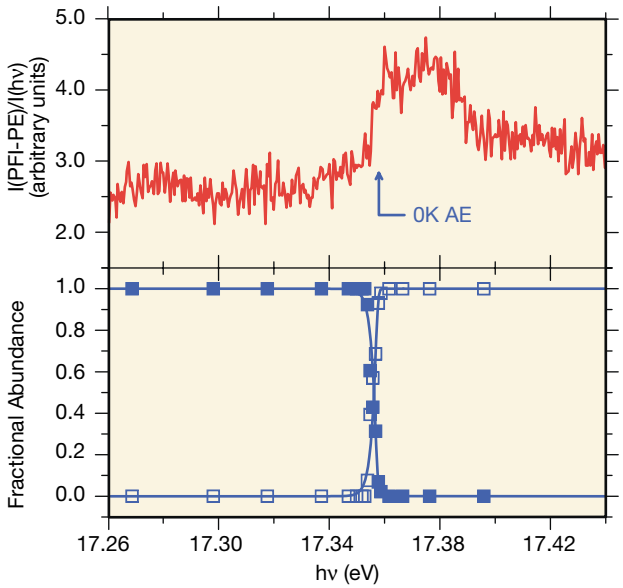

Figure 2 Comparison of the PFI–PE spectrum and breakdown diagram for C_2H_2 in the energy range of 17.26–17.40 eV. *Top,* PFI–PE spectrum for C_2H_2. I(PFI–PE) and I(hν) represent the PFI–PE and VUV intensity, respectively. The arrow marks the 0 K AE for C_2H^+. *Bottom,* the breakdown curves for C_2H^+ *(open squares)* and $C_2H_2^+$ *(solid squares).*

This mechanism is operative for all molecules for which fragmentation at the threshold is fast compared to the time scale of the experiment (a few hundred nanoseconds). Consequently, the step in the PFI–PE spectrum is also observed for acetylene molecules (see Figure 2). However, no step is observed for molecules like C_2H_4, for which the fragmentation rate constant is known to be on the order of 10^5 s^{-1}.

In summary, we report here the first observation of a step in the PFI–PE spectrum of CH_4 and C_2H_2 at the 0 K AE for CH_3^+ and $C_2H_2^+$ and have established the mechanism for step formation. This observation in PFI–PE measurements, together with the breakdown curves obtained in PFI–PEPICO studies, can provide unambiguous 0 K AE values for the dissociation reactions involved, which in turn can yield highly accurate energetic information for simple neutrals and cations.

INVESTIGATORS

K.-M. Weitzel and M. Malow (Freie Universität Berlin, Germany); G. Jarvis (Lawrence Berkeley National Laboratory), T. Baer (University of North Carolina, Chapel Hill); and Y. Song and C.Y. Ng (Iowa State University).

FUNDING

U.S. Department of Energy, Office of Basic Energy Sciences; German Science Foundation (DFG).

PUBLICATION

1. K.-M. Weitzel, G.K. Jarvis, M. Malow, T. Baer, Y. Song, and C.Y. Ng, "Observation of accurate ion dissociation thresholds in pulsed field ionization–photoelectron studies," *Phys. Rev. Lett.,* **86**, 3526 (2001).

Accelerator Physics

A New Method to Understand the Momentum Aperture in Particle Accelerators

Over the last decades, synchrotrons have evolved from rapid cycling machines, where the beam typically circulates for only fractions of a second, to a newer type generally called a storage ring. Once accelerated to their maximum energy, particles (such as electrons, protons, and atomic nuclei) in storage rings coast for long periods (several hours). Storage rings are useful in both science and technology—for example, as synchrotron light sources like the ALS, in which circulating electrons emit intense beams of x rays, or as colliders for high-energy physics, in which counter-rotating beams of particles meet head on, creating new particles in the encounters. For users of synchrotron light sources, long beam lifetimes are important, since they maximize the total amount of light produced, minimize the time lost to refilling the ring, and improve the beam stability. This accelerator development has made many advanced scientific experiments possible. Steier et al. have applied a new method for examining one of the principal causes of short lifetime, known technically as a reduced momentum aperture, and for determining what to do to lengthen the lifetime.

The motion of a particle in a storage ring can be described in terms of transverse (betatron) and longitudinal (synchrotron) motions with respect to the orbit of a reference particle. In addition, some particles may be lost from the beam because of various aperture limitations. In many cases, the momentum aperture is the dominating factor determining the beam lifetime. The momentum aperture is defined as the maximum momentum deviation that a particle can have without becoming unstable and being lost. Because of the complexity of the six-dimensional dynamics that determine the momentum aperture, up to now there have been unexplained discrepancies between the predicted and measured values of the aperture.

In those storage rings where the dominant lifetime process is Touschek scattering, the lifetime has a stronger than quadratic dependence on the momentum aperture. The Touschek lifetime at the ALS of nine hours is much shorter than the vacuum lifetime of 60 hours, so the ALS would benefit greatly from a larger momentum aperture. Therefore it is important to understand what limits the momentum aperture. We have extensively studied the particle dynamics and momentum aperture of the ALS. The knowledge gained will help improve the performance of existing light sources and help predict and optimize the performance of future storage rings.

Figure 1 gives a schematic representation of the process leading to particle loss after Touschek scattering. Because of

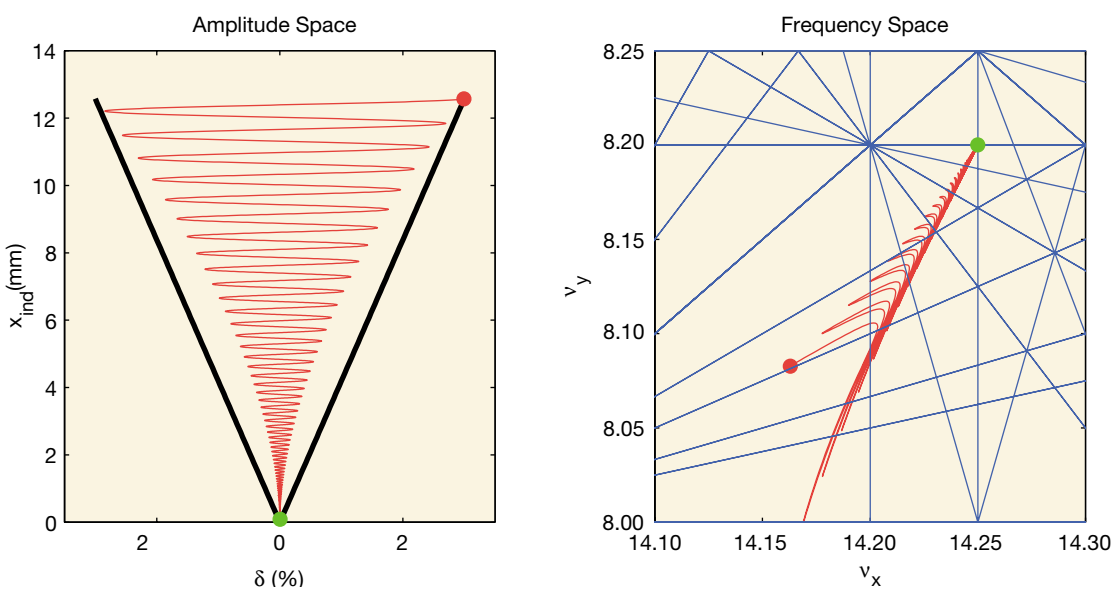

Figure 1 *Left,* schematic representation of particle behavior after Touschek scattering. From the initial scattering-induced transverse oscillation amplitude x_{ind} and energy offset δ *(red circle),* the particle oscillates in energy and amplitude *(solid line)* while damping back down to the nominal orbit *(green circle). Right,* the same particle motion tracked in the tune space, ν_x, ν_y, showing the effects of tune shifts with betatron amplitude and with energy during the damping from the scattered *(red)* to the nominal *(green)* tunes. Resonances up to the fifth order are shown.

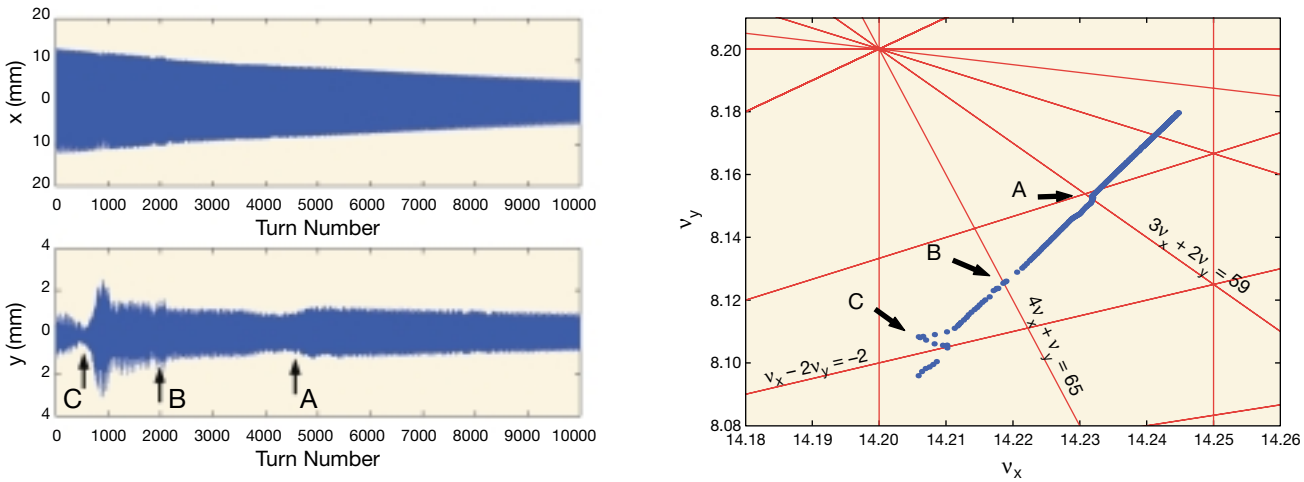

Figure 2 Tracking of a particle with synchrotron oscillations and radiation damping in configuration space *(left)* and tune space *(right)* (calculated every 300 turns). When the trajectory crosses a region with high diffusion *(regions A, B, and C),* the vertical oscillation amplitude *y* increases, and at *C,* the particle gets very close to the vacuum chamber aperture of 4 mm.

the scattering, a particle receives a certain energy offset (here, 3%). If the scattering happens at a position of the ring with dispersion, this energy change will also induce a transverse oscillation (red circle in the figure). Because of their dependence on energy (chromaticities) and betatron amplitude, the betatron tunes (i.e., the number of transverse oscillations in one revolution) of the particle change as well. Afterwards, the particle undergoes energy oscillations and slowly damps back to the nominal orbit (green circle). Because of the chromaticities and the tune shift with amplitude, during this process the particle might eventually encounter a resonance or an area of high diffusion and might be lost.

Tracking particle trajectories by using a realistic representation of the ALS lattice confirmed that this model of particle loss is correct. Figure 2 shows the trajectory of a particle tracked for 10,000 turns, including the effects of synchrotron

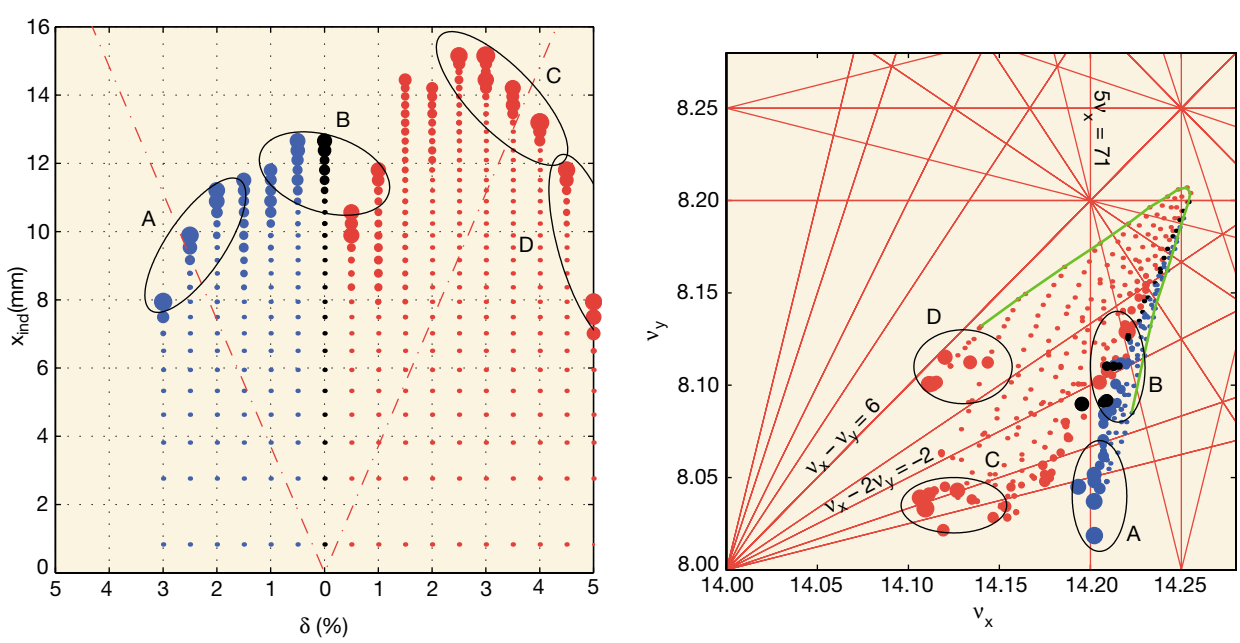

Figure 3 Measured momentum aperture in configuration space *(left)* and in tune space *(right)* for a chromaticity of ($\xi_x = 0.4$, $\xi_y = 1.4$). The sizes of the points indicate relative beam loss, and the labels point out specific resonance areas responsible for these losses. Resonances up to the fifth order are shown in tune space.

radiation on the horizontal and vertical position of the particle and on the betatron tunes. At certain times, when the tunes cross resonances, growth of the oscillation amplitude is observed. On some of those occasions, the particle got very close to the surface of the vacuum chamber (±4 mm). Particles with slightly different initial conditions can be lost.

Experimental measurements clearly show that the major limitation to the momentum aperture is the transverse beam dynamics, causing Touschek-scattered particles to eventually reach large vertical amplitudes where they are lost at the vacuum-chamber wall. The new method developed at the ALS was to analyze the measured data by using frequency-map techniques. This method allows us to understand the details of the beam loss, identifying those resonances that limit the momentum aperture.

One example for the nominal ALS lattice is shown in Figure 3, which displays the relative beam loss in the configuration space formed by energy offset and horizontal oscillation amplitude. One can clearly see the complicated structure at the boundary of the stable area. The figure also shows the same data in frequency space. By recording the tunes of the particles after they have been kicked, one can clearly identify which resonance areas are causing the beam loss. With this information, one can now understand what caused particular loss regions (compare areas A–D). The knowledge gained as a result of these measurements allows us to adjust the machine parameters to improve the lifetime. For two-bunch operation, a better choice of the linear chromaticities resulted in a 25% increase in the lifetime.

INVESTIGATORS

C. Steier, L. Nadolski, D. Robin, and Y. Wu (ALS); W. Decking (DESY, Germany); J. Laskar (Astronomie et Systèmes Dynamiques, IMC-CNRS, France).

FUNDING

This work was supported by the U.S. Department of Energy, Office of Basic Energy Sciences; Centre National de la Recherche Scientifique (France); and Bundesministerium für Bildung und Forschung (Germany).

PUBLICATION

1. C. Steier et al., "Measuring and optimizing the momentum aperture in a particle accelerator," *Phys. Rev. E* **65,** 056506 (2002).

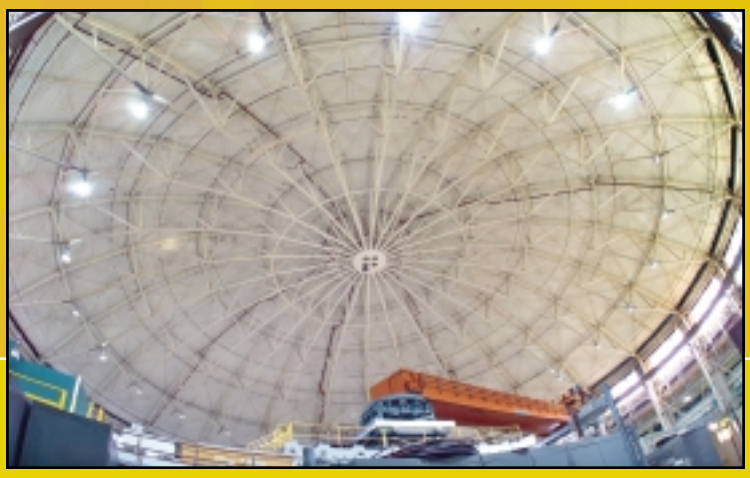

Facility Report

Keeping the Advanced Light Source running smoothly requires the efforts of many minds and many hands. In this section, the leaders of the various teams responsible for making the facility available to its users discuss the year's work. The largest group, Operations, is responsible for day-to-day running and optimization of the accelerators, while the Accelerator Physics Group works to develop the accelerator systems in order to meet the changing needs of the user community. The Experimental Systems Group engages in the design and construction of new beamlines and advocacy for new projects. The Scientific Support Group helps researchers using ALS beamlines through scientific and technical collaboration and outreach. All of these groups work closely with ALS engineering, whose work is so integral to their efforts that a separate engineering report would be redundant. The User Services Group supports the users through administrative services, logistics, and technical information. Requiring teamwork on the grandest of scales, the superbend project benefited from the talents of all the ALS groups. We therefore begin with this most inclusive of projects.

Superbends at the ALS

A Perfect Fit

One by one, the pieces fell into place. Slowly but surely, the story lines converged. The development of superconducting bend magnets ("superbends"), intended to expand the capabilities of the ALS in general, dovetailed neatly with the extraordinary growth of protein crystallography research in recent years. The superbends will allow up to 12 new hard x-ray beamlines (from 7 to 40 keV) without sacrificing the quality or quantity of light available at the lower energies. This will be more than enough to accommodate the fast-growing protein crystallography community and to provide complementary diffraction, spectroscopy, and imaging capability for materials science in the higher energy range. Superbends, in other words, are tailor-made for the future of the ALS. When the superbend-enhanced ALS started up for user operations on October 4, 2001, it marked the beginning of a new era in its history. It was a testament to the vision, ingenuity, and dedication of the multitude of people who contributed over the course of many years to this resounding success story.

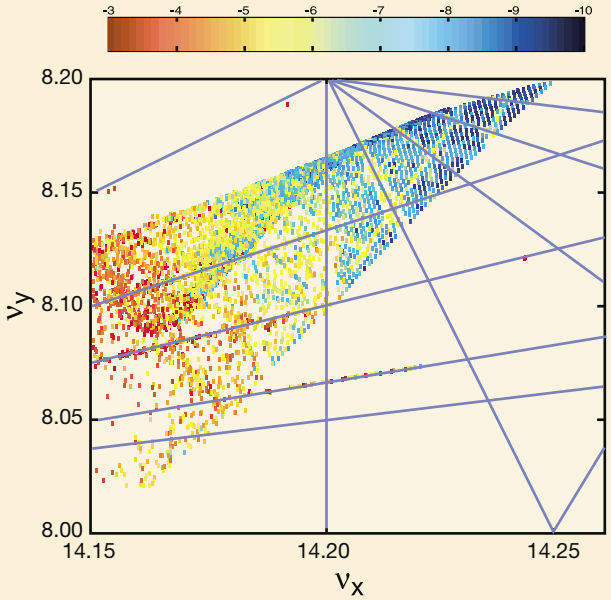

Frequency map analysis of an electron bunch. Stable electrons near the center of the bunch are represented by blue dots in the upper right; less stable electrons are represented by red dots at the lower left. This map was made after installation of the superbends, and it shows gratifyingly little change from the maps made before installation.

The first discussions on incorporating superbends into the ALS took place in 1993, between Alan Jackson, who was the ALS Accelerator Physics Group Leader at the time, and Werner Joho, who was here on sabbatical from the Paul Scherrer Institute in Switzerland. The ALS, somewhat constrained by its available acreage, was originally designed to be a 1- to 2-GeV third-generation light source, with long straight sections for undulators, optimized to serve the vacuum-ultraviolet (VUV) and soft x-ray (SXR) communities. Since then, however, light sources have been trending upwards in beam energy, generating more high-energy photons. One way for the ALS to enhance its flux at high energies would have been to use some of its scarce straight sections for higher-energy wiggler insertion devices. Jackson and Joho proposed an alternative that preserved the straight sections for high-brightness undulators: to replace the ALS's normal dipole bend magnets with superconducting dipoles that could generate higher magnetic fields within the available space.

In 1993, newly hired accelerator physicist David Robin was assigned the task of performing preliminary modeling studies to see how superbends could fit into the storage ring's magnetic lattice and to determine whether the lattice symmetry would be broken as a result. He concluded that three 5-Tesla superbends (compared to the 1.3-Tesla normal bend magnets), deflecting the electron beam through 10 degrees each, could indeed be successfully incorporated into the storage ring.

Then, beginning in 1995, Clyde Taylor of Berkeley Lab's Accelerator and Fusion Research Division (AFRD) led a Laboratory Directed Research and Development (LDRD) project to design and build a proof-of-principle superconducting magnet. By 1998, the collaboration (which included the ALS Accelerator Physics Group, the AFRD Superconducting Magnet Program, and Wang NMR, Inc.) produced a robust magnet that reached the design current and field without quenching (i.e., loss of superconductivity). The basic design, which has remained unchanged through the production phase, includes a C-shaped iron yoke with two oval-shaped poles protruding into the gap. The superconducting material consists of wire made of niobium-titanium alloy in a copper

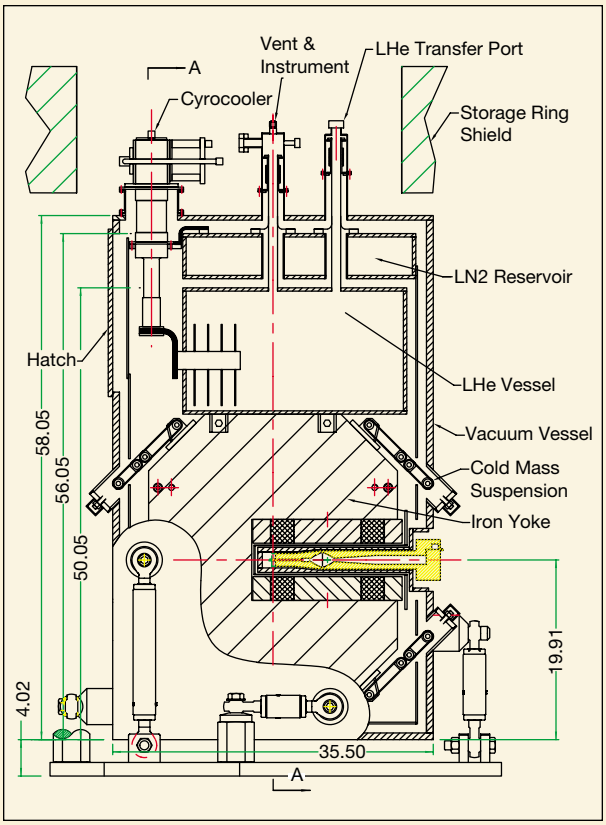

Technical drawing for a superconducting bend magnet, a design that went essentially unchanged throughout the production phase.

matrix, over a mile long, wound more than 2000 times around each pole. The operating temperature is about 4 K.

By this time, wiggler Beamline 5.0.2 of the Macromolecular Crystallography Facility (MCF) had already debuted in 1997 with spectacular success, and protein crystallographers were soon clamoring for more beam time. Howard Padmore, head of the ALS Experimental Systems Group (ESG), developed a "figure of merit" to get a handle on how well superbends would meet the needs of the protein crystallography community. He concluded that a superbend would be an excellent x-ray source for most protein crystallography projects, with performance similar to that of the existing wiggler beamline. Furthermore, the ALS had undergone the upheaval generated by the Department of Energy's Birgeneau review in 1997, which asserted (controversially) that "important scientific issues which require UV radiation have decreased in number compared to those which require hard x rays." The subsequent ALS Workshop on Scientific Directions supported the development of superbends as a way to provide higher-energy photons without diminishing support for the vital and active core VUV/SXR community.

This direction was also endorsed by the ALS Science Policy Board and the ALS Scientific Advisory Committee. Against this backdrop and with the strong support of Berkeley Lab Director Charles Shank, ALS Director Brian Kincaid made the decision to proceed with the superbend upgrade, and his successor, Daniel Chemla, made the final commitment to follow through.

The Superbend Project Team held a kickoff meeting in September 1998, with David Robin as Project Leader, Jim Krupnick as Project Manager, and Ross Schlueter as Lead Engineer. This team was solidified by the inclusion of members of the Lab's Engineering Division. Christoph Steier came aboard a year later as Lead Physicist. Over the next three years, the team worked toward making the ALS storage ring the best understood such ring in the world. In every dimension of the project, from beam dynamics to the cryosystem, from the physical layout inside the ring to the timing of the shutdowns, there was very little margin for error. Though it represented the first time that superconducting magnets

The arrival of the first superbend at the ALS on February 28, 2001.

would be retrofitted into the magnet lattice of an already operating synchrotron light source, the installation and commissioning had to proceed quickly and transparently to users of the ALS.

To study the beam dynamics, the accelerator physicists adapted an analytical technique used in astronomy called frequency mapping. This provided a way to "experiment" with the superbends' effect on beam dynamics without actually requiring the use of the storage ring. Another technical challenge was to design a reliable, efficient, and economical cryosystem capable of maintaining a 1.5-ton cold mass at 4 K with a heat leakage of less than a watt. Wang NMR was contracted to construct the superbend systems (three plus one spare). Because so much was at stake, the storage ring was studied and modeled down to the level of individual bolts and screws to ensure a smooth, problem-free installation into the very confined space within the storage ring.

One of three superbends being lifted over the shielding wall just before installation in the storage ring, August 20, 2001.

Meanwhile, on the beamline end, Alastair MacDowell, Richard Celestre, and Padmore of the ALS Experimental Systems Group and Carl Cork of the MCF had demonstrated, at Beamline 7.3.3, the feasibility of doing protein crystallography easily and cheaply at a normal bend-magnet beamline. On the strength of this demonstration, users Tom Alber and James Berger of the University of California, Berkeley (UCB), with David Agard of the University of California, San Francisco (UCSF), agreed to build "Beamline 9.1," a normal bend-magnet beamline for protein crystallography. Fortunately, it was soon recognized that, right next door in

Superbend Timeline

1993

Alan Jackson (ALS) and Werner Joho (Paul Scherrer Institut) discuss idea of incorporating superbends into the ALS.

1995

Clyde Taylor of the LBNL Superconducting Magnet Program begins LDRD project to build proof-of-principle coil.

Accelerator physicists run simulations to test effects of superbends in ALS storage ring.

2000

Mar.—First of two shutdowns for superbend installation; vacuum chambers in remaining sectors machined; QDA magnets, QFA power supplies, and new controls installed.

Dec.— Contract for first magnet system released, awarded to Wang NMR. Construction begins.

Jul.—Second technical review assesses installation plan. Positive results lead to release of UCDRD funds.

Jul.—Construction of Beamline 8.3.1 begins.

2001

Feb. 28—First superbend arrives at ALS.

Jun. 7—First light from normal-conducting magnets delivered to Beamline 8.3.1 hutch.

Jul. 6—Last superbend required for installation delivered to ALS.

Jul. 31—Superbend readiness review: full steam ahead.

Aug.—Final superbend magnet (spare) delivered to ALS.

Aug. 20–30—Superbends installed.

Sector 8, a superbend would become available that would be an even better source. The UCB/UCSF Participating Research Team (PRT) decided to take the plunge and committed to building the first-ever superbend beamline (Beamline 8.3.1). The detailed plans that were developed for this beamline were subsequently instrumental in convincing representatives of the Howard Hughes Medical Institute (HHMI), which was interested in investing in a West Coast facility for its protein crystallography investigators, to fund two more superbend beamlines in Sector 8.

The UCB/UCSF and HHMI beamlines provided the necessary momentum for other groups to follow suit: additional proposals were submitted and construction of beamlines was begun even before a single superbend had been installed. The Molecular Biology Consortium (MBC, affiliated with the University of Chicago) and a PRT from The Scripps Research

One of the superbends about to be placed around the section of vacuum chamber previously machined to accommodate it. The machining work is clearly visible above the head of the technician in light blue.

1998

Collaboration between Taylor's group, ALS accelerator physicists, and Wang NMR completes robust proof-of-principle coil that meets design goals.

Feb.—ALS Director Brian Kincaid approves project to place superbend magnets in the ALS lattice.

Jun.—Daniel Chemla takes over as ALS Director.

Sep. 23—Kickoff meeting, superbend project team formed, to be led by David Robin.

Howard Padmore and ESG group demonstrate feasibility of protein crystallography on a bend magnet. UCB/UCSF group agrees to build a bend-magnet beamline for crystallography.

1999

1998

Jun.—Technicians machine vacuum chamber in first of three sectors. Scientific Advisory Committee approves move of proposed UCB/UCSF beamline to superbend Beamline 8.3.1.

Mar./Apr.—First test of prototype cryogenic system.

Feb.—Critical Energy Working Group reports to Daniel Chemla, Chemla approves addition of three 5-Tesla superbends to ALS lattice.

Dec.—First technical review determines that the physics behind the superbend idea is sound.

Oct.—At ALS Users' Meeting, decision is made to form a user committee (the Critical Energy Working Group) to study the effects of superbends on the ALS's service to its user community.

Aug. 31, 1:00 am—First beam stored just five minutes after first injection. One hour later, 100 mA stored at 1.5 GeV. Later that day, ring ramped to 1.9 GeV.

Sep. 5—Storage ring ramped to its usual 400 mA at 1.9 GeV.

Sep. 16—Effect of new magnets in storage ring fully evaluated, no negative impact on user operations.

Oct. 4— During DOE onsite review, light delivered to Beamline 8.3.1. Berkeley Lab Director Charles Shank presses the "open shutter" button to dedicate the ALS's first superbend beamline. Scheduled superbend user operations begin.

Superbends

- extend the spectral range of the ALS to 40 keV for hard x-ray experiments
- do not degrade the high brightness of the ALS in the soft x-ray region for which the ALS was originally designed
- do not degrade other performance specs such as beam stability and lifetime
- do not require any straight sections be sacrificed to obtain high photon energies
- are already serving the first of a new set of protein crystallography beamlines

Institute have also committed to building superbend beamlines. Noncrystallography beamlines currently in the works include one for tomography and one for high-pressure research, two areas for which superbends are even more advantageous than they are for protein crystallography, because they more fully exploit the higher energies that superbends can generate. Many other areas, including microfocus diffraction and spectroscopy, would also benefit enormously through use of the superbend sources. In addition to paying for their beamlines, the PRTs contributed funds to help offset the cost of the superbends (estimated at $4.5 million). The PRTs will get 75% of the beam time on their respective beamlines, with 25% of the beam time allocated to independent investigators.

After some preparatory work during previous shutdowns, installation of the superbends began in August 2001. The initial installation plan was very tight. From August 20 to 30 (11 days including a weekend), the superbend team removed three normal bend magnets and a portion of the injection line, installed the superbends, modified cryogenic systems, and completed extensive control system upgrades. They also installed many other storage-ring items and prepared for startup with beam.

Beamline 8.3.1, the first beamline to accept light from a superbend magnet at the ALS.

The Superbend Celebration, a festive luncheon hosted by Wang NMR on the ALS patio, marked the successful completion of the project.

Commissioning proceeded much faster than expected. At the end of the first day, a current of 100 mA and an energy of 1.9 GeV were attained. At the end of the first weekend, the injection rate and beam stability were near normal. By the end of the first week, the full 400-mA beam current was ramped to 1.9 GeV, and studies of a new low-emittance lattice with a nonzero dispersion in the straight sections (designed to retain the high brightness the storage ring had without superbends) were begun. By the end of the second week, test spectra taken in some beamlines showed no change

The superbend that delivers light to Sector 12 is situated incredibly close to the injection line coming from the ALS booster ring.

in quality due to the presence of superbends. And so it went. Data taken at Beamline 8.3.1 had been used to solve a protein structure before the year's end.

Eight years in the making, with a large supporting cast of physicists, engineers, technicians, and others too numerous to list, the remarkably successful installation and commissioning of the superbends marked—not the end of the story—but the beginning of a new chapter in the history of the ALS. Well-deserved thanks go to all the Superbend Project Team members, all of whom assumed the full measure of their responsibilities in ensuring the success of the project. Their technical achievement of integrating three superbends into the ALS storage ring will permit this facility to achieve balanced growth in many areas of science, well into the future.

During the Superbend Celebration, project leader David Robin displays one of the commemorative t-shirts featuring a frequency map.

What's the Big Deal?

Because the superbends are responsible for directing the paths of the electrons circulating in the storage ring, it is essential that they work properly and continuously. Unlike straight-section insertion devices such as wigglers and undulators, superbends cannot simply be turned off in case of failure or malfunction. No other third-generation synchrotron light source has been retrofitted in this fundamental way.

The stakes were very high: the payoff would be an expanded spectrum of photons to offer users; the risks included the possibility of ruining a perfectly good light source or, at the very least, causing unacceptable down time. Needless to say, the superbends had to work right, and they had to work right away.

Superbend project leaders were bracing for up to a six-week adjustment period. Instead, thanks to extensive modeling and planning beforehand, it took less than two weeks after installation began before the machine was ramped up to full strength. Superbend Project Team Leader David Robin describes it this way: "It's as if you performed major surgery and the patient immediately got up and walked away."

The Superbend Team: Barry Bailey, Bill Baldock, Bob Benjegerdes, Alan Biocca, Paul Bish, William Brown, Terry Byrne, Dennis Calais, Mike Chin, Richard DeMarco, Mike Fahmie, Alan Geyer, Dennis Gibson, Michael Green, Joe Harkins, Dennis Hull, Susanna Jacobson, Jim Krupnick, James McDonald, Steve Marks, Paul Molinari, Bob Mueller, Laurent Nadolski, Fred Ottens, Alan Paterson, Paul Pipersky, Art Ritchie, Dave Robin, Steve Rossi, Benoit Salvant, Ross Schlueter, Christoph Steier, Clyde Taylor, Monroe Thomas, and Jon Zbasnik. Not pictured: Robert Armstrong, Loren Shalz, John Spring, Chris Timossi, Alan Wandesforde, and Tim Williams.

Operations

Ben Feinberg, *Division Deputy for Operations*

Operations and Availability

The mission of the ALS is to "support users in doing outstanding science." The most fundamental support offered to users by the ALS is delivery of high-quality beams. Thus, to best support the work of ALS researchers, the ALS operations groups make the delivery of high-quality beams their prime goal. Delivering these beams according to a published schedule along with an efficient, effective safety program allows our researchers to make maximum use of their limited beam time.

In 2001, the ALS once again maintained its exemplary operations record while making continuing improvements in beam quality and reliability. In addition, the operations groups installed the new superconducting bend magnets (superbends) to greatly expand the capacity of the program in hard x rays and also designed, constructed, and installed new beamlines for protein crystallography, which will make use of the superbends. Figure 1 shows the installation of the first superbend magnet into the storage ring, which took place during the installation shutdown in August.

The research community at the ALS has become accustomed to high operational efficiency and reliability, and it was not disappointed during this period. As shown in Figure 2, the ALS delivered beam to the users more than 96% of the time scheduled for user operations in FY2001, maintaining the excellent record of the last several years. In addition, there was significant improvement in reliability (defined as the number of completed fills versus the number of scheduled fills) over previous years. The ALS realized fewer interruptions in operation, completing nearly 90% of all scheduled fills without interruption. This was a result of early identification and correction of problems as they occurred. The Accelerator Physics section provides more information on efforts to improve beam quality and reliability.

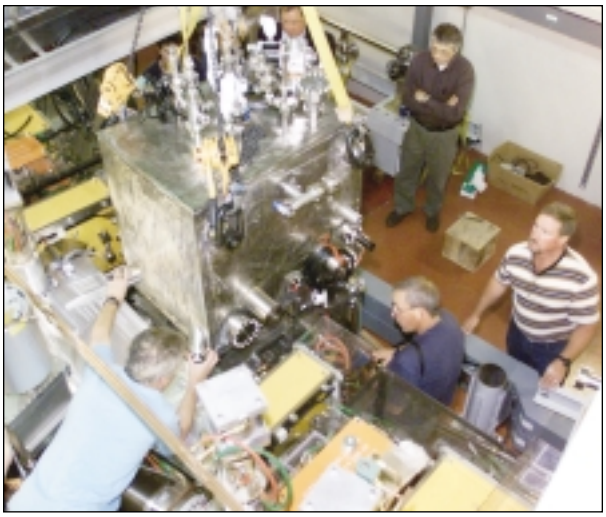

Figure 1 The first superbend magnet was installed as an integral part of the storage ring lattice in August.

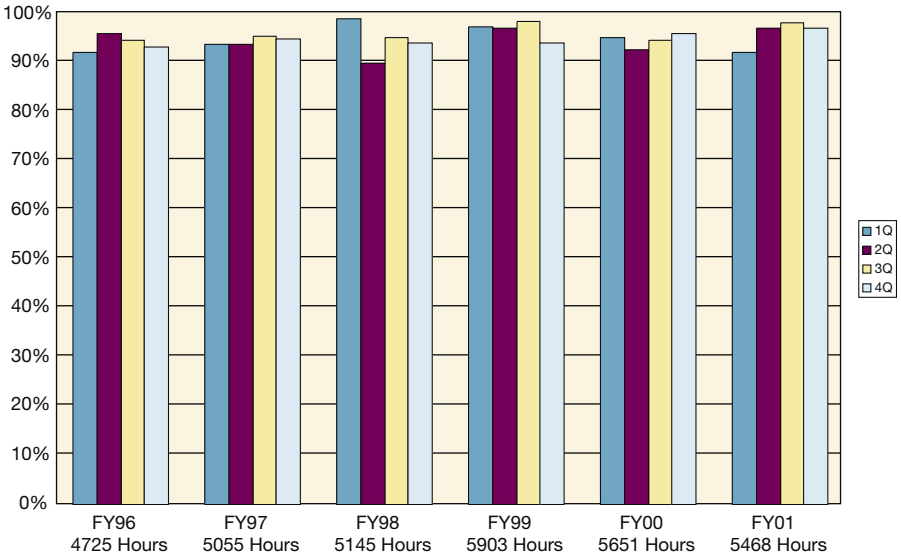

Figure 2 ALS operational availability (percentage of scheduled user beam time actually delivered).

Changes in User and Instrument Hours

The operations schedule continued with the minimal number of maintenance and installation periods in use during the last several years, although we have increased the number of "special shifts" from two to three per month, based upon user requests. This schedule has provided the maximum number of hours for user operations while allowing for needed maintenance and installation of new instrumentation. In addition to these monthly periods, this year we had one six-week installation shutdown, two weeks of which were to install the new superbend magnets and four of which were to commission the accelerator. The Accelerator Physics section provides more details on the superbend installation and commissioning. As a result of this longer installation period, the scheduled operating hours decreased from 5,651 hours in FY2000 to 5,468 hours in FY2001.

Even with the decrease in the number of scheduled operating hours, we were able to increase the number of instrument hours (user hours multiplied by the number of simultaneous beamlines that can accept beam), as shown in Figure 3. We finished the calendar year with 28 beamlines operating simultaneously, up from 24 at the end of the previous fiscal year. This increase resulted in the delivery of 135,348 instrument hours, an increase of 17% over FY2000.

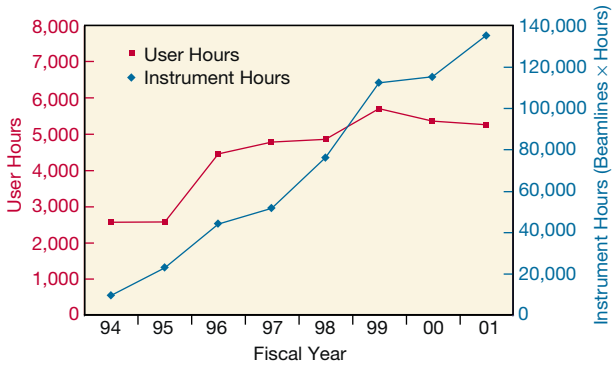

Figure 3 Number of delivered user hours and instrument hours from FY1994 through FY2001.

Facility Growth

One major shutdown was scheduled during 2001 for the installation and commissioning of new equipment. In August and September, three superbend magnets were installed and commissioned. In addition, during 2001, construction of multiple superbend beamlines was started, and one beamline was operated with the normal bend magnet in anticipation of superbend installation. This major initiative, more fully described in the special section on superbends, will greatly increase the range of science and the user base of the ALS.

Digital Controls for Superbends

The extremely tight requirements for stability and resolution in superbend control called for improvements in our control systems. The Controls Group responded by selecting and developing support for the DeviceNet field bus, and the manufacturer of the power supplies incorporated extended-precision controls directly into the supplies. This combination meets the new requirements and has been reliable in production.

Beam Stability

During this period, the horizontal orbit stability in the twelve arcs of the ALS was greatly improved by the introduction of a feedback system that adjusts the rf frequency. The feedback uses newly installed, very stable beam-position monitors, which were added in four arcs as a part of the superbend project. It compensates for changes in the ring circumference caused by several sources, including changes in insertion-device gaps (on the time scale of several seconds), changes in air or magnet-support temperatures (on the time scale of an eight-hour user fill), or seasonal changes of the accelerator ground plate (especially at the beginning and end of the rainy season). By correcting the beam orbit in the arcs, it also improves the long-term stability of the beam energy. Without the feedback, the electron beam energy could drift by as much as 0.1% over the course of a week. Now the energy stability is much better than 0.01%.

Figure 4 shows an example of the improved stability in the horizontal plane. Without rf-frequency feedback, the orbit in

one arc drifted by as much as 80 μm over the four days after startup in January 2001. With feedback over the same period in 2002, the drift was reduced to close to the noise of the beam-position monitors. With this new addition to the orbit feedback system, the orbit stability in the arcs of the ALS is now about as good as that in the straight sections.

Preparing for Fast Orbit Feedback

Increasing the quality of the beam for users includes increasing the stability. In preparation for a fast (1-kHz update rate) global orbit feedback loop, the power supplies for the storage-ring horizontal and vertical correctors have been moved to new controls. These controls were developed to meet myriad requirements, ranging from tight control of drift and noise to plug compatibility with existing cable plants. The majority of the components are off the shelf, with the exception of the input/output cards. These cards had to be designed in-house by the Instrumentation Electronics Section and manufactured by local industry to meet our stringent tolerances. The systems were deployed during the superbend shutdown. Soon the commissioning of the fast orbit feedback will begin, as we continue our ongoing improvements to the operation of the facility.

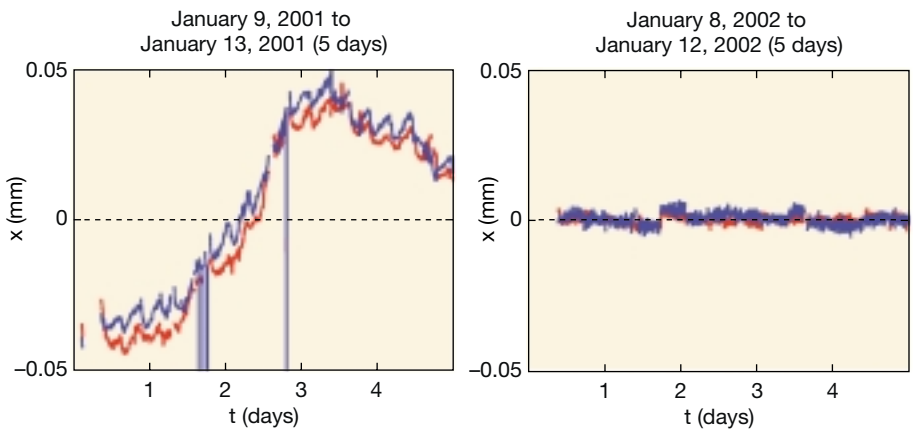

Figure 4 Horizontal orbit drift over four days in the ALS arcs, *left,* without and, *right,* with rf-frequency feedback.

Accelerator Physics

David Robin, *Accelerator Physics Group Leader*
John Byrd, *Accelerator Physics Deputy Group Leader*

Introduction

To achieve the ALS's mission, supporting its users in doing outstanding science, the ALS Accelerator Physics Group (Figure 1) plays several important roles. The first is to make certain that the ALS provides high-quality beam in a reliable manner to users. The second is to strive to understand and continually improve the performance of the facility, keeping it at the forefront of synchrotron radiation sources. The third role is to ensure that machine upgrades are implemented smoothly and with minimal adverse impact to users. The fourth is to study potential upgrades to the facility that will enhance the capabilities and capacity of the ALS. In all these roles, the Accelerator Physics Group works very closely with other groups both within the ALS and elsewhere at Berkeley Lab.

In 2001, the ALS storage ring went through a major transition with the installation of three high-field superconducting bend magnets, or superbends, to extend the wavelength of ALS-generated light up to 40 keV. The superbend project is the largest transformation of the ALS facility since the ring was commissioned in 1993. This was a very important project that brought challenges in many areas, including accelerator physics, engineering, and controls. A large fraction of the ALS Accelerator Physics Group as well as the Mechanical Engineering, Electrical Engineering, and Controls Groups worked on the project, ensuring that the transition to superbend operation was transparent to our users. The upgrade went very smoothly, and the success of the project marks the beginning of a new era for the ALS. The superbends have greatly extended the capabilities and capacity of the facility to serve the hard x-ray community. Our role in the superbend project is discussed in greater detail below.

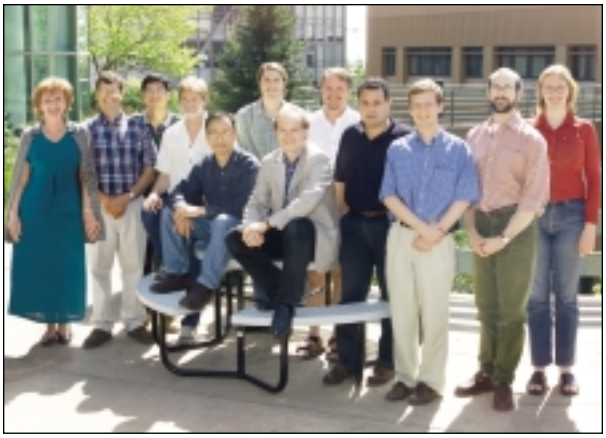

Figure 1 Accelerator Physics Group: *left to right,* Linda Senft, David Robin, Weishi Wan, Terry Byrne, Hiroshi Nishimura, Tom Scarvie, Christoph Steier, John Byrd, Fernando Sannibale, Laurent Nadolski, Steve Lidia, and Agusta Loftsdottir. Not pictured: Ying Wu.

In addition to the superbend project, the group continued to improve its understanding and control of the ring's performance, particularly through studies of the momentum aperture (the range of electron momentums that are stable in the storage ring). The momentum aperture is one of the main limitations on the electron beam's lifetime. Through our enhanced understanding of the momentum aperture, we were able to accurately predict the impact of superbends on the lifetime of electrons in the storage ring. The results of these studies are outlined in the highlight on page 55.

We also continued ongoing studies looking at the effects of insertion devices on the performance of the facility (in terms of lifetime, orbit, and beam size stability). Most of the efforts have been focusing on understanding and controlling the effects of the elliptical polarization undulator (EPU). The EPU operates in a different mode than the other insertion devices, rapidly and mechanically switching the insertion-device jaws to change the polarization of the light. Improving our understanding and control of these devices will be important as more of them are installed in the storage ring. In fact, the second EPU is scheduled to be installed in Sector 11 in April 2002 for the molecular environmental science beamline. The Accelerator Physics Group is involved in ensuring that the addition of this second EPU goes smoothly.

The Accelerator Physics Group has been investigating several possible upgrades to the ALS facility: the femtosecond undulator project, a far-infrared (FIR) storage ring, and a high-resolution photoemission electron microscope (PEEM 3). As with the superbends, the intention of both the femtosecond undulator project and the FIR project is to extend the capabilities of the ALS in new directions. These latter projects will increase the ALS's capabilities in generating short x-ray pulses and long wavelengths. The femtosecond undulator project is an upgrade to the beam-slicing experiment currently running on bend-magnet Beamline 5.3.1, increasing the flux and brightness of the ALS as a subpicosecond x-ray source by several orders of magnitude. The far-infrared storage ring is a

dedicated storage ring to be placed on top of the booster shielding tunnel for the generation of far-infrared radiation. Work on the far-infrared ring is detailed in a separate highlight below. The Accelerator Physics Group is working with engineering and the Experimental Systems Group on the design and analysis of the high-resolution PEEM 3 microscope. The accelerator group has concentrated its efforts on a critical component of the microscope, the beam separator.

In addition, the group is involved in helping support Berkeley Lab's Center for Beam Physics in its efforts to create a dedicated femtosecond radiation source for pump-probe experiments. This source will use a recirculating linac and will be much brighter than the undulator slicing source. Finally, there is a small effort (based on Laboratory Directed Research and Development funds) to investigate the possibility of capturing and cooling neutral molecules with a storage ring. This work is done in collaboration with the Chemical Sciences Division as well as the Center for Beam Physics.

The Superbend Project

The superbend project was completed on October 4, 2001. On that date, the ALS began first operation with superbends installed in the storage ring. It marked the end of a very busy and exciting project whose success has significantly enhanced the capacity of the facility to serve the hard-x-ray community. The history of the project is detailed in the special section on superbends. We review here the work done in the past year.

This project was a joint effort between three of LBNL's divisions (ALS, Engineering, and AFRD) together with our vendor, Wang NMR. At the end of 2000, Wang NMR made modifications to the first superbend to improve its thermal performance. A picture of this "first article" is shown in Figure 2. These modifications were needed to reduce the heat leaks to the 4.2 Kelvin stage so that the refrigeration system (a 1.5-W Sumitomo system) would have enough capacity to cool the magnet under normal operation without requiring external cryogenics. The goal of the cryosystem was to be self sustaining in order to simplify the operation of the superbends. It was a challenging task to reduce the heat leak to the several-ton cold mass to as little as 1 Watt.

Before the cryosystem modifications, the heat leaks were larger than could be accommodated by the cryocooler alone. After the modifications were completed, tests of the cryogenic performance demonstrated that the heat leaks were low enough that the magnet could be operated at 1.9 GeV and ramped sufficiently quickly between 1.5 GeV and 1.9 GeV. Figure 3 shows the performance of the system after the cryosystem was modified. Based upon successful test results in February 2001, the system was delivered to LBNL later that same month. The second, third, and fourth articles were delivered in June, July, and August, respectively.

In preparing for the final installation and commissioning of the ALS with superbends, the superbend team was busy thoroughly testing all of the superbend subsystems. The team conducted extensive testing of the magnetic, cryogenic, power supply, control, and diagnostic systems. These tests were performed to reduce risk and to ensure a smooth transition to superbend operation. All magnets were ramped to 320 A—more than 6% above the current required for 1.9-GeV operation. They proved to be very robust. Two of the four magnets experienced a training quench (where the coils become normal conducting) on their first ramp but not on subsequent ramps. Tests for quenches at different ramp rates were also conducted, and the magnets performed well. The first magnet underwent an equivalent of four years' worth of ramping without a problem, demonstrating the robustness of the cryocooler and magnet.

Figure 2 First ALS superbend magnet produced by Wang NMR.

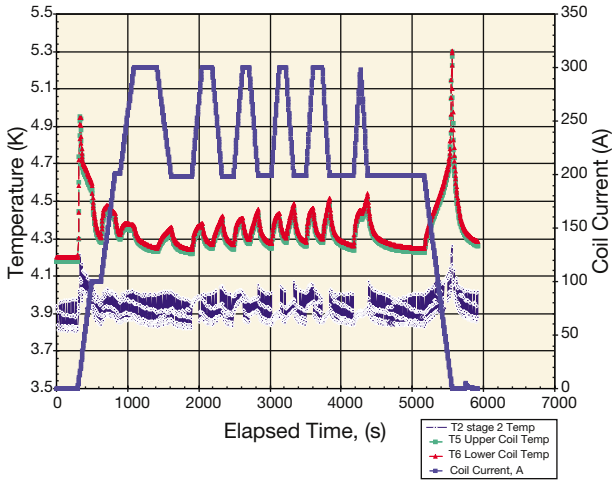

Figure 3 The performance of the superbend magnet system after the cryosystem was modified. The magnet can ramp between 1.5 GeV and 1.9 GeV operation solely under the cooling power of the cryocooler.

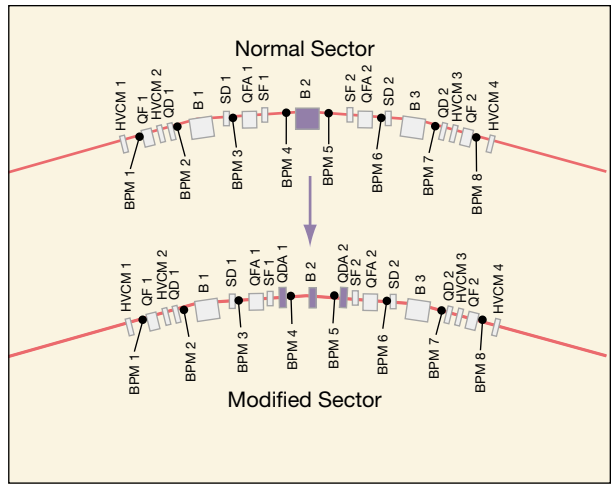

Figure 4 Changes made to the ALS lattice in a typical superbend sector. One normal-conducting bend magnet (B2, *top*) was replaced by a superconducting magnet and two quadrupole magnets (B2, QDA1, QDA2, *bottom*).

Nevertheless, the superbends do not require a working cryocooler in order to operate. In the event of a cryocooler failure, a superbend can be operated on external cryogens. The system was designed to be able to transition from cryocooler operation to cryogen operation with no interruption in user time. The superbend team conducted extensive tests of the four superbend systems operating on external cryogens.

On August 20, the ALS was shut down for the installation of the superbends. In three of the 12 sectors (4, 8, and 12), the normal-conducting gradient magnet was removed and replaced with a superbend as shown in Figure 4. In Sector 12, part of the injection straight needed to be disassembled to accommodate the superbends. Within five days, all magnets were installed and re-aligned. Within 11 days, power supplies were connected, controls were modified, external cryogenic lines were installed, and the machine was prepared for commissioning.

On August 31, the first injection was attempted at 1:00 A.M. A plot of the beam current history on August 31 can be seen in Figure 5. Within minutes of attempting injection, beam was stored. Within an hour, 100 mA of current was accumulated. The current was vacuum limited, so we ran in scrubbing mode overnight. Within one day, the beam was ramped to 1.9 GeV for the first time.

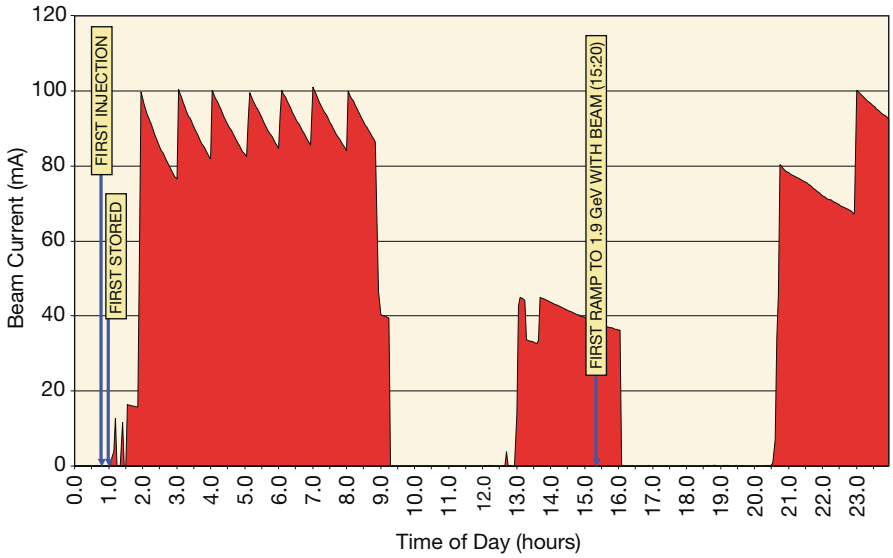

Figure 5 Beam current history on August 31, 2002, the first day of commissioning the superbends.

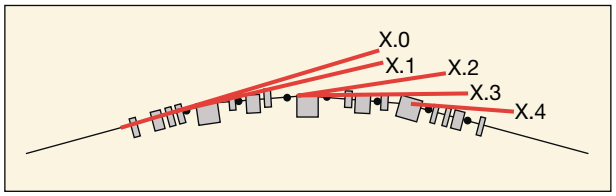

Table 1 Comparison of beam parameters at the various insertion-device and bend-magnet ports before and after the installation of superbends.

	BEFORE SUPERBENDS	AFTER SUPERBENDS
Horizontal emittance	5.5 nm-rad	6.75 nm-rad
Vertical emittance	0.2 nm-rad	0.15 nm-rad
Energy spread	0.080%	0.10%
Horizontal beam size in x.0 magnets	250 µm	310 µm
Horizontal beam size in x.1 magnets	50 µm	57 µm
Horizontal beam size in x.2 magnets	100 µm	100 µm
Horizontal beam size in x.3 magnets	100 µm	100 µm
Horizontal beam size in x.4 magnets	60 µm	65 µm
Vertical beam size in x.0 magnets	30 µm	23 µm
Vertical beam size in x.1 magnets	65 µm	54 µm
Vertical beam size in x.2 magnets	20 µm	15 µm
Vertical beam size in x.3 magnets	20 µm	15 µm
Vertical beam size in x.4 magnets	60 µm	52 µm

By the end of two weeks, the operation of the ALS with superbends was thoroughly tested, and we found that the new magnets had no negative impact on the performance of the machine. The beam lifetime, injection times, and orbit stability were as before superbend installation. In addition, we introduced and commissioned a new lattice with 6 cm of dispersion in the straight sections. (Previously, we were operating with zero dispersion.) This was done to minimize the growth in emittance when operating with the superbends. As a result, the horizontal emittance increased only from 5.5 nm-rad to 6.7 nm-rad. The difference was minimal when compared with the predicted value of 12 nm-rad that would have been obtained without the change in the lattice. The dispersion change resulted in a small change in the beam parameters, as shown in Table 1.

After several months of ALS operation with superbends in place, we can confidently say that the transition to superbend operation exceeded our expectation. The impact on nonsuperbend users was minimal, as there were only small changes in the beam sizes. In addition, it was anticipated that there would be a "teething period" for several months after installation, during which there might be a drop in reliability as compared with presuperbend operation. This teething period did not come to pass, however, and the operation of the ALS with superbends has been excellent.

Far-Infrared Storage Ring

Infrared spectroscopy and microscopy have been gaining popularity at synchrotron sources in recent years, as evidenced by the design and construction of several new infrared beamlines at existing light sources. Most of these beamlines are being retrofitted to rings originally designed as high-brightness soft and hard x-ray sources and thus have several performance limitations. The foremost is the vertical angular acceptance of

the radiation from the beam. Because long-wavelength synchrotron radiation has a larger vertical opening angle than light of shorter wavelengths, the vacuum chamber acts as a high-pass filter, cutting off much of the long-wavelength radiation. This limitation is particularly severe in rings with vacuum chambers that have antechambers in which most of the far-infrared radiation is suppressed.

Given this limitation and the potential for exciting, new science at far-infrared wavelengths, we have been considering ideas for a storage ring optimized for the production of synchrotron radiation over the infrared wavelength range from 1 to 1000 µm. Such an infrared ring would represent an extension of the capabilities of the ALS facility, much like the superbend project. The main goals of the design are to increase the range of transmitted wavelengths up to 1 mm and beyond and to minimize the sources of noise. We also hope to achieve bunches short enough to emit coherent light over the wavelength range from 200 to 1000 µm.

INFRARED RING DESIGN

Most synchrotron light sources require a large floor space outside the main ring to accommodate beamlines. However, infrared beamlines require relatively little space and are best located as close to the source as possible. Given the layout of the ALS facility, as shown in Figure 6, the ideal location for an infrared ring is either in or atop the ALS booster tunnel. The minimum circumference of a ring that would fit on the existing booster-tunnel shielding is about 65 meters. Full energy injection to the ring can be done from the booster without interfering with injection to the main ring.

Because the brightness and flux of the synchrotron infrared light have little dependence on beam energy, we have chosen 700 MeV as the nominal energy for the conventional mode of ring operation. This choice represents an optimal balance between performance and cost. (Beam stability and lifetime favor higher energies, whereas heat loading and accelerator component lifetimes favor lower energy.)

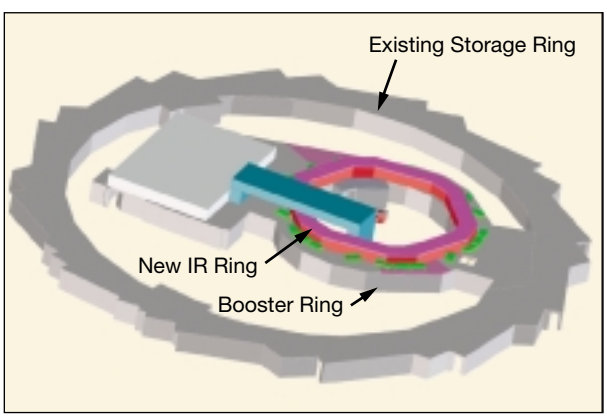

Figure 6 The infrared ring location atop the ALS booster synchrotron. The ring circumference is 66 meters.

The lattice is a sixfold symmetric double-bend achromat. One of the significant differences in the lattice compared to that of a third-generation storage ring is that the electron beam emittance can be much larger without degrading the beam brightness over the infrared spectrum. This significantly relaxes the focusing on the lattice, which gives it less sensitivity to vibration and power-supply jitter, better dynamic aperture (a broader range of electron energies over which we can inject), and more robust operation. Furthermore, infrared measurement techniques do not require small vertical beam sizes; thus, the requirement on the vertical emittance can be strongly relaxed. The larger electron beam emittances strongly reduce Touschek and intrabeam scattering.

A view of a ring arc sector is shown in Figure 7. We expect to use circular stainless-steel pipe for most of the vacuum chamber except for the dipole chambers, which are specially shaped for maximum vertical and azimuthal acceptance.

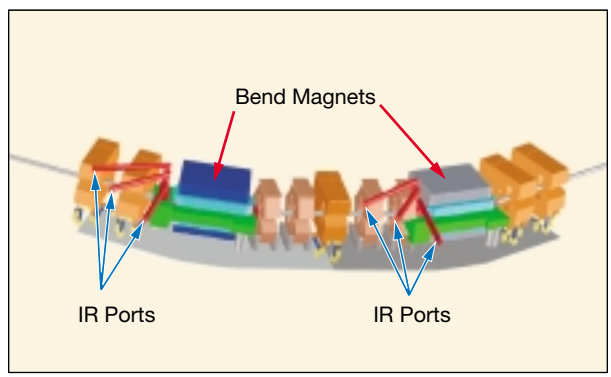

Figure 7 Conceptual view of ring arc sector, showing how infrared light ports are extracted from the end of each dipole vacuum chamber.

BRIGHTNESS AND FLUX

Conventional Mode

Shown in Figure 8 is the brightness curve for the new infrared ring, calculated by using our preliminary ring parameters. Also shown is the brightness of the ALS main ring with a 10-mrad vertical aperture. The main improvement with the infrared ring comes in the far-infrared range. As discussed below, we also expect to increase the horizontal collection angle from 40 mrad to 100 mrad.

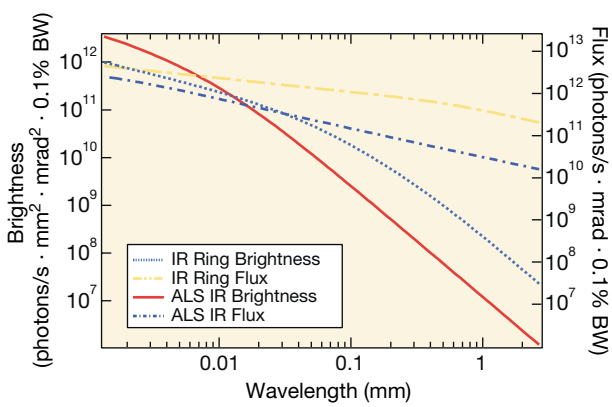

Figure 8 Brightness and flux of the ALS infrared ring (in coherent mode) and of the existing ALS infrared beamline.

Coherent Mode

When the electron bunch length becomes comparable to the wavelength of emitted synchrotron radiation, the radiation becomes coherent and the power becomes proportional to the square of the number of electrons in the bunch. We refer to this effect as a superradiant mode of emission. Many attempts have been made to reach submillimeter bunch lengths in electron rings, with little success. However, if such short bunch lengths can be achieved, high gains can be made from coherent emission in the far-infrared range, even at very low currents. For example, Figure 9 shows the computed flux in the infrared ring for the conventional (1 A, 10-mm bunches) and superradiant (only 3.3 mA, 70-µm bunches) modes. The long-wavelength transmission is limited by the waveguide cutoff of the vacuum chamber, and the short-wavelength regime is limited only by how short the bunch length can be made.

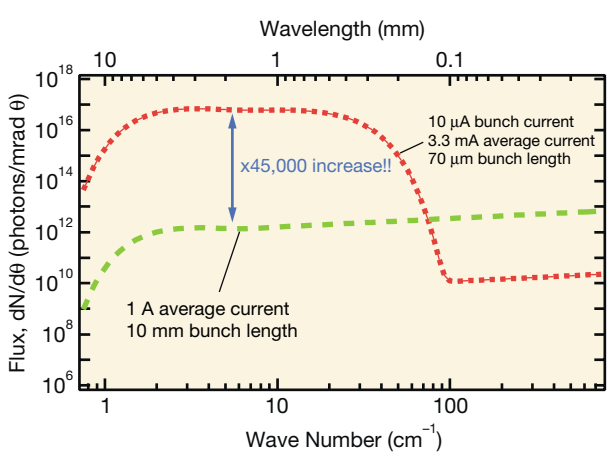

Figure 9 Flux enhancement from coherent emission for a 3.3-mA average bunch current and 70-µm bunch length.

The flux with 3.3 mA at a bunch length of 70 µm is almost five orders of magnitude larger than the flux with 1 A and long bunch lengths. The peak bunch current of 85 A used in this computation has been achieved in many rings. We are actively studying limitations in the bunch length imposed by both the vacuum chamber and radiation impedance.

We hope to use a combination of increased rf voltage at higher frequencies and reduction in momentum compaction (the relative change in beam energy with changes in rf frequency). The necessary rf voltage is achievable only with the use of superconducting rf systems.

BEAMLINE INTEGRATION

Another of the improvements we hope to achieve with the ALS infrared ring is a smoother integration of the beamline front end with the ring vacuum chamber. This will increase the transmission at long wavelengths and significantly reduce potential sources of beamline motion relative to the electron beam.

Shown in Figure 10 is a drawing of the vacuum chamber in one of the infrared-producing dipole magnets, illustrating the extraction of infrared light from the ring. The vertical opening of the dipole chamber is matched to the vertical opening of the gradient dipole, resulting in a 100-mrad full vertical aperture, collecting 90% of the light with a 1-mm wavelength. We plan to use a single first mirror collecting 300 mrad of horizontal angle with the light split into three beamlines by subsequent focusing mirrors.

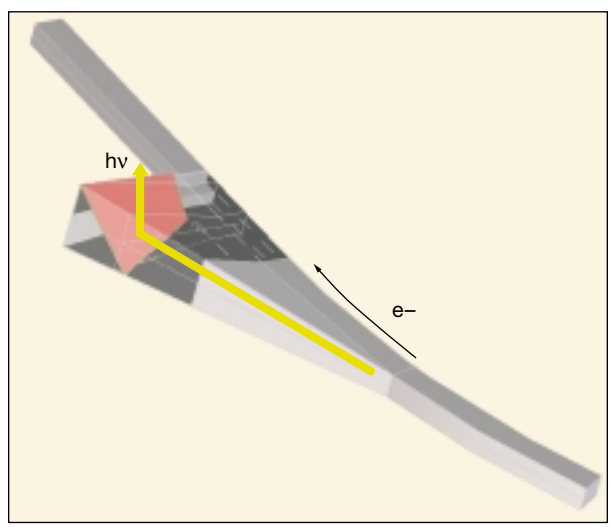

Figure 10 Layout of vacuum chamber with integrated front-end mirror *(red trapezoid)*, which collects 100 mrad vertically and 300 mrad horizontally.

Experimental Systems

H. A. Padmore, *Experimental Systems Group Leader*

Introduction

The past year has been extremely challenging for the Experimental Systems Group (ESG, Figure 1). We have had very high levels of activity in all areas of our work, from beamline construction to research and advocacy for new projects. In addition, the group also operates beamlines for the independent-investigator community. This includes Beamlines 5.3.1, 7.3.1.1, 7.3.3, and 10.3.2, and Beamline 11.3.1 will join them in 2002. A considerable fraction of the group's resources are thus going into direct user operation.

The focused research and development that ESG undertakes can have a large impact on the ALS as a facility. One of our main activities for the year 2001 was the completion and commissioning of the first three superbend protein crystallography beamlines. This work evolved from collaborative development work with a group from the University of California, Berkeley (UCB). Another example of such an effort is the development of high-pressure research at the ALS. Exploratory work undertaken in collaboration with two groups from UCB has proved to be extremely successful, and it has enabled us to progress toward a now-funded superbend high-pressure beamline. Finally, we have pioneered the use of "application-specific" soft x-ray bend-magnet beamlines that are focused on a narrow range of performance goals and thus can have extremely well optimized performance. One beamline that exemplifies this approach came on line this year: Beamline 5.3.2, for scanning transmission x-ray microscopy. In each case, ESG has been highly proactive in developing new user programs by acting as a technical resource and as a catalyst to create new scientific opportunities.

As these three projects exemplify the type of work that ESG does and have come to fruition during the last year, I have chosen to highlight them in greater detail below. First, though, I will give short updates on some of our other current projects.

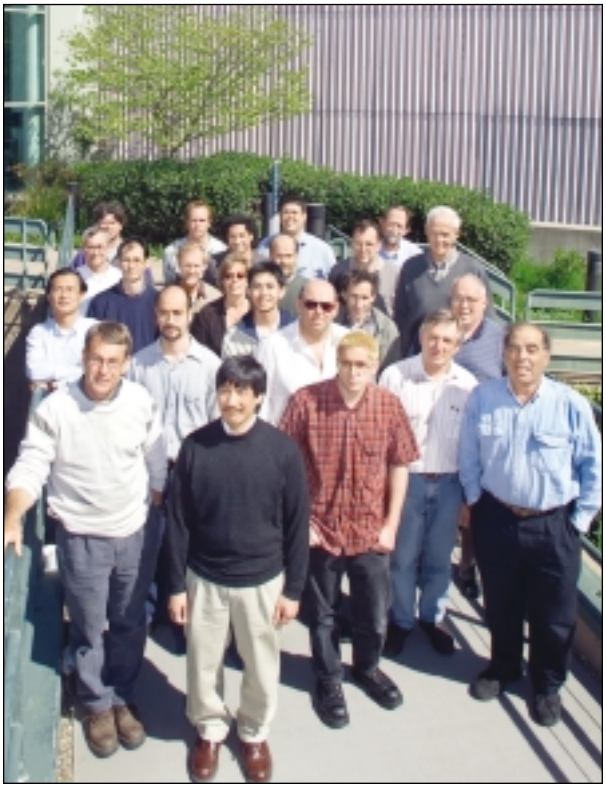

Figure 1 Members of the Experimental Systems Group: *left to right, front row,* Tony Warwick, Tony Young, Andrew Franck, Bob Batterman; *second row,* Andrew Doran, Simon Clark, Malcolm Howells; *third row,* Jun Feng, Marvin Paik, Phil Heimann, Wayne McKinney; *fourth row,* Nobumichi Tamura, Marsha Fenner, Al Thompson; *fifth row,* Steve Irick, Alastair MacDowell, Matthew Marcus, Howard Padmore; *back row,* Andreas Scholl, Sander Caldwell, Ernie Glover, Rich Celestre, Everett Harvey. Not pictured: Sug-Bong Choe, Sirine Fakra, Haifeng He, David Kilcoyne, Scott Locklin, Alan Manceau, Jim Patel, John Spence, Robert Sublett.

BEAMLINE 11.0.2: MOLECULAR ENVIRONMENTAL SCIENCE

The molecular environmental science (MES) project, under the technical leadership of Tony Warwick (ESG), is approaching its final phases after several years of design and construction. The undulator, front end, and first mirror will be installed in Sector 11 in April 2002. The monochromator will be installed in May, commissioning will start in June, and user operation is scheduled to begin in October. The photon source is a 5-cm-period elliptical polarization undulator, almost identical to the system installed in straight-section 4. Like 4, this straight is chicaned to accommodate two undulators and two separate beamlines in the future.

The MES beamline is based on the collimated-light Petersen monochromator, pioneered at BESSY II. We have addressed the challenge of water cooling such a high-power monochromator by running the water down the axis of rotation of the sine bar drives. This prevents unconstrained force from being applied to the system during a scan—a major advantage over other designs. We have also been able to avoid the time-consuming recalibration requirements of changing gratings by having a single grating with multiple rulings and then a system that translates the whole monochromator laterally the few millimeters required. The monochromator tank is a single piece of aluminum, resulting in a highly compact, stable, and ultraclean system. The cleanliness is extremely important, as carbon K-edge NEXAFS will be a major use of the beamline. We believe that this system will set a new standard for monochromator design. The overall engineering effort has been led by Jim Commins (Mechanical Engineering Group), and Nord Andresen (Mechanical Engineering Group) has played a key role in designing the monochromator.

Three endstations will be used on the MES beamline, two for spectroscopy and one for microscopy. The microscopy station will have a scanning transmission x-ray microscope (STXM) that has already been built and tested on Beamline 7.0.1. A two-axis differential interferometer that effectively encodes the position difference between the microfocus zone plate and the sample stage gives the system exceptional stability. The system now performs at diffraction-limited resolution, as shown by the test pattern in Figure 2. The STXM was developed by a group led by Tony Warwick (ESG) and including Keith Franck (Mechanical Engineering Group), Sirene Fakra (ESG), and Rick Steele (Controls Group).

BEAMLINE 11.3.1: SMALL-MOLECULE CHEMICAL CRYSTALLOGRAPHY

Although the ALS has superb facilities for solving protein structures, we do not yet have facilities for the solution of smaller-unit-cell structures to very high resolution. In chemical crystallography, the crystals are usually much more perfect than protein crystals, but they are typically much smaller, down to the few-micron range, and structural data is required to well below 1 Å in resolution. In some cases, the technique can yield structure factors accurate enough to determine the locations of bonding orbitals.

A growing trend in chemistry is the design of new materials based on some form of directed assembly, so a rapid way of measuring to see whether the structure formed is as desired is absolutely essential. These materials quite often have rather large unit cell sizes, up to the scale of small proteins, and they often only exist in small crystals. These two facts mean that the high flux and brightness of a synchrotron source are required.

We have built a new type of beamline for crystals with either large or small unit cells: Beamline 11.3.1. In order to reduce costs and yield a robust design, we have miniaturized the whole optical system and placed it inside the shield wall of the storage ring. It consists of a cryocooled, channel-cut silicon[111] crystal monochromator and a single toroidal mirror focusing at 1:1. All the primary functions, such as crystal rotation, mirror bend, mirror angle, and yaw are

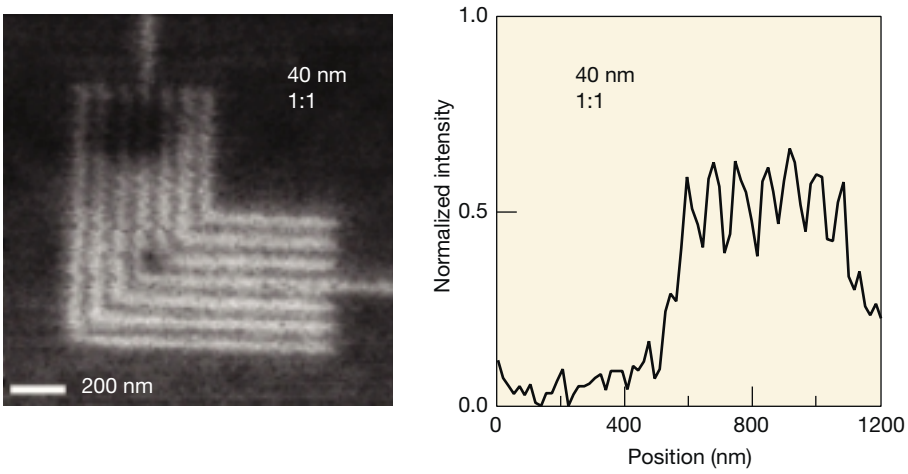

Figure 2 *Left,* image of a test pattern taken on Beamline 7.0.1 with the new scanning transmission x-ray microscope destined for the MES beamline; *right,* the modulation of the intensity along a vertical line through the test pattern.

remotely actuated from the endstation. Outside the shield wall, there is just a vacuum tube leading to a small hutch. The hutch contains a Bruker diffractometer and a state-of-the-art x-ray CCD camera (Proteum 300). This effort, undertaken in collaboration with the UCB chemistry department, is led by Al Thompson, Haifeng He, and Rich Celestre (ESG), and the engineering is led by Keith Franck and Greg Morrison (Mechanical Engineering Group).

BEAMLINE 10.3.2: MICRO X-RAY ABSORPTION SPECTROSCOPY

The 10.3.2 beamline system has evolved out of a project to evaluate x-ray absorption spectroscopy on the micron spatial scale. The present system is novel in that it has a horizontally deflecting toroidal mirror to focus the light with unity magnification to a slit. Downstream, light is first collimated with a parabolic mirror then monochromatized with a four-crystal monochromator and then re-imaged by a second parabolic mirror (vertical) and an elliptical mirror (horizontal). The mirrors are all small (less than 100 mm) because of their proximity to the intermediate focus, and all are shaped by bending. The endstation hutch contains all of these downstream optics, plus a fast-scanning sample stage and a seven-element fluorescence detector. The system was completed during 2001 and is now open to independent investigators. In 2002, we plan to modify the beamline to allow microdiffraction studies to be carried out. This work is led by Matthew Marcus and Bob Sublett (ESG), and the engineering work is led by Keith Franck and Greg Morrison.

BEAMLINE 7.3.1.1: PHOTOEMISSION ELECTRON MICROSCOPY

The photoemission electron microscopy (PEEM 2) beamline and electron imaging endstation have now been operational for several years. There have been many enhancements to the sample preparation system during the year, but the main technical effort at present is devoted to developing time-resolved PEEM for magnetic materials. Experiments will be done in a synchronous pump-probe manner, in which a sample is pumped many times to the same state, and images are integrated over thousands of cycles. For magnetic materials, the pump is provided by a magnetic field impulse in the PEEM main chamber. The impulse is generated by a fast laser pulse that hits the semiconductor substrate on which the sample is built, inducing a current to flow in a small one-loop coil lithographed around the sample. In this way, it should be possible to observe repetitive excitation of a sample with a time resolution equal to the storage-ring bunch length of around 50 picoseconds. The PEEM 2 effort is led by Andreas Scholl and Andrew Doran (ESG), and the time-resolved work is a joint development with S.-B. Choe (ESG) and Yves Acreman (Stanford Synchrotron Radiation Laboratory).

BEAMLINE 5.3.1: ULTRAFAST X-RAY SPECTROSCOPY AND DIFFRACTION

This beamline has been in operation for more than a year, and it functions as a test-bed for the development of ultrafast x-ray techniques and ultrafast x-ray science. It is used by the group of Roger Falcone (UCB), which uses a streak camera for measurements down to a time resolution of a few picoseconds. This group, supported by Phil Heimann, has made measurements of the melting of silicon and carbon. A Berkeley Lab team led by Ali Belkacem (Chemical Sciences Division) uses the beamline for atomic physics experiments, and a group from the University of Lausanne has used the beamline for studying the dynamics of various systems in solution, all so far at 50-picosecond time resolution. To go beyond this time resolution, the Berkeley Lab group of Bob Schoenlein (Materials Science Division) and Sasha Zholents (Center for Beam Physics) is developing laser-driven "slicing" of the electron beam. This has yielded optical pulses close to 100 femtoseconds in duration. In order to utilize these ultrashort pulses, we have installed a dispersive-grating spectrometer in the endstation hutch and begun the first generation of soft x-ray ultrafast experiments at transition-metal L edges. The ESG work in this collaboration is led by Ernie Glover and Phil Heimann.

BEAMLINE 7.3.3: X-RAY MICRODIFFRACTION

The microdiffraction beamline has now been in operation for two years, and during 2001, the system was opened up to independent investigators. Under the project leadership of Nobumichi Tamura, it is operating superbly. We have achieved a spatial resolution of 0.7 μm and can take Laue diffraction images with the shutter open for less than one second. The system was upgraded during the year with a new, fast Bruker 6000 x-ray camera (1-MHz readout) and with enhanced storage (1 terabyte) and processing capabilities. The Participating Research Team that operates the beamline focuses on issues in thin-film metal physics, but the independent-investigator program has seen a wide range of materials applications, from measuring strain in silicon microelectromechanical systems to understanding stress in high-T_c superconductor thin films.

Since the influx of independent investigators, the demand for beam time has grown to several times that available, and it is clear that an expansion to a superbend beamline would be extremely beneficial.

PEEM 3

The PEEM 3 project is a large one, encompassing the construction of a new state-of-the-art EPU-based beamline (the second EPU on the Sector-4 straight) and an aberration-corrected photoemission electron microscope capable of 5-nm resolution. Although the project was approved in 2000, the rate of funding has been slow. The current funding profile has the whole system operational in summer of 2004.

The beamline will be based on the technology developed for the MES project but with additional focusing elements to compress the beam to nearly 1 μm in both planes. This requires two stages of demagnification in both the vertical and horizontal directions.

The microscope is largely similar to the SMART microscope pioneered by Harald Rose, which is being built for operation at BESSY II. There are key differences, however. One difference is that we intend to image a wide energy range of secondary electrons, so care must be taken to have as good a chromatic correction as possible. Also, our microscope is designed to focus specifically on magnetic materials and polymer science, so the design can be simpler. The instrument is designed to work in two modes, a high-throughput mode with a resolution of around 50 nm and a high-resolution mode with a resolution around 5 nm, where an aperture is used to reduce the beam transmission.

As compared to PEEM 2, the key components of the microscope are a magnetic separator to allow separation of the beams going to and from an electron mirror, and the electron mirror itself, which performs the aberration correction. The separator cannot be axially symmetric and so must not introduce any additional aberrations, or the axially symmetric mirror would be unable to compensate them. The separator has been designed, and we have now moved on to a full study of the mirror. Thus far, we have shown that fairly simple mirrors compensate aberrations to the required level.

We can now start the engineering design of the complete system. We intend to build the microscope as a prototype, building in the ability to reconfigure components and perform many test functions that may be eliminated in the final design. The work is a joint effort between Jun Feng and Alastair MacDowell of ESG; David Robin, Ying Wu (now at Duke University), and Weishi Wan of the Accelerator Physics Group; and Ross Schlueter, Rob Duarte, and Nicholas Kelez of ALS engineering.

Superbend Protein Crystallography

Three new superbend beamlines have been installed in Sector 8 for protein crystallography. Beamline 8.3.1, now in routine use, was built for a UCB/University of California, San Francisco, consortium. It served as the prototype for the two subsequent beamlines (8.2.1 and 8.2.2), built for the Howard Hughes Medical Institute. The project originated in 1998, when it became clear that wiggler Beamline 5.0.2 would not be able to accommodate the tremendous interest in multiple-wavelength anomalous diffraction (MAD) it had generated, and that the storage ring would not have room for a second wiggler. Working with the UCB group of Tom Alber on Beamline 7.3.3, we showed that the single high-field pole of an optimized superbend source could be competitive with the much lower field but many poles of the existing wiggler for MAD studies.

The design for the superbend beamlines consists of a bent parabolic premirror inside the shield wall, a monochromator (Kohzu) with two flat crystals, and a bent toroidal mirror. The latter takes the source from infinity in the vertical direction and the real source demagnified by two in the horizontal direction. This arrangement eliminates the low-order aberrations of the toroid and gives a theoretical image size of 150 (hor.) × 70 (vert.) μm FWHM. The aberration-free image size would be 120 (hor.) × 40 (vert.) μm FWHM, so in each plane we are nearly—but not quite—brightness limited. Other designs can produce theoretically perfect foci, but in practice this is extremely difficult and is generally incompatible with the rapid energy scans required for MAD. The toroidal mirror arrangement we have adopted only requires rotation of the goniometer during MAD energy scans. With its intrinsic simplicity, this gives a robust design. The premirror is nickel-plated Invar coated with rhodium on platinum (to eliminate the platinum L edges but retain good high-energy performance) and is internally water cooled. The first monochromator crystal is intensively water cooled, with internal channels drilled perpendicular to the beam axis and with a depth below the surface matched to the power distribution at the selenium K edge.

Figure 3 shows a new version of this design that is being developed for the Sibyls beamline for small-angle scattering

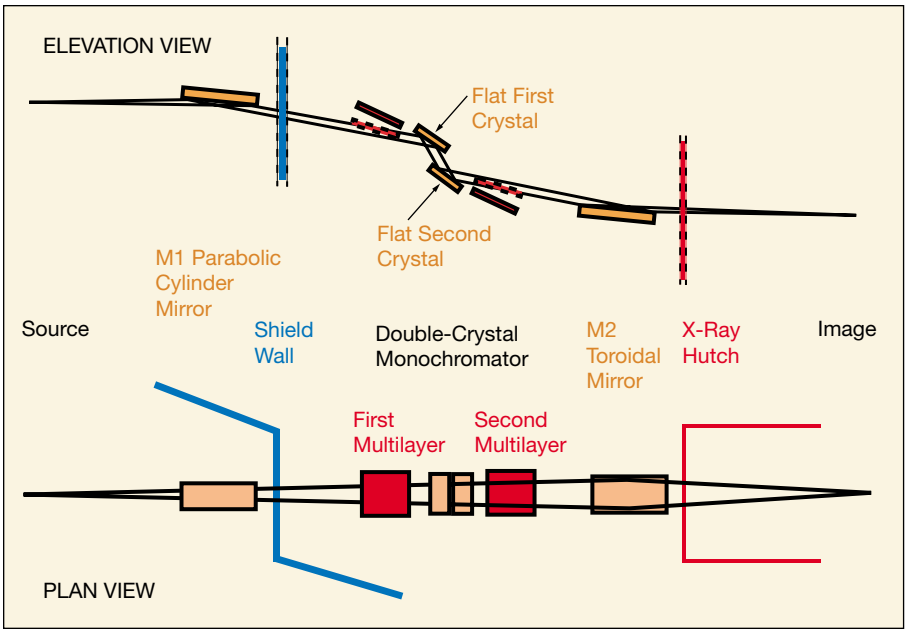

Figure 3 Optical layout of the protein crystallography and small-angle scattering beamline (Sibyls) in Sector 12. This layout is nearly identical to the design used in Sector 8.

studies, Beamline 12.3.1 [Principal investigators, Priscilla Cooper (Berkeley Lab Life Sciences Division) and John Tainer (Scripps Institute)]. The newer system contains a monochromator with two multilayers and two crystals. The multilayers are mounted eccentrically with respect to the crystal rotation axis, and they rotate into the beam at a Bragg angle lower than that used for the highest energy in the crystal mode. The multilayers will give a much broader bandpass and significantly higher flux.

Figure 4 shows the measured flux from each of the three Sector-8 protein crystallography beamlines compared to theory.

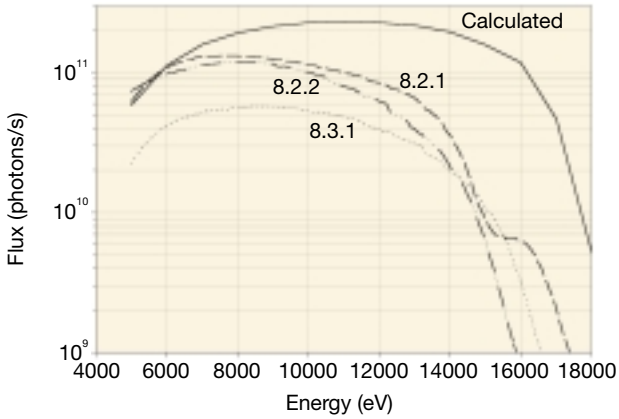

Figure 4 Flux output for each of the three Sector-8 protein crystallography beamlines, measured through a 100-µm aperture in a convergence angle of 1.5 mrad (hor.) and 0.33 mrad (vert.) for a 400-mA current in the storage ring at 1.9 GeV, and calculated output for a superbend beamline.

The differences in high-energy performance and the discrepancy with theory are due to the poor quality of the premirror surfaces. The manufacturer failed to meet specification in both slope error and microroughness, resulting in an enlarged vertical beam size and poor high-energy reflectivity. Still, even with a rather imperfect premirror, the flux is close to or as high as that from the high-power wiggler beamline. This is a major success and ensures that challenging structures will be accessible with these new beamlines. The premirrors in all three Sector-8 beamlines will be replaced toward the end of 2002, and we should then get close to the theoretical flux of 2×10^{11} photons/s (through a 100-µm collimator in a convergence angle of 1.5 mrad), almost three times that of the wiggler beamline.

Figure 5 shows the general endstation area in Sector 8. The endstations are what we call minihutches, which have the interesting feature that the operator only manipulates the sample from outside the hutch, through a sliding window. The sample area is shown in Figure 6. The main features are a high-speed air-bearing rotary stage for crystal rotation, a sophisticated on-axis crystal viewing system, and a drive that lowers the whole assembly around the crystal out of the way to ease sample mounting. The detector is mounted on a very large Cartesian framework that allows the detector to move back up to one meter from the sample and tilt up to 45 degrees.

The ESG effort in technical design was led by Alastair MacDowell, the superb new beamline control system was put together by Ed Domning (Controls Group) and Rich Celestre (ESG), and the Mechanical Engineering Group's

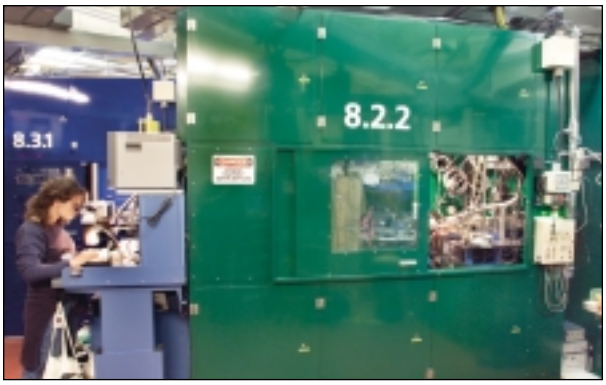

Figure 5 Minihutch endstations in Sector 8. The back panel of the Beamline 8.2.1 minihutch is visible to the far right.

Figure 6 The inside of the Beamline 8.2.2 hutch, showing the x-ray detector *(left)* and the single-axis air-bearing rotation stage *(center).*

effort was led by Rob Duarte and Dave Plate. Staff from the Macromolecular Crystallography Facility contributed to the endstation design and control system, and James Holton of UCB, working with Alastair, was essential to the success of the commissioning work.

High-Pressure Research

A two-year Laboratory Directed Research and Development grant has enabled us to develop the upstream section of the Beamline 7.3.3 x-ray hutch as a high-pressure research facility. The grant enabled a two-year sabbatical in ESG for Simon Clark from the Synchrotron Radiation Source at the CLRC Daresbury Laboratory. This, together with initial work by Alastair MacDowell and Rich Celestre, has led to a successful high-pressure program. The high-pressure research program has been a collaborative development between ESG and the UCB groups of Paul Alivisatos and Raymond Jeanloz.

It was realized early on that, although the ALS bend magnets do not produce a high flux of hard x rays, the brightness is high, approximately 10^{15} photons/s·mm^2·mrad^2·0.1% BW at 10 keV. Conventionally, high-pressure work is done at 17–30 keV, because of the high penetrating power required to pass through the thick diamonds required for compression to high pressure. With the advent of drilled thin-window diamonds, some significant work can be done at much lower energies, and in fact there is a need to go to even lower energies to do spectroscopy under pressure and at high temperature. Beamline 7.3.3 has been used to develop these new methodologies.

The station uses the same 1:1 focus as the microdiffraction system on the same beamline, but it has its own cryocooled channel-cut silicon monochromator, alignment system, diamond anvil cell, pressure measurement spectrometer, and a choice of a Mar Research 135-mm x-ray CCD or Mar345 image-plate detector. The idea here was to develop techniques, to enable local groups to build up a scientific program, and to demonstrate that challenging high-pressure research could be done, thus nucleating a new high-pressure community. Our success on all fronts has led to the funding of a dedicated high-pressure superbend beamline in Sector 12.

Here we show one example of the type of challenging new science that can be done, even on a low-energy bend-magnet source, with optimized endstation instrumentation. The Jeanloz group has been studying the phase diagram of oxygen at extreme pressures and temperatures, and it has discovered the formation of a new phase. This work was headed by Robin Benedetti of the Jeanloz group in close collaboration with Simon Clark. Samples of liquid oxygen were compressed between single-crystal diamond anvils to pressures up to 46.5 GPa and simultaneously heated to temperatures up to 5000 K. X-ray diffraction patterns revealed that a new phase of oxygen had been formed (Figure 7). This new "μ" phase has the astonishing property that it remains stable when the pressure and temperature are reduced to ambient levels. This is the first solid phase of oxygen that has been discovered to exist at atmospheric conditions. The work has major implications for our understanding of the structures of the Earth and the giant planets.

This type of work was used in our request for funding to DOE, leading to approval to begin construction. The design has advanced well, and we expect first beam into the hutch in summer 2003. The overall layout is shown in Figure 8. The Beamline 12.2/12.3 complex will have four beamlines and hutches, and the rear two, Beamline 12.2.2 for high pressure

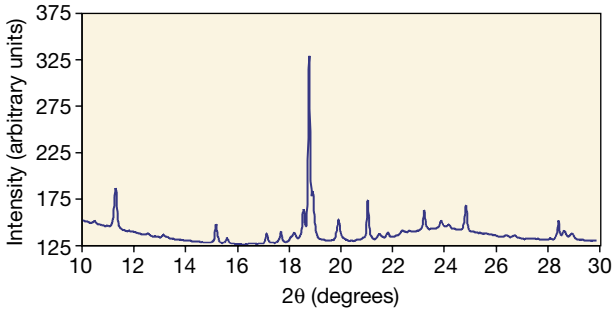

Figure 7 Diffraction pattern for oxygen at 3.2 GPa inside a diamond anvil cell, taken on Beamline 7.3.3. This work showed the existence of a new phase of oxygen.

and Beamline 12.3.1 for structural biology (Sibyls), will be constructed first. The high-pressure beamline is largely based on the superbend protein crystallography design, but with 2-mrad mirror grazing angles, allowing good performance up to 40 keV. It will produce an intermediate focus for relatively low pressure experiments at the front of the rear hutch. The very high pressure experiments will be performed further downstream, after the beam has been demagnified to around 10 µm by a Kirkpatrick–Baez elliptical mirror pair. A request has also been made to the National Nuclear Security Administration for funding of an upstream hutch and beamline, in a collaboration between UCB, Berkeley Lab, and Lawrence Livermore National Laboratory. The system would be complementary to the diamond anvil system in the rear hutch and would be equipped with a large-volume press.

Polymer X-Ray Microscopy

Scanning transmission x-ray microscopy (STXM) has been successfully applied to a wide range of problems, from environmental science to the study of magnetic materials. As the micro–zone plates used for focusing only collect a very small angular cone, STXMs have traditionally been used in conjunction with undulator sources. At the ALS, this has meant that our existing STXM shares its beamline (Beamline 7.0.1) with several other systems. The resulting paucity of dedicated microscope time has prevented the instrument from being fully developed, and though good research has come out of it, the quantity of results has been low. Moreover, the shared beamline could not be optimized for microscopy.

Following the "application-specific design" philosophy, we investigated the possibility of using an ALS bend magnet for this application and found that, together with an optimized optical design, the brightness of the bend-magnet source was sufficient for a state-of-the-art scanning x-ray microscope. This led to the development of a new bend-magnet beamline (Beamline 5.3.2) together with a new microscope (similar to the one for MES) by a consortium of groups from North Carolina State University (Harald Ade), the ALS (Tony Warwick), McMaster University (Adam Hitchcock), and the Dow Chemical Company (Ed Rightor).

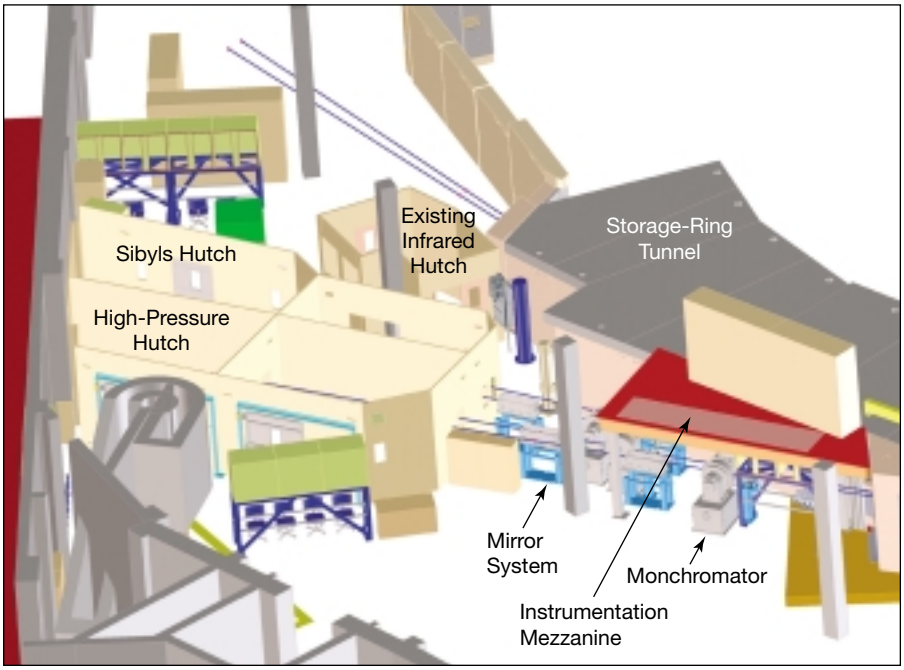

Figure 8 Superbend Sector 12, showing the high-pressure (12.2.2) and Sibyls (12.3.1) beamlines currently under construction.

The beamline is highly optimized and covers the energy range between 250 and 600 eV for access to the carbon, nitrogen, and oxygen 1s edges. The optical system is simple and highly optimized. Figure 9 shows the arrangement, consisting of a horizontally deflecting toroid to produce a horizontal focus at the monochromator entrance slit and a vertical focus at the exit slit, together with a horizontally deflecting and dispersing spherical-grating monochromator. The grating has a density of 300 lines/mm and achieves a diffraction efficiency of 28% at 300 eV. Figure 10 shows the measured flux through a silicon nitride window into the acceptance of the zone plate, showing that, near the carbon K edge, fluxes of around 3×10^8 photons/s are achieved. The only other loss factors are the efficiencies of the zone plate and pulse counting detector, so data rates of several MHz can be easily achieved. This is sufficient for state-of-the-art scanning x-ray microscopy. Because of the relatively high sagittal slope errors on the toroidal mirror (12 µrad), the vertical brightness is degraded by a factor of 3, so future replacement of this mirror should lead to a substantial increase in signal.

One of the great advantages of this beamline is that it is dedicated to one instrument. From day to day, incremental improvements can be made, and more and more challenging measurements can be made. It has very good overall performance. Because it is also simple and inexpensive, it can easily be duplicated when demand requires more capacity. The system is now in routine use for studies of polymer systems by the North Carolina State/McMaster/Dow team. The beamline team was led by Tony Warwick, assisted by Sirene Fakra, and Mike Kritcher (Mechanical Engineering Group) led the engineering effort. Tolek Tylisczcak (McMaster University), David Kilcoyne (North Carolina State University), and ALS summer student Peter Hitchcock have also played key roles.

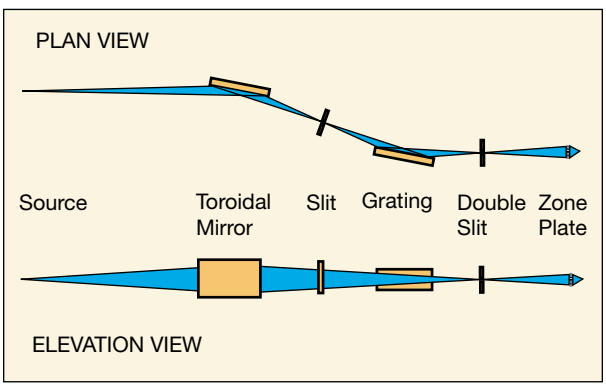

Figure 9 Schematic layout of the polymer STXM bend-magnet beamline (Beamline 5.3.2).

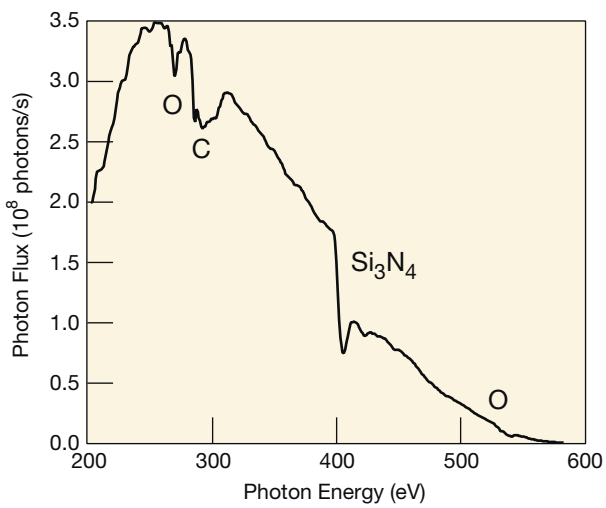

Figure 10 Flux through a 100-nm silicon nitride window into the acceptance of a diffraction-limited zone plate from Beamline 5.3.2 in a bandpass of 1/2000. The flux above 400 eV is highly suppressed by the nitrogen K edge of the window.

Scientific Support

Zahid Hussain, *Scientific Support Group Leader*
John Bozek, *Scientific Support Group Deputy Leader*

Introduction

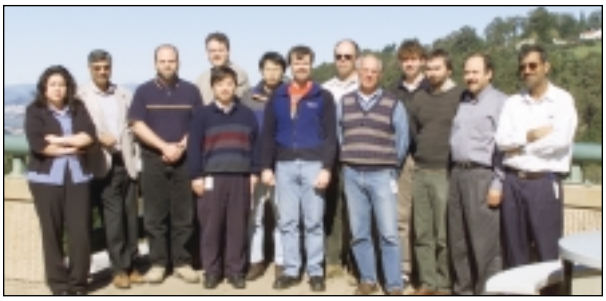

Figure 1 Scientific Support Group members: *left to right,* Adriana Reza, Zahid Hussain, Jason Akre, *(behind)* Eli Rotenberg, Jinghua Guo, Yi-De Chuang, Wayne Stolte, Gennadi Lebedev, Fred Schlachter, Jonathan Denlinger, Alexei Fedorov, Nasser Hamdan, and Mushtaq Salim. Not pictured: Glenn Ackerman, Elke Arenholz, John Bozek, Byron Freelon, Mike Martin, Bruce Rude, Xingjiang Zhou.

The primary mission of the Scientific Support Group (SSG, Figure 1) is to support the efforts of researchers at the ALS through scientific and technical collaboration and scientific outreach. Working with the users of the ALS, SSG members play an important role in developing novel instrumentation that enables those at the cutting edge of science to tackle challenging scientific problems. Depending on the needs of the user, the degree of collaboration can range from technical assistance with the beamline to full partnership in developing new research programs.

Staff scientists within SSG are also expected to maintain scientific and technical excellence in areas of synchrotron radiation research. Participation in active scientific programs is essential for such development, and all of the SSG scientists are active members of research programs at the ALS.

SCIENTIFIC OUTREACH

The SSG strives to expand the scientific program of the ALS and broaden its user base through publications and presentations. The group organizes a variety of seminars, including the weekly ALS/CXRO seminar series and a targeted weekly SSG Lecture Series. The weekly lectures focus on a topic of wide interest through a series of many lectures given by world-renowned scientists. The group has also initiated the quarterly ALS Colloquium.

The group, working together with the Users' Executive Committee (UEC), also helps to organize workshops exploring new scientific opportunities and needs for new beamlines or experimental facilities. Seven such workshops were conducted during the 2001 ALS Users' Meeting. These were heavily attended by enthusiastic scientists and triggered many fruitful discussions that should spark further advances in scientific endeavors at the ALS.

The SSG has also initiated a new ALS Doctoral Fellowship in Residence program. These doctoral fellowships allow beginning researchers to work at the frontier of synchrotron radiation research and to help advance state-of-the-art applications in many areas of physical and biological science. A selection committee consisting of Harald Ade (UEC Chair, North Carolina State University), David Attwood (UCB), Zahid Hussain (SSG), Stephen Kevan (Scientific Advisory Committee Chair, University of Oregon) and Neville Smith (ALS Division Deputy for Science) recommended five candidates for doctoral fellowships for academic year 2002. The award recipients in the field of physical sciences (Figure 2) and their research areas are as follows:

Alejandro Aguilar (University of Nevada, Reno)
Ion spectroscopy
Henry Chong (University of California, Berkeley)
Femtosecond x-ray spectroscopy with a slicing source
Steven Johnson (University of California, Berkeley)
Femtosecond x-ray spectroscopy with a streak camera
Cynthia Morin (McMaster University, Canada)
Characterization of protein interactions with biomaterials
Kevin Wilson (University of California, Berkeley)
X-ray spectroscopy of liquid jets

Figure 2 ALS Doctoral Fellows: *Back row, left to right,* Alejandro Aguilar, Henry Chong, and Kevin Wilson; *front row,* Steven Johnson and Cynthia Morin.

SUPPORT

Members of SSG are responsible for the operation, upgrade, and maintenance of most of the facility beamlines and many of the permanent endstations at the ALS. The undulator-based beamlines, Beamlines 4.0.2, 7.0.1, 8.0.1, and 10.0.1 and a photoemission branchline on Beamline 12.0.1, each have one or two SSG staff members responsible for their continued operation. The group is also playing an active role in fixing some of the problems in operation of the chemical dynamics Beamline 9.0.2 complex, which is operated by Berkeley Lab's Chemical Sciences Division through separate funding from the DOE Office of Basic Energy Sciences (more details below). Members of SSG are putting great emphasis on building the necessary infrastructure at the ALS to develop novel instrumentation most efficiently. In addition, continuing efforts are made in making the existing development system more user friendly. The year 2001 also saw the designing of several new experimental systems. Some of these are described below.

Advances in Infrared Research: Instrumentation and Future Directions

NEW IR MICROSCOPE AND BENCH FOR BIOLOGY

New infrared spectromicroscopy equipment was purchased for and installed on the ALS infrared beamlines on beam port 1.4. It includes the latest step-scan-capable Fourier-transform infrared (FTIR) bench and an infinity-corrected infrared microscope that will allow for a number of new sample visualization methods. This equipment was purchased with funding from the DOE Office of Biological and Environmental Research (the Principal Investigator is Hoi-Ying Holman of the Berkeley Lab Earth Sciences Division, with help from Mike Martin and Wayne McKinney of SSG) with the express purpose of developing biomedical and biological applications of synchrotron-based infrared spectromicroscopy.

The new spectromicroscopy equipment includes a Thermo Nicolet Nexus 870 step- and rapid-scan FTIR bench and a Thermo Spectra-Tech Continuum infrared microscope (Figure 3). The microscope includes two infrared detectors, a wide-band mercury cadmium telluride detector (MCT) and a fast (20-ns) MCT for time-resolved experiments. A fast digitizer (up to 100 MHz) complements the fast MCT detector. The synchrotron beam coupled into the infrared microscope continues to have a diffraction-limited spot size, thereby attaining a 200-fold increase in signal from a small (3–10-µm) sample spot compared to the spot for a conventional thermal infrared source. The infinity-corrected microscope optics allow for a number of additional sample visualization accessories that can help the user identify the important location within their sample for microinfrared analysis: visual and infrared polarizers, dark-field illumination, differential-interference-contrast optics, and ultraviolet fluorescence.

The new instrument will aid in user scientific research across many fields. For example, studies of individual living cells, toxic contaminants, bioremediation samples, protein microcrystals, rhizoids, and forensic evidence will all be enhanced by the additional capabilities of this new synchrotron FTIR spectromicroscopy system.

DEVELOPMENT OF A COHERENT FAR-INFRARED SOURCE

The first measurements at the ALS of coherent far-infrared synchrotron emission were performed during 2001 (an effort led by Mike Martin of SSG and John Byrd of the Accelerator Physics Group). Coherent bursts are observed coming from instabilities within high-current electron bunches. These measurements are leading toward the understanding and development of a stable, high-intensity coherent infrared source many orders of magnitude brighter than the best presently available sources.

We have used a number of accelerator physics shifts to make measurements with well-controlled sets of machine operating parameters. Light was measured at beam port 1.4 by using two liquid-helium-cooled silicon bolometers. We observed large intensity bursts when the single-bunch current was above about 7 mA at 1.5 GeV and above 12 mA at 1.9 GeV. We used the Bruker 66v/S FTIR spectrometer on Beamline 1.4.2 to measure the far-infrared spectrum of the bursts that

Figure 3 The new infinity-corrected infrared microscope on Beamline 1.4.3.

occur at the very top of the fill during regular two-bunch operations (Figure 4). The emission is peaked at ~27 cm^{-1}, indicating a microbunching within the electron bunch having a period on the order of 400 µm (or approximately 30 times smaller than the normal ALS bunch length). The bursting was clearly dependent on the beam energy (E), with higher intensity at 1.5 GeV. This energy dependence is to be expected, as the bunch length is proportional to $E^{3/2}$. Thus we expect higher peak currents, and therefore a greater tendency for instabilities and hence microbunching, at 1.5 GeV than at 1.9 GeV.

We are continuing these and other measurements to gain a greater understanding of coherent synchrotron emission. We will measure the coherent emission from a femtosecond laser-sliced electron bunch, as well as from short electron bunches, at Jefferson Lab and at BESSY II.

High-Precision Element- and Chemical-Site-Specific Vector Magnetometry

Beamline 4.0.2 is the first undulator beamline at the ALS to allow full control of the polarization of the x rays, from linear horizontal to helical to linear vertical, making it a unique tool to study dichroic effects, especially magnetic circular and linear dichroism. The undulator, in combination with a plane-grating, variable-included-angle monochromator, is designed to provide high-flux photon beams from 50 eV to 2000 eV. This beamline has gone through a long commissioning period but is now fully operational. The focus has now shifted to developing new instrumentation that could make the best use of the unique capability of this beamline.

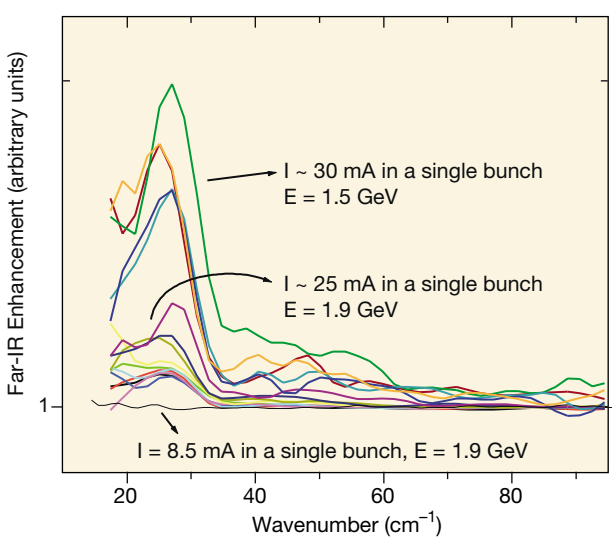

Figure 4 Far-infrared spectra taken at the very top of the fill during regular two-bunch operations show large-intensity bursts of coherent radiation that vary with beam energy and bunch current. The bursts are particularly strong at 1.5 GeV.

Multilayered, multielement, and heteromagnetic nanostructures are currently the subject of intense research activity, mainly because of their importance for magnetic data storage. For most multilayered magnetic device applications [magnetic recording media, giant magnetoresistance (GMR) read heads, magnetic random access memory (MRAM), spin-tunnel junctions (STJ), etc.], it is the change of the relative magnetization directions that defines the operation of the device and is therefore necessarily the critical process that must be thoroughly characterized and understood. To satisfy this need for detailed magnetic characterization of complex magnetic systems, we are currently developing a high-precision, element-specific and chemical-site-specific vector magnetometry endstation to be used for measurement of soft x-ray magnetic circular dichroism.

A team led by Elke Arenholz of SSG and Soren Prestemon of the Mechanical Engineering Group have completed the initial design of a four-axis electromagnet compatible with a sample manipulator that allows 360-degree polar and azimuthal rotation of the sample (Figure 5). This capability will give us access to any geometry of applied magnetic field, sample orientation, and x-ray incidence direction without any modifications of the experimental setup, thus allowing a complete characterization of the field dependence of the magnetization vector. The electromagnet will be able to achieve a maximum field of 0.8 T in any orientation relative to the sample to allow us to saturate the magnetization of many types of samples.

Photon-In–Photon-Out Spectroscopy of Materials

The Beamline 8.0.1 emission spectrograph developed by the Callcott group (University of Tennessee) has been the endstation of choice for independent investigators interested in carrying out photon-in–photon-out experiments. (See, for example, the water jet studies described below.) With the addition of Jinghua Guo to the SSG group, we have the expertise needed to make another system available on Beamline 7.0.1 with the help of the Nordgren group (Uppsala University, Sweden). Some progress has also been made in

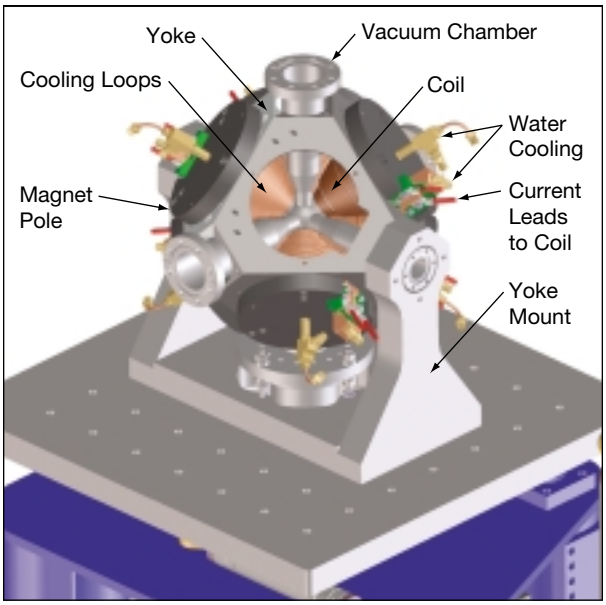

Figure 5 The design for the vector magnetometer on Beamline 4.0.2. The four-axis electromagnet gives access to any geometry of applied magnetic field, sample orientation, and x-ray incidence direction.

designing a new nanoscience characterization system that will be installed as a permanent endstation on Beamline 8.0.1. The principal investigators include Franz Himpsel (University of Wisconsin–Madison), Lou Terminello (Lawrence Livermore National Laboratory), and Stan Williams (Hewlett–Packard Laboratories). The Department of Energy has earmarked funds for the three-year project.

WATER JET STUDIES

Inner-shell photoionization studies of liquid water in vacuum were carried out on Beamlines 8.0.1 and 9.3.2 by University of California chemistry professor Richard Saykally and graduate student Kevin Wilson with the tireless assistance of SSG member Bruce Rude. A jet of liquid water is introduced into the vacuum chamber with a high backing pressure through a small aperture (tens of microns wide). The water moves through the vacuum as a well-defined jet for several tens of centimeters before breaking up into droplets. Total electron, total ion, fluorescence, and—most recently—partial ion yields have been measured from the water jet at photon energies around the oxygen 1s ionization edge (~550 eV). The trick is to minimize the exposure (in time and surface area) of the liquid water to the vacuum in order to keep the pressure at a low enough level to permit charged-particle detection. An endstation with a unique arrangement for pumping has been implemented to carry out these experiments, and it maintains a pressure of 10^{-5} Torr in the main chamber with the water jet flowing. Differential pumping separates the main chamber from the beamline and allows for windowless operation of the experiment on an ultrahigh-vacuum synchrotron beamline. Clear differences were observed between the total ion and electron yields from the liquid water, and both are different from the gas-phase yields that can be observed by moving the liquid jet out of the photon beam. Salt solutions as well as mixtures of ethanol and methanol have also been studied recently with this unique apparatus.

Further Improvements to the HERS System on Beamline 10.0.1

The high-energy-resolution spectrometer has been considered one of the world's premier facilities for carrying out angle-resolved photoemission experiments. Further improvements to the experimental capability were made in 2001 by incorporating a new custom-designed, improved Scienta analyzer (SES 2002) that will take us to the next level in ultrahigh angular and energy resolution in photoemission spectroscopy. The new analyzer, through the use of two different magnification angle modes, enables us to run the analyzer with an angular resolution of either ±0.05° or ±0.15°. Furthermore, it provides a maximum energy resolution of <1.8 meV. This is the result of a close collaboration between Z.-X. Shen's group from Stanford University and SSG's Zahid Hussain, carried out with funding from the DOE Office of Basic Energy Sciences and the ALS.

New Angle-Resolved Photoemission Branchline on Beamline 12.0.1

Through a collaboration between Daniel Dessau (University of Colorado) and Alexei Fedorov (University of Colorado and SSG), a new branchline for carrying out high-resolution photoemission experiments has been developed on Beamline 12.0 (Figure 6). The beamline, used primarily for EUV lithography metrology, used to be home to the MAXIMUM photoelectron microscope. When MAXIMUM was retired in early 2001, room was made available for a new branchline and endstation. The experimental station for angle-resolved photoemission spectroscopy (ARPES) has

been built up with an SES 100 electron energy analyzer, a sample transfer system with a liquid-helium-cooled sample manipulator, and a high-intensity ultraviolet lamp with a monochromator.

High-Efficiency Spin Detector for Photoemission Experiments

To date, spin-resolved photoemission has contributed a wealth of information about the physics of magnetic metals and alloys. In contrast, applications of this method to the new classes of complex materials with strong electron correlations and somewhat unusual magnetic properties (e.g., manganites, ruthenites, and hexaborides) have so far been very limited. The limitation, mainly due to the low efficiency of spin detection, has restricted its applicability for high energy resolution. To remedy this situation, we have developed a new mini-Mott detector (up to 30 keV) that achieves extremely high throughput by accepting and focusing the full line-source output slit (2 mm × 10 mm) of an energy analyzer rather than a small circular aperture.

Our design (Figure 7) includes a 90-degree bend and four channel electron multipliers (channeltrons). This allows us to simultaneously measure photoemission intensity and two components of spin polarization and to measure the third polarization component simply by rotating the detector. The use of a large exit slit, a clear beam path (no grid), and separate focusing elements for each channeltron (to collect over a larger solid angle) makes this spin detector about a factor of 30 more efficient than most other designs. The spin detector will be mounted to the exit plane of a high-throughput and -resolution Scienta SES 200 analyzer and is expected to allow us to carry out spin-resolved photoemission spectroscopy with an unprecedented energy resolution of 10–20 meV, comparable to kT. The scientists involved in this project include Alessandra Lanzara, Yulin Chen, and Z.-X. Shen from Stanford University and Alexei Fedorov, Gennadi Lebedev, Gary Krebs, Neville Smith, and Zahid Hussain from the ALS. After commissioning off line, the system will be installed in tandem with the ARPES chamber on Beamline 12.0.1.

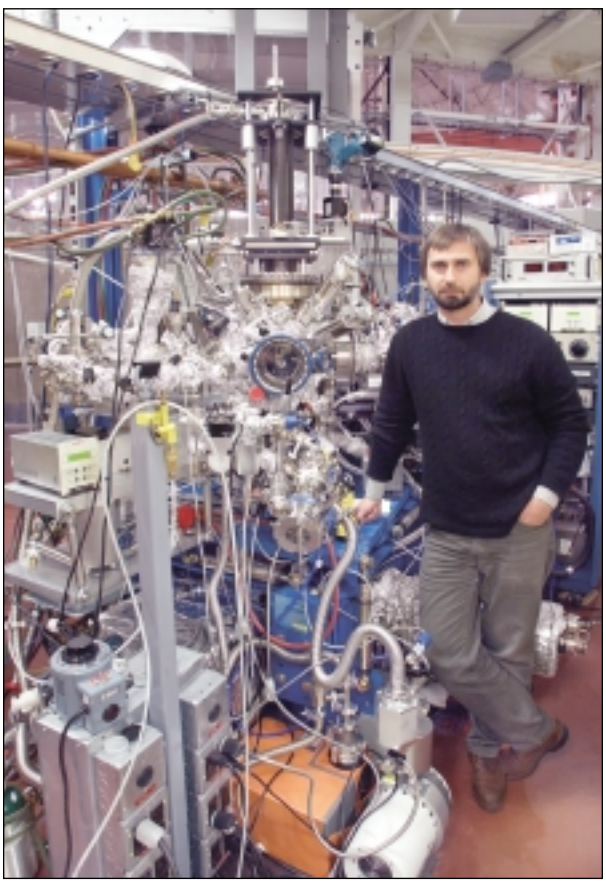

Figure 6 The endstation for Beamline 12.0.1's new high-resolution photoemission branchline.

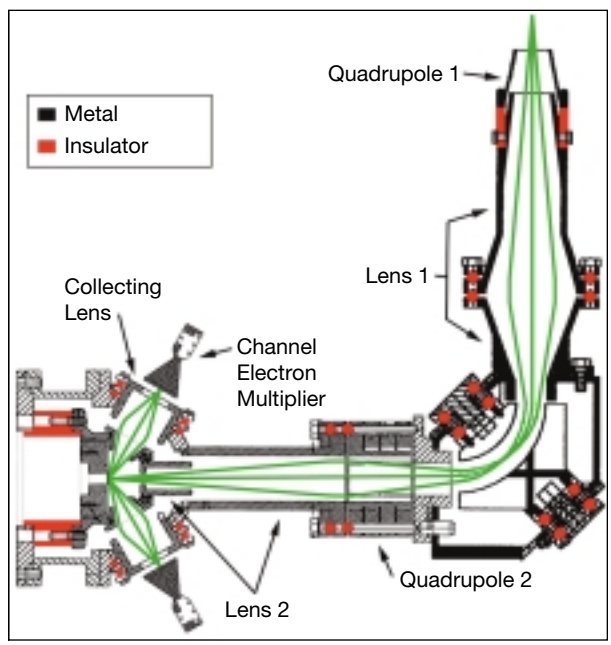

Figure 7 The use of a large exit slit, a clear beam path, and separate focusing elements for each channeltron makes this spin detector about 30 times as efficient as most other designs.

Momentum-Resolved Resonant Soft X-Ray Inelastic Scattering

Despite extensive research efforts, the electronic structure of strongly correlated quantum systems continues to be a major class of unsolved problems in physics. Well-developed momentum-resolved spectroscopies such as photoemission and neutron scattering cannot directly probe valence charge–charge correlation (fluctuation) spectra in a momentum-resolved manner, as angle-resolved photoemission probes the single-particle occupied states, and neutrons do not couple to the electron's charge directly. A good understanding of momentum-resolved charge–charge correlation functions is of paramount importance to gain insights into the charge-transport mechanisms in correlated systems.

A relatively new technique, resonant inelastic scattering at the transition-metal K edges, has recently been used to obtain intriguing results regarding excitons and the anisotropy and dispersion of the Mott Gap in correlated systems. For the 3d transition-metal oxides, the resonant scattering at the transition-metal $L_{2,3}$ edges promises to be very spectacular and should also, according to theory, have at least several orders of magnitude more scattering intensity in the inelastic channel. We are building, for use on Beamline 8.0.1, a novel soft x-ray spectrometer with a variable-line-spacing grating and a pre-mirror that is estimated to be 100–1000 times as efficient as those based on previous designs.

The prototype emission spectrograph (Figure 8) is optimized for Mn 2p at 650 eV and will provide an energy resolution of about 100 meV. The momentum transfer is enough to cover almost the whole Brillouin zone for manganites. This project, funded through Laboratory Directed Research and Development funds, is being developed in collaboration with M.D. Hasan from Princeton University and Z.-X. Shen from Stanford University. The project leader is SSG's Zahid Hussain. The optical design was done by James Underwood, and the mechanical engineering design was by Phil Batson, both from CXRO. Yi-De Chuang (a postdoctoral fellow) is taking care of the commissioning of the system. The same emission spectrograph will also be used by David Shuh (Berkeley Lab Chemical Sciences Division) et al. for the molecular environmental science project on Beamline 11.0.2.

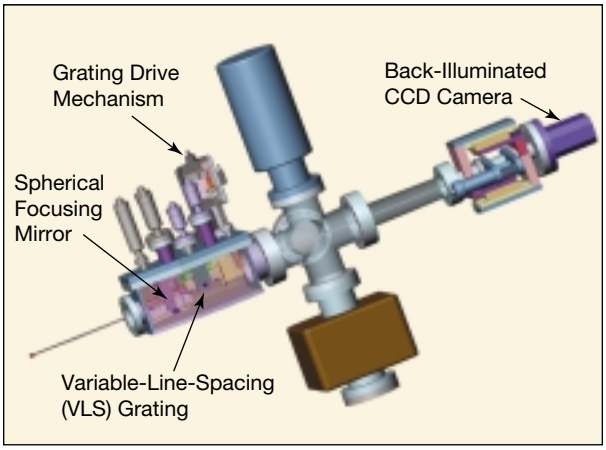

Figure 8 Design of the new soft x-ray spectrograph for Beamline 8.0.1, which uses a variable-line-spacing grating and a premirror that is estimated to be 100–1000 times as efficient as those based on previous designs.

Negative Ion Inner-Shell Photoionization Studies on Beamline 10.0.1

Until recently, research on the photoexcitation and photoionization of negative ions was concentrated on outer-shell photodetachment processes. Inner-shell (K-shell) photodetachment and excitation of negative ions provide a unique opportunity for exploring the dynamics of strongly correlated electron–electron interactions

A collaboration between John Bozek, Glenn Ackerman, and Bruce Rude of SSG and a group from Western Michigan University led by Nora Berrah has produced a negative-ion test facility comprising commercially produced negative-ion sources from the National Electrostatics Corporation and an ALS-designed support system, which couples them to the existing ion–photon facility (IPF) on Beamline 10.0. Negative lithium ions are produced in the SNICS II cesium-sputter ion source, and negative helium ions are produced by using an Alphatros source.

These ion sources operate at high potentials relative to ground, and it was necessary to design an elaborate interlocked enclosure to provide for personal safety and an interlock chain for equipment protection. The IPF beamline is a shared facility, designed, built, and used by Ron Phaneuf of the University of Nevada, Reno, to study multiply charged positive ions. Thus, the negative-ion-source enclosure also needed to be portable to facilitate changing the sources on the ion beamline. The enclosure contains the ion sources, an isolation transformer, a floating electrical rack for the necessary power supplies, and an ALS-designed chassis containing the relay logic for all of the interlocks.

The high probability of gas stripping for negative ions required that we design a vacuum system with a high pumping speed and low conductivity. In particular, the Alphatros source, used to generate negative helium ions, leaks a considerable amount of gas downstream from the charge-exchange chamber. So, a turbopumped differential pumping section was incorporated into the design. The ion sources have exceeded our expectations, and we plan to add additional diagnostics in the coming year.

New Staff and Upgraded Instrumentation for Beamline 7.0.1

This year, three new members joined the staff at Beamline 7.0.1. Aran Guy (shared with Beamline 8.0.1) is the new associate beamline scientist and is responsible for beamline maintenance and operations and for assisting users with experiment installation and operation. Jinghua Guo is a new beamline scientist with expertise in soft x-ray fluorescence spectroscopy (SXFS). He is responsible for scientific support of the soft x-ray fluorescence program at Beamline 7.0.1 as well as for conducting research into next-generation SXFS experiments. Kai Rossnagel, a Feodor Lynen postdoctoral fellow from Germany, provides scientific support for angle-resolved photoemission experiments and conducts his own program in the study of correlated materials.

The sample preparation endstation of the UltraESCA (a.k.a. "XPD") endstation has been redesigned by Byron Freelon of SSG. A new and separate chamber, pumps, and stand have been procured and will be installed in spring 2002. The new chamber features greatly expanded space for growth and characterization as well as a new capability for reverse-view low-energy electron diffraction (LEED).

Beamline 9.3.1 Monochromator Upgrade

The double-crystal monochromator on beamline 9.3.1 has been successfully upgraded to achieve considerably improved performance for experiments using extended x-ray absorption fine structure and those requiring photons in the energy range 2.3–5.5 keV. The monochromator was redesigned to include water cooling for the first crystal, a new control system, and a user-friendly interface; the result is greatly improved thermal and mechanical stability for energy scans over hundreds of eV. The beamline is presently in operation for users. The first experiments are near-edge absorption spectroscopy (XANES) measurements of complex materials containing titanium and vanadium by a group from the University of California, Berkeley. A sample absorption spectrum for crystalline barium titanate (Figure 9, courtesy of Heinz Frei of the Berkeley Lab Physical Biosciences Division) shows absorption at the titanium K edge and the barium L edge. This effort was headed by SSG's Fred Schlachter with help from the Mechanical Engineering Group and Alastair MacDowell and Tony Warwick from the Experimental Systems Group.

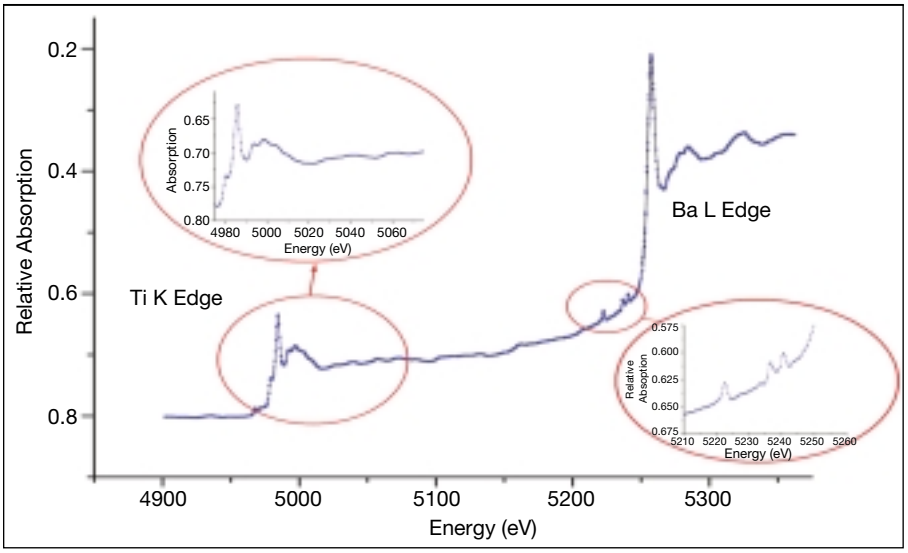

Figure 9 Sample absorption spectrum for barium titanate crystals, taken at Beamline 9.3.1. The monochromator upgrade significantly improved performance for scans in the 2.3–5.5 keV energy range.

User Services

Gary Krebs, *User Services Group Leader*

Introduction

The User Services Group provides an interface to the facility for new and continuing users at the ALS. The group is made up of the User Services Administration, Beamline Coordination, and Technical Information Sections. These groups work together to provide users with a wide range of services. It is the goal of the ALS to continue to provide these varied services in a friendly and efficient manner.

Figure 1 The User Services Administration Section: *left to right,* Jeremy Coyne, Bernadette Dixon, Barbara Srulovitz, Adriana Reza, and Barbara Phillips. Not pictured, Ruth Pepe and Sharon Fujimura.

User Services Administration

The User Services Office is located on the mezzanine floor of the ALS. Recently, to consolidate activities, the office moved down the hall from its previous location. The reception area, still located on the second floor directly across from the lobby elevator, provides a convenient point of contact for ALS users. The User Services Office is staffed by members of the User Services Administration Section (Figure 1), who help new users through the required registration process before they begin work at the ALS. All users receive an electronic identification card, which allows them access to the ALS experiment floor. New users also watch a short safety video that describes some of the potential safety hazards at the facility and outlines the experiment safety-checkout process. New users can complete much of the processing before they arrive by preregistering on the ALS Web site (www-als.lbl.gov). Through its oversight of the registration process, the User Services Administration Section also collects data about user publications and demographics. As a national user facility, the ALS is required to report these statistics annually to the U.S. Department of Energy.

In another of its many functions, the User Services Administration Section coordinates the allocation of beam time through a peer-review process. For all the sciences except protein crystallography, independent-investigator requests for beamtime are received through the ALS Web site twice annually. Protein crystallography proposals, also submitted over the Web, are reviewed by a separate panel but are received and evaluated monthly to better meet the need of this scientific community for rapid access. All proposals for beam time are reviewed by one of the two Proposal Study Panels and, under the direction of ALS Division Deputy for Science Neville Smith, beam time is allocated based on principles and guidelines agreed upon by the ALS and the Users' Executive Committee (UEC). These principles and guidelines adhere to those of the International Union of Pure and Applied Physics. The UEC, elected annually by the users, is the voice of that diverse group and represents them at the ALS as an advisory body. Proposal Study Panel members are chosen in consultation with the UEC to cover the wide range of sciences represented at the ALS. The User Services Administration Section provides administrative and logistical support to both the PSP and the UEC. The proposal submission and beam time allocation process is described in greater detail on the ALS Web site (www-als.lbl.gov/als/quickguide/independinvest.html).

For out-of-towners, the User Services Office can also help in finding a place to stay while working at the ALS. The office manages the ALS apartments (Figure 2), which are located near Berkeley Lab on the main shuttle-bus route. The apartments, recently increased in number, are available to all ALS users, and detailed information about costs and other factors can be found on the Web at www-als.lbl.gov/als/quickguide/housing.html.

The User Services Administration Section was managed by Ruth Pepe through June, 2001, and Bernie Dixon took over as manager in July 2001. It includes Jeremy Coyne, Sharon Fujimura, Adriana Reza, Barbara Srulovitz, and Barbara Phillips.

Figure 2 The ALS maintains a number of apartments for its users from out of town.

Beamline Coordination

The Beamline Coordination Section (Figure 3) serves as a point of contact for users on the experiment floor. Section members act as liaisons between users and both ALS and Berkeley Lab resources. They provide shipping and receiving and temporary storage services as well as endstation setup and safety-checkout support. Ensuring that all user experiments are checked for safety is a crucial function of this group. Section members work closely with various Berkeley Lab safety specialists in the areas of electrical, mechanical, chemical, radiation, and laser safety. This safety checkout process is required in order to assure the safety of all users on the experiment floor. Upon the successful completion of the required safety checks, section members enable the beamlines for use. The Beamline Coordination Section also maintains a stock room of parts and equipment commonly needed by ALS users and ALS technicians (Figure 4). These supplies are accessible by proximity card 24 hours a day. The Beamline Coordination Section is led by Donna Hamamoto and includes Gary Giangrasso, Cheryl Hauck, Alex Lobodovsky, Tony Marquez, Todd Anderson, and Ken Winters.

Figure 3 The Beamline Coordination Section: *front,* Donna Hamamoto; *back,* Cheryl Hauck, Alex Lobodovsky, Ken Winters, Todd Anderson, Tony Marquez, and Gary Giangrasso.

Figure 4 The ALS user stock room makes a wide variety of beamline necessities easily available.

Technical Information

The Technical Information Section (Figure 5) is responsible for this Activity Report as well as the annual Compendium of User Abstracts. The group's members also prepare special brochures and create posters and announcements for countless workshops and conferences. They are responsible for the "Science Highlights" shown in the ALS lobby, around the experiment floor, and on the ALS Web site. In addition, the section maintains and develops the ALS Web site and writes and edits the electronic newsletter, ALSNews. The section, composed of science writers along with graphics and Web experts, provides the ALS scientific community as well as the general public with information about the science carried out at the ALS. The group maintains a strong tie to the educational community, both within the state of California and internationally. In conjunction with the User Services Office, this group coordinates tours for the thousands of visitors—often from high schools, universities, and industry—who come to glimpse the ALS annually. The Technical Information section is led by Art Robinson and includes Annette Greiner, Elizabeth Moxon, Lori Tamura, and Greg Vierra.

Figure 5 The Technical Information Section: *left to right,* Art Robinson, Lori Tamura, Annette Greiner, Greg Vierra, and Elizabeth Moxon.

Special Events

2001 was an especially exciting and eventful year at the ALS. The facility hosted its largest user meeting ever, introduced its first commercial beamline and its first superbend beamlines, and welcomed an unprecedented number of distinguished visitors. Though finding itself the object of much attention in the scientific world, the ALS continued its outreach and diversity efforts, reaching out to the general public, students, and teachers both locally and abroad.

2001 ALS Users' Meeting

A busy schedule of facility updates, scientific highlights, workshops, a poster session, and a student poster competition attracted more than 350 participants to this year's ALS Users' Meeting. The record number of attendees reflected the ever increasing interest in the diverse research capabilities at the ALS, as did the seven workshops, which covered topics including future directions in soft x-ray molecular environmental science; advanced detectors for synchrotron experiments; infrared spectromicroscopy and future infrared sources; correlated materials and nanoscale phenomena; macromolecular crystallography; and a synchrotron radiation research theory network (SRRTNet) workshop on theory, computation, and synchrotron experiments.

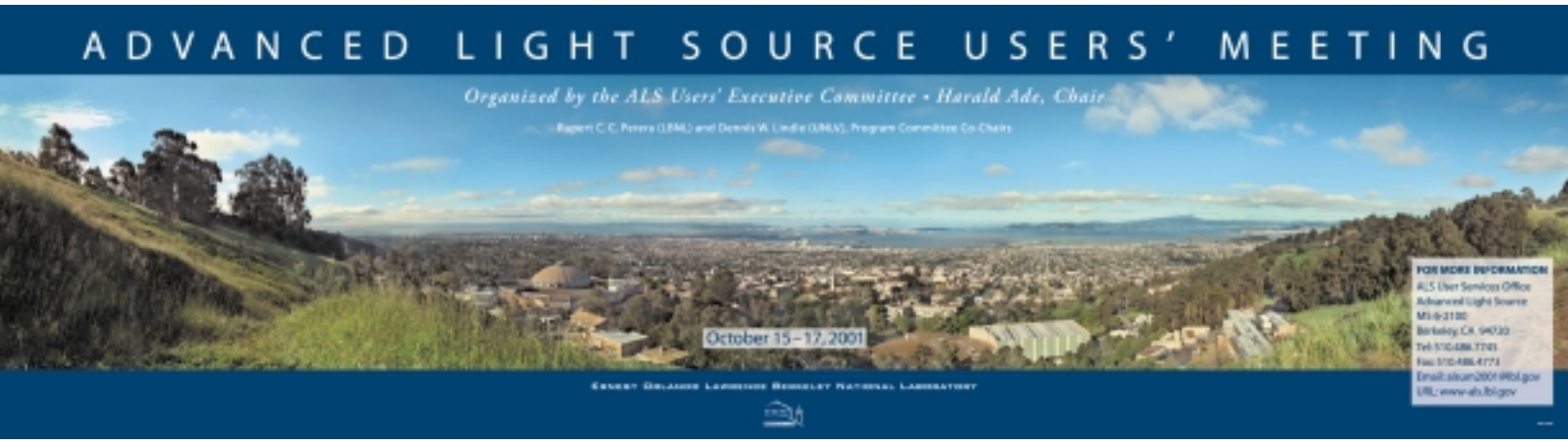

During the morning session, Patricia Dehmer *(left)*, U.S. Department of Energy Associate Director for Basic Energy Sciences, presented the perspective from Washington. Her talk was followed by ALS Division Director Daniel Chemla's *(center)* facility update highlighting the growth and diversity of the ALS scientific program. *Bottom,* Yves Petroff (Senior Advisor on sabbatical from the European Synchrotron Radiation Facility) kicked off the scientific highlights session with an analysis of recent scientific successes at the ALS and possible routes for continued productivity.

Capacity crowds attended the seven workshops that followed the conclusion of the meeting.

In a departure from recent years, the Users' Meeting Awards Banquet was held on the ALS patio. The early evening event also showcased vendor exhibits *(center),* the poster session *(left)*, and the student poster competition (*right).*

This year, the Halbach Award for Outstanding Instrumentation went to the team responsible for the successful design and installation of the superbend magnets. Accelerator Physics Group Leader David Robin (*left,* with UEC Chair Harald Ade) accepted on behalf of the Superbend Team (photo, page 65).

ALS Beamline Scientist Elke Arenholz (upper right, with Ade) and Laser Safety Officer Ken Barat (lower right) shared the Tim Renner User Services Award.

Gary Mitchell *(above, right)* and Ed Rightor (Dow Chemical Company) received the David A. Shirley Award for Science at the ALS for their research on superabsorbent polymers.

Left to right, Christoph Bostedt (Lawrence Livermore National Laboratory and ALS) and Hendrik Ohldag (SSRL and ALS) shared the student poster award.

Berkeley–Stanford Summer School in Synchrotron Radiation

The summer of 2001 marked the inaugural session of the Berkeley–Stanford Summer School in Synchrotron Radiation. Sponsored by the University of California, Berkeley; Stanford University; Berkeley Lab; Stanford Synchrotron Radiation Laboratory (SSRL); and the Division of Continuing Education in Engineering, UC Berkeley Extension, the week-long residential program provided a comprehensive overview of synchrotron radiation, its technologies, and a broad range of scientific applications. The summer school, which will be held at Stanford in 2002, is intended for graduate students in the physical sciences.

Participants of the first Berkeley–Stanford Summer School. David Attwood *(fourth from right)* of the Center for X-Ray Optics (Berkeley Lab) and UC Berkeley and Anders Nilsson of SSRL and Stockholm University *(second from right)* organized this year's session.

As part of the summer school, students toured the ALS and spoke with many ALS scientists, including Tony Warwick *(top, left)*, Jonathan Denlinger *(middle, left)*, and Tony Young *(bottom, right).*

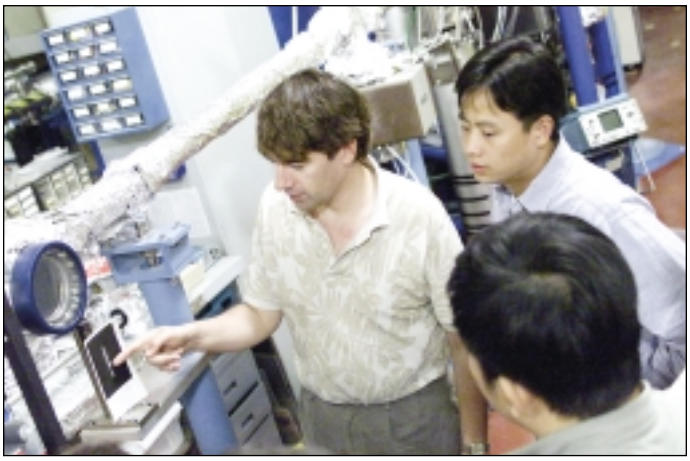

AXSUN Beamline Dedication

A new era of public–private sector collaboration was celebrated in June when Beamline 3.3.1, funded entirely by AXSUN Technologies, was dedicated at the ALS. Using x-ray lithography, the AXSUN beamline will make miniature molds for the microcomponents required for manufacturing advanced microelectro-mechanical structures that are used in the assembly of integrated photonic products.

During the dedication ceremony, AXSUN president Dale Flanders gave an overview of the lithography process.

Dale Boehme, director of LIGA technology for AXSUN, presented a plaque to the ALS in recognition of the project's successful completion.

From left, ALS Director Daniel Chemla, AXSUN president Dale Flanders, Berkeley Lab Director Charles Shank, and Jim Lewis, vice president of sales for AXSUN, cut the ceremonial ribbon in front of Beamline 3.3.1.

ALS staff and invited guests joined the celebration on the ALS patio with food and music courtesy of AXSUN Technologies.

Nitschke Award

Former ALS project manager Ron Yourd *(above, second from left)* was presented with the J.M. Nitschke Technical Excellence Award for his success in the enormous job of managing the ALS construction project to completion, on budget and on schedule. The award was presented by Berkeley Lab nuclear chemist Albert Ghiorso *(right)* and ALS Mechanical Engineering Group Leader Alan Paterson *(left)* as ALS Director Daniel Chemla looked on.

The J.M. Nitschke award is made through the East Bay Community Foundation, with funds from the estate of the late Michael Nitschke, a long-time physicist in Berkeley Lab's Nuclear Science Division who died in 1995.

Pappy's Boys

Pappy's Boys, a University of California, Berkeley, Alumni club, visited the ALS in February 2001. The club, made up of former football players who played for Cal's legendary coach "Pappy" Waldorf during the period from 1947 to 1956, saw the ALS from the top of the storage ring with ALS engineer Art Ritchie *(top)* and got an introduction to x-ray microscopy from Deborah Yager of Life Sciences *(bottom).*

Distinguished Visitors

Former Berkley Lab employee Muriel Miller *(left)* and ALS Division Deputy for Science Neville Smith *(right)* stop for a moment atop the storage ring shielding. Ms. Miller worked at the 184-inch cyclotron (the precursor to the ALS) in the 1940s, and was known for her ability to tune the beam better than any of her peers. She was visiting Berkley Lab this year as part of the 100th birthday celebration of LBNL's founder E.O.Lawrence.

In September, Neville Smith *(left)* and Scientific Support Group Leader Zahid Hussain *(second from left)* hosted visiting scientists from the National Science Council of Taiwan, Republic of China.

Department of Energy Undersecretary Robert. G. Card *(fourth from right)* listened as Keith Jackson of the Center for X-Ray Optics described the scientific applications of the EUV (extreme ultraviolet) lithography metrology beamline at the ALS.

Pierre Nzila *(left)*, Minister of Education for the Republic of Congo, spoke with Greg Denbeaux *(right)* of the Center for X-Ray Optics about x-ray microscopy during a visit to the ALS. The minister, accompanied by the Education Advisor to the Congo president and the Chancellor of the Marein Ngouabi University in Brazzaville, was visiting Berkeley Lab to find out about educational and research opportunities for Congolese students.

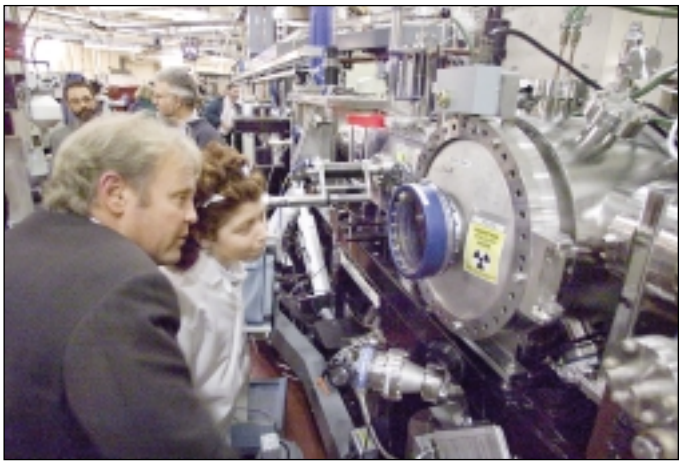

Berkeley Lab's David Shuh *(upper right)* shows young inventor Annie Austin the intricacies of an ALS beamline. Annie joined three other winning young inventors as they listened to Hoi-Ying Holman *(lower right)* of Earth Sciences discuss the applications of infrared spectromicroscopy. The four young students were winners of a contest to design energy-efficient products. The contest was sponsored by the Department of Energy's EnergySmart Schools program and supported by Owens Corning.

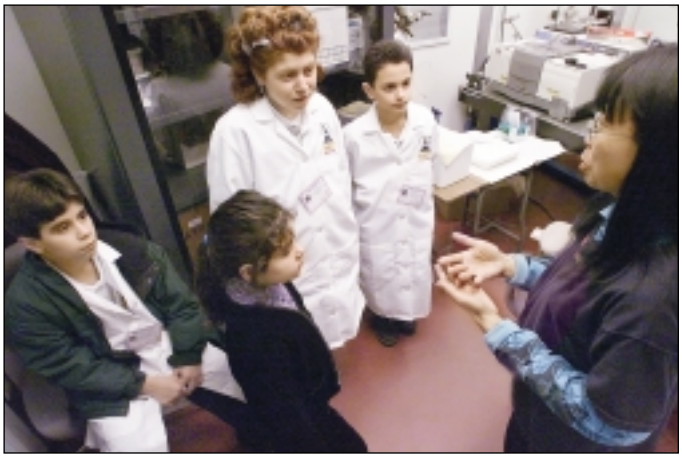

James Decker *(left)*, acting director of the U.S. Department of Energy's Office of Science, joined Berkeley Lab Director Charles Shank at the dedication of superbend Beamline 8.3.1. During the brief ceremony, Mr. Decker congratulated ALS management and staff for the successful completion of the superbend project.

U.S Congresswoman for the Sixth Congressional District Lynn Woolsey got the "inside story" as she toured the storage ring with, *from left,* Neville Smith, Zahid Hussain, and Charles Shank.

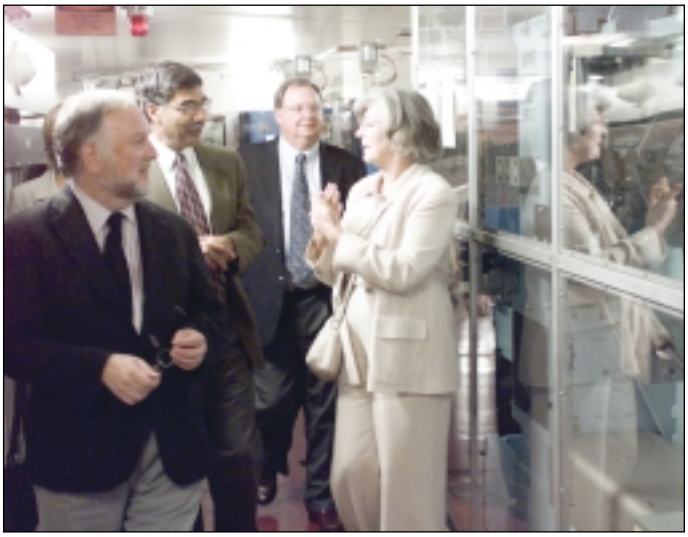

Educational Outreach and Diversity

The ALS continues to keep its doors open to the scientists of the future by being an accessible learning resource for teachers and students at home and abroad. Locally, on-site tours, mentoring of students and teachers from underrepresented school populations, and special events like Daughters and Sons to Work Day provide opportunities for budding scientists from all backgrounds to grasp the possibilities of careers in science and technology. MicroWorlds (www.lbl.gov/MicroWorlds), our interactive educational Web site, continues to provide information about synchrotron-related science to an international audience of students and educators.

Students from the Ecole Polytechnique de Tunisie (Polytechnic School of Tunisia) visited the ALS as part of a Northern California tour of high-tech manufacturing and research facilities. At the ALS , the visitors listened as Beamline Scientist Michael Martin *(left)* discussed recent research in infrared spectromicroscopy and later paused for a group photo on the patio with ALS Division Director Daniel Chemla, an alumnus of the school.

Future scientists from Montera Middle School in Oakland visited the ALS as part of their after-school science club program. The Techbridge science and technology program for girls is coordinated in conjunction with Oakland's Chabot Science Center. Gretchen Giedt *(left)* of Physical Biosciences gave the young women tips on making protein crystals, while ALS Division Deputy for Operations Ben Feinberg *(right)* gave them the opportunity to see an undulator up close.

ALS editor Annette Greiner prepares her charges for a scientific scavenger hunt during Berkeley Lab's 2001 Daughters and Sons to Work Day.

Mhairi Donohoe of the Physical Biosciences Division introduced high-school students from a small Inupiat village in Alaska to the inner workings of a protein crystallography endstation.

Latino students from Richmond High School visited the ALS to get an idea about career opportunities in science and possible summer mentorships. Elizabeth Moxon *(above, in black vest)* of the ALS talked to the students atop the storage ring. The students later posed on the ALS patio. The visit was sponsored by the Berkeley Lab Workforce Diversity Office and the Latino and Native American Association.

ALS Advisory Panels

Science Policy Board

Advises the Berkeley Lab Director on major policy issues concerning the ALS.

William Brinkman, Lucent Technologies/Bell Laboratories

John Carruthers, Intel Corporation

Chien-Te Chen, Synchrotron Radiation Research Center, Taiwan

Peter Eisenberger, Columbia Earth Institute

Paul Fleury, University of New Mexico

Franz J. Himpsel, University of Wisconsin–Madison

Yuan T. Lee, Academia Sinica, Taiwan

Albert Narath, Lockheed Martin Corporation (retired)

Yves Petroff, Lawrence Berkeley National Laboratory/European Synchrotron Radiation Facility

Stephen D. Kevan (ex officio), University of Oregon

Scientific Advisory Committee

Advises Berkeley Lab and ALS management on issues relating to ALS operations, resource allocation, strategic planning, and Participating Research Team proposals and research.

Harald Ade, North Carolina State University

Ernst G. Bauer, Arizona State University

James M. Berger, University of California, Berkeley

Jeffrey Bokor, University of California, Berkeley

John Carruthers, Intel Corporation

Wolfgang Eberhardt, BESSY GmbH, Germany

Yves Idzerda, Montana State University

Stephen D. Kevan (chair), University of Oregon

Alain Manceau, Université Joseph Fourier, France

Anders Nilsson, Stanford Synchrotron Radiation Laboratory/Stockholm University

Sunil Sinha, University of California, San Diego

Janet Smith, Purdue University

John Spence, Lawrence Berkeley National Laboratory/Arizona State University

Anthony Starace, University of Nebraska, Lincoln

Louis J. Terminello, Lawrence Livermore National Laboratory

Users' Executive Committee

Elected by the members of the Advanced Light Source Users' Association to act as the official voice of the user community in its interactions with ALS management.

Harald Ade (Chair), North Carolina State University

Nora Berrah (Past Chair), Western Michigan University

Aaron Covington, University of Nevada, Reno

Jennifer A. Doudna, Yale University

Roger Falcone, University of California, Berkeley

Lewis Johnson, Florida A & M University, Tallahassee

Carolyn A. Larabell, University of California, San Francisco

Dennis W. Lindle, University of Nevada, Las Vegas

Gerry McDermott, Lawrence Berkeley National Laboratory

Cheuk-Yiu Ng, Iowa State University

Rupert C. Perera, Lawrence Berkeley National Laboratory

ALS Staff

This is a cumulative list of all those who worked at the ALS during the 2001 calendar year. The list includes visitors, students, and staff members from other divisions who were matrixed to the ALS.

MANAGEMENT

D. Chemla
B. Feinberg
Z. Hussain
G. Krebs
J. Krupnick
H. Padmore
Y. Petroff
D. Robin
N. Smith

ACCELERATOR PHYSICS

J. Byrd
T. Byrne
S. Lidia
A. Loftsdottir
H. Nishimura
F. Sannibale
T. Scarvie
C. Steier
W. Wan
Y. Wu

ADMINISTRATION

P. Epps
M. Fenner
R. Pepe
A. Reza
M. Sattar
L. Senft

BUDGET

S. Rossi
J. Zelver

CONTROLS

A. Biocca
W. Brown, Jr.
E. Domning
K. Fowler
C. Ikami
S. Jacobson
J. McDonald
A. Robb
L. Shalz
J. Spring
R. Steele
C. Timossi
J. Tunis
E. Williams

ENVIRONMENT, HEALTH & SAFETY

W. Agot
R. Baker
G. Perdue
P. Thomas

ELECTRICAL ENGINEERING

B. Bailey
M. Balagot
K. Baptiste
W. Barry
M. Bell
R. Benjegerdes
T. Bilstein
K. Bolin
R. Candelario
M. Chin
R. Cole
R. Colston
L. Dominguez
J. Elkins
M. Estrema
D. Edwards
M. Fahmie
M. Foster
R. Gassaway
R. Gervasoni
A. Geyer
J. Gregor
J. Hellmers
M. Hilburn
L. Holzer
L. Jordan
J. Julian
S. Kwiatkowski
E. Lee
A. Lindner
P. Molinari
D. Narron
T. Nhan
J. Nomura
F. Ottens
A. Ritchie
P. Rosado
S. Rogoff
H. Scheid
A. Sippio
R. Slater
G. Stover
M. Thomas
M. Vinco
S. Warner
J. Weber
M. Williams
K. Woolfe

EXPERIMENTAL SYSTEMS

R. Celestre
S.-B. Choe
A. Doran
S. Fakra
J. Feng
A. Franck
E. Glover
E. Harvey
H. He
P. Heimann
M. Howells
S. Irick
A. MacDowell
M. Marcus
W. McKinney
A. Scholl
R. Sublett
N. Tamura
A. Thompson
A. Warwick
A. Young

MECHANICAL ENGINEERING

J. Akre
N. Andresen
R. Armstrong
W. Baldock

D. Baum
L. Bonifas
D. Calais
D. Cambie
M. Coleman
D. Colomb
J. Comins
C. Cummings
D. Davis
M. Decool
R. DeMarco
R. Duarte
D. Eastman
Z. Eisentraut
K. Franck
A. Gavidia
D. Gibson
C. Hopkins
D. Hull
D. Jones
J.Y. Jung
N. Kelez
S. Klingler
C. Knopf
G. Koehler
M. Kritscher
K. Krueger
A. Lim
B. Macdonell
D. MacGill
S. Marks
C. Matuk
P. McKean
H. Meyer
V. Moroz
G. Morrison
W. Oglesby
J. Osborne
A. Paterson
R. Patton
J. Pepper
P. Pipersky
D. Plate
S. Prestemon
K. Rex
R. Schlueter
N. Searls
K. Sihler
T. Stevens
H. Stewart
M. Thomas
W. Thur
A. Wandesforde
R. Weidenbach
E. Wong
J. Zbasnik
F. Zucca

OPERATIONS

D. Bentsen
J. Bishop
D. Brothers
E. Diaz
O. Jones
J. Pusina
B. Samuelson
T. Scarvie
S. Stricklin
M. Wolfe

PROCEDURE CENTER

R. Jones

PROJECT MANAGEMENT

A. Catalano
J. Harkins

QUALITY ASSURANCE

E. Lampo

SCIENTIFIC SUPPORT

G. Ackerman
E. Arenholz
J. Bozek
J. Denlinger
B. Freelon
J. Guo
N. Hamdan
G. Lebedev
M. Martin
E. Rotenberg
B. Rude
F. Schlachter

USER SERVICES

T. Anderson
J. Coyne
B. Dixon
S. Fujimura
G. Giangrasso
A. Greiner
D. Hamamoto
C. Hauck
A. Lobodovsky
A. Marquez
E. Moxon
B. Phillips
A. Robinson
B. Srulovitz
L. Tamura
G. Vierra

VISITORS AND STUDENTS

B. Batterman
P. Bogdanov*
V. Brouet
W. Caldwell*
S. Canton
Y. Chen*
H. Chong*
Y.-D. Chuang
S. Clark
J. Diaz
A. Fedorov
Z. Hasan*
S. Johnson*
D. Kilcoyne
W. Ling*
A. Lanzara
A. Lindenberg*
S. Locklin*
A. Manceau
C. Morin*
J. Patel
J. Spence
W. Stolte
G. Turri
E. Umbach
M. Van Hove
Y. Wang
K. Wilson*
C. Won*
W. Yang
X. Zhou

**Graduate Student Research Assistant*

Facts and Figures

Using the Advanced Light Source

The ALS, a Department of Energy national user facility, welcomes researchers from universities, industry, and government laboratories. Qualified users have access either as members of Participating Research Teams (PRTs) or as independent investigators. PRTs (groups of researchers with related interests from one or more institutions) construct and operate beamlines and have primary responsibility for experiment endstation equipment. They are entitled to a certain percentage of their beamline's operating time according to the resources contributed by the PRT. Through a peer-reviewed proposal process, the remaining beamtime is granted to independent investigators, who may provide their own endstation or negotiate access to a PRT-owned endstation.

The ALS does not charge users for beam access if their research is nonproprietary. Users performing proprietary research are charged a fee based on full cost recovery for ALS usage. All users are responsible for the day-to-day costs of research (e.g., supplies, phone calls, technical support).

The nominal operating energy of the ALS storage ring is 1.9 GeV, although it can run from 1.0 to 1.9 GeV, allowing flexibility for user operations. At 1.9 GeV, the normal maximum operating current is 400 mA in multibunch operation. The spectral range of undulator and wiggler beamlines extends from photon energies of roughly 5 eV to 21 keV. On superbend beamlines the range is between 2.4 and 60 keV. Bend magnets produce radiation from the infrared to about 20 keV.

The ALS is capable of accommodating approximately 50 beamlines and more than 100 endstations. The first user beamlines began operation in October 1993, and there were 28 operating beamlines, with several more under construction, by the end of 2001.

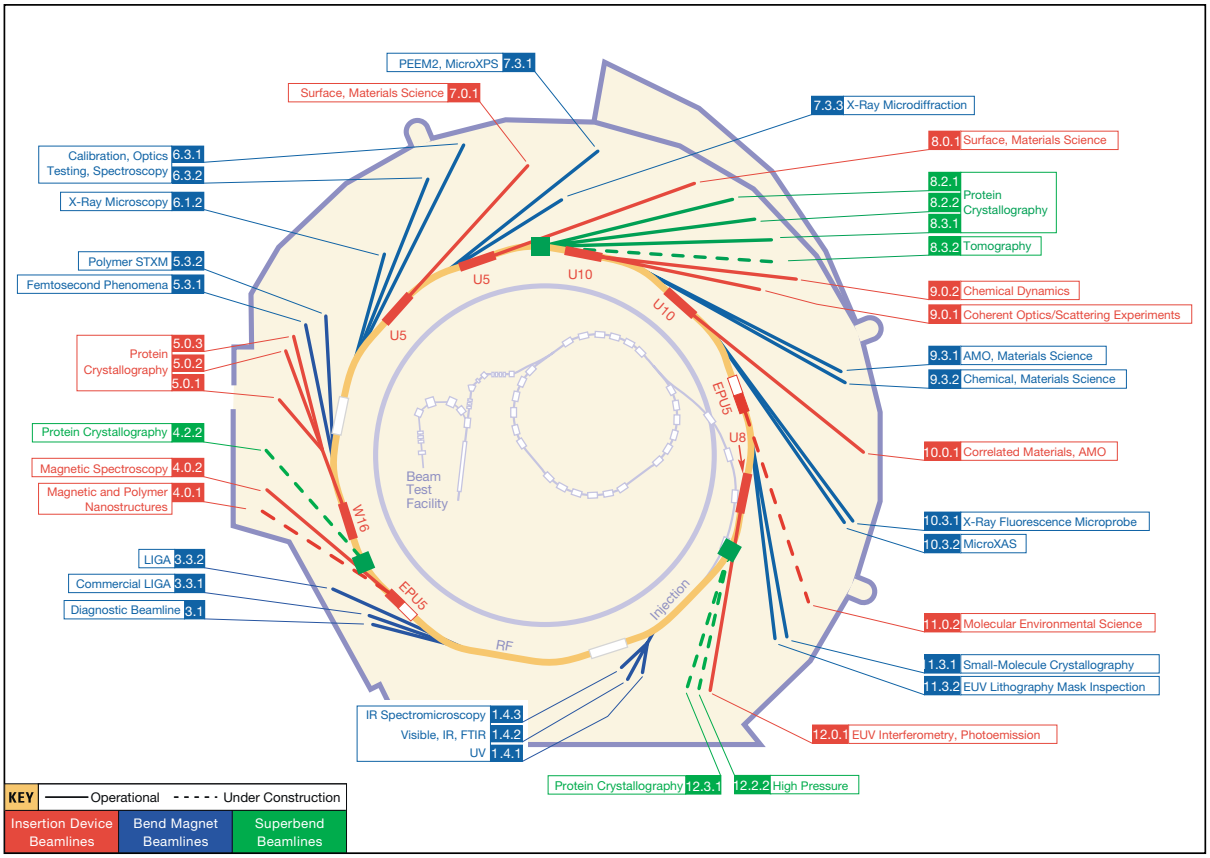

ALS Beamlines*

BEAMLINE	SOURCE**	AREAS OF RESEARCH/TECHNIQUES	MONOCHROMATOR	ENERGY RANGE	OPERATIONAL
1.4.1	Bend	Ultraviolet photoluminescence	0.5 m single grating	1.6–6.2 eV	Now
1.4.2	Bend	Visible and infrared Fourier transform spectroscopy (FTIR)	Interferometer	0.002–3 eV (15–25,000 cm^{-1})	Now
1.4.3	Bend	Infrared spectromicroscopy	Interferometer	0.05–1 eV (550–10,000 cm^{-1})	Now
3.1	Bend	Diagnostic beamline	Mirror/filter	1–2 keV	Now
3.3.1	Bend	Commercial deep-etch x-ray lithography (LIGA)	None	3–12 keV	Now
3.3.2	Bend	Deep-etch x-ray lithography (LIGA)	None	1–20 keV	Now
4.0.2	EPU5	Magnetic spectroscopy			
		XMCD chamber	Variable-included-angle PGM	52–1900 eV	Now
		X-ray absorption chamber	Variable-included-angle PGM	52–1900 eV	Now
		Advanced photoelectron spectrometer/diffractometer	Variable-included-angle PGM	52–1900 eV	Now
		Gas-phase absorption cell	Variable-included-angle PGM	52–1900 eV	Now
		Spin spectrometer	Variable-included-angle PGM	52–1900 eV	Now
		MXCD cryo-chamber	Variable-included-angle PGM	52–1900 eV	Now
		L-edge chamber with superconducting spectrometer	Variable-included-angle PGM	52–1900 eV	Now
		XMCD chamber (6 T, 2 K)	Variable-included-angle PGM	52–1900 eV	Now
		Photoemission electron microscope	Variable-included-angle PGM	52–1900 eV	Now
4.2.2	S-bend	Multiple-wavelength anomalous diffraction (MAD) and monochromatic protein crystallography	Double crystal	6–18 keV	2002
5.0.1	W16	Monochromatic protein crystallography	Curved crystal	12.4 keV	Now
5.0.2	W16	Multiple-wavelength anomalous diffraction (MAD) and monochromatic protein crystallography	Double crystal	3.5–14 keV	Now
5.0.3	W16	Monochromatic protein crystallography	Curved crystal	12.4 keV	Now
5.3.1	Bend	Femtosecond phenomena	Double crystal	1.8–12 keV	Now
5.3.2	Bend	Polymer scanning transmission x-ray microscopy	SGM	150–650 eV	Now
6.1.2	Bend	High-resolution zone-plate microscopy	Zone-plate linear	300–900 eV	Now
6.3.1	Bend	Calibration and standards, EUV/soft x-ray optics testing, solid-state chemistry	VLS-PGM	500–2000 eV	Now
6.3.2	Bend	Calibration and standards; EUV optics testing; atomic, molecular, and materials science	VLS-PGM	50–1300 eV	Now

* This table is valid as of March 2002. The most current information on ALS beamlines is available on the World Wide Web (http://www-als.lbl.gov/als/als_users_bl/bl_table.html).

** Bend = bend magnet; S-bend = superbend magnet; EPU5 = 5-cm-period elliptical polarization undulator; W16 = 16-cm-period wiggler; Ux = x-cm-period undulator.

ALS Beamlines (continued)

BEAMLINE	SOURCE**	AREAS OF RESEARCH/TECHNIQUES	MONOCHROMATOR	ENERGY RANGE	OPERATIONAL
7.0.1	U5	Surface and materials science, spectromicroscopy, spin resolution, photon-polarization dichroism			
		Scanning photoemission microscope (SPEM)	SGM	100–800 eV	Now
		Scanning transmission x-ray microscope (STXM)	SGM	180–900 eV	Now
		Spin-resolved endstation (SPIN)	SGM	60–1200 eV	Now
		UltraESCA	SGM	60–1200 eV	Now
		Soft x-ray fluorescence spectrometer (SXF)	SGM	50–1200 eV	Now
7.3.1.1	Bend	Magnetic microscopy, spectromicroscopy	SGM	175–1500 eV	Now
7.3.1.2	Bend	Surface and materials science, micro x-ray photoelectron spectroscopy	SGM	175–1500 eV	Now
7.3.3	Bend	X-ray microdiffraction	White light, two or four crystal	6–12 keV	Now
8.0.1	U5	Surface and materials science, imaging photoelectron spectroscopy, soft x-ray fluorescence			
		Ellipsoidal-mirror electron energy analyzer (EMA)	SGM	65–1400 eV	Now
		Soft x-ray fluorescence spectrometer (SXF)	SGM	65–1400 eV	Now
8.2.1	S-bend	Multiple-wavelength anomalous diffraction (MAD) and monochromatic protein crystallography	Double crystal	6–18 keV	Now
8.2.2	S-bend	Multiple-wavelength anomalous diffraction (MAD) and monochromatic protein crystallography	Double crystal	6–18 keV	2002
8.3.1	S-bend	Multiple-wavelength anomalous diffraction (MAD) and monochromatic protein crystallography	Double crystal	2.4–15 keV	Now
8.3.2	S-bend	Tomography	Double crystal	3–60 keV	2003
9.0.1	U10	Coherent optics/scattering experiments	None or off-axis zone plate	10–800 eV	Now
9.0.2	U10	Chemical reaction dynamics, photochemistry, high-resolution photoelectron and photoionization spectroscopy, photoelectron and photoionization imaging and spectroscopy			
		Crossed molecular beam	None	5–30 eV	Now
		Molecular-beam photoelectron/photoion imaging and spectroscopy	Off-plane Eagle	5–30 eV	Now
		Molecular-beam photoelectron/photoion spectroscopy	Off-plane Eagle	5–30 eV	Now
9.3.1	Bend	Atomic, molecular, and materials science			
		Angle-resolved time-of-flight electron spectrometer	Double crystal	2.2–6.0 keV	Now
		Ion time-of-flight spectrometer	Double crystal	2.2–6.0 keV	Now
		Magnetic mass analyzer	Double crystal	2.2–6.0 keV	Now
		Polarized-x-ray emission spectrometer	Double crystal	2.2–6.0 keV	2002
		X-ray absorption cell	Double crystal	2.2–6.0 keV	Now
9.3.2	Bend	Chemical and materials science, circular dichroism, spin resolution			
		Advanced materials chamber (AMC)	SGM	30–1400 eV	Now
		Ambient-pressure photoemission	SGM	30–1400 eV	Now

BEAMLINE	SOURCE**	AREAS OF RESEARCH/TECHNIQUES	MONOCHROMATOR	ENERGY RANGE	OPERATIONAL
10.0.1	U10	Photoemission of highly correlated materials; high-resolution atomic, molecular, and optical physics			
		High-energy-resolution spectrometer (HERS)	SGM	17–340 eV	Now
		Electron spin polarization (ESP)	SGM	17–340 eV	Now
		High-resolution atomic and molecular electron spectrometer (HiRAMES)	SGM	17–340 eV	Now
		Ion–photon facility (IPF)	SGM	17–340 eV	Now
10.3.1	Bend	X-ray fluorescence microprobe	White light, multilayer mirrors	3–20 keV	Now
10.3.2	Bend	Environmental and materials science, micro x-ray absorption spectroscopy	White light, four crystal	3–17 keV	Now
11.0.2	EPU5	Molecular environmental science			
		Wet spectroscopy	Variable-included-angle PGM	75–2000 eV	2002
		High-pressure photoemission spectroscopy	Variable-included-angle PGM	75–2000 eV	2002
		Scanning transmission x-ray microscope (STXM)	Variable-included-angle PGM	180–1000 eV	2002
11.3.1	Bend	Small-molecule crystallography	Channel-cut Si(111)	6–17 keV	2002
11.3.2	Bend	Inspection of EUV lithography masks	VLS-PGM	50–1000 eV	Now
12.0.1	U8	EUV optics testing, interferometry, coherent optics; angle- and spin-resolved photoemission			
		EUV interferometer (two available)	VLS-PGM	60–320 eV	Now
		Angle- and spin-resolved photoemission	VLS-PGM	20–320 eV	2002
12.2.2	S-bend	California High-Pressure Science Observatory (CALIPSO)			
		Nanoscience/materials chemistry	Double crystal	6–40 keV	2002
		Solid-state physics/geoscience	Double crystal	6–40 keV	2002
12.3.1	S-bend	Multiple-wavelength anomalous diffraction (MAD) protein crystallography and small-angle x-ray scattering (SAXS)	Double crystal and double multilayer	6–18 keV	2002
BTF	Linac	Beam Test Facility	None	50-MeV electrons	Now

ALS Insertion Device Parameters

DEVICE	BEAMLINE	STATUS	ENERGY RANGE (AT 1.5 GEV)	ENERGY RANGE (AT 1.9 GEV)	PERIOD LENGTH	NUMBER OF PERIODS	OPERATING GAP RANGE	PEAK EFFECTIVE FIELD RANGE
U5 Undulator	8.0	Operational	130–1900 eV	210–3000 eV	5.0 cm	89	1.4–4.5 cm	0.85–0.10 T
U5 Undulator	7.0	Operational	50–1900 eV	80–3000 eV	5.0 cm	89	1.4–4.5 cm	0.85–0.10 T
U8 Undulator	12.0	Operational	18–1200 eV	30–1900 eV	8.0 cm	55	2.5–8.3 cm	0.80–0.07 T
U10 Undulator	9.0	Operational	5–950 eV	8–1500 eV	10.0 cm	43	2.4–11.6 cm	0.98–0.05 T
U10 Undulator	10.0	Operational	8–950 eV	12–1500 eV	10.0 cm	43	2.4–11.6 cm	0.80–0.05 T
EPU5 Elliptical Polarization Undulator	4.0	Operational	60–1000 eV*	100–1500 eV*	5.0 cm	37	1.45–5.5 cm	0.79–0.10 T (vertical field) 0.54–0.10 T (horizontal field)
W16 Wiggler	5.0	Operational	5–13 keV	5–21 keV	16.0 cm	19	1.4–18.0 cm	2.1 T

* Elliptical polarization mode

ALS Storage Ring Parameters

PARAMETER	VALUE
Beam particle	electron
Beam energy	1.0–1.9 GeV
Injection energy	1.0–1.5 GeV
Beam current	
multibunch mode	400 mA
two-bunch mode	2×30 mA
Filling pattern (multibunch mode)	276 to 320 bunches possibility of 10-mA "camshaft" bunch in filling gap
Bunch spacing	
multibunch mode	2 ns
two-bunch mode	328 ns
Circumference	196.8 m
Number of straight sections	12
Current number of insertion devices	7
Radio frequency	500 MHz
Beam size in straight sections, rms	250 microns hor. $\times$ 28 microns vert. at 1.9 GeV

PARAMETER	VALUE AT 1.5 GEV	VALUE AT 1.9 GEV
Beam lifetime		
multibunch mode*	~3.5 hours at 400 mA	~8.0 hours at 400 mA
two-bunch mode	not used	~35 min. at 40 mA
Horizontal emittance	4.2 nm-rad	6.75 nm-rad
Vertical emittance**	0.2 nm-rad	0.15 nm-rad
Energy spread ($\Delta E/E$, rms)	8×10^{-4}	1×10^{-3}

*In multibunch mode, the storage ring is typically filled every six hours or as requested by our users.

**Vertical emittance is deliberately increased to improve beam lifetime.

2001 Publications

Agui, A., J. Guo, C. Såthe, J.E. Nordgren, M. Hidaka, and I. Yamada, "Resonant O K alpha emission spectra of $CuGeO_3$ single-crystal," *Solid State Commun.* **118**(12), 619–622 (Summer 2001).

Ahmed, M., D.S. Peterka, and A.G. Suits, "New directions in reaction dynamics using velocity map imaging," in *Imaging in Chemical Dynamics, ACS Symposium Series: 770*, edited by A.G. Suits and R.E. Continetti (American Chemical Society, Washington, 2001), pp. 167–195.

Arce, J.C., J.A. Sheehy, P.W. Langhoff, O. Hemmers, H. Wang, P. Focke, I.A. Sellin, and D.W. Lindle, "On the angular distributions of molecular photoelectrons: Dipole cross-sections for fixed-in-space and randomly oriented molecules," *Chem. Phys. Lett.* **346**(3–4), 341–346 (October 2001).

Arce, J.C., J.A. Sheehy, P.W. Langhoff, O. Hemmers, H. Wang, P. Focke, I.A. Sellin, and D.W. Lindle, Erratum to "On the angular distributions of molecular photoelectrons: Dipole cross-sections for fixed-in-space and randomly oriented molecules," *Chem. Phys. Lett.* **349**(3–4), 349–350 (November 2001).

Armitage, N.P., D.H. Lu, C. Kim, A. Damascelli, K.M. Shen, F. Ronning, D.L. Feng, P. Bogdanov, Z.-X. Shen, Y. Onose, Y. Taguchi, Y. Tokura, P.K. Mang, N. Kaneko, and M. Greven, "Anomalous electronic structure and pseudogap effects in $Nd_{1.85}Ce_{0.15}CuO_4$," *Phys. Rev. Lett.* **87**(14), 123–125 (October 2001).

Assoufid, L., O. Hignette, M. Howells, S. Irick, H. Lammert, P. Takacs, "Future metrology needs for synchrotron radiation grazing-incidence optics," *Nucl. Instrum. Meth.* **467**, 267–270 (2001).

Atkinson, D., J. Corlett, C. Steier, J. Byrd, S. de Santis, A. Wolski, K. Bane, and M. Ross et al., "Measurements of intra-beam scattering at low emittance in the Advanced Light Source," in *Proceedings of the 18th International Conference on High Energy Accelerators (HEACC2001)* (Tsukuba, Japan, March 26–30, 2001).

Atwell, S., E. Meggers, G. Spraggon, and P.G. Schultz, "Structure of a copper-mediated base pair in DNA," *J. Am. Chem. Soc.* **123**(49), 12364–12367 (December 2001).

Bajt, S., D.G. Stearns, and P. Kearney, "Investigation of the amorphous-to-crystalline transition in Mo/Si multilayers," *J. Appl. Phys.* **90**(2), 1010–1017 (July 2001).

Barnosa, L.R., "High-resolution angle-resolved photoemission of high-temperature superconductors," M.S. Thesis, Claude Bernard University, France, 2001.

Barry, W., A. Biocca, J. Byrd, S. Kwiatkowski, M.C. Martin, W.R. McKinney, H. Nishimura, F. Sannibale, C. Steier, K. Rex, D. Robin, G. Stover, G.Will Thur, Y. Wu, et al., "A dedicated infrared synchrotron radiation source at the Advanced Light Source,"in *Proceedings of the 2001 Particle Accelerator Conference* (Chicago, Illinois, June 18–22, 2001).

Batey, R.T., M.B. Sagar, and J.A. Doudna, "Structural and energetic analysis of RNA recognition by a universally conserved protein from the signal recognition particle," *J. Mol. Biol.* **307**(1), 229–246 (March 2001).

Bauer, E.G., "Photoelectron spectromicroscopy: Present and future," *J. Electron Spectrosc.* **114–116,** 975–987 (March 2001).

Beernink, P.T., B.W. Segelke, M.Z. Hadi, J.P. Erzberger, D.M. Wilson, and B. Rupp, "Two divalent metal ions in the active site of a new crystal form of human apurinic/apyrimidinic endonuclease, Ape1: Implications for the catalytic mechanism," *J. Mol. Biol.* **307**(4), 1023–1034 (April 2001).

Berrah, N., J.D. Bozek, A.A. Wills, G. Turri, H.L. Zhou, S.T. Manson, G. Ackerman, B. Rude, N.D. Gibson, C.W. Walter, et al., "K-shell photodetachment of Li^-: Experiment and theory," *Phys. Rev. Lett.* **87**(25), 253002 (December 2001).

Bethelsen, B.O., G.M. Lamble, A.A. MacDowell, and D.G. Nicholson, "Analysis of metal speciation and distribution in symbiotic fungi (ectomycorrhiza) studied by micro x-ray absorption spectroscopy and x-ray fluorescence microscopy,"

in *Trace Elements in the Rhizosphere,* edited by G. Gobran, E. Lombi, and W. Wenzel (CRC Press, Boca Raton, 2001), pp. 149–164.

Birtalan, S., and P. Ghosh, "Structure of the Yersinia type III secretory system chaperone SycE," *Nat. Struct. Biol.* **8**(11), 974–978 (November 2001).

Bogdanov, P.V., "Angle-resolved photoemission spectroscopy of Bi and La based cuprates," Ph.D. Thesis, Stanford University, 2001.

Bogdanov, P.V., A. Lanzara, X. Zhou, S.A. Kellar, D.L. Feng, E.D. Lu, H. Eisaki, A. Fujimori, Z. Hussain, and Z.X. Shen, et al., "Photoemission study of Pb doped Bi2212—A Fermi surface picture," *Phys. Rev. B* **64,** 29957–29954 (Fall 2001).

Bressler, C.G., M. Saes, M. Chergui, R. Abela, and P. Pattison, "Optimizing a time-resolved x-ray absorption experiment," *Nucl. Instrum. Meth. A* **467–468,** 1444–1446 (November 2001).

Byrd, J., and M. Georgsson, "Lifetime increase using passive harmonic cavities in synchrotron light sources," *Phys. Rev. ST Accel. Beams* **4**(3), 1–10 (March 2001).

Byrd, J.M., and S. De Santis, "A novel method for measuring energy loss in electron rings," in *Proceedings of the 2001 Particle Accelerator Conference,* (Chicago, Illinois, June 18–22, 2001).

Byrd, J.M., and S. De Santis, "Longitudinal injection transients in an electron storage ring," *Phys. Rev. ST Accel. Beams* **4**(2), 1–11 (February 2001).

Byrd, J.M., S. De Santis, G. Stover, J. Jacob, V. Serriere, M. Georgsson, J. Fox, and D. Teytelman, "Harmonic cavities and longitudinal beam stability in electron storage rings," in *Proceedings of the 2001 Particle Accelerator Conference* (Chicago, Illinois, June 18–22, 2001).

Byrd, J.M., J. Jacob, V. Serriere, and S. De Santis, "Computed Transient beam loading effects with harmonic RF systems," in *Proceedings of the 2001 Particle Accelerator Conference* (Chicago, Illinois, June 18–22, 2001).

Callcott, T.A., L. Lin, G.T. Woods, G.P. Zhang, J.R. Thompson, M. Paranthaman, and D.L. Ederer, "Soft-x-ray spectroscopy measurements of the p-like density of states of B in MgB_2 and evidence for surface boron oxides on exposed surfaces," *Phys. Rev. B* **64**(13), 1–3 (October 2001).

Carlisle, J.A., I.N. Germanenko, Y.B. Pithawalla, and M.S. El-Shall, "Morphology, photoluminescence and electronic structure in oxidized silicon nanoclusters," *J. Electron Spectrosc.* **114–116,** 229–234 (March 2001).

Carroll, T.X., J.D. Bozek, E. Kukk, V. Myrseth, L.J. Saethre, and T.D. Thomas, "Line shape and lifetime in argon 2p electron spectroscopy," *J. Electron Spectrosc.* **120**(1–3), 67–76 (October 2001).

Chang, C., P.P. Naulleau, E.H. Anderson, and D.T. Attwood, "Spatial coherence properties of undulator radiation based on Thompson-Wolf two-pinhole measurement," *Nucl. Instrum. Meth. A* **467**(PT 2), 913–916 (July 2001).

Chang, G.S., S.-H. Kim, K.H. Chae, E.Z. Kurmaev, V. Galakhov, A. Moewes, Y.P. Lee, K. Jeong, and C.N. Whang, "Electronic structure of ion beam mixed ferromagnetic multilayered films," *J. Electron Spectrosc.* **114–116**, 807–811 (March 2001).

Chang, G.S., J.H. Son, K.H. Chang, C.N. Whang, E.Z. Kurmaev, S.N. Shamin, V.R. Galakhov, A. Moewes, and D.L. Ederer, "Soft x-ray fluorescence and photoluminescence of Si nanocrystals embedded in SiO_2," *Appl. Phys. A–Mater.* **72**(3), 303–306 (February 2001).

Chao, W., E. Anderson, G. Denbeaux, B. Harteneck, A. Pearson, D. Olynick, G. Schneider, and D. Attwood, "Experimental analysis of high-resolution soft x-ray microscopy," in *SPIE Annual Meeting 2001*, (San Diego, California, July 29–August 3, 2001).

Chapados, B.R., Q. Chai, D. Hosfield, J. Qiu, B. Shen, and J.A. Tainer, "Structural biochemistry of a type 2 RNase H: RNA primer recognition and removal during DNA replication," *J. Mol. Biol.* **307**(2), 541–556 (March 2001).

Chapman, H.N., A.K. Ray-Chaaudhuri, D.A. Tichenor, W.C. Replogle, R.H. Stulen, G.D. Kubiak, P.D. Rokett, L.E. Klebanoff, D. O'Connell, A.H. Leung, et al., "First litho-

graphic results from the extreme ultraviolet engineering test stand," *J. Vac. Sci. Technol. B* **19**(6), 2389–2396 (November 2001).

Charkraborty, H.S., D. L. Hansen, O. Hemmers, P.C. Deshmukh, P. Focke, I.A. Sellin, C. Heske, D.W. Lindle, and S.T. Manson, " interchannel coupling in the photoionization of the M shell of Kr well above threshold: Experiment and theory," *Phys. Rev. A* **63**(4), 1–4 (March 2001).

Chen, Z., C.D. Wells, P.C. Sternweis, and S.R. Sprang, "Structure of the rgRGS domain of p115RhoGEF," *Nat. Struct. Biol.* **8**(9), 805–809 (September 2001).

Cherkashenko, V.M., E.Z. Kurmaev, S.Z. Nazarova, A.L. Ivanovskii, A.I. Gusev, A. Moewes, and D.L. Ederer, "X-ray emission TaN_3 and Nb L_3 spectra of NbC-TaC solid solutions," *Russian Journal of Inorganic Chemistry* **46**(6), 892–897 (June 2001).

Chevalier, B.S., R.J. Monnat, Jr., and B.L. Stoddard, "The homing endonuclease I-CreI uses three metals, one of which is shared between two active sites," *Nat. Struct. Biol.* **8**(4), 312–316 (April 2001).

Chow, D.C., X.L. He, A.L. Snow, S. Rose-John, and K.C. Garcia, "Structure of an extracellular gp130 cytokine receptor signaling complex," *Science* **291**(5511), 2150–2155 (March 2001).

Chuang, Y.D., A.D. Gromko, D.S. Dessau, T. Kimura, and Y. Tokura, "Fermi surface nesting and nanoscale fluctuating charge/orbital ordering in colossal magnetoresistive oxides," *Science* **292**(5521), 1509–1513 (May 2001).

Chuang, Y.D., A.D. Gromko, A. Fedorov, Y. Aiura, K. Oka, Y. Ando, H. Eisaki, S.I. Uchida, and D.S. Dessau, "Doubling of the bands in overdoped $Bi_2Sr_2CaCu_2O_{8+\delta}$: Evidence for *c*-axis bilayer coupling," *Phys. Rev. Lett.* **87**(11), 1–4 (September 2001).

Corbett, K.D., and T. Alber, "The many faces of Ras: Recognition of small GTP-binding proteins," *Trends Biochem. Sci.* **26**(12), 711–716 (December 2001).

Covington, A.M., A. Aguilar, I. Alvarez, C. Cisneros, I.R. Covington, I. Dominguez, M.F. Gharaibeh, G. Hinojosa, M.M. Sant'Anna, R.A. Phaneuf, and A.S. Schlachter, "Absolute cross sections for photoionization of Ne^+ and Ar^+," in *ICPAEC 2001, Proceedings of the 22nd International Conference on Photonic, Electronic, and Atomic Collisions* (Santa Fe, New Mexico, July 18–24, 2001).

Covington, A., A. Aguilar, I.R. Covington, M. Gharaibeh, C.A. Shirley, R.A. Phaneuf, I. Alvarez, C. Cisneros, G. Hinojosa, J.D. Bozek, et al., "Photoionization of metastable O^+ Ions: Experiment and theory," *Phys. Rev. Lett.* **87**(24), 243002 (December 2001).

Covington, A.M., A. Aguilar, V.T. Davis, I. Alvarez-Torres, H.C. Bryant, C. Cisneros, M.H. Halka, D. Hanstorp, G.A. Hinojosa, A.S. Schlachter, J.S. Thompson, and D.J. Pegg, "Correlated processes in inner-shell photodetachment of the Na^- ion," *J. Phys. B–At. Mol. Opt.* **34**, 735–740 (November 2001).

Critchley, A.D., G.C. King, P. Kreynin, M.C.A. Lopes, I.R. McNab, and A.J. Yencha, "TPEsCO spectra of HCl^{2+} and DCl^{2+}: Experiment and theory," *Chem. Phys. Lett.* **349**(1–2), 79–83 (November 2001).

Cronk, J., J.A. Endrizzi, M. Cronk, J. O'Neill, and K. Zhang, "Crystal structure of *E. coli* beta-carbonic anhydrase, an enzyme with an unusual pH-dependent activity," *Protein Sci.* **10**(5), 911–922 (May 2001).

Crowder, S., J. Holton, and T. Alber, "Covariance analysis of RNA recognition motifs identifies functionally linked amino acids," *J. Mol. Biol.* **310**(4), 793–800 (July 2001).

Daniels, D.S., "Structural studies of the human DNA repair protein O6-Alkylguanine-DNA alkyltransferase," Ph. D. Thesis, Scripps Research Institute, 2001.

Demeter, M., M. Neumann, A.V. Postnikov, V.M. Cherkashenko, V.R. Galakhov, and E.Z. Kurmaev, "Electronic structure of the mixed-valent system $V_{2-x}Mo_xO_5$," *Surf. Sci.* **482**(1), 708–711 (June 2001).

Denbeaux, G., "A full field x-ray microscope for high-resolution imaging: Advances and applications," in

Proceedings of the Fifth Harima International Forum (HIF2001) (Himeji, Japan, July 12–14, 2001).

Denbeaux, G., "X-ray microscopy: Imaging with short wavelengths for high spatial resolution," in *Proceedings of OSA Annual Meeting* (Long Beach, California, October 14–18, 2001).

Denbeaux, G., E. Anderson, W. Chao, T. Eimueller, L. Johnson, M. Koehler, C. Larabell, M. Le Gros, P. Fischer, D. Attwood, et al., "Soft x-ray microscopy to 25 nm with applications to biology and magnetic materials," *Nucl. Instrum. Meth. A* **467**(2), 841–844 (July 2001).

Denbeaux, G., P. Fischer, G. Kuskinski, M. Le Gros, A. Pearson, and D. Attwood, "A full field transmission x-ray microscope as a tool for high-resolution magnetic imaging," *IEEE T. Magn.* **37**(4, Part 1), 2764–2766 (July 2001).

Denlinger, J.D., G.-H. Gweon, J.W. Allen, C.G. Olson, M.B. Maple, J.L. Sarrao, P.E. Armstrong, Z. Fisk, and H. Yamagami, "Comparative study of the electronic structure of XRu_2Si_2: Probing the Anderson lattice," *J. Electron Spectrosc.* **117**, 347–369 (June 2001).

Dessau, D. S, Y. D Chuang, A. Gromko, T. Saitoh, T. Kimura, and Y. Tokura, "Electronic structure of CMR oxides: High resolution electron-spectroscopic studies and a pseudogap," *J. Electron Spectrosc.* **117–118**, 265–276 (June 2001).

Diaz, J., S. Anders, X. Zhou, E.J. Moler, S.A. Kellar, and Z. Hussain, "Analysis of the pi* and sigma* bands of the x-ray absorption spectrum of amorphous carbon," *Phys. Rev. B* **64**(12), 5204 (September 2001).

Diez Muino, R., D. Rolles, F.J. Garcia de Abajo, F. Starrost, W. Schattke, C.S. Fadley, and M.A. Van Hove, "Multiple scattering theory for non-spherical potentials: Application to photoelectron angular distributions from oriented diatomic molecules and the study of shape resonances," *J. Electron Spectrosc.* **114–116**, 99–105 (March 2001).

Dittmar, M., "Photoelectron spectroscopy of liquid water and of aqueous solutions of simple alkali halide salts," Ph.D. Thesis, Max-Planck-Institut Strömungsforschung, Universität Göttingen, Germany, 2001.

Domeier, L.A., M. Gonzles, J. Hachman, J.M. Hruby, R. Janek, and A.M. Morales, "Microscreen-based replication of electroforming micromolds," in *Proceedings of the Fourth International Conference on High Aspect Ratio Microstructure Technology (HARMST '01)* (Baden-Baden, Germany, June 17–19, 2001).

Doyle, S.A., P.T. Beernink, and D.E. Koshland, "Structural basis for a change in substrate specificity: Crystal structure of S113E isocitrate dehydrogenase in a complex with isopropylmalate, Mg^{2+} and NADP," *Biochemistry–US* **40**(14), 4234–4241 (April 2001).

Drennan, C.L., J. Heo, M.D. Sintchak, E.R. Schreiter, and P.W. Ludden, "Life on carbon monoxide: X-ray structure of *Rhodospirillum rubrum* Ni-Fe-S carbon monoxide dehydrogenase," *Proc. Natl. Acad. Sci. USA* **98**(21), 11973–11978 (October 2001).

Du, X., W. Wang, R. Kim, H. Yakota, H. Nguyen, and S.-H. Kim, "Crystal structure and mechanism of catalysis of a pyrazinamidase from *Pyrococcus horikoshii," Biochemistry–US* **40**(47), 14166–14172 (November 2001).

Eigenbrot, C., D. Kirchhofer, M.S. Dennis, L. Santell, R.A. Lazarus, J. Stamos, and M.H. Ultsch, "The factor VII zymogen structure reveals reregistration of beta-strands during activation," *Structure* **9**(7), 627–636 (July 2001).

Eigenbrot, C., J. Stamos, and M.H. Ultsch, "The factor VII zymogen structure implies re-registration of b-strands during activation," in *Proceedings of the 15th West Coast Protein Crystallography Workshop* (Pacific Grove, California, March 25–28, 2001).

Eimueller, T., P. Fischer, M.R. Koehler, M. Scholz, P. Guttmann, G. Denbeaux, S. Glueck, G. Bayreauther, G. Schmahl, D. Attwood, and G. Schutz, "Transmission x-ray microscopy using x-ray magnetic circular dichroism," *Appl. Phys. A–Mater.* **73**(6), 697–701 (October 2001).

Eimuller, T., M. Scholz, P. Guttmann, P. Fischer, M. Koehler, G. Bayreuther, G. Schmahl, and G. Schutz, "Magnetization reversal of a multilayered FeGd dot array imaged by transmission x-ray microscopy," *J. Appl. Phys.* **89**, 7162–7164 (June 2001).

Endo, K., S. Shimada, T. Ida, M. Suhara, E.Z. Kurmaev, A. Moewes, and D.P. Chong, "Theoretical x-ray photoelectron and emission spectra of Si- and S-containing polymers by density-functional theory calculations using model molecules," *J. Mol. Struct.* **561**(1–3), 17–28 (April 2001).

Facciotti, M.T., S. Rouhani, F.T. Burkard, F.M. Betancourt, K.H. Downing, R.B. Rose, G. McDermott, and R.M. Glaeser, "Structure of an early intermediate in the m-state phase of the bacteriorhodopsin photocycle," *Biophys. J.* **81**(6), 3442–3455 (December 2001).

Fadley, C.S., M.A. Van Hove, A. Kaduwela, S. Omori, L. Zhao, and S. Marchesini, "Photoelectron and x-ray holography by contrast: Enhancing image quality and dimensionality," *J. Phys–Condens. Mat.* **13**(47), 10517–10532 (November 2001).

Fedorov, D.G., M.S. Gordon, Y. Song, and C.Y. Ng, "A theoretical study of spin-orbit coupling constants for O_2^+ ($A^2\pi_{3/2,1/2u}$, v^+ = 0–17 and $a^4\pi_{5/2,3/2,1/2,-1/2u}$, v^+ = 0–25)," *J. Chem. Phys.* **115**(16), 7393–7400 (October 2001).

Feese, M.D., B.P. Ingason, J. Goranson-Siekierke, R.K. Holmes, and W.G.J. Hol, "Crystal structure of the iron-dependent regulator (IdeR) from *Mycobacterium tuberculosis* at 2.0 M-E resolution reveals the Src homology domain 3-like fold and metal binding function of the third domain," *J. Biol. Chem.* **276**(8), 5959–5966 (February 2001).

Finkelstein, L.D., A.V. Postnikov, E.Z. Kurmaev, M. Matteucci, G. Robert, B. Schneider, M. Neumann, and C. Bellitto, " inelastic x-ray scattering measurements of iron organophosphonate," *Phys. Rev. B* **63**(7), 188–193 (February 2001).

Fischer, P., T. Eimueller, S. Glueck, G. Schuetz, S. Tsunashima, M. Kumazawa, N. Takagi, G. Denbeaux, and D. Attwood, "High resolution imaging of magnetic domains with magnetic soft x-ray microscopy," *J. Magnetics Soc. of Japan* **25**, 186–191 (June 2001).

Fischer, P., T. Eimueller, G. Schutz, G. Bayreuther, S. Tsunashima, N. Takagi, G. Denbeaux, and D.T. Attwood, "Magnetic domains in nanostructured media studied with M-TXM," *J. Synchrotron Radiat.* **8**(2), 325–327 (March 2001).

Fischer, P., T. Eimueller, G. Schutz, G. Denbeaux, A. Pearson, L.E. Johnson, D.T. Attwood, S. Tsunashima, M. Kumazawa, N. Takagi, et al., "Element-specific imaging of magnetic domains at 25 nm spatial resolution using soft x-ray microscopy," *Rev. Sci. Instrum.* **72**(5), 2322–2324 (May 2001).

Fischer, P., T. Eimueller, G. Schutz, M. Koehler, G. Bayreuther, G. Denbeaux, and D. Attwood, "Study of in-plane magnetic domains with magnetic transmission x-ray microscopy," *J. Appl. Phys.* **89**(11, Part 2), 7159–7161 (June 2001).

Franco Cerame, N., J.E. Klepeis, C.F.O. Bostedt, A. Van Buuren, C. Heske, O. Pankratov, and L.J. Terminello, "Valence band study of the PtSi by synchrotron radiation photoelectron spectroscopy," *J. Electron Spectrosc.* **114–116**, 1191–1196 (March 2001).

Franklin, M.C., "Structure of an RB69 DNA polymerase ternary complex," Ph. D. Thesis, Yale University, 2001.

Franklin, M.C., J.M. Wang, and T.A. Steitz, "Structure of the replicating complex of alpha pol family DNA polymerase," *Cell* **105**(5), 657–667 (June 2001).

Fried, D., and T.M. Breunig, " infrared spectroscopy of laser irradiated dental hard tissues using the Advanced Light Source," in *Proceedings of SPIE, Photonics West 2001: Lasers in Dentistry VII* (San Jose, California, January 20–26, 2001).

Friedrich, S., T. Niedermayr, T. Funk, O. Drury, M.L. van den Berg, M.F. Cunningham, J.N. Ullom, S.P. Cramer, M. Frank, and S.E. Labov, "A multichannel cryogenic detector system for synchrotron-based x-ray spectroscopy," in *Proceedings of the Ninth International Workshop on Low Temperature Detectors (LTD-9)* (Madison, Wisconsin, July 23–27, 2001).

Fuchs, O.K., "Resonant inelastic x-ray scattering of beryllium sulfide," Master's Thesis, University of Wurzburg, Germany, 2001.

Garcia de Abajo, F.J., M.A. Van Hove, and C.S. Fadley, "Multiple scattering of electrons in solids and molecules: A novel cluster approach," *Phys. Rev. B* **63**(7), 5404 (February 2001).

Georgsson, M., "Higher harmonic cavities at third generation synchrotron Light sources," Ph.D. Thesis, University of Lund, Sweden, 2001.

Georgsson, M., W. Anders, D. Krämer, and J.M. Byrd, "Design and commissioning of third harmonic cavities at BESSY II," *Nucl. Instrum. Meth. A* **469** (3), 373–381 (August 2001).

Ghosh, U., J.W. Talley, and R.G. Luthy, "Particle-scale investigation of PAH desorption kinetics and thermodynamics from sediment," *Environ. Sci. Technol.* **35**(17), 3468–3475 (September 2001).

Glover, T.E., G.D. Ackermann, A. Belkacem, B. Feinberg, P. A. Heimann, Z. Hussain, H.A. Padmore, C. Ray, R.W. Schoenlein, and W.F. Steele, "Measurement of synchrotron pulse durations using surface photovoltage transients," *Nucl. Instrum. Meth. A* **467–468**(2), 1438–1440 (July 2001).

Glover, T.E., A.H. Chin, and R.W. Schoenlein, "High-order harmonic pulse broadening in an ionizing medium," *Phys. Rev. A* **63**(2), 496–503 (February 2001).

Goedken, E.R., and S. Marqusee, "Co-crystal of *Escherichia coli* RNase HI with Mn^{2+} ions reveals two divalent metals bound in the active site," *J. Biol. Chem.* **276**(10), 7266–7271 (March 2001).

Goldberg, K.A., and K. Geary, "Wave-front measurement errors from restricted concentric subdomains," *J. Opt. Soc. Am. A* **18**(9), 2146–2152 (September 2001).

Gomez-Vega, J.M., A. Hozumi, E. Saiz, A.P. Tomsia, H. Sugimura, and O. Takai, "Bioactive glass-mesoporous silica coatings on Ti_6Al_4V through enameling and triblock-copolymer-templated sol-gel processing," *J. Biomed. Mater. Res.* **56**(3), 382–389 (September 2001).

Goudeau, P., "X-ray diffraction stress mapping: Application to thin film buckling analysis," in *Proceedings of Photomechanics 2001 Study of the Behavior of Materials and Structures* (Futuroscope, France, April 24–26, 2001).

Greasley, S.E., P. Horton, J. Ramcharan, G.P. Beardsley, S. Benkovic, and I.A. Wilson, "Crystal structure of a bifunctional transformylase and cyclohydrolase enzyme in purine biosynthesis," *Nat. Struct. Biol.* **8**(5), 402–406 (May 2001).

Griffiths, S.K., and A. Ting, "The influence of x-ray fluorescence on LIGA sidewall tolerances," in *Proceedings of the Fourth International Conference on High Aspect Ratio Microstructure Technology (HARMST '01)* (Baden-Baden Germany, June 17–19, 2001).

Gullikson, E.M., S. Mrowka, and B.B. Kaufmann, "Recent developments in EUV reflectometry at the Advanced Light Source," in *Proceedings of SPIE, Microlithography 2001: Emerging Lithographic Technologies V* (Santa Clara, California, February 27–March 2, 2001).

Guo, J.H., "Resonant soft-x-ray emission of molecular materials," in *Proceedings of VUV-XIII Satellite Meeting—Decay Processes in Core-Excited Species* (Monte Porzio Catone, Italy, July 30–August 2, 2001).

Guo, J.H., "Resonant soft-x-ray emission spectroscopy of correlated systems," in *Proceedings of the Third International Symposium on Electronic and Atomic Structures (ISEAS-3)* (Taiwan, China, December 13–14, 2001).

Guo, J., S. Butorin, N. Wassdahl, A. Warwick, and J.E. Nordgren, "The electronic structure of K_6C_{60} studied by soft x-ray spectroscopy," *J. Electron Spectrosc.* **114–116**, 885–888 (March 2001).

Hague, C.F., M. Tronc, Y. Yanagida, and A. Kotani, "Resonant x-ray emission from gas-phase $TiCl_4$," *Phys. Rev. A* **63**(1), 2511–2514 (January 2001).

Hambach, D., G. Schneider, and E.M. Gullikson, "Efficient high-order diffraction of extreme-ultraviolet light and soft x-rays by nanostructured volume gratings," *Opt. Lett.* **26**(15), 1200–1202 (August 2001).

Hamdan, N., and M.M. Faiz, "An x-ray photoemission study of the effect of gamma-irradiation on fluorinated $(Tl_{0.5}Pb_{0.5})\ Sr_{1.6}Ba_{0.4}Ca_2Cu_3O_y$ high-T_c superconductor," *J. Electron Spectrosc.* **114–116**, 291–294 (March 2001).

Hasan, Z., "Angle-resolved photoemission and inelastic x-ray scattering of high temperature superconductors and nickelates," Ph.D. Thesis, Stanford University, 2001.

He, X.-L., D.C. Chow, M.M. Martick, and K.C. Garcia, "Allosteric activation of a spring-loaded natriuretic peptide receptor dimer by hormone," *Science* **293**(5535), 1657–1662 (August 2001).

Head-Gordon, T., G. Hura, J.M. Sorenson, and R.M. Glaeser, "New kinds of phase transitions: Transformations in disordered substances," in *Proceedings of NATO Advanced Research Workshop* (Volga River, Russia, May 24–28, 2001).

Heimann, P.A., A.M. Lindenberg, I. Kang, S. Johnson, T. Missalla, Z. Chang, R.W. Falcone, R.W. Schoenlein, T.E. Glover, and H.A. Padmore, "Ultrafast x-ray diffraction of laser-irradiated crystals," *Nucl. Instrum. Meth. A* **467–468**, 986–989 (July 2001).

Hellgren, N., J. Guo, C. Sathe, A. Agui, J. Nordgren, Y. Luo, H. Agren, and J. Sundgren, "Nitrogen bonding structure in carbon nitride thin films studied by soft x-ray spectroscopy," *Appl. Phys. Lett.* **76**(26), 4348–4350 (December 2001).

Hellwig, O., S. Maat, J.B. Kortright, and E. Fullerton, "Magnetic reversal of perpendicularly-biased Co/Pt multilayers," *Phys. Rev. B* **65** (March 2002).

Hemmers, O., and D.W. Lindle, "Photoelectron spectroscopy and the dipole approximation," in *Proceedings of the 16th International Conference on the Application of Accelerators in Research and Industry (CAARI)* (Denton, Texas, November 1–4, 2002).

Hemmers, O., S.T. Manson, M.M. Sant'Anna, P. Focke, H. Wang, I.A. Sellin, and D.W. Lindle, "Relativistic effects on interchannel coupling in atomic photoionization: The photoelectron angular distribution of Xe 5s," *Phys. Rev. A* **64**(2), 1–3 (August 2001).

Hemmers, O., H. Wang, P. Focke, I.A. Sellin, D.W. Lindle, J.C. Arce, J.A. Sheehy, and P.W. Langhoff, "Large nondipole effects in the angular dstributions of K-shell photoelectrons from molecular nitrogen," *Phys. Rev. Lett.* **87**(27), 1–4 (December 2001).

Heske, C., U. Groh, O. Fuchs, E. Umbach, N. Franco, C. Bostedt, L.J. Terminello, R.C. Perera, K.H. Hallmeier, and A. Preobrajenski, "X-ray emission spectroscopy of $Cu(In,Ga)(S,Se)_2$-based thin film solar cells: Electronic structure, surface oxidation, and buried interfaces," *Phys. Status Solidi A* **187**(1), 13–24 (September 2001).

Hitchcock, A.P., "Chemical mapping with soft x-ray spectromicroscopy," *American Laboratory* **33**(16), 30–36 (August 2001).

Hitchcock, A.P., "Soft x-ray spectromicroscopy of polymers and biopolymer interfaces," *J. Synchrotron Radiat.* **8**(2), 66–71 (March 2001).

Hitchcock, A.P., I.N. Koprinarov, T. Tyliszczak, E.G. Rightor, G.E. Mitchell, M.T. Dineen, F. Hayes, W. Lidy, S.G. Urquhart, H. Ade, et al ., "Copolymer polyol particles in polyurethanes studied by soft x-ray spectromicroscopy," *Ultramicroscopy* **88**(1), 33–49 (June 2001).

Hlawatsch et al., "Trace metal fluxes to ferromanganese nodules from the western Baltic Sea as a record for long-term environmental changes," *Chemical Geology* **182**, 697 (2001).

Ho, C., W. Wang, R. Kim, H. Yokota, S. Damo, S.-H. Kim, D. Wemmer, S. Kustu, and D. Yan, "BeF_3^- acts as a phosphate analog in proteins phosphorylated on aspartate: Structure of a BeF_3^- complex with phosphoserine phosphatase," *Proc. Natl. Acad. Sci. USA* **98**(15), 8525–8530 (July 2001).

Hoang, C., and A.R. Ferré-D'Amaré, "Cocrystal structure of a tRNA psi55 pseudouridine synthase: Nucleotide flipping by an RNA-modifying enzyme," *Cell* **107**, 929–939 (December 2001).

Hopfner, K.P., A. Karcher, L. Craig, T.T. Woo, J.P. Carney, and J.A. Tainer, "Structural biochemistry and interaction architecture of the DNA double-strand break repair Mre11 nuclease and Rad50-ATPase," *Cell* **105**(4), 473–485 (May 2001).

Hou, P.Y., and G.D. Ackerman, "Chemical state of segregants at Al_2O_3/alloy interfaces studied using micro-XPS," *Appl. Surf. Sci.* **178**, 156–164 (June 2001).

Howells, M. R., "Gratings and monochromators in the soft x-ray spectral region," in *Handbook of Optics, Vol. IV,* edited

by M. Bass and C. Macdonald, Optical Society of America, Washington DC, 2001.

Howells, M.R., C.J. Jacobsen, S. Marchesini, S. Miller, J.C. Spence, and U. Weirstall, "Toward a practical x-ray Fourier holography at high resolution," *Nucl. Instrum. Meth. A* **468**(2), 864–867 (July 2001).

Hsu, L.-S., G.Y. Guo, J.D. Denlinger, and J.W. Allen, "Experimental and theoretical study of the electronic structure of $AuAl_2$," *J. Phys. Chem. Solids* **62**(6), 1047–1054 (June 2001).

Hsu, L.-S., G.Y. Guo, J.D. Denlinger, and J.W. Allen, "Experimental and theoretical study of the electronic structure of $PtGa_2$," *Phys. Rev. B* **63**(155105), 1–8 (April 2001).

Hu, B., P. Geissbuhler, L.B. Sorensen, S.D. Kevan, J. Kortright, and E.E. Wullerton, "Coherent soft x-ray magnetic scattering," *Synchrotron Radiation News* **14**(2), 11–19 (March 2001).

Hüfner, S., F.O. Schumann, E. Rotenberg, J.G. Tobin, S.H. Wang, B.S. Mun, S.A. Morton, J. Schafer, and D. Ehm, "3d and 4d resonant photoemission in Pr and Nd metal," *Phys. Rev. B* **63**(8), 93–97 (February 2001).

Huxford, T., " inactivation of transcription factor NF-kappaB through its association with the IkappaBalpha Inhibitor Protein," Ph. D. Thesis, University of California, San Diego, 2001.

Isaure, M.P., A. Laboudigue, A. Manceau, G. Sarret, C. Tiffreau, and P. Trocellier, "Characterisation of zinc in slags originated from a contaminated sediment by coupling micro-PIXE, micro-RBS, micro-EXAFS and powder EXAFS spectroscopy," *Nucl. Instrum. Meth. B* **181**, 598–602 (July 2001).

Istvan, E.S., and J. Deisenhofer, "Structural mechanism for statin inhibition of HMG-CoA reductase," *Science* **292**(5519), 1160–1164 (May 2001).

Jeruzalmi, D., M. O'Donnell, and J. Kuriyan, "Crystal structure of the processivity clamp loader gamma (γ) complex of *E. coli* DNA polymerase III.," *Cell* **106**(4), 429–441 (August 2001).

Jeruzalmi, D., O. Yurieva, Y.X. Zhao, M. Young, J. Stewart, M. Hingorani, M. O'Donnell, and J. Kuriyan, "Mechanism of processivity clamp opening by the delta subunit wrench of the clamp loader complex of *E. coli* DNA polymerase III," *Cell* **106**(4), 417–428 (August 2001).

Johnson, T.F., S. Chiang, Y. Sato, D.A. Arena, S.A. Morton, M. Hochstrasser, J.G. Tobin, J.D. Shine, J.A. Giacomo, G.E. Thayer, et al., "X-ray magnetic linear dichroism of Fe-Ni Alloys on Cu(111)," in *Applications of Ferromagnetic and Optical Materials, Storage and Magnetoelectronics,* edited by W.C. Black, H.J. Borg, K. Bussmann, L. Hesselink, S.A. Majetich, and E.S. Murdock, Materials Research Society Symposium Proceedings Vol. 674 (Pittsburgh, 2001).

Jones, S.J., and H.E. Doner, "Micro-scale distribution and associations of metals in an urban soil," in *Proceedings of the Soil Science Society of America Annual Meeting* (Charlotte, North Carolina, October 21–25, 2001).

Juneau, K.M., E.R. Podell, D.J. Harrington, and T. Cech, "Structural basis of the enhanced stability of a mutant ribozyme domain and a detailed view of RNA-solvent interactions," *Struct. Fold. Des.* **9**, 221–231 (March 2001).

Kaambre, T., L. Qin, J. Rubensson, J. Guo, C. Sathe, J. Nordgren, J. Palmqvist, and U. Jansson, "Study of oxygen-C60 compound formation by NEXAFS and RIXS," *European Physical Journal D* **16**, 357–360 (2001).

Karis, O., M. Magnusson, T. Wiell, M. Weinelt, N. Wassdahl, A. Nilsson, N. Mårtensson, E. Holmström, A.M.N. Niklasson, O. Eriksson, et al., "Probing surface states of Cu/Ni thin films using x-ray absorption spectroscopy," *Phys. Rev. B* **63**(11), 1–4 (February 2001).

Karlsen, T., L.J. Saethre, K.J. Borve, N. Berrah, E. Kukk, J.D. Bozek, T.X. Carroll, and T.D. Thomas, "Vibrational structure and vibronic coupling in the carbon 1s photoelectron spectra of ethane and deuteroethane," *J. Phys. Chem. A* **105**, 7700–7706 (July 2001).

Kauffman, M.E., W.K. Keener, R.M. Lehman, M.E. Watwood, H.-Y Holman, and M.C. Martin, "Effects of bacterial attachment on the production of toluene 2-monooxygenase," in *Proceedings*

of the Sixth International Symposium on Batelle In Situ and On-Site Bioremediation (San Diego, California, June 4–7, 2001).

Kay, A.W., F.J. Garcia de Abajo, S.-H. Yang, E. Arenholz, B.S. Mun, N. Mannella, Z. Hussain, M.A. Van Hove, and C.S. Fadley, "Multi-atom resonant photoemission," *J. Electron Spectrosc.* **114–116**, 1179–1189 (March 2001).

Kay, A.W., F.J. Garcia de Abajo, S.-H. Yang, E. Arenholz, B.S. Mun, N. Mannella, Z. Hussain, M.A. Van Hove, and C.S. Fadley, "Multi-atom resonant photoemission," *Phys. Rev. B* **63**(11), 214–222 (March 2001).

Kikkawa, M., E.P. Sablin, Y. Okada, H. Yajima, R.J. Fletterick, and N. Hirokawa, "Switch-based mechanism of kinesin motors," *Nature* **411**(6836), 439–445 (May 2001).

Kim, K.H., and Y.M. Koo, "New interpretation about deviation of guide strains: In-situ measurement by synchrotron radiation of lattice rotation in a copper single crystal," *J. Mater. Sci. Lett.* **20**(7), 625–627 (April 2001).

Kim, S., J. Kortright, and S.-C. Shin, "Vector magnetization imaging in ferromagnetic thin films using soft x-rays," *Appl. Phys. Lett.* **78**(18), 2742–2744 (April 2001).

Kim, S.-K., and J.B. Kortright, "Modified magnetism at a buried Co/Pd interface resolved with x-ray standing waves," *Phys. Rev. Lett.* **86**(7), 1347–1350 (February 2001).

Kim, S.-K., J.-R Jeong, J.B. Kortright, and S.-C. Shin, "Experimental observation of magnetically dead layers in Ni/Pt multilayer films," *Phys. Rev. B* **64**(5), 224–227 (July 2001).

King, G.C., A.J. Yencha, and M.C.A. Lopes, "Threshold photoelectron spectroscopy using synchrotron radiation," *J. Electron Spectrosc.* **114–116**, 33–40 (March 2001).

Kleineberg, U., G. Haindl, A. Hütten, G. Reiss, E.M. Gullikson, M.S. Jones, S. Mrowka, S.B. Rekawa, and J.H. Underwood, "Microcharacterization of the surface oxidation of Py/Cu multilayers by scanning x-ray absorption spectromicroscopy," *Appl. Phys. A–Mater.* **73**(4), 515–519 (March 2001).

Kolczewski, C., R. Püttner, O. Plashkevych, H. Ågren, V. Staemmler, M. Martins, G. Snell, A.S. Schlachter, M. Sant'Anna, G. Kaindl, et al., "Detailed study of pyridine at the C 1s and N 1s ionization thresholds: The influence of the vibrational fine structure," *J. Chem. Phys.* **115**(14), 6426–6437 (October 2001).

Koprinarov, I.N., A.P. Hitchcock, W.H. Li, Y.M. Heng, and H.D. Stöver, "Quantitative compositional mapping of core-shell polymer microspheres by soft x-ray spectromicroscopy," *Macromolecules* **34**(13), 4424–4429 (June 2001).

Kortright, J.B., S.-K Kim, G.P. Denbeaux, G. Zeltzer, K. Takano, and E.E. Fullerton, "Soft x-ray small-angle scattering as a sensitive probe of magnetic and charge heterogeneity," *Phys. Rev. B* **64**(9), 18–20 (September 2001).

Kortright, J.B., S.-K Kim, E.E. Fullerton, J.S. Jiang, and S.D. Bader, "X-ray magneto-optic Kerr effect studies of spring magnet heterostructures," *Nucl. Instrum. Meth. A* **467–468**, 1396–1403 (July 2001).

Kukk, E., "High resolution auger spectroscopy of molecules," in *Proceedings of the 31st Annual Meeting of Estonian Physical Society* (Tartu, Estonia, February 12–15, 2001).

Kukk, E., "Molecular vibrations and electronic structure by resonant auger spectroscopy," in *Proceedings of 5th International Workshop on Auger Spectroscopy & Electronic Structure (IWASES-5)* (Cortona, Italy, July 2–6, 2001).

Kukk, E., G.P. Snell, J.D. Bozek, W.T. Cheng, and N. Berrah, "Vibrational structure and partial rates of resonant Auger decay of the N 1s $\rightarrow 2\pi$ core excitations in nitric oxide," *Phys. Rev. A* **6306**(6), 249–256 (June 2001).

Kumar, A., C. Roach, I.S. Hirsh, S. Turley, S. deWalque, P.A.M. Michels, and W.G.J. Hol, "An unexpected extended conformation for the third TPR motif of the peroxin PEX5 from *Trypanosoma brucei,*" *J. Mol. Biol.* **307**(1), 271–282 (March 2001).

Kurmaev, E.Z., M.I. Katsnelson, A.P. Moewes, M. Magnuson, J.-H. Guo, S.M. Butorin, J.E. Nordgren, D.L. Ederer, and M. Iwami, "Spectroscopic observation of polaron-lattice band structure in conducting polymers: X-ray fluorescence measurements of polyaniline," *J. Phys.–Condens. Mat.* **13**(17), 3907–3912 (April 2001).

Kurmaev, E.Z., A.P. Moewes, D.L. Ederer, H. Ishii, K. Seki, M. Yanagihara, F. Okino, and H. Touhara, "Electronic structure of graphite fluorides," *Phys. Lett. A* **288**(5–6), 340–344 (October 2001).

Kurmaev, E.Z., A.P. Moewes, Z.V. Pchelkina, I.A. Nekrasov, A.A. Rempel, and D.L. Ederer, "X-ray transitions for studying the electronic structure of 5d-metals," *Phys. Rev. B* **64**(7), 3108–3121 (August 2001).

Kurmaev, E.Z., A.P. Moewes, U. Schwingenschlögl, R. Claessen, M.I. Katsnelson, H. Kobayashi, S. Kagoshima, Y. Misaki, D.L. Ederer, K. Endo, et al., "Electronic structure of charge transfer salts," *Phys. Rev. B* **64**(23), 28222–28225 (December 2001).

Kurmaev, E.Z., A.P. Moewes, N.D. Zhigadlo, E. Takayama-Muromachi, Y.M. Yarmoshenko, S.N. Shamin, I.A. Nekrasov, O.A. Bureev, and D.L. Ederer, "Local and electronic structure of carbon and nitrogen atoms in oxycarbonitrate superconductors," *Physica C* **363**(1), 55–59 (October 2001).

Kurmaev, E.Z., S.N. Shamin, V.R. Galakhov, A.P. Moewes, T. Otsuka, S. Koizume, K. Endo, H.E. Katz, M. Bach, M. Neumann, D.L. Ederer, M. Iwami, et al., "Electronic structure of thiophenes and phtalocyanines," *Phys. Rev. B* **64**(4), 344–349 (July 2001).

Kusinski, G.J., "Structure and properties of co-based thin films and multilayers with perpendicular magnetic anisotropy," Ph.D. Thesis, University of California, Berkeley, 2001.

Kusinski, G.J., K.M. Krishnan, G. Denbeaux, G. Thomas, B.D. Terris, and D. Weller, "Magnetic imaging of ion-irradiation patterned Co/Pt multilayers using complementary electron and photon probes," *Appl. Phys. Lett.* **79**(14), 2211–2213 (October 2001).

Landers, A., T. Weber, I. Ali, A. Cassimi, M. Hattass, O. Jagutzki, A. Nauert, T. Osipov, A. Staudte, M.H. Prior, H. Schmidt-Böcking, C.L. Cocke, and R. Doerner, "Photoelectron diffraction mapping: Molecules illuminated from within," *Phys. Rev. Lett.* **87**(1), 13002 (July 2001).

Langhoff, P.W., J.C. Arce, J.A. Sheehy, O. Hemmers, H. Wang, P. Focke, I.A. Sellin, and D.W. Lindle, "On the angular distributions of electrons photoejected from fixed-in-space and randomly oriented molecules," *J. Electron Spectrosc.* **114–116**, 23–32 (March 2001).

Lanyi, J.K., and H. Luecke, "Bacteriorhodopsin," *Curr. Opin. Struct. Biol.* **11**, 415–419 (August 2001).

Lanzara, A., P.V. Bogdanov, S.A. Kellar, X.J. Zhou, E.D. Lu, G. Gu, J.-I. Shinoyama, K. Kishio, Z. Hussain, and Z.-X. Shen, et al., "Evidence for abrupt change in dispersion and scattering rate of quasiparticles in $Bi_2Sr_2CaCu_2O_8$," *J. Phys. Chem. Solids* **62**(1–2), 21–24 (January 2001).

Lanzara, A., P.V. Bogdanov, X.J. Zhou, S.A. Kellar, D.L. Feng, E.D. Lu, T. Yoshida, H. Eisaki, A. Fujimori, K. Kishio, J.I. Shimoyama, T. Noda, S. Uchida, Z. Hussain, Z.X. Shen, et al., "Evidence for ubiquitous strong electron-phonon coupling in high-temperature superconductors," *Nature* **412**(6846), 510–514 (August 2001).

Lawniczak-Jablonska, K., R.J. Iwanowski, I.N. Demchenko, T. Boettcher, S. Einfeldt, D. Hommel, R. Cortes, and R.C. Perera, "Polarization dependent x-ray absorption studies of the chemical bonds anisotropy in wurtzite GaN grown at different conditions," *J. Alloys Cmpd.* **328**(1–2), 77–83 (October 2001).

Lee, S.H., P. Naulleau, K.A. Goldberg, C.H. Cho, S. Jeong, and J. Bokor, "Extreme-ultraviolet lensless Fourier-transform holography," *Appl. Optics* **40**(16), 2655–2661 (June 2001).

Lee, S.Y., H.S. Cho, J.G. Pelton, D. Yan, E.A. Berry, and D.E. Wemmer, "Crystal structure of activated CheY. Comparison with other activated receiver domains," *J. Biol. Chem.* **276**(19), 16425–16431 (May 2001).

Lee, S.Y., H.S. Cho, J.G. Pelton, D.L. Yan, R.K. Henderson, D.S. King, L.S. Huang, S. Kustu, E.A. Berry, and D.E. Wemmer, "Crystal structure of an activated response regulator bound to its target," *Nat. Struct. Biol.* **8**(1), 52–56 (January 2001).

Li, P., D. Morris, B. Willcox, A. Steinle, T. Spies, and R. Strong, "Complex structure of the activating immunoreceptor NKG2D and its MHC classI-like ligand MICA," *Nature Immunol.* **2**(5), 443–451 (May 2001).

Lin, L., G.T. Woods, and T.A. Callcott, "Soft-x-ray fluorescence spectra of III-V phosphides BP, GaP, and InP," *Phys. Rev. B* **63**(23), 119–126 (June 2001).

Lindenberg, A.M., "Ultrafast lattice dynamics probed by time-resolved x-ray diffraction," Ph.D. Thesis, University of California, Berkeley, 2001.

Lindle, D.W., and O. Hemmers, "Time-of-flight photoelectron spectroscopy of atoms and molecules," *J. Alloys Cmpd.* **328**(1–2), 27–34 (October 2001).

Liu, J.B., M. Hochlaf, G. Chambaud, P. Rosmus, and C.Y. Ng, "High resolution pulsed field ionization-photoelectron bands for $CS_2^+(\tilde{A}^2\Pi_u)$: An experimental and theoretical study," *J. Phys. Chem.* **105**(11), 2183–2191 (March 2001).

Liu, P., and D.K. Shuh, "Adsorption of O_2 on polycrystalline rhenium metal at room temperature studied by synchrotron x-ray photoemission spectroscopy," *J. Electron Spectrosc.* **114–116**, 319–325 (March 2001).

Liu, Y., A. Manna, R. Li, W.E. Martin, R.C. Murphy, A.L. Cheung, and G. Zhang, "Crystal structure of the SarR protein from *Staphylococcus aureus,*" *Proc. Natl. Acad. Sci. USA* **98**(12), 6877–6882 (June 2001).

Loo, B.W., I.M. Sauerwald, A.P. Hitchcock, and S.S. Rothman, "A new sample preparation method for biological soft x-ray microscopy: Nitrogen-based contrast and radiation tolerance properties of glycol methacrylate-embedded and sectioned tissue," *J. Microsc.–Oxford* **204**(1), 69–86 (October 2001).

Lougheed, J.C., J.M. Holton, T. Alber, J.F. Bazan, and T.M. Handel, "Structure of melanoma inhibitory activity protein, a member of a recently identified family of proteins," *Proc. Natl. Acad. Sci. USA* **98**(10), 5515–5555 (May 2001).

Lucas, R.W., Y.G. Kuznetsov, S.B. Larson, and A. McPherson, "Crystallization of Brome Mosaic Virus and T=1 BMV particles following a structural transition," *Virology* **286**(2), 290–303 (August 2001).

MacDowell, A.A., R.S. Celestre, N. Tamura, R. Spolenak, B. Valek, W.L. Brown, J.C. Bravman, H.A. Padmore, B.W. Batterman, and J.R. Patel, "Submicron x-ray diffraction," *Nucl. Instrum. Meth. A* **467–468**(2), 936–943 (July 2001).

Magnuson, M., S. Butorin, J. Guo, A. Agui, J.E. Nordgren, H. Ogasawara, A. Kotani, T. Takahashi, and S. Kunii, "Electronic-structure investigation of CeB_6 by means of soft-x-ray-scattering," *Phys. Rev. B* **63**(7), 1–5 (February 2001).

Malinowski, M.E., P.A. Grunow, C.A. Steinhaus, M. Clift, and L. Klebanoff, "Use of molecular oxygen to reduce EUV-induced carbon contamination of optics," in *Proceedings of SPIE, Microlithography 2001: Emerging Lithographic Technologies V* (Santa Clara, California, February 27–March 2, 2001).

Martin, M.C., N.M. Tsvetkova, J.H. Crowe, and W.R. McKinney, "Negligible sample heating from synchrotron infrared beam," *Appl. Spectrosc.* **55**(2), 111–113 (February 2001).

Matsuo, S., N. Sakaguchi, E. Obuchi, K. Nakano, R.C.C. Perera, T. Watanabe, T. Matsuo, and H. Wakita, "X-ray absorption spectral analyses by theoretical calculations for TiO_2 and Ni-Doped TiO_2 thin films on glass plates," *Anal. Sci.* **17**(1), 149–153 (January 2001).

McGrail, B.P., J.P. Icenhower, D.K. Shuh, P. Liu, J.G. Darab, D.R. Baer, S. Thevuthasen, V. Shutthanandan, C.H. Booth, and P. Nachimuthu, "The structure of Na_2O-Al_2O_3-SiO_2 glasses: Impact on sodium ion exchange in H_2O, D_2O, and $D_2{}^{18}O$," *J. Non-Cryst. Solids* **296**(1–2), 10–26 (December 2001).

McGuinness, C., K.E. Smith, S.M. Butorin, J.H. Guo, J. Nordgren, T. Vogt, G. Schneider, J. Reilly, J.J. Tu, P.D. Johnson, D.K. Shuh, et al., "High-resolution x-ray emission and absorption study of the B 2p valence band electronic structure of MgB_2," *Europhys. Lett.* **56**(1), 112–118 (October 2001).

McHugo, S., A.C. Thompson, A. Mohammed, G. Lamble, I. Perichaud, S. Martinuzzi, M. Werner, M. Rinio, W. Koch, and H. Hoefs, "Nanometer-scale metal percipitates in multicrystalline silicon solar cells," *J. Appl. Phys.* **89**(8), 4282–4288 (April 2001).

Meng, S., B.R. Schroeder, A. Bostwick, M.A. Olmstead, E. Rotenberg, and F.S. Ohuchi, "Low-energy photoelectron diffraction structure determination of GaSe-bilayer passivated Si(111)," *Phys. Rev. B* **64**(23), 235314 (December 2001).

Meyer-Ilse, W., D. Hamamoto, A. Nair, S. Lelievre, G. Denbeaux, L. Johnson, A.L. Pearson, D. Yager, M.A. Le Gros, and C.A. Larabell, "High resolution protein localization using soft x-ray microscopy," *J. Microsc.–Oxford* **201**(3), 395–403 (March 2001).

Mirkarimi, P.B., D.G. Stearns, S.L. Baker, J.W. Elmer, D.W. Sweeney, and E.M. Gullikson, "Method for repairing Mo/Si multilayer thin film phase defects in reticles for extreme ultraviolet lithography," *Appl. Phys. B–Photo.* **91**(1), 81–89, (January 2001).

Misura, K.M.S., R. Scheller, and W.I. Weis, "Self-association of the H3 region of syntaxin 1A: Implications for intermediates in SNARE complex assembly," *J. Biol. Chem.* **276**(16), 13273–13282 (April 2001).

Mitchell, G.E., et al., "Quantitative characterization of microscopic variations in the crosslink density of gels," *Macromolecules* **35,** 1336 (2002).

Moewes, A.P., and E.Z. Kurmaev, "Multi-atom resonances and soft x-ray emission," *Nucl. Instrum. Meth. A* **467–468**(2), 1529–1532, (July 2001).

Morais, J., G.H. Fecher, R. Denecke, J. Liesegang, and C.S. Fadley, "Dichroism in angular resolved XPS from gadolinium core-levels," *J. Electron Spectrosc.* **114–116**, 783–788 (March 2001).

Morin, C., H. Ikeura-Sekiguchi, T. Tyliszczak, R. Cornelius, J.L. Brash, A.P. Hitchcock, A. Scholl, F. Nolting, G. Appel, A.D. Winesett, et al., "X-ray spectromicroscopy of immiscible polymer blends: Polystyrene-poly(methyl methacrylate)," *J. Electron Spectrosc.* **121**(1–3), 203–224 (December 2001).

Mueller, J.A., B.F. Parsons, L.J. Butler, F. Qi, O. Sorkhabi, and A.G. Suits, "Competing isomeric product channels in the 193 nm photolysis of 2-chloropropene and in the unimolecular dissociation of the 2-propenyl radical," *J. Chem. Phys.* **114**(10), 4505–4521 (March 2001).

Müller, A., S. Schippers, A.M. Covington, A. Aguilar, G. Hinojosa, R.A. Phaneuf, M.M. Sant'Anna, A.S. Schlachter, J.D. Bozek, and C. Cisneros, "Photoionization of Ca^+ Ions by Synchrotron Radiation," *Proceedings of the 22nd International Conference on Photonic, Electronic, and Atomic Collisions (ICPAEC 2001)* (Santa Fe, New Mexico, July 18–24, 2001).

Muramatsu, Y., M. Watanabe, Y. Ueno, S. Shin, and R.C.C. Perera, "Soft x-ray emission spectra in the O K region of oxygen incorporated in microporous carbon," *J. Electron Spectrosc.* **114–116**, 301–305 (March 2001).

Nadolski, L.S., "Application de l'analyse en fréquence a l'étude de la dynamique des sources de lumière," Ph. D. Thesis, Université de Paris XI, France, 2001.

Nakamura, J., N. Yamada, K. Kuroki, T.A. Callcott, J. Denlinger, R.C. Perrera, and D.L. Ederer, "Soft x-ray spectroscopy experiments on the near K-edge of B in MB_2 (M=Mg, Al, Ta, and Nb)," *Phys. Rev. B* **64**(17), 433–435 (November 2001).

Naulleau, P., K.A. Goldberg, P.J. Batson, S. Jeong, and J.H. Underwood, "Tolerancing of diffraction-limited Kirkpatrick–Baez synchrotron beamline optics for extreme-ultraviolet metrology," *Appl. Optics* **40**(22), 3703–3709 (August 2001).

Naulleau, P.P., K.A. Goldberg, E.H. Anderson, P.J. Batson, P. Denham, S. Rekawa, and J. Bokor, "Adding static printing capabilities ot the EUV phase-shifting point diffraction interferometer," in *Proceedings of SPIE, Microlithography 2001: Emerging Lithographic Technologies V* (Santa Clara, California, February 27–March 2, 2001).

Naulleau, P.P., K.A. Goldberg, E.H. Anderson, P.J. Batson, P.E. Denham, K.H. Jackson, E.M. Gullikson, S. Rekawa, and J. Bokor, "At-wavelength characterization of the extreme ultraviolet engineering test stand set-2 optic," *J. Vac. Sci. Technol. B* **19**(6), 2396–2400 (November 2001).

Nayandin, O.Y., "High-resolution photoelectron studies in Ar and Cl_2," Ph.D. Thesis, Western Michigan University, 2001.

Nayandin, O.Y., T.W. Gorczyca, A.A. Wills, B. Langer, J.D. Bozek, and N. Berrah, " interference effects in the Auger decay of the Ar $2p^{-1}$ 3d resonances," *Phys. Rev. A* **64**(1), 1–7 (July 2001).

Nayandin, O.Y., E. Kukk, A.A. Wills, B. Langer, J.D. Bozek, S.E. Canton, M.F. Wiedenhoeft, D. Cubaynes, and N. Berrah, "Angle-resolved two-dimensional mapping of electron emission from the inner-shell 2p excitations in Cl_2," *Phys. Rev. A* **63**(6), 396–402 (June 2001).

Nelson, A.J., A. Van Buuren, E. Miller, T.A. Land, C.F.O. Bostedt, N. Franco Cerame, P.K. Whitman, P.A. Baisden, L.J. Terminello, and T.A. Callcott, "X-ray absorption analysis of KDP optics," *J. Electron Spectrosc.* **114–116**, 873–878 (March 2001).

Nilsson, P., S. Mankefors, J. Guo, J. Nordgren, D. Debowska-Nilsson, W. Ni, and G. Hansson, "Electronic structure of ultrathin Ge layers buried in Si(100)," *Phys. Rev. B* **64**(11), 27587–26582 (August 2001).

Nollert, P., W.E. Harries, D. Fu, L.J. Miercke, and R.M. Stroud, "Atomic structure of a glycerol channel and implications for substrate permeation in aqua(glycero)porins," *FEBS Lett.* **504**, 112–117 (August 2001).

Nollert, P.K., D. Fu, L. Miercke, W.E. Harries, and R.M. Stroud, "Structure and function of an aquaglyceroporin and the basis for water conductance and its selectivity against protons and ion," in *Proceedings of the International Conference on Sequence, Structure, and Function in Membrane Protein Systems* (Zichron Ya'acov, Israel, November 4–8,2001).

Nyberg, M., Y. Luo, L. Qian, J.E. Rubensson, C. Såthe, D. Ding, J.H. Guo, T. Käämbre, and J.E. Nordgren, "Bond formation in titanium fulleride compounds studied through x-ray emission spectroscopy," *Phys. Rev. B* **63**(11), 202–207 (March 2001).

Ohldag, H., T.J. Regab, J. Stoehr, A. Scholl, F. Nolting, J. Luening, C. Stamm, S. Anders, and R.L. White, "Spectroscopic identification and direct imaging of interfacial magnetic spins," *Phys. Rev. Lett.* **87**(24), 7201–7204 (December 2001).

Ohldag, H., A. Scholl, F. Nolting, S. Anders, U. Hillebrecht, and J. Stöhr, "Spin reorientation at the antiferromagnetic NiO(001) surface in response to an adjacent ferromagnet," *Phys. Rev. Lett.* **86**(13), 2878–2881 (March 2001).

Ollman-Saphire, E., P.W.H.I. Parren, C.F. Barbas, D.R. Burton, and I.A. Wilson, "Crystallization and preliminary structure determination of an intact human immunoglobulin, b12: An antibody that broadly neutralizes primary isolates of HIV-1," *Acta Crystallogr. D* **57**(PT1), 168–171 (January 2001).

Omori, S., Y. Nehei, E. Rotenberg, J.D. Denlinger, S.D. Kevan, B.P. Tonner, M.A. Van Hove, and C.S. Fadley, "Imaging of Cu(001) atoms by a new differential approach to photoelectron holography," *J. Electron Spectrosc.* **114–116**, 455–460 (March 2001).

Orencia, C., J. Yoon, J.E. Ness, W.P.C. Stemmer, and R.C. Stevens, "Predicting the emergence of antibiotic resistance by directed evolution and structural analysis," *Nat. Struct. Biol.* **8**(3), 238–242 (March 2001).

Orgad, D., S.A. Kivelson, E.W. Carlson, V.J. Emery, X.J. Zhou, and Z.X. Shen, "Evidence of electron fractionalization from photoemission spectra in the high-temperature superconductors," *Phys. Rev. Lett.* **86**(19), 4362–4365 (May 2001).

Padmore, H.A., A.C. Thompson, and J. Feng, "A double-crystal monochromator using tangentially bent crystals in combination with toroidal mirror focusing," *Nucl. Instrum. Meth. A* **467**, 650–653 (June 2001).

Panero, W., "Experimental observations of basaltic crust in the lower mantle," Ph.D. Thesis, University of California, Berkeley, 2001.

Prabhakar, S., J.D. Fox, and D. Teytelman, "Curing coupled-bunch instabilities with uneven fills," *Phys. Rev. Lett.* **86**(10), 2022–2025 (March 2001).

Püttner, R., B. Gremaud, D. Delande, M. Domke, M. Martins, A.S. Schlachter, and G. Kaindl, "Statistical properties of inter-series mixing in helium: From integrability to chaos," *Phys. Rev. Lett.* **86**(17), 3747–3750 (April 2001).

Qi, F., O. Sorkhabi, A.G. Suits, S.-H. Chien, and W.-K. Li, "Photodissociation of ethylene sulfide at 193 nm: A photofragment translational spectroscopy study with VUV synchrotron radiation and ab initio calculations," *J. Am. Chem. Soc.* **123**(1), 148–161 (January 2001).

Qian, L., "Soft x-ray spectroscopy study of fullerene based transition-metal compounds and related systems," Ph.D. Thesis, Uppsala University, Sweden, 2001.

Qian, L., M. Nyberg, Y. Luo, J. Rubensson, A. Talyzine, C. Såthe, D. Ding, J. Guo, H. Hogberg, T. Käämbre, U. Jansson, J.E. Nordgren, et al., "Bonding mechanism in the transition-metal fullerides studied by symmetry-selective resonant x-ray inelastic scattering," *Phys. Rev. B* **63**(8), 524–526 (February 2001).

Quitman, C., U. Flechsig, L. Patthey, T. Schmidt, G. Ingold, M. Howells, M. Janousch, and R. Abela, "A beamline for time-resolved photoelectron microscopy on magnetic materials at the Swiss Light Source," *Surface Science,* **480**, 173–179 (2001).

Raab, T.K., and M.C. Martin, "Visualizing rhizosphere chemistry of legumes with mid-infrared synchrotron radiation," *Planta* **213**(6), 881–887 (October 2001).

Rahmim, A., "Analysis of coherent resonant x-ray scattering and reconstruction of magnetic domains," Master's Thesis, University of British Columbia, Canada, 2001.

Raman, C.S., H. Li, P. Martasek, G. Southan, and B.S. T.L. Poulos, "Crystal structure of nitric oxide synthase bound to nitro indazole reveals a novel inactivation mechanism," *Biochemistry–US* **40**(45), 13448–13455 (November 2001).

Rathbone, G.J., E. Poliakoff, J.D. Bozek, and R.R. Lucchese, "Resonantly amplified vibronic symmetry breaking," *J. Chem. Phys.* **114**(19), 8240–8243 (May 2001).

Regan, T.J., et al., "Chemical effects at metal/oxide interfaces studied by x-ray-absorption spectroscopy," *Phys. Rev. B* **64**, 214422 (2001).

Roberge, M., L. Santell, M.S. Dennis, C. Eigenbrot, M.A. Dwyer, and R.A. Lazarus, "A novel exosite on coagulation factor VIIa and its molecular interactions with a new class of peptide inhibitors," *Biochemistry–US* **40**(32), 9522–9531 (August 2001).

Robin, D., R. Schlueter, J. Zbasnik, S. Marks, C. Steier, J. Krupnick, B. Wang, E. Hoyer, T. Henderson, M. Fahmie, et al., "Superbend project at the Advanced Light Source," in *Proceedings of the 2001 Particle Accelerator Conference* (Chicago, Illlinois, June 18–22, 2001).

Robinson, J.C., W. Sun, S.A. Harris, F. Qi, and D.M. Neumark, "Photofragment translational spectroscopy of 1,2-butadiene at 193 nm," *J. Chem. Phys.* **115**(18), 8359–8365 (November 2001).

Rolles, D., D. Diez Muino, F.J. Garcia de Abajo, C.S. Fadley, and M.A. Van Hove, "Elastic scattering of low-energy electrons by randomly oriented and aligned molecules: Influence of full non-spherical potentials," *J. Electron Spectrosc.* **114–116**, 107–113 (March 2001).

Rose, R.B., J.A. Endrizzi, J.D. Cronk, J. Holton, and T. Alber, "High-resolution structure of the HNF-1 α dimerization," *Biochemistry–US* **40**(10), 3242 (March 2001).

Rosengarth, A.A., V. Gerke, and H. Luecke, "X-ray structure of full-length annexin 1 and implications for membrane aggregation," *J. Mol. Biol.* **306**(3), 489–498 (February 2001).

Rouhani, S., J.-P. Cartailler, M.T. Facciotti, P. Walian, R. Needleman, J.K. Lanyi, R.M. Glaeser, and H. Luecke, "Crystal structure of the D85S mutant of bacteriorhodopsin: Model of an O-like photocycle intermediate," *J. Mol. Biol.* **313**(3), 615–628 (October 2001).

Rupert, P.B., and A.R. Ferré D'Amaré, "Crystal structure of a hairpin ribozyme–inhibitor complex with implications for catalysis," *Nature* **410**, 780–786 (April 2001).

Sacchi, M., A. Mirone, C.F. Hague, P. Castrucci, R. Gunnella, and M. De Crescenzi, "Resonant magnetic scattering from fcc Cu/Fe/Cu/Si(111) heterostructures," *Phys. Rev. B* **64**(1), 27–29 (July 2001).

Sae-Lao, B., and C. Montcalm, "Molybdenum-strontium multilayer mirrors for the 8–12 nm extreme-ultraviolet wavelength region," *Opt. Lett.* **26**(7), 468–470 (April 2001).

Saethre, L.J., N. Berrah, J.D. Bozek, K.J. Børve, T.X. Carroll, E. Kukk, G.L. Gard, R. Winter, and T.D. Thomas, "Chemical insights from high-resolution x-ray photoelectron spectroscopy and ab initio theory: Propyne, trifluoropropyne, and ethynylsulfur pentafluoride," *J. Am. Chem. Soc.* **123**(43), 10729–10737 (October 2001).

Schäfer, J.H., E. Rotenberg, S.D. Kevan, P. Blaha, R. Claessen, and R.E. Thorne, "High-temperature symmetry breaking in the electronic band structure of the quasi-one-dimensional solid $NbSe_3$," *Phys. Rev. Lett.* **87**(19), 1–4 (November 2001).

Schippers, S., A. Müller, A. Covington, A. Aguilar, G. Hinojosa, R.A. Phaneuf, M.M. Sant'Anna, A.S. Schlachter, J.D. Bozek, and C. Cisneros, "Photoionization of Ca^+ ions by synchrotron radiation," in *Proceedings of the Seventh European Conference on Atomic and Molecular Physics* (Berlin, Germany, April 2–6, 2001).

Schmidt, T.J., Z. Jusys, H.A. Gasteiger, R.J. Behm, U. Endruschat, and H. Boennemann, "On the CO tolerance of novel colloidal PdAu/carbon electrocatalysts," *J. of Electroanal. Chem.* **501**(1–2), 132–140 (March 2001).

Schneider, B., "Untersuchungen zur elektronischen und geometrischen Struktur ausgewaehlter oxidischer und sulfidischer mittels Photoelektronen- und Roentgenspektroskopie," Ph.D. Thesis, University of Osnabrueck, Germany, 2001.

Schoenlein, R.W., H.H.W. Chong, T.E. Glover, P.A. Heimann, W.P. Leemans, H.A. Padmore, C.V. Shank, A. Zholents, M. Zolotorev, and J.S. Corlett, "Femtosecond x-rays from relativistic electrons: New tools for probing structural dynamics," *CR Acad. Sci. IV–Phys.* **2**, 1373 (2001).

Scholl, A., F. Nolting, J. Stöhr, T. Regan, J.M. Lüning, J.W. Seo, J.P. Locquet, J. Fompeyrine, S. Anders, H. Ohldag, H.A. Padmore, et al., "Exploring the microscopic origin of exchange bias with photoelectron emission microscopy," *J. Appl. Phys.* **89**(11), 7266–7268 (June 2001).

Schuler, T.M., D.L. Ederer, N. Rudzycki, G. Glass, W.A. Hollerman, A. Moewes, M. Kuhn, and T.A. Callcott, "Diffusion of TiN into aluminum films measured by soft x-ray spectroscopy and Rutherford backscattering spectroscopy," *J. Vac. Sci. Technol. A* **19**(5), 2259–2266 (October 2001).

Schulze-Gahmen, U., and S.-H. Kim, "Crystallization of a complex between human CDK6 and a virus-encoded cyclin is critically dependent on the addition of small charged organic molecules," *Acta Crystallogr. D* **57**(9), 1287–1289 (September 2001).

Schumann, F.O., and J.G. Tobin, "Observation of component fine structure in the linear dichroism of the Fe 3p photoelectron emission," *Surf. Sci.* **476**, 235–240 (March 2001).

Seeman, J.T., Y. Cai, J. Clendenin, F.-J Decker, M. Donald, S. Ecklund, I. Reichel, C. Steier, M. Zisman, et al., "Status and future plans of the PEP-II B-factory," in *Proceedings of the 2001 Particle Accelerator Conference* (Chicago, Illlinois, June 18–22, 2001).

Shin, N., C. Chang, Y. Mo Koo, and H.A. Padmore, "Background spectrum of synchrotron radiation: Excited total reflection x-ray fluorescence for Si wafer analysis," *X-Ray Spectrom.* **30**(2), 127–131 (March 2001).

Shin, N., C. Chang, Y. Mo Koo, and H.A. Padmore, "Synchrotron radiation excited total reflection x-ray fluorescence quantitative analysis of Si wafer by absolute fluorescence intensity calculation," *Mater. Lett.* **49**(1), 38–42. (May 2001).

Shirley, E.L., J.A. Soininen, G.P. Zhang, J.A. Carlisle, T.A. Callcott, D.L. Ederer, L.J. Terminello, and R.C.C. Perera, "Modeling final-state interaction effects in inelastic x-ray scattering from solids: Resonant and non-resonant," *J. Electron Spectrosc.* **114–116**, 939–946 (March 2001).

Shumway, M.D., S.H. Lee, C.H. Cho, P. Naulleau, K.A. Goldberg, and J. Bokor, "Extremely fine-pitch printing with a 10× Schwarzschild optic at extreme-ultraviolet wavelengths," in *Proceedings of SPIE, Microlithography 2001: Emerging Lithographic Technologies V* (Santa Clara, California, February 27–March 2, 2001).

Sintchak, M.D, G. Arjara, C.C. Lawrence, L. Shu, B.A. Kellogg, J. Stubbe, and C.L. Drennan, "B12-dependent ribonucleotide reductase: Paradox or paradigm?" in *Proceedings of the 15th West Coast Protein Crystallography Workshop* (Pacific Grove, Cailfornia, March 25–28, 2001).

Smith, N.V., "Classical generalization of the Drude formula for the optical conductivity," *Phys. Rev. B* **64**(15), 110–114 (October 2001).

Snell, G.P., M. Martins, E. Kukk, W.T. Cheng, and N. Berrah, "High-resolution electron spectroscopy of a strongly correlated system: Atomic barium," *Phys. Rev. A* **63**(6), 362–367 (June 2001).

Solak, H.H., Y. Yang, and F. Cerrina, "Observation of speckles in extreme ultraviolet imaging," *J. Vac. Sci. Technol. B* **19**(6), 2406 (November 2001).

Song, Y., C.Y. Ng, G.K. Jarvis, and R.A. Dressler, "Rotational-resolved pulsed field ionization–photoelectron study of NO^+ ($A'\ ^1\Sigma^-$, $v^+ = 0$–17) in the energy range of 17.20–20.10 eV," *J. Chem. Phys.* **115**(5), 2101–2108 (August 2001).

Song, Y., X. Qian, K.-C. Lau, and C.Y. Ng, "A pulsed field ionization study of the dissociative photoionization reaction $CD_4 + h\nu \rightarrow CD_3^+ + D + e^-$," *Chem. Phys. Lett.* **347**(1–3), 51–58 (October 2001).

Song, Y., X.M. Qian, K.C. Lau, C.Y. Ng, J.B. Liu, and W.W. Chen, "High-resolution energy-selected study of the reaction $CH_3X \rightarrow CH_3^+ + X$: Accurate thermochemistry for the CH_3X/CH_3X^+ (X=Br,I) system," *J. Chem. Phys.* **115**(9), 4095–4104 (September 2001).

Song, Y., X.M. Qian, K.C. Lau, C.Y. Ng, J.B. Liu, and W.W. Chen, "High-resolution energy-selected study of the reaction $NH_3^+ \rightarrow NH_2^+ + H$: Accurate thermochemistry for the NH_2/NH_2^+ and NH_3/NH_3^+ systems," *J. Chem. Phys.* **115**(6), 2582–2589 (August 2001).

Sorkhabi, O., F. Qi, A.H. Rivzi, and A.G. Suits, "The ultraviolet photochemistry of phenylacetylene and the enthalpy of formation of 1,3,5-hexatriyne," *J. Am. Chem. Soc.* **123**(4), 671–676 (January 2001).

Soufli, R., E.A. Spiller, M.A. Schmidt, J.C. Davidson, R.F. Grabner, E.M. Gullikson, B.B. Kaufmann, S. Mrowka, S.L. Baker, H.N. Chapman, R.M. Hudyma, J.S. Taylor, C.C. Walton, C. Montcalm, and J.A. Folta, "Multilayer optics for an extreme ultraviolet lithography tool with 70 nm resolution," in *Proceedings of SPIE, Microlithography 2001: Emerging Lithographic Technologies V* (Santa Clara, California, February 27–March 2, 2001).

Spassov, V.Z., H. Luecke, D. Bashford, and K. Gerwert, "pK_a calculations suggest storage of an excess proton in a hydrogen-bonded water network in bacteriorhodopsin," *J. Mol. Biol.* **312**(1), 203–219 (September 2001).

Spence, J., "Optics: Holograms of atoms," *Nature* **410**(6382), 1037–1040 (April 2001).

Spence, J., M. Howells, L. Marks, and J. Miao, "Lensless imaging: A workshop on new approaches to the phase problem for non-periodic objects," *Ultramicroscopy* **90**(1), 1–6 (November 2001).

Spence, J., M. Howells, J. Miao, and L. Marks, "Workshop on lensless imaging," *Ultramicroscopy* **14**(6), 21–23 (Fall 2001).

Spence, J.C.H., and C. Koch, "Atomic String holography," *Phys. Rev. Lett.* **86**(24), 5510–5513 (June 2001).

Spiegel, P.C., M. Jacquemin, J.R. Saint-Remy, B.L. Stoddard, and K.P. Pratt, "Structure of a factor VIII C2 domain–immunoglobulin G4k Fab complex: Identification of an inhibitory antibody epitope on the surface of factor VIII," *Blood* **98**(1), 13–19 (July 2001).

Spolenak, R., N. Tamura, B.C. Valek, A.A. MacDowell, H.A. Padmore, W.L. Brown, T. Marieb, B.W. Batterman, and J.R. Patel, "High resolution microdiffraction studies using synchrotron radiation," in *Proceedings of the Sixth International Workshop on Stress Induced Phenomena in Metallization* (Ithaca, New York, July 25–27, 2001).

Stamper, C.C., Y. Zhang, J.G. Tobin, D. Erbe, S. Ikemizu, S.J. Davis, M.L. Stahl, J. Seehra, W.S. Somers, and L. Mosyak, "Crystal structure of the B7-1/CTLA-4 complex that inhibits human immune responses," *Nature* **410**(6828), 608–611 (March 2001).

Steier, C., A. Biocca, E. Domning, S. Jacobson, G. Portmann, and Y. Wu, "Design of a fast global orbit feedback system for the Advanced Light Source," in *Proceedings of the 2001 Particle Accelerator Conference* (Chicago, Illlinois, June 18–22, 2001).

Steier, C., J. Byrd, J. Corlett, S. de Santis, A. Wolski, K. Bane, M. Ross, T. Smith, et al., " intra-beam scattering and minimum achievable emittance in the Advanced Light Source," in *Proceedings of the 2001 Particle Accelerator Conference* (Chicago, Illlinois, June 18–22, 2001).

Steier, C., D. Robin, Y. Wu, W. Decking, J. Laskar, and L. Nadolski, "Understanding the dynamic momentum aperture of the Advanced Light Source," in *Proceedings of the 2001 Particle Accelerator Conference* (Chicago, Illlinois, June 18–22, 2001).

Stewart, J., et al., "Mechanism of beta clamp opening by the delta subunit of *Escherichia coli* DNA polymerase III holoenzyme," *J. Biol. Chem.* **276**, 19182 (2001).

Stolte, W.C., D.L. Hansen, M.N. Piancastelli, I. Dominguez-Lopez, A.H. Rizvi, O.A. Hemmers, H. Wang, A.S. Schlachter, M.S. Lubell, and D.W. Lindle, "Anionic photofragmentation of CO: A selective probe of core-level resonances," *Phys. Rev. Lett.* **86**(20), 4504–4507 (May 2001).

Story, R.M., H. Li, and J.N. Abelson, "Crystal structure of a DEAD box protein from the hyperthermophile *Methanococcus jannaschii,*" *Proc. Natl. Acad. Sci. USA* **98**(4), 1465–1470 (March 2001).

Strasser, T., C. Solterbeck, W. Schattke, I. Bartos, M. Cukr, P. Jiricek, C.S. Fadley, and M.A. Van Hove, "A theoretical investigation of photoemission spectra from $(GaAs)_2(AlAs)_2$ superlattices," *J. Electron Spectrosc.* **114–116**, 1127–1132 (March 2001).

Strasser, T., C. Solterbeck, W. Schattke, I. Bartos, M. Cukr, P. Jiricek, C.S. Fadley, and M.A. Van Hove, "One-step photoemission calculations for ideal GaAs(001) and AlAs(001) surfaces and $(GaAs)_m(AlAs)_n$ superlattices," *Phys. Rev. B* **63**(19), 402–410 (May 2001).

Sui, H., B. Han, J. Lee, P. Wallen, and B. Jap, "Structural basis of water-specific transport through the AQP1 water channel," *Nature* **414**, 872–878 (December 2001).

Suits, A.G., and F. Qi, "The photodissociation dynamics of cyclic sulfides probed with tunable undulator radiation," *J. Electron Spectrosc.* **119**(2–3), 127–145 (August 2001).

Sundaram, S.K., M.A. Haller, Y. Su, V. Shutthanandan, J.S. Young, S. Thevuthasan, P. Nachimuthu, R.C. Perera, and D.K. Shuh, "Structural investigation of ion irradiated simulated high-level waste glass," in *Proceedings of the 48th International Symposium of the American Vacuum Society* (San Francisco, California, October 29–November 2, 2001).

Suresh, S., J.C. Bressi, K.J. Kennedy, C.L.M.J. Verlinde, M.H. Gelb, and W.G.J. Hol, "Conformational changes in *Leishmania mexicana* glyceraldehyde–3-phosphate dehydrogenase induced by designed inhibitors," *J. Mol. Biol.* **309**(2), 423–435 (June 2001).

Takagi, H., H. Daimon, F.J. Palomares, and C.S. Fadley, "Photoelectron holography analysis of W(110)(1×1)–O surface," *Surf. Sci.* **470**(3), 189–196 (January 2001).

Takagi, N., P. Fischer, S. Tsunashima, M. Kumazawa, H. Ishida, A. Yamyguchi, H. Noguchi, and M. Kume, "Observation of thermomagnetically recorded magnetic domains in TbFeCo films with x-ray microscopy," *Jpn. J. Appl. Phys. 1* **40**(4B), 380–382 (April 2001).

Tamura, N., B.C. Valek, R. Spolenak, A.A. Macdowell, R.S. Celestre, H.A. Padmore, W.L. Brown, T. Marieb, J.C. Bravman, B.W. Batterman, and J.R. Patel, "Grain orientation and strain measurements in sub-micron wide passivated individual aluminum test structures," in *Proceedings of Materials Research Society Spring Meeting* 2000 (San Francisco, California, April 23–27, 2000).

Taylor, A.B., B.S. Smith, S. Kitada, K. Kojima, H. Miyaura, Z. Otwinowski, A. Ito, and J. Deisenhofer, "Crystal structures of mitochondrial processing peptidase reveal the mode for specific cleavage of import signal sequences," *Structure* **9**(7), 615–625 (July 2001).

Ter Haar, E., J.T. Coll, D.A. Austen, H.-M. Hsiao, L. Swenson, and J. Jain, "Structure of GSK3b reveals a primed phosphorylation mechanism," *Nat. Struct. Biol.* **8**(7), 593–596 (July 2001).

Terry, J., R.K. Schulze, J.D. Farr, T. Zocco, K. Heinzelman, E. Rotenberg, D.K. Shuh, G. van der Laan, D.A. Arena, and J.G. Tobin, "5f resonant photoemission from Pu," *Surf. Sci.* **480**, 1–6 (November 2001).

Teytelman, D., "Arthitectures and algorithms for control and diagnostics of coupled-bunch instabilities in circular accelerators," Ph.D Thesis, Stanford University, 2001.

Teytelman, D., J. Fox, S. Prabhakar, and J.M. Byrd, "Characterization of longitudinal impedances in storage rings via multibunch effects," *Phys. Rev. ST Accel. Beams* **411**(11), 2801 (November 2001).

Teytelman, D., J.D. Fox, S. Prabhakar, and J. Byrd, "Frequency resolved measurement of longitudinal impedances using transient beam diagnostics," in *Proceedings of the 2001 Particle Accelerator Conference* (Chicago, Illlinois, June 18–22, 2001).

Thevuthasan, S., V. Shutthanandan, M.A. Henderson, G.S. Herman, S.A. Chambers, S. Mun, N.H. Hamdan, D.K. Shuh, and C.S. Fadley, "Valence band photoemission from pure and Sr diffused single crystal anatase TiO_2(001) surfaces," in *Proceedings of the 48th International Symposium of the American Vacuum Society* (San Francisco, California, October 29–November 2, 2001).

Tichenor, D.A., A.K. Ray-Chaudhuri, S.H. Lee, W.C. Replogle, R.H. Stulen, G.D. Kublak, P.D. Rockett, L.E. Klebanoff, K.J. Jefferson, A. Leung, et al., " initial results from the EUV engineering test stand," in *SPIE Annual Meeting 2001* (San Diego, California, July 29–August 3, 2001).

Tichenor, D.A., A.K. Ray-Chaudhuri, W.C. Replogle, R.H. Stulen, G.D. Kubiak, P.D. Rockett, L.E. Klebanoff, K.L. Jefferson, A.H. Leung, J.B. Wronosky, et al., "System integration and performance of the EUV engineering test stand," in *Proceedings of SPIE, Microlithography 2001: Emerging Lithographic Technologies V* (Santa Clara, California, February 27–March 2, 2001).

Tobin, J.G., and F.O. Schumann, "Element-specific magnetometry with photoelectron dichroism: FeCo and FeNi," *Surf. Sci.* **478**(3), 211–228 (May 2001).

Uda, M., D. Yamashita, D. Terashi, T. Yamamoto, H. Osawa, K. Kanai, H. Nakamatsu, and R.C.C. Perera, "XANES spectra of sesqui-oxides of Al, Cr and Fe," *J. Electron Spectrosc.* **114–116**, 819–823, (March 2001).

Valek, B.C., N. Tamura, R. Spolenak, A.A. MacDowell, R.S. Celestre, H.A. Padmore, J.C. Bravman, W.L. Brown, B.W Batterman, and J.R. Patel, "Local microstructure and stress in Al(Cu) thin film structures studied by x-ray microdiffraction," *Mater. Res. Soc. Symp. Proc.* **673**, 771–776 (April 2001).

Vargason, J.M., K. Henderson, and P.S. Ho, "A crystallographic map of the transition from B-DNA to A-DNA," *Proc. Natl. Acad. Sci. USA* **98**(13), 7265–7270 (June 2001).

Vyvenko, O.F., A.A. Istratov, T. Buonassisi, E.R. Weber, and R. Schindler, "Application of x-ray fluorescence microprobe technique for the analysis of fully processed solar cells," in *Proceedings of the 11th Workshop on Crystalline Silicon Solar Cell Materials and Processes* (Estes Park, Colorado, August 19–22, 2001).

Wang, H., G. Snell, O. Hemmers, M.M. Sant'Anna, I. Sellin, N. Berrah, D.W. Lindle, P.C. Deshmukh, N. Haque, and S.T. Manson, "Dynamical relativistic effects in photoionization: Spin-orbit-resolved angular distributions of xenon 4d photoelectrons near the cooper minimum," *Phys. Rev. Lett.* **87**(12), 1–4 (September 2001).

Wang, H-X., D.S. Patil, W-W. Gu, L. Jacquamet, S. Friedrich, T. Funk, and S.P. Cramer, "L-edge x-ray absorption spectroscopy of some Ni enzymes: Probe of Ni electronic structure," *J. Electron Spectrosc.* **114–116**, 855–863 (June 2001).

Wang, N., K.K. Fung, S. Wang, and S. Yang, "Oxide-assisted nucleation and growth of copper sulphide nanowire arrays," *J. Cryst. Growth* **233**(1–2), 226–232 (November 2001).

Wang, W., H.S. Cho, R. Kim, J. Jancarik, H. Yokota, H.T. Nguyen, I.V. Grigoriety, D.E. Wemmer, and S.-H. Kim, "Crystallographic 'snapshots' of the reversible protein phosphorylation in phosphoserine phosphatase," in *Proceedings of the Gordon Research Conference on Enzymes, Coenzymes, and Metabolic Pathways* (Meriden, New Hamphshire, July 15–20, 2001).

Wang, W., R. Kim, J. Jancarik, H. Yokota, and S.H. Kim, "Crystal structure of phosphoserine phosphatase from *Methanococcus jannaschii,* a hypertheromophile, at 1.8 Å resolution," *Structure* **9**(1), 65–71 (January 2001).

Wang, W., and S.-H. Kim, "Mechanism of a phosphatransfer reaction in biology, crystallographic studies," in *Proceedings of the World Molecular Engineering Network of the 12th Annual Meeting on Structural Biology* (San Jose del Cabo, Mexico, May 6–10, 2001).

Warwick, T., D. Cambie, H. A. Padmore, and M. R. Howells, "A variable-included-angle plane-grating monochromator on an undulator for spectroscopy and microscopy at the Advanced Light Source," *Nucl. Instrum. Meth. A* **467**, 525–528 (2001).

Weber, E.R., S.A. McHugo, A.A. Istratov, C. Flink, and H. Hieslmair, "Identification of metal–oxygen complexes as lifetime limiting defects in solar cell materials," in *Proceedings of the NCPV Program Review Meeting* (Denver, Colorado, April 16–19, 2001).

Weber, Th., O. Jagutzki, M. Hattass, A. Staudte, A. Nauert, L. Schmidt, M.H. Prior, A.L. Landers, A. Braeuning-Demian, H. Braeuning, C.L. Cocke, T.Y. Osipov, I.M. Ali, R. Diez Muino, D. Rolles, F.J. Garcia de Abajo, C.S. Fadley, M.A. Van Hove, A. Cassimi, H. Schmidt-Böcking, and R. Doerner, "K-shell photoionization of CO and N_2: Is there a link between the photoelectron angular distribution and the molecular decay dynamics?" *J. Phys. B–At. Mol. Opt.* **34**(18), 3669–3678 (September 2001).

Weber, Th., M. Weckenbrock, A. Staudte, M. Hattass, L. Spielberger, O. Jagutzki, V. Mergel, H. Schmidt-Boecking, G. Urbasch, H. Giessen, H.P. Braeuning, C.L. Cocke, M.H. Prior, and R. Doerner, "Atomic dynamics in single and multi-photon double ionization: An experimental comparison," *Optics Express* **8**(7), 368–376, March 2001.

Weitzel, K.M., G.K. Jarvis, M. Malow, T. Baer, Y. Song, and C.Y. Ng, "Observation of accurate ion dissociation thresholds in pulsed field ionization-photoelectron studies," *Phys. Rev. Lett.* **86**(17), 3526–3529 (April 2001).

White, C.L., R.K. Suto, and K. Luger, "Structure of the yeast nucleosome core particle reveals fundamental changes in internucleosome interactions," *EMBO J.* **20**(18), 5207–5218 (September 2001).

Wilson, N., D. Fremont, P. Marrack, and J. Kappler, "Mutations changing the kinetics of class II MHC peptide exchange," *Immunity* **14**(5), 513–522 (May 2001).

Wilson, K.R., B.S. Rude, T. Catalano, R.D. Schaller, J.G. Tobin, D.T. Co, and R.J. Saykally, "X-ray spectroscopy of liquid water microjets," *J. Phys. Chem. B* **105**(17), 3346–3349 (May 2001).

Wood, Z.A., L. Poole, and P. Karplus, "Structure of intact AhpF reveals a mirrored thioredoxin-like active site and implies large domain rotations during catalysis," *Biochemistry–US* **40**(13), 3900–3911 (April 2001).

Yang, S.-H., B.S. Mun, A.W. Kay, J.B. Kortright, J.H. Underwood, Z. Hussain, and C.S. Fadley, "Depth-resolved photoemission spectroscopy with soft x-ray standing waves," *J. Electron Spectrosc.* **114–116**, 1089–1095 (March 2001).

Yee, N., L.G. Benning, M.J. Tobin, and K.O. Konhauser, "Synchrotron radiation fourier transform infrared study of bacteria–water interactions: Towards a molecular understanding of bacterial surface reactivity," in *Proceedings of the Synchrotron Radiation Source User Meeting 2001* (Warrington UK, September 4–5, 2001).

Yencha, A.J., S. Canton, J.D. Bozek, and N. Berrah, "A photoelectron spectroscopic study of iron pentacarbonyl," in *Proceedings of the 22nd International Conference on Photonic, Electronic, and Atomic Collisions (ICPAEC 2001)* (Santa Fe, New Mexico, July 18–24, 2001).

Yenen, O., K. McLaughlin, D.H. Jaecks, M.M. Sant'Anna, and E.A. Seddon, "Quantifying relativistic interactions from angular momentum partitioning measurements during photoionization," *Phys. Rev. Lett.* **86**(6), 979–982 (February 2001).

Yeom, H., "Self-organized quantum wires on semiconductor surfaces: The new frontier provided by reduced dimensionality," *J. Electron Spectrosc.* **114–116**, 283–290 (March 2001).

Yeom, Y.H., and H. Frei, "Photoactivation of CO in Ti silicalite molecular sieve," *J. Phys. Chem. A* **105**(22), 5334–5339 (June 2001).

Yi, M., T. Haga, C. Walton, and J. Bokor, "High sensitivity actinic detection of native defects on exterme ultraviolet

lithography mask blanks," *J. Vac. Sci. Technol. B* **19**(6), 2930–2934 (November 2001).

Yi, M., T. Haga, C.C. Walton, and J. Bokor, "'Actinic-only' defects in EUVL mask blanks—Native defects, barely detectable by visible-light inspection," in *Proceedings of the 2001 International Microprocesses and Nanotechnology Conference* (Matsue-shi, Japan, October 31–November 2, 2001).

Yi, M., T. Haga, C.C. Walton, and J. Bokor, "High sensitivity actinic detection of native defects on EUVL mask blanks," in *Proceedings of the 44th International Conference on Electron, Ion, and Photon Beam Technology and Nanofabrication Conference 2001* (Washington, DC, May 28–30, 2001).

Yoshida, T., "Angle-resolved photoemission spectroscopy of $(La,Sr)_2CuO_4$," Ph.D. Thesis, University of Tokyo, Japan, 2001.

Yoshida, T., X.J. Zhou, M. Nakamura, S.A. Kellar, P.V. Bogdanov, E.D. Lu, A. Lanzara, Z. Hussain, A. Ino, T. Mizokawa, A. Fujimori, H. Eisaki, C. Kim, Z.X. Shen, T. Kakeshita, S. Uchida, et al., "Electronlike Fermi surface and remnant (pi,0) feature in overdoped $La_{1.78}Sr_{0.22}CuO_4$," *Phys. Rev. B* **63**(22), 22–24 (June 2001).

Young, A.T., J. Feng, E. Arenholz, H.A. Padmore, T. Henderson, S. Marks, E. Hoyer, R. Schlueter, C. Steier, G. Portmann, et al., "First commissioning results for the elliptically polarizing undulator beamline at the Advanced Light Source," *Nucl. Instrum. Meth. A* **467**(Part 1), 549–552 (July 2001).

Yusupov, M., G. Yusupova, A.E. Baucom, K. Lieberman, T. Earnest, J.H. Cate, and H.F. Noller, "Crystal structure of the ribosome at 5.5 Å resolution," *Science* **292**, 883–896 (May 2001).

Yusupova, G.Z., M.M. Yusupov, J.H.D. Cate, and H.F. Noller, "The path of messenger RNA through the ribosome," *Cell* **106**(2), 233–241 (July 2001).

Zhang, X., R. Kostecki, T.J. Richardson, J.K. Pugh, and P.N. Ross, "Electrochemical and infrared studies of the reduction of organic carbonates," *J. Electrochem. Soc.* **148**(12), 1341–1345 (December 2001).

Zhang, X., J.K. Pugh, and P.N. Ross, "Evidence for epoxide formation from the electrochemical reduction of ethylene carbonate," *Electrochem. Solid-State Lett.* **4**(6), 82–84 (April 2001).

Zhang, X., P.N. Ross, R. Kostecki, F. Kong, S. Sloop, J.B. Kerr, K. Striebel, E.J. Cairns, and F. McLarnon, "Diagnostic characterization of high power lithium-ion batteries for use in hybrid electric vehicles," *J. Electrochem. Soc.* **148**(5), 463–470 (May 2001).

Zhang, X.H., R.S. Gates, S. Anders, and S.M. Hsu, "An accelerated wear test method to evaluate lubricant thin films on magnetic hard disks," *Tribology Letters* **11**(1), 15–21 (July 2001).

Zheng, W.T., J.H. Guo, Y. Sakamoto, M. Takaya, X.T. Li, P.J. Cao, Z.S. Jin, K.Z. Xing, and J.E. Sundgren, "Chemical bonding in carbon nitride films studied by x-ray spectroscopies," *Diam. Relat. Mater.* **10**(9–10), 1897–1900 (October 2001).

Zheng, W.T., Y. Sakamoto, J.H. Guo, X.T. Li, P.J. Cao, Z.S. Jin, and M. Takaya, "Correlation of x-ray absorption and x-ray photoemission spectroscopies in amorphous carbon nitride," *Phys. Rev. B* **64**(1), 6201 (July 2001).

Zhou, X.J., T. Yoshida, S.A. Kellar, P.V. Bogdanov, E.D. Lu, A. Lanzara, S. Fujimora, M. Nakamura, M. Noda, T. Kakeshita, H. Eisaka, H. Uchida, Z. Hussain, and Z.X. Shen, "Dual nature of the electronic structure of $(La_{2-x-y}Nd_ySr_x)CuO_4$ and $La_{1.85}Sr_{0.15}CuO_4$," *Phys. Rev. Lett.* **86**(24), 5578–5581 (June 2001).

Ziegelbauer, J., B. Shan, D. Yager, C. Larabell, B. Hoffmann, and R. Tjian, "Transcription factor MIZ-1 is regulated via microtubule association," *Mol. Cell* **8**, 339–349 (August 2001).